NOVEL CELL-PENETRATING PEPTIDES IN THE DELIVERY OF FUNCTIONAL PROTEIN CONJUGATES INTO LIVING CELLS

Inaugural-Dissertation
to obtain the academic degree
Doctor rerum naturalium (Dr. rer. nat.)

submitted to the Department of Biology, Chemistry, Pharmacy
of Freie Universität Berlin

by

ANSELM FABIAN LOWELL SCHNEIDER

2020

This dissertation was written between the 15.04.2016 and 16.11.2020 under the supervision of Prof. Dr. Christian P. R. Hackenberger at the Leibniz-Forschungsinstitut für Molekulare Pharmakologie (FMP). I declare that I have authored this thesis independently using only the cited literature.

1st Reviewer: Prof. Dr. Christian P. R. Hackenberger

2nd Reviewer: Prof. Dr. Markus C. Wahl

Defense on the: 19.02.2021

The work shown in this dissertation has thus far resulted in the following publications, conference talks and posters:

Original research articles

1. Henry D. Herce, Dominik Schumacher, Anselm F. L. Schneider, Anne K. Ludwig, Florian A. Mann, Marion Fillies, Marc-André Kasper, Stefan Reinke, Eberhard Krause, Heinrich Leonhardt, M. Cristina Cardoso and Christian P. R. Hackenberger*, *Nat. Chem.* **2017**, 9, 762–771.
   Cell-permeable nanobodies for targeted immunolabelling and antigen manipulation in living cells.
   DOI: 10.1038/nchem.2811

2. Anselm F. L. Schneider, Luise Franz, Antoine L. D. Wallabregue and Christian P. R. Hackenberger*, *Bioconjug. Chem.* **2019**, 30, 400-404. Targeted Subcellular Protein Delivery Using Cleavable Cyclic Cell-Penetrating Peptides.
   DOI: 10.1021/acs.bioconjchem.8b00855

3. Anselm F. L. Schneider, Marina Kithil, M. Cristina Cardoso, Martin Lehmann and Christian P. R. Hackenberger*, *Nat. Chem.* **2020**, accepted.
   Cellular uptake of Large Biomolecules Enabled by Cell-surface-reactive Cell-penetrating Peptide additives.
   DOI link not yet available.

Talks

1. Anselm F. L. Schneider, "Schwerpunktprogramm 1623, PhD student meeting", Nürnberg, 27-29.3.**2017**.
   Site-specific functionalization of nanobodies: From labelling to cellular uptake.

2. Anselm F. L. Schneider, Fellowship meeting of the "Fonds der chemischen Industrie", Berlin, 30.11.**2017**.
   Cell-Permeable Nanobodies for Microscopy and Antigen Manipulation in living cells.

3. Anselm F. L. Schneider, 2nd research training group (RTG) 2473 (SynPepBio) Seminar, Berlin, 23-24.01.**2020**.
   Cell-Penetrating Peptides in the Delivery of Fucntional Proteins into Living Cells.

Posters

1. Anselm F. L. Schneider, Henry D. Herce, Dominik Schumacher, Jonas Helma, Alice Baumann, Heinrich Leonhardt, M. Cristina Cardoso, Christian P. R. Hackenberger. GDCh Wissenschaftsforum, Berlin, 10-14.9.**2017**. "Generation of Cell-Penetrating Nanobodies for Microscopy, Interaction Studies and Antigen Manipulation in Live Cells."

2. Anselm F. L. Schneider, Henry D. Herce, Dominik Schumacher, Jonas Helma, Alice Baumann, Heinrich Leonhardt, M. Cristina Cardoso, Christian P. R. Hackenberger. 4th joint meeting of the SPP 1623, Darmstadt, 19-22.6.**2018**. "Generation of Cell-Penetrating Nanobodies for Microscopy, Interaction Studies and Antigen Manipulation in Live Cells."

3. Anselm F. L. Schneider, Henry D. Herce, Dominik Schumacher, Jonas Helma, Heinrich Leonhardt, M. Cristina Cardoso, Christian P. R. Hackenberger. 20th EMBL PhD symposium, Heidelberg, 22-24.11.**2018**.
   "Cell-Permeable Nanobodies for Live-Cell Microscopy and Proteomics."

4. Anselm F. L. Schneider, Henry D. Herce, Alice Baumann, Luise Franz, Heinrich Leonhardt, M. Cristina Cardoso, Christian P. R. Hackenberger. 8th Chemical Protein Synthesis Meeting, Berlin, 16-19.6.**2019**.
   "Making Proteins Cell-permeable with Cell-Penetrating Peptides."

5. Anselm F. L. Schneider, Luise Franz, Alice Baumann, Heinrich Leonhardt, M. Cristina Cardoso, Christian P. R. Hackenberger. Chemical Biology and Physiology 2019, OHSU, Portland, Oregon, 12-15.12.**2019**. "Making Proteins Cell-Permeable for Microscopy and Targeted Protein Modulation."

Other published works not included in this thesis

1. Anselm F. L. Schneider and Christian P. R. Hackenberger*, *Curr. Opin. Biotechnol.* **2017**, 48, 61-68.
   Fluorescent labelling in living cells. (Review article)
   DOI: 10.1016/j.copbio.2017.03.012

2. Dominik Schumacher, Jonas Helma, Anselm F. L. Schneider, Heinrich Leonhardt and Christian P. R. Hackenberger*, *Angew. Chem. Int. Ed. Engl.* **2018**. 57:2314-2333.
   Nanobodies: chemical functionalization strategies and intracellular applications. (Review article)
   DOI: 10.1002/anie.201708459
3. Marc-André Kasper, Marcus Gerlach, Anselm F. L. Schneider, Christiane Groneberg, Philipp Ochtrop, Stefanie Boldt, Dominik Schumacher, Jonas Helma, Heinrich Leonhardt, Matthias Christmann and Christian P. R. Hackenberger*, *ChemBioChem* **2019**.
   NHS-modified ethynylphosphonamidates enable the synthesis of configurationally defined protein conjugatesion strategies and intracellular applications.
   DOI: 10.1002/cbic.201900587

Acknowledgments

First, my gratitude is to my supervisor Prof. Dr. Christian P. R. Hackenberger. He gave me the opportunity to work in his research group and provided the basis for what became a research project that I have thoroughly enjoyed throughout my entire stay. I thank him especially for being a mentor, but also for trusting me to make my decisions that impacted the direction of the project. I owe him especially for his commitment in encouraging me to pursue scientific exchange with other scientists about my work as well as theirs, a habit that will surely be valuable for the rest of my career.

I would also like to thank Prof. Dr. Markus Wahl for his willingness to be the second reviewer of this thesis and for his advice during our thesis committee meetings. I am also grateful to Dr. Martin Lehmann for teaching a lot about microscopy and for making several projects possible that would otherwise not have gone as smoothly. I also thank Profs. Cristina Cardoso and Heinrich Leonhardt and their labs for fruitful collaborations.

My thanks also go to Ines Kretzschmar and Kristin Kemnitz-Hassanin for their great and constant technical support in the peptide- and biology labs. I also want to thank Marianne Dreißigacker, Katrin Wittig and Jennifer Trümpler for their assistance with all kinds of administrative tasks.

I also want to thank all other members of the Hackenberger lab. I want to highlight Dominik Schumacher, Marc-André Kasper and Sergej Schwagerus for long discussions about science and many other things that do not matter as much. During my work, I have had the pleasure to supervise many students on internships, including Alen Kocak, Natalie Agarwala, Kevin Schiefelbein, Luise Franz, Felix Schonebeck and Laila Benz. They have taught me much and I am very grateful that they were a part of my journey.

I want to thank my family and friends. My mother, Stefanie Schneider B. Schneider, for the financial support during my studies and for believing in me throughout. Also, my brother, Lewin L. F. Schneider, for his continuing support and life advice. I also want to thank my grandparents, Siegrid and Karl-Dieter Schneider, for their encouragements. My friends Andras Bittner, Sebastián Florez-Rueda, Eleftheria Poulou, Pia Rautenstrauch, Camilla Ciolli-Mattioli and many others were also instrumental during this long time.

Finally, I wish to dedicate this thesis to my late uncle, Dr. Bernd Christian Schneider. An inspiration to everyone around him - he is proof that being smart, knowledgeable, and well-spoken is very cool indeed.

Abbreviations

Ar	argon
ATP	adenosine triphosphate
Boc	tert-butyloxycarbonyl
CBD	chitin-binding domain
CPP	cell-penetrating peptide
cCPP	cyclic cell-penetrating peptide
CuAAC	copper-catalysed azide–alkyne cycloaddition
DIPEA	*N*,*N*-diisopropylethylamine
DMF	*N*,*N*-dimethylformamide
DNA	deoxyribonucleic acid
DTNB	5,5'-dithiobis-2-nitrobenzoic acid
DTT	dithiothreitol
EPL	expressed protein ligation
Et_3N	triethylamine
ESI	electrospray ionization
Fab	antibody fragment of the variable region
Fmoc	fluorenylmethyloxycarbonyl
h	hour
HEPES	(4-(2-hydroxyethyl)-1-piperazineethanesulfonic acid)
HBTU	2-(1*H*-benzotriazole-1-yl)-1,1,3,3-tetramethyluronium hexafluorophosphate
HCl	hydrochloric acid
HOBt	1-hydroxybenzotriazole
HPLC	high-performance liquid chromatography
HR	high-resolution
IgG	Immunoglobulin G, a type of antibody
IMAC	immobilized metal ion affinity chromatography

MALDI	matrix-assisted laser desorption/ionization
MeCN	acetonitrile
MHz	Megahertz
min	minute
MS	mass spectrometry
MS/MS	tandem mass spectrometry
NaOH	sodium hydroxide
NCL	native chemical ligation
NMR	nuclear magnetic resonance
PBS	Phosphate-buffered saline
ppm	parts per milion
PTM	post-translational modification
RNA	Ribonucleic acid
RP	reversed-phase
SPPS	solid-phase peptide syntesis
TFA	trifluoroacetic acid
THPTA	tris(hydroxypropyltriazolyl)methylamine
TIS	triisopropylsilane
tRNA	Transfer-RNA
Tris	tris(hydroxymethyl)aminomethane
UDP	uridine diphosphate glucose
UPLC	ultra-performance liquid chromatography
UV	ultraviolet
VhH	single-domain antibody (nanobody)
XIC	extracted ion chromatogram

Table of contents

1 Introduction

1.1 Motivation: Cellular Delivery of Proteins

Proteins offer an incredible diversity in form and function. Enzymes, nature's biological catalysts, enable life itself. Today, proteins can even be created *de novo* with entirely new functions[1]. Unlike drugs and drug-like molecules however, proteins are somewhat limited in their potential by their large size and hydrophilicity, two properties which generally render them cell impermeable. What is, under normal circumstances, an important feature in the compartmentalization of living organisms into cells and subcellular organelles, can become a problem when a protein is dysregulated, dysfunctional or missing entirely.

In these cases, the delivery of functional proteins into cells has immediate therapeutic potential[2], for example in the treatment of protein deficiencies like Rett syndrome[3]. The advent of protein-based DNA-editing approaches such as CRISPR-Cas[4] holds promise for *ex vivo* cell-based therapies, *in vivo* genome-editing, and a limitless array of research applications[5] – if the biomolecules involved can be delivered. Antibodies, a class of proteins that has become crucial in fundamental biological research, are also typically limited to extracellular applications[6,7]. The delivery of antibodies, which can be raised against virtually any target and are therefore reliable targeting agents and inhibitors, has tremendous potential for therapeutic and research applications[8,9].

Several methods already exist for the cellular delivery of biomolecules, each with their own advantages and disadvantages[10,11]. A particular challenge in the delivery of proteins is also the delivery to the correct subcellular compartment. During delivery proteins can become trapped in endosomes or lysosomes, which will lead to their degradation[12].

The ideal method of protein delivery would therefore:

- be simple to use and scalable
- be applicable to any given cargo and cell system
- be specific to a certain type of cell or target
- be traceless such that the protein is restored to its original state once delivered
- not be harmful to the cell or organism
- lead to delivery of the protein to its intended location[10,11,13,14].

1.2 The Cell Membrane

In general, when considering the delivery of proteins into mammalian cells, the obstacle to overcome is the cell membrane. The cell membrane, or plasma membrane, consists of a phospholipid bilayer made up out of three major classes of lipids: glycerophospholipids, sphingolipids and cholesterol[15]. The formation of this bilayer is a direct consequence of the structures of lipids that possess a hydrophobic and hydrophilic moiety, which will arrange spontaneously into bilayers in aqueous medium[16]. The plasma membrane has a width of approximately 5 nanometers. Lipids are distributed asymmetrically and are in constant motion, both laterally as well as trans-bilayer. Because of this motility, the original model of plasma membranes pioneered by Singer and Nicolson is called the "fluid mosaic" model[17].

Since their original model, the general understanding of the structure of membranes has changed much, although the changes were mostly focused not on lipids, but rather on the protein components of membranes[18]. In the original model, transmembrane proteins played a minor role, but more recent research has shown that they occur rather frequently, with a protein:lipid ratio of approximately 1:40[19]. Moreover, transmembrane and membrane-anchored proteins often have very bulky protein domains on the surface of the cell. Proteins have also been found to attach to membranes transiently[20]. They can also themselves reorganize the bilayer through protein-protein and protein-lipid interactions[21] and several specific interactions of proteins with lipids have been described[22].

Additionally, many membrane proteins are proteoglycans, meaning they carry complex carbohydrate chains such as heparan sulfate, which also shape the surface of the plasma membrane[23]. These carbohydrate chains mediate cell-cell recognition and many other intercellular activities including infection by bacteria and viruses[24]. The negative charge of many proteoglycans is also often made responsible for the effective binding of positively charged molecules to the surface of the cell[25-27].

The basic function of the cell membrane is to physically separate intracellular components from extracellular environment. However, it is evident that for cells to function, transport of molecules across the cell membrane must occur. Various types of molecules cross the membrane in different ways. Typically, smaller and more hydrophobic molecules can diffuse across the cell membrane passively, driven by electric and concentration gradient of the

solute[28]. As it is of great significance in pharmacology and drug development, much research has been done into understanding and predicting the membrane permeability of given molecules[29]. Several parameters that are important for cellular permeability have been determined, famously summarized in Lipinski's "rule of 5" and other rulesets, although not all compounds comply with these parameters and behave as predicted[30].

The cellular entry of molecules that do not permeate passively is accomplished through active transport, mediated by membrane transporters. It is estimated that around 10% of human genes are related to transporters, which shows how significant these proteins are[31]. Active transport is complex, and there are many pathways into the cell[32,33]. For larger molecules, active transport generally results in the inclusion of a transported cargo into a vesicle, and the eventual delivery of the cargo into lysosomes for degradation[34]. Because of this, successful delivery of proteins into the cytosol of cells requires specialized methods[11,14,35,36].

1.3 Methods for the Cellular Delivery of Proteins

A variety of methods has been established to transport cargoes across the cell membrane. They can be broadly divided into five categories: physical methods, nanocarriers, endosomal escape, cell-penetrating peptides, and other methods.

1.3.1 Physical Methods

Physical methods of biomolecule delivery generally rely on the temporary disruption of the cell membrane, after which the cellular uptake of biomolecules into the cell can occur through simple diffusion. Ideally, the uptake of the biomolecule of interest is followed by the quick recovery of the cell membrane before the cell is damaged. Over the years, many methods for the disruption of biomembranes have been developed[13,37].

Being over 100 years old, microinjection is likely the first ever method to provide intracellular delivery of biomolecules[38]. Conceptually, microinjection is very simple: a capillary is inserted into the cytosol or nucleus of a cell, and a biomolecule is injected through it (figure 1a). In practice however, microinjection is very laborious, as only one cell at a time can be injected, which typically limits the scale of experiments to a few hundred cells[39]. Because of this, the

most important development in the field of microinjections has been the automation and standardization of the cell preparation and injection processes, which can greatly improve the throughput of the method[40-42]. Nevertheless, microinjection also requires very specialized equipment.

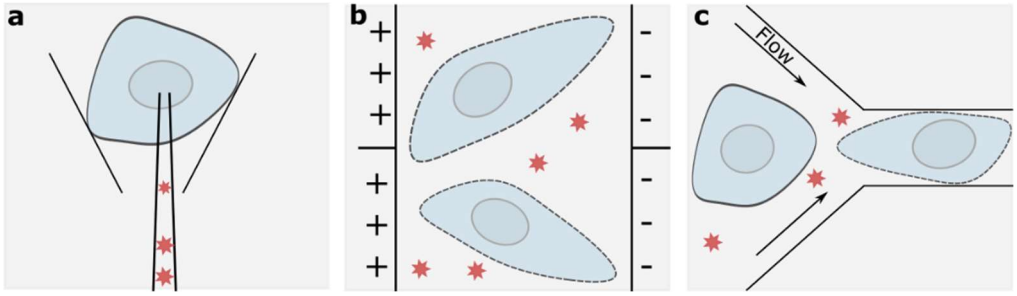

Figure 1. Selected physical methods for protein delivery into cells. **a**, For microinjection, a capillary is inserted into the cytosol or nucleus of the cell and the cargo is injected. **b**, In electroporation an electric field is applied to a cell suspension, leading to the formation of pores in the cell membrane. **c**, Cells are squeezed through a constriction using an applied flow, leading to the deformation of the membrane.

The most popular physical method to ensure protein delivery is electroporation. The physical principle underlying electroporation is that cell membranes maintain an electrical potential between the cytosol and the extracellular environment. By applying a potential difference across that membrane, the membrane forms small openings (pores) to compensate. The cargo that one wants to deliver can then diffuse through these openings into the cell (figure 1b). An inherent problem with electroporation-type approaches is the heterogeneity of permeabilization, making it difficult to control the amount of cargo delivered[43]. Miniaturized electroporation approaches such as microelectroporation and nanoelectroporation promise to improve on this by performing electroporation in smaller scales. These approaches have a much higher level of control of the membrane disruption; however the throughput of the methods is reduced in turn, although recent methods try to overcome this using microfluidics[44,45].

A more modern, physical approach to cargo delivery is cell squeezing[46]. This is a microfluidic approach that relies on the deformation of cells as they pass through a constriction (figure 1c). The shear forces result in deformation of the membrane, generating transient holes into the cytosol[46]. In contrast to the aforementioned methods, cell squeezing is both high throughput (1’000’000 cells per second) and can be used to deliver well defined concentrations of cargo[47].

While cell squeezing also promises to be less harmful to cells than electroporation[48], it is still a relatively new method that requires specialized equipment and has yet to establish itself as a contender.

There are also many other physical methods to disrupt the lipid bilayer, such as scrape loading[49], sonoporation[50] and chemical detergents[51]. The inherent problem with nearly all physical delivery methods is that that membrane disruption can lead to toxicity and leakage of the cellular interior. Also, physical delivery methods are limited to *in vitro* or *ex vivo* applications[13]. However, when it comes to throughput and reliability, these methods have made tremendous progress and there is still much potential for this field to grow and develop further.

1.3.2 Nanocarrier-mediated Delivery

There are many kinds of nanocarriers that have been developed for various kinds of applications in science and therapy[52,53]. The great potential of nanocarrier-mediated delivery lies in the tunability of their properties for their applications in different fields[14,54]. Proteins can be loaded onto nanocarriers in many ways, and the nanocarriers can enter cells through different pathways as well[55].

Liposomes are perhaps the most widely used nanocarriers in the delivery of therapeutic proteins and antibodies[56,57]. Liposomes consist of a lipid bilayer that is often positively charged on the surface, thereby binds to cell-membranes and is endocytosed. An advantage of using liposomes is that the lipid bilayer will shield the cargo from extracellular proteases, making it a promising approach for *in vivo* applications. Proteins can be loaded into these cationic particles, for example through fusion to a super-negatively charged protein domain (figure 2a)[58]. The uptake into cells then typically occurs through endocytosis, and liposomes can fuse or destabilize the endosomal membrane to release the cargo into the cytosol[58]. Despite this straightforward concept, this process can be inefficient, and cargo can remain trapped in endosomes. Still, approaches which improve upon this endosomal escape exist[59].

To circumvent endosomal entrapment entirely, fusogenic liposomes were developed. These liposomes can fuse with the cellular plasma membrane and deliver the liposomal content directly into the cytoplasm[60,61]. While quite efficient, it was originally only possible to load

negatively charged cargoes into the cationic liposomes, as electrostatic repulsion would prevent cationic cargoes from being loaded. To overcome this, it was shown that it is possible to incorporate mesoporous silica nanoparticles that bind to proteins into fusogenic liposomes[62].

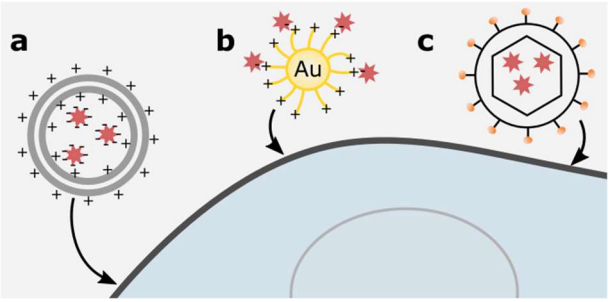

Figure 2. Selected nanocarrier-based methods for protein delivery. **a**, Delivery based on cationic liposomes with negatively charged cargo loaded into the liposome. **b**, Gold nanoparticle functionalized with cationic headgroups in the delivery of an anionic protein cargo. **c**, Cargo delivery by encapsulation into a virus-like-particle.

Exosomes are naturally occurring, secreted vesicles that can transport macromolecules between cells[63]. Because they are a naturally occurring mechanism, they are a promising avenue to protein delivery *in vivo*[64,65]. However, loading exosomes with a protein of interest has proven difficult. A chosen protein cargo can be fused to a protein that naturally occurs in exosomes to generate exosomes with the cargo inside it, but this limits the breadth of proteins that can be loaded[66]. A more sophisticated approach uses a light-triggered protein interaction to recruit proteins into exosomes, at which point the interaction can be removed again for cargo release[67]. It is also possible to load isolated exosomes with exogenous cargo, although this process seems to be inefficient[68].

Completely synthetic polymer species can also be used to deliver proteins into cells. For example, polysaccharides and nanogels have been used for this purpose[69,70]. However, the cellular uptake of polymers is mostly through endocytosis, and cargo will thus generally remain trapped in endosomes[71]. One notable exception to this are cell-penetrating-polydisulfides (CPDs), which contain positively charged guanidinium head groups like polyarginine peptides but in which the backbone linkage consists of disulfides. These polymers can reportedly deliver a cargo directly in the cytosol and are de-polymerized by reduction with intracellular glutathione. Since it was not possible to generate the polymer directly on a protein cargo, conjugation of the cargo to the polymer had to be done using affinity tags such as biotin and streptavidin[72]. In a new approach these tags could be removed once inside the cell, improving the method somewhat[73].

Alternatively protein cargoes can be conjugated to carbon nanotubes for cellular delivery. By using biotin-conjugated nanotubes, it was possible to deliver fluorescently labelled streptavidin into cells[71]. In this first report, however, cargoes were also trapped in endosomes after delivery, although other reports exist in which cargoes reach the cytosol[74]. More recent reports include light-cleavable protein-nanotube conjugates that can be used to deliver proteins into the nucleus of cells and can even be used *in vivo*[75].

Gold nanoparticles have been widely used in drug delivery approaches[76]. In protein delivery, the surface of the gold nanoparticles can be tailored to suit the cargo, such as cationic sequences binding to the enzyme β-galactosidase (figure 2b)[77]. The resulting delivery is then often a mixture of cytosolic and endosomal uptake. To improve upon this concept, gold particles can be incorporated into so-called nanoparticle-stabilized capsules (NPSCs) which contain a fatty acid interior that can fuse with cell membranes to deliver proteins directly into the cytosol[78,79].

Virus-like-particles (VLPs) are based on the self-assembly of viral coat proteins. From different viral origin exist different coat proteins with different structures and functionalities. The protein cargoes can usually be recombinantly expressed as fusions to a viral protein and thereby loaded into the viral capsid (figure 2c)[80,81]. A newer method in which the surface of the particle expresses an antibody-binding domain has even been used to deliver antibodies into cells[82]. All VLP-based approaches, like many other methods, show a mixture of cytosolic delivery and endosomal entrapment.

In summary, nanoparticle-based delivery approaches often struggle with achieving cytosolic delivery without endosomal entrapment. Due to their flexibility and tunability however, these approaches can often be combined with triggers for efficient endosomal release[83].

1.3.3 Endosomal Escape

A very attractive way to ensure the delivery of biomolecules into cells is endosomal escape. Endocytosis is the major way for cells to take up macromolecules and loading cargoes into endosomes is relatively straightforward[84]. For example, modification of proteins with folic acid

leads to their uptake into endosomes via receptor-mediated endocytosis[85]. Endosomes are, however, also loaded with proteases and acidify over time to digest any proteins within[86], so escape of the cargo must be quick.

Anthrax toxin is a secreted, multi-protein complex from the bacterium *Bacillus anthracis*. It contains the protective antigen (PA) protein, that can bind to cell-surface receptors, oligomerize and, after uptake into endosomes and acidification, form a channel through the endosomal membrane and release the lethal and edema factor proteins into the cytosol[87]. This is a promising system to hijack for intracellular protein delivery, since every step can be modified to suit the application[88]. For example, a linker on the protective antigen must be cleaved by the ubiquitous protease furin before binding to the cell membrane. By exchanging this linker to be cleavable by matrix metalloproteases that are overexpressed on cancer cells, specific cell killing could be achieved[89]. Exchanging the delivered lethal and edema factor proteins for a cargo of choice is simple and can be achieved by recombinant expression of the cargo of interest fused to the *N*-terminal domain of the lethal factor[90]. Small, linear peptide cargoes are easy to transport, although more bulky constructs cannot pass through the pore generated by the protective antigen[91]. Proteins such as antibody mimics have also been delivered into cells using anthrax toxin, although such uptake requires the unfolding and subsequent refolding of the proteins[92].

Instead of using a rather complex protein system, several peptide-based approaches to get cargoes from endosomes into the cytosol have been developed. GALA is a 30-mer peptide with a glutamic acid-alanine-leucine-alanine repeat. It was designed with two criteria in mind: enough length to span a lipid bilayer, and a low-pH mediated trigger where at neutral pH GALA does not bind membranes but does so at pH 5[93]. GALA is unstructured at neutral pH but can take on an α-helical structure at the lower endosomal pH and insert into the membrane to form a channel. However, one major drawback of GALA is that due to its negative charge, efficient delivery requires complex formation with a cationic lipid that will bind to the cell[94]. The combination of GALA with a cationic lipid has been used to deliver proteins into the cytosol that were trapped in endosomes in absence of the peptide (figure 3)[95].

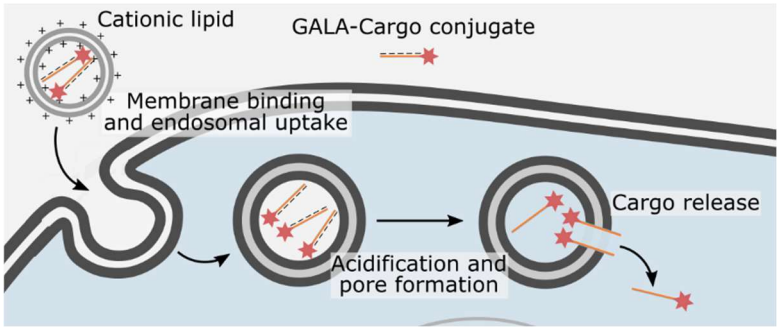

Figure 3. Delivery of cargo-GALA conjugates in combination with cationic lipids. The conjugate forms complexes with the cationic lipid that are taken up into endosomes. Through acidification of the endosome, the GALA peptide is protonated and becomes helical (not shown), allowing insertion into the membrane, formation of a pore and release of the cargo into the cytosol.

More recently, a 13 amino acid long peptide named aurein 1.2 was discovered that could also efficiently release proteins from proteins into the cytosol. To achieve efficient delivery, cargo proteins had to be fused to a supercharged mutant of GFP that contains a net 36 positive charges[96]. The peptide showed relatively high cytotoxicity but could be applied to the delivery of the gene-editing enzyme Cre recombinase in a mouse model.

To circumvent the issues with negatively charged peptides, a new endosomolytic peptide was developed originating from a spider toxin. The peptide is named “L17E” after the mutation that sets it apart from the M-lycotoxin peptide that it is based on. It was designed with a helical structure, with a cationic face and an anionic face that contains a single negatively charged amino acid that would be protonated to be more hydrophobic in endosomes[97]. This protonation was proposed to lead to endosomal rupture. Indeed, it could successfully be used in the delivery of several cargoes, including intact IgG antibodies into cells by simple co-incubation of the cargo with the peptide. Recently, however, it was suggested that the peptide may in fact not lead to endosomal rupture at all, but instead induce membrane ruffling that leads to direct cytosolic uptake of cargoes[98].

Other endosomal escape peptides have also been obtained through rational design. Notably, cyclization of an amphipathic arginine-rich peptide conferred efficient endosomal escape activity to it[99]. It could later be shown that this cyclic peptide escapes from early endosomes and does not require endosome acidification[100]. The peptide was also able to transport EGFP and a phosphatase into the cytosol of HeLa cells.

An interesting finding in this context is that Tat, a cell-penetrating peptide with an affinity for biomembranes (see 1.3.4.1 for a detailed description of the peptide) was able to bring the fluorophore tetramethylrhodamine into contact with membranes and, upon irradiation, the fluorophore would lead to membrane leakage[101]. By making a dimer of the fluorescent Tat, named "dfTat", it was possible to deliver cargoes into cells by simple co-incubation with a low concentration of the peptide. Amongst the delivered proteins were the fluorescent protein EGFP and an intact antibody[102]. A fluorescent Tat-trimer was also effective at delivering protein cargoes at a low concentration, but the peptide also showed noticeable cytotoxicity over a low concentration threshhold[103].

Through rational design and evaluation of various hydrophobic moieties fused to Tat, several candidates for endosomolytic peptides could also be evaluated in the delivery of a peptide fragment of EGFP. But these hydrophobic sequences also showed cytotoxicity at elevated concentrations[104].

The small molecule chloroquine, an anti-malarial drug that raises endosomal pH and stops fusion of endosomes with lysosomes[105], has also been used to aid in endosomal escape[104,106,107]. Chloroquine is quite inefficient and has significant side effects and so research has been done into alternative small molecules for endosomal release. As a potential candidate, the small molecule UNC7938 was proposed, which is structurally similar but proved to be more potent than chloroquine in the release of molecules entrapped in endosomes[108]. The delivery of proteins was still quite ineffective with UNC7938 alone however, and had to be improved by the addition of an endosomal escape peptide[109].

In summary, endosomal escape is a promising route for cellular delivery, as it promises ease of use and has seen successful applications *in vivo*. However, efficient cytosolic localization of the cargo can for the most part only be achieved if the cargo is actively taken up into endosomes, and toxicity of endosomal escape agents is also often a problem[110].

1.3.4 Cell-Penetrating Peptides

1.3.4.1 Origin and Classification

The first cell-penetrating peptides (CPPs) or "protein transduction domains" (PTDs) have been discovered a little over 30 years ago, when researchers found that the transactivator of transcription (TAT) protein of the human immunodeficiency virus 1 (HIV-1) could be efficiently taken up by simple co-incubation with cells[111]. What later turned out to be an important mechanism for HIV-triggered progression towards the acquired immune deficiency syndrome (AIDS)[112,113], also had immediate implications for biotechnological applications. More close examinations of the sequence of TAT determined that a relatively short stretch of the protein, ranging from amino acids 37-62, was responsible for its transactivation activity, and the key sequence for passing cell membranes was identified as a strongly basic stretch from amino acids 48-60 (figure 4a)[114,115]. This 12 amino acid-long peptide (GRKKRRQRRRPPQ) became known as the TAT-peptide over the following years, developing into a focal point of research into this new class of peptides.

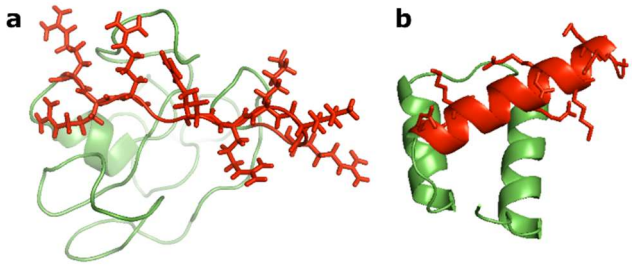

Figure 4. Cartoon models of structures of the **a**: TAT (PDB: 1K5K) and **b**: pAntp (PDB: 9ANT) peptides. The sequences that are commonly used as cell-penetrating peptides are shown in red, with cationic residues highlighted as stick-models.

Shortly after the original discovery of the properties of the TAT protein, a similar phenomenon was observed with the pAntp peptide, which is the DNA binding domain of the *Drosophila* antennapedia protein[116]. A fluorescently labelled version of the peptide was taken up into neurons, and could induce neural differentiation by itself[117,118]. Truncations of the peptide revealed that only 16 amino acids (43-58, figure 4b) were required for cellular uptake, and this uptake could also occur at 4°C, in conditions where classical endocytosis does not happen[119]. This peptide is now known as penetratin and is still one of the most used CPPs to date. It could also later be shown that a version of the peptide consisting only of D-amino acids was taken up into cells just as well, suggesting that recognition by a receptor on the surface of the cells is most likely not required in the uptake either[120].

Since the discovery of these archetypical cell-penetrating peptides, much has been accomplished in the field. There are now thousands of experimentally validated cell-penetrating peptide sequences[121]. Many CPPs come from viral or other biological origin, but there are also synthetic CPPs, and it is even possible to predict novel CPP sequences using machine learning algorithms[122,123].

Typically, CPPs are peptides ranging from 5-30 amino acids that can pass through cell membranes without interacting with specific receptors. Classification of cell-penetrating peptides is challenging, because CPPs have various origins and show little sequence homology. However, it is possible to classify CPPs by the prevalent type of amino acid within the peptide. There are cationic CPPs, like TAT and penetratin, but also amphipathic[124], hydrophobic[125] and even some anionic CPPs[126]. Most CPPs by far (>80%) have a net positive charge[127]. An overview of some cell-penetrating peptides of different types can be found in Table 1.

Table 1: Select Cell-Penetrating Peptides and their sequences.

Type	Name	Sequence	Origin	Ref.
Cationic	TAT	GRKKRRQRRRPPQ	HIV TAT protein	[115]
	Penetratin	RQIKIWFQNRRMKWKK	*Drosophila Melanogaster* Antennapedia	[119]
	Polyarginines	R7-R12	Synthetic	[128,129]
	PPC3	KKYRGRKRHPR	Synthetic	[123]
	hPP3	KPKRKRRKKKGHGWSR	*Homo Sapiens* SP140-like protein	[130]
	Cyclic W(RW)4	Cyclic [W(RW)4]	Synthetic	[131]
Amphipathic	SAP	(VRLPPP)3	*Zea Mays* γ-Zein protein	[132]
	Transportan	GWTLNSAGYLLGKINLKALAALAKKIL	Chimeric of protein origin	[133]
	Pep-1	KETWWETWWTEWSQPKKKRKV	Chimeric of protein and	[134]

			synthetic origin	
	MAP	KLALKLALKALKAALKLA	Synthetic	[135]
Hydrophobic	C105Y	CSIPPEVKFNKPFVYLI	*Homo Sapiens* α1-antitrypsin	[136]
	Pep7	SDLWEMMMVSLACQY	Phage display library	[125]
Anionic	SAP(E)	(VELPPP)3	Synthetic, derived from SAP	[126]
	P28	LSTAADMQGVVTDGMASGLDKDYL KPDD	*Pseudomonas aeruginosa* azurin	[137]

1.3.4.2 Structural Features of Cationic CPPs

The first step in the membrane entry of cationic CPPs is generally accepted to be electrostatic interaction between the positively charged headgroups with negatively charged proteoglycans and phospholipids[138,139]. The importance of the positive charges for the ability of cationic CPPs to cross membranes has been proven several times. Replacement of charged residues within the Tat peptide by alanines strongly reduced uptake[129], and this was also true for penetratin[140]. Interestingly, substituting lysine residues for arginine residues also increased the rates of cellular uptake[129]. Studies on the differences between oligoarginines and oligolysines have shown that the guanidinium group in arginine leads to higher affinity for membranes[141] and more efficient clustering of peptides at the membrane interface[142]. Polyarginines also bind to membranes cooperatively, which polylysines do not do[143]. These effects have been attributed to the guanidinium groups' ability to form bidentate hydrogen bonds with negatively charged phosphate, sulfate and carboxylate groups (fig. 5a), all of which can be present on the cell surface[144]. Lysine, on the other hand, can only donate one hydrogen bond (fig. 5b). To explore this further, symmetrical dimethylated arginine (SDMA) was also tested, which should retain the charge of typical arginine but can only donate one hydrogen bond as well (fig. 5c). The dimethylated arginine peptide was substantially worse in its uptake, suggesting that the bidentate hydrogen bonding of arginines is indeed a crucial feature for uptake[145]. Lysine that had been guadinylated to generate homoarginine (fig. 5d) showed similar uptake to arginine peptides[146] and a recent study even suggested homoarginine may be more effective than

conventional arginine[147].

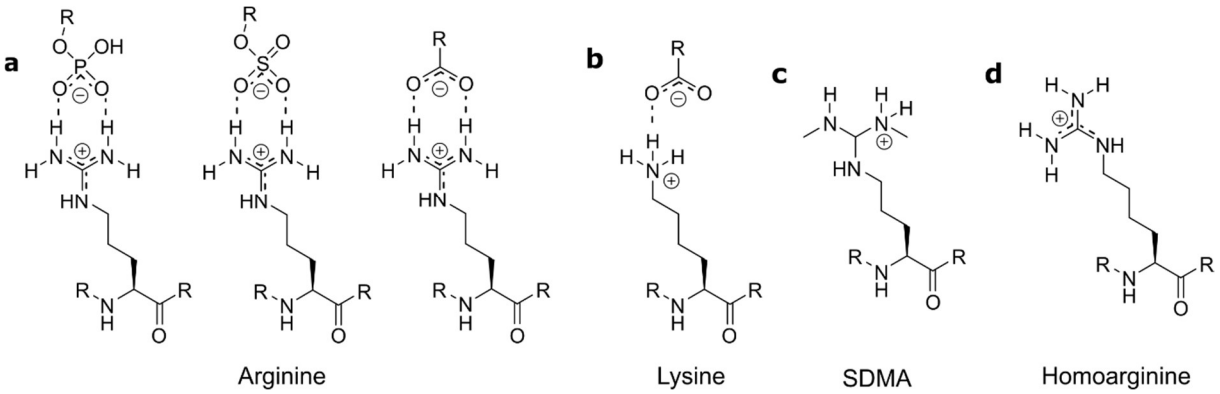

Figure 5. Structures at physiological pH of **a**: arginine in its bidentate interaction with phosphate, sulfate or carboxylate groups, **b**: lysine in its monodentate interaction with a carboxylate, **c**: symmetrical dimethylated arginine (SDMA) and **d**: homoarginine (also known as guanidyl-lysine).

Hydrophobicity is another component that is often a part of cationic CPPs and a key factor in their interaction with the lipid bilayer[148]. Introducing a hydrophobic tryptophan residue into a Tat peptide increased vesicular leakage and altered the translocation mechanism[149]. Increasing hydrophobicity can also lead to a decrease in uptake efficiency, which may be due to peptides being "stuck" in the membrane[150]. Tryptophan may also play a role in CPPs beyond its hydrophobicity, as deletion of other hydrophobic acids in the peptide penetratin did not lead to a reduction in cellular uptake but the removal of tryptophan did[140]. Appending tryptophan residues to polyarginine peptides was also linked to an improvement in cellular uptake in several studies[151,152]. This effect may result from increased binding to proteoglycans on the surface of cells[153].

It is still not completely clear if there is a relationship between the secondary structure of cell-penetrating peptides and their cellular uptake. Cell-penetrating peptides are often unstructured in aqueous environments, but adapt a secondary structure upon interaction with the lipid bilayer[150,154]. Interestingly, polyarginines and Tat seem to remain unstructured even when interacting with the membrane[155]. The peptide penetratin adopts a helical structure when interacting with cell membranes, but this may have a negative impact on cellular uptake[156], and is not actually required for the uptake of the peptide[157]. Generally, flexibility seems to be an important structural feature for the uptake of CPPs[158,159].

1.3.4.3 Synthetic Derivatives of Cell-Penetrating Peptides

To improve upon the cellular uptake of naturally occurring cell-penetrating peptide sequences, several strategies have been explored[160]. Increasing stability towards proteolysis, adding hydrophobicity, and enhancing structure and/or rigidity are common goals in the engineering of synthetic CPPs.

The replacement of the naturally occurring L-amino acids with D-amino acids is commonly done in the development of peptides for biological applications. The substitution can retain the activity of the parent peptide while making it more resistant to proteolysis[161]. This concept has also been applied to cell-penetrating peptides, increasing the amount of delivered peptide[162]. Interestingly, in some studies the substitution of L- to D-amino acids has also been linked to a decrease in uptake of cell-penetrating peptides in some cell types[163].

Peptoids are peptidomimetics in which the amino acid side chain is on the nitrogen atom instead of the α-carbon. They are resistant to proteolysis and have been used to improve conventional cell-penetrating peptide sequences[164,165].

Lipidation of cell-penetrating peptides allows tuning of the behaviour of the peptides while crossing the lipid bilayer[166]. Lipidation has also been shown to sometimes increase helical content in peptides through micelle formation[167]. This was also accomplished for a cell-penetrating peptide, increasing its uptake into cells[168]. Using a long acyl chain (decyl), a very effective cell-penetrating peptide containing only four arginine residues could be generated[169].

To induce helicity in a peptide sequence, the unnatural amino acid α-aminoisobutyric acid can be used[170]. Cell-penetrating peptides incorporating this amino acid showed improved uptake into cells with increasing helicity[171]. Alternative strategies to induce helicity in cell-penetrating peptides were also successful[172,173], suggesting that this may be a general strategy in improving uptake.

To pre-arrange positive charges in defined distances, oligoproline peptides bearing guanidinium groups can be used[174]. Oligoprolines provide a rigid helical structure with a defined distance between individual residues. The rigid guanidinium-bearing oligoproline proved to be more effective at transporting a fluorophore into cells than an equivalent polyarginine peptide. The same oligoproline could recently be used to transport inositol phosphate into cells[175].

Cyclization of peptide sequences can provide both structural rigidity as well as increased proteolytic stability[176]. When designing functional peptides, it also seems to be a general rule that cyclic peptides have increased cell-permeability over their linear counterparts[177,178]. Significant work has been put into understanding how cyclization affects the conformations of peptides and, in turn, their cell permeability[179,180].

The advantages of cyclic peptides over their linear counterparts also apply to CPPs[181]. Cyclic analogues of the Tat peptide and a decaarginine showed increased cellular uptake due to more rapid crossing of the cell membrane[182]. There are also several reports on improved delivery using cyclic variants of amphipathic CPPs[183]. The mode and site of cyclization also seems to impact the efficiency of the resulting uptake into cells[184]. Bicyclic cell-penetrating peptides have also been generated using different chemistries[185,186]. One approach makes use of cyclization of a CPP-cargo fusion through a disulfide bond that is reduced inside cells, making the cyclization reversible[187].

1.3.4.4 Cellular Uptake Mechanism

The mechanism of uptake of CPPs has been a long-standing research objective in the field, but it is challenged by the fact that the variety in CPP sequences comes along with a variety in modes of uptake. A given CPP-cargo-conjugate can also take different roads into the cell depending factors other than the peptide sequence. The concentration of the CPP[188], the size and nature of the cargo[189], the linker between CPP and cargo[190], type of lipid or cell[191] and temperature[192] all have effects on the mechanism that the CPP uses to get into the cell. Generally, the pathways into the cell can be divided into energy-dependent endocytosis and energy-independent membrane transduction. First however, the methods that can be used to study these mechanisms of entry will be discussed.

1.3.4.4.1 Methods to Study Cellular Uptake

No single method has emerged that would allow complete characterization of the cellular uptake mechanism and often a combination of methods is required to elucidate the mechanism

for a given system. Different methods each have their own biases, which also makes using multiple assays a requirement to avoid drawing false conclusions.

Cellular uptake of peptides is often studied by using a coupled fluorophore to detect the peptide either by flow cytometry or microscopy. Flow cytometry allows high throughput screening of peptides in many cells but cannot discriminate peptides bound to the outside of the cell, peptide in endosomes or peptides in the cytosol. Through the application of the non-permeant dye trypan blue, some fluorophores bound to the outside of the cell can be quenched, allowing quantification of only intracellular fluorescence[193]. Nevertheless. endosomal and cytosolic localization of the peptide could still not be distinguished. Using conventional fluorescence microscopy it can also be difficult to distinguish intracellular localization, although protocols have been developed to digest membrane-bound CPP with the enzyme trypsin to remove bias originating from it[194]. Confocal microscopy allows distinguishing intracellular compartments. Still, it is important to choose the right fluorophore for the experiment, as fluorophores that lose fluorescence at lower pH can appear cytosolic while in reality being mostly localized to endosomes[195]. Another important factor is the self-quenching of fluorophores. When the concentration of a given organic fluorophore in a compartment is too high, fluorescence can decrease. To avoid this, it is possible to use a mixture of fluorescently labelled and unlabelled cell-penetrating peptide. Contrary to expectations, this method could reveal that the majority of an arginine-rich CPP was localized to lysosomes instead of the cytosol in one experiment[196].

Electron microscopy presents an attractive method to study alterations of the plasma membrane caused by CPPs down to a few nanometres of resolution. For example, it could be shown that an R9-CPP could cause local deformations and multilamellarity of the membrane in areas where the peptide was particularly enriched[197].

As a qualitative measure of uptake, the delivery of functional molecules and proteins can be used. A common assay here is the delivery of the cre recombinase enzyme, that can be used in conjunction with a reporter cell line. When delivered, the enzyme will lead to expression of a fluorescent protein, which can be read out by flow cytometry or microscopy[198]. The advantage of this assay is that it requires an active enzyme in the correct subcellular compartment, but the amount of delivered enzyme is difficult to quantify. An alternative methodology relies on the delivery of D-cysteine. This unnatural amino acid can react with a cell-permeable building block to form D-luciferin, which serves as the substrate for a luciferase enzyme expressed within a reporter cell line. Thereby, luminescence is generated which is

proportional to the amount of D-cysteine delivered[199]. This method could even be used to quantify delivery of cell-penetrating peptides in a mouse model.
An alternative method for quantification of delivered CPP and cargo is mass spectrometry. CPPs can be modified with an affinity tag such as biotin and, after pulldown of the tag, quantification can be done to compare different conditions during uptake. Subcellular fractionation may be able to help distinguish the intracellular fate of the CPP and cargo, but this has not been done so far[200].

To study the fundamental mechanism of the uptake, inhibiting certain pathways and monitoring the response is commonly done. Here, experiments can be performed at 4°C, conditions under which active transport should not occur[201]. Chemical inhibitors of active transport processes can also be used, but they are often not specific and have side effects[202].

Energy-independent uptake can also be studied with the help of model membrane systems such as giant unilamellar vesicles (GUVs). Uptake of peptides into these vesicles proves that the peptides can pass through model membranes without any active transport[203]. Model membrane systems can also be useful to gain knowledge about how CPPs interact with membranes of different composition[204].

Molecular dynamics can also assist in understanding the membrane interactions[205] and cell entry of CPPs[206]. A recent study makes use of molecular dynamics simulations to show that translocation of CPPs across the membrane is driven by the electrostatic potential of the membrane[207]. These simulations are typically limited to model membranes as well, however.

1.3.4.4.2 Energy-Independent Uptake

Membrane transduction, also known as non-endocytic translocation or direct penetration, is a term coined to describe the energy- and receptor-independent membrane-crossing of proteins and peptides[208]. Although the process has been described in many individual reports, it is not without controversy[11], also because membrane transduction and energy-dependent endocytic uptake often occur in parallel and it is difficult to separate them[188].

All the postulated energy-independent pathways into the cell involve some form of membrane interaction or disruption. The notable common ground between them is that uptake can occur

at low temperatures (e.g. 4°C) or in presence of endocytotic inhibitors[209]. Besides direct translocation through the membrane (figure 6a)[210,211], a "carpet-like"-model was also proposed, in which the peptides alter the fluidity of the membrane through electrostatic interactions of positively charged peptides with negative charges on the cell surface (figure 6b) and then pass through the membrane[212,213].

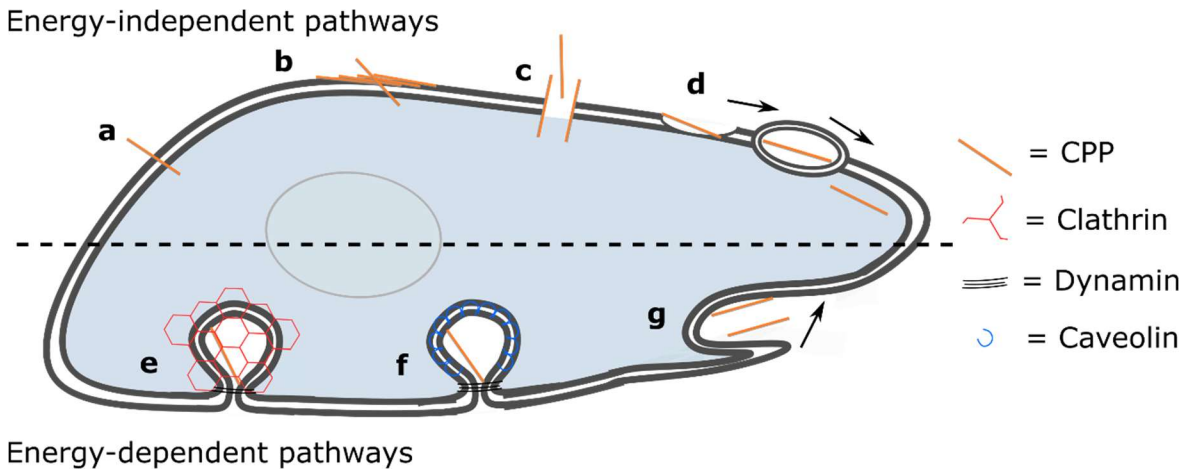

Figure 6. Pathways into the cells for cell-penetrating peptides. **a**, Direct penetration through the membrane. **b**, "Carpet-like" alteration of membrane fluidity through interaction with peptides. **c**, Pore-formation of Cell-penetrating peptides. **d**, Inverted micelle formation followed by release of the peptide. **e**, Clathrin-mediated endocytosis. **f**, Caveolae-mediated endocytosis. **g**, macropinocytosis.

Another current model postulates that CPPs form a pore through the membrane (figure 6c)[214]. Here, research has shown that at a higher, extracellular pH, fatty acids can bind to the guanidinium groups of cationic CPPs, at which point they form a toroidal pore and mediate the CPP transport into the cells. Once inside, the lower pH leads to the release of the CPPs and the reformation of the membrane[215]. Alternatively, the barrel-stave model of uptake suggests that the peptides can assume a helical structure within the membrane, where a hydrophobic side of the peptide faces towards the membrane and a hydrophilic side towards the inside of the pore[216].

An important finding in this context is that at a high concentration (20 µM), arginine rich, hydrophilic CPPs seem to form foci on the cell membrane where the peptides are highly enriched[217]. These "nucleation zones" seem to be crucial for the energy-independent uptake of this class of peptides. An enrichment of the sphingolipid ceramide on the outer leaflet of the plasma membrane was found to be crucial for this type of membrane transduction[218]. A recent study using combined confocal fluorescence and electron microscopy could show that at the

foci where CPPs are enriched, the peptides can induce changes in the membrane which likely lead to the formation of a pore into the cell[197].

Another proposed energy-independent pathway is the "inverted-micelle" mechanism (figure 6d). In this mechanism, the lipid bilayer invaginates to accommodate the CPP and eventually forms a micelle that encapsulates the peptide. Through opening of the micelle towards the cytosol, the peptide is released into the cytosol[219].

1.3.4.4.3 Energy-Dependent Uptake

Active transport can be broadly classified into two categories: phagocytosis and pinocytosis, with only specialized cell types (generally of the immune system) undergoing phagocytosis[220]. All cell types undergo pinocytosis on the other hand and the process can be further divided into several types. The great majority of active transport through endosomes arises through clathrin coated pits (figure 6e)[221]. As the main function of clathrin-coated pits is the internalization and recycling of membrane receptors, cargoes that go through this pathway are usually bound by a receptor and sorted into a pit. Clathrin, a triskelion-shaped protein is recruited and induces a curvature of the membrane. The protein dynamin is then recruited and, through GTP hydrolysis, leads to membrane fusion and release of the vesicle into the cytosol[222]. While many CPPs have been proven to enter cells without any type of specific receptor interaction[119,128], others have been shown to enter through clathrin-coated pits[223].

Caveolae are invaginations of the cell membrane that are very rich in proteins, cholesterol and sphingolipids (figure 6f)[224]. They are especially relevant in signal transduction and mechanosensation, but also play a role in endocytosis[225]. The formation of caveolae is often accompanied by the protein caveolin, although recently the cavin-family proteins have been shown to be more important[226]. Caveolae-mediated uptake is important for the uptake of some CPPs. For example, the tat peptide was shown to colocalize with caveolin[227], although other reports suggest that knocking down caveolin[228] or inhibiting caveolae-mediated uptake[229] did not affect the internalization of the peptide.

Macropinocytosis is a lipid-raft-dependent but receptor-independent endocytic pathway (figure 6g). It is actin-dependent, and is initiated by ruffles on the membrane surface that produce large endocytic vacuoles[230]. Macropinocytosis has a major rule in immune surveillance, as well as virus and cancer pathologies, but also seems to play an important role

in the cellular delivery of various cargoes[231,232]. For cell-penetrating peptides, macropinocytosis has been shown to be important for the uptake of polyarginines and the Tat peptide[233,234]. Inhibiting macropinocytosis had a strong effect on the uptake of polyarginine peptides at low concentrations especially[217]. Interestingly, some findings suggest that the Tat peptide can induce its own uptake by macropinocytosis, with one report showing the peptide interacting with the actin cytoskeleton[149] and another demonstrating the induction of the activity of the small GTPase Rac1[235], both of which led to increased macropinocytosis. A recent study also showed that the Tat peptide is taken up via macropinocytosis, and that this is dependent on the presence of proteins on the cell surface[236].

1.3.4.5 Toxicity

Several reports investigate the toxicity of CPPs. *In vitro*, cationic CPPs have been shown to be generally less toxic than more hydrophobic, amphipathic CPPs[237]. When investigating polyarginines of different length, it was found that cytotoxicity of polyarginines increases with chain length, where 9 arginines or fewer have only minor cytotoxicity[162]. The cytotoxicity of cell-penetrating peptides also changed based on the cargo attached, but this may simply be a consequence of the altered mode of uptake due to the cargo[238]. A metabolic profiling analysis compared the alterations in the metabolome of cells treated by five different CPPs and found that penetratin as well as an R9-peptide only had a very minor effect on the cells[239].

There is only limited data on the toxicity of CPPs *in vivo*. In one study, the toxicity of an intravenously injected CPP was found to be concentration dependent in rats, with concentrations under 15 mg/kg being non-toxic[240]. Another study also found concentration-dependent toxicity after intravenous injection of a polyarginine CPP into mice, and this toxicity could be strongly decreased when using a CPP with a caging group that would mask the positive charges until it reached the target tissue of the CPP[241]. In a long-term study, rats treated with multiple administrations of penetratin showed no change in the release of inflammatory or immunogenicity mediators[242]. Interestingly, there is research into applying CPPs to the delivery of antigens to trigger more effective immune responses[243].

1.3.4.6 Applications in Imaging

Imaging of subcellular compartments or specific cell types has potential both in research applications as well as in the detection of disease markers or tissue. CPPs have found many applications in the labelling of subcellular structures. Arginine-rich CPPs localize to the nucleolus, an RNA-rich compartment within the nucleus, and so can directly be used to image the nucleolus in living cells when fluorescently labelled[244]. Using a fluorescent fusion of the Tat peptide to the *N*-terminal 15 amino acids of the human ventricular MLC-1 protein led to staining of sarcomers in primary cells[245]. Similarly, the actin-binding peptide lifeact can be fluorescently labelled and fused to a cell-penetrating peptide via an intracellularly cleavable disulfide bond to generate a live-cell actin marker[246]. Conjugates of the Tat peptide with the radioactive isotope (99m)Tc have also been used in the delivery of the isotope into the nuclei of cancer cells, where it could be used for imaging as well as radiotherapy[247,248].

CPPs can also be used for imaging *in vivo*, for example by loading nanoparticle-CPP conjugates into cells *ex vivo* and then injecting the cells intravenously, which allowed tracking of the injected cells[249]. CPPs have also been used to transport luciferin, the substrate of luciferases, into transgenic mice expressing luciferase[250]. A fluorescently labelled, caged cell-penetrating peptide that is uncaged and becomes active when exposed to matrix metalloproteases overexpressed in cancerous tissue was also used to label cells within that tissue[251] (figure 7). This could then later also be applied to imaging cells producing hydrogen peroxide, by utilizing a linker cleaved by the reactive oxygen species[252]. Quantum dots are semiconductor particles with advantageous photoluminescent properties when compared to conventional fluorophores[253]. Tat-conjugates with quantum dots were taken up into cells in culture[254], and cells loaded with quantum dots could also be injected into live mice to track the movement of the quantum dot-loaded cells within the mice using fluorescence microscopy[255].

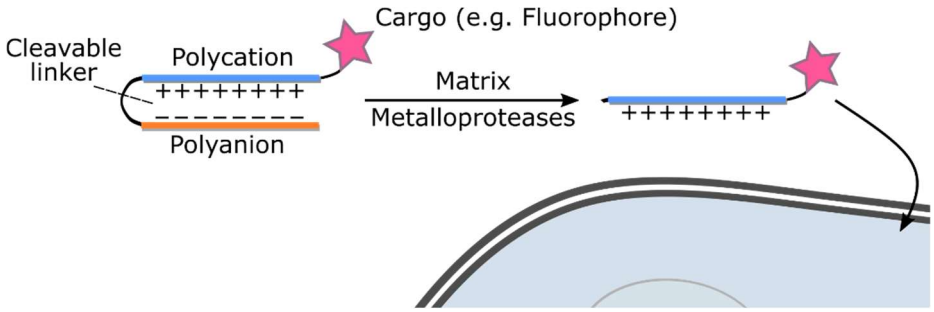

Figure 7. Application of a fluorescent, "caged" CPP conjugate. The polycationic CPP is initially inactive as the positive charges are blocked by an anion through a cleavable linker. Upon cleavage by matrix metalloproteases which are overexpressed in some cancers, the CPP is released and can enter cells[251].

1.3.4.7 Applications in Drug Delivery

As CPPs are very versatile when it comes to the cargo being delivered, there are many drug delivery approaches using various payloads in the treatment of several diseases under clinical or pre-clinical development.

In many drug delivery applications, the special ability of some CPPs to cross the blood-brain barrier is of interest. Brain ischemia is caused by insufficient blood flow to the brain, which can lead to cell death, infarction, and ischemic stroke. The anti-apoptotic protein Bcl-X_L has been associated with improved resistance to ischemia in mice[256]. Based on this finding, a fusion of the Tat peptide with the Bcl-X_L protein was administered to a mouse ischemia model prior to the induction of ischemia. The mice treated with the protein-CPP conjugate showed increased protection to ischemia and improved neurological performance when compared to the control[257]. Even after the ischemic event, administration of the CPP conjugate still led to an improvement. Similar effects were later also reported with a mutant of Bcl-X_L[258]. A fusion of the Tat peptide fused to the Bcl-2 homology domain 4 (BH4) of Bcl-X_L could also prevent the death of neurons caused by amyotrophic lateral sclerosis (ALS)[259]. A fusion of Tat with a peptide-inhibitor of the Jun N-terminal Kinase (JNK), a mediator of cell death during ischemia, could also reduce the impact of ischemic events in a mouse model[260]. This same fusion peptide could also be shown to reduce neuron death in an Alzheimer's disease model[261] and is now under clinical development as a drug for hearing loss[262] and intraocular pain[263]. Taken together, these findings demonstrate the significant potential of CPPs in the treatment of neurological diseases.

CPPs are an attractive option for drug delivery in chemotherapy as they can strongly increase cellular uptake of the. The cytostatic agent methotrexate is hindered by the fact that many tumorous diseases show resistance toward it. Coupling methotrexate to the CPP penetratin increased its efficacy, especially in resistant cells[264]. Very similar effects could also be observed when coupling several cationic CPPs to the cytotoxic drug doxorubicin[265-267]. A recent approach with a novel CPP-doxorubicin conjugate could show that the conjugate was also more effective in reaching cancerous tissue as compared to the free drug. Once there, it effectively killed cancer cells in a mouse xenograft model[268]. The protein p53 is a pro-apoptotic protein that acts as a tumour suppressor and prevents cancer formation. Dysregulation of p53 is involved in many cancers, and reactivation of the protein can in some cases be used in cancer therapy[269]. Interestingly, a peptide derived from the *C*-terminus of p53 is sufficient to

activate wild-type p53 and cause cell death in cancer cells. A fusion of this *C*-terminal peptide to the Tat CPP was an effective treatment option in peritoneal cancer models[270].

CPPs have also found an application in the treatment of inflammation. The transcription factor nuclear factor kappa B (NF-κB) regulates transcription of several genes related to inflammation and suppressing it is likely a viable therapeutic avenue in the treatment of inflammatory diseases[271]. A fusion of a peptide inhibitor of NF-κB with penetratin was cell-permeable and could prevent NF-κB activation and inflammatory response in cell culture[272]. This was later also confirmed to be effective in a mouse model of the inflammatory disease Duchenne muscular dystrophy[273]. A similar anti-inflammatory effect could also be observed with a novel cell-penetrating peptide designed from a peptide inhibitor of NF-κB[274].

Because of the similarity of cell-penetrating peptide sequences to antimicrobial peptides (AMPs), the antimicrobial activity of several CPPs has also been investigated[275]. Derivatives of the Tat and Pep-1 CPPs were shown to be potent antimicrobials[276-278]. It is also possible to combine CPPs with AMPs to make them more efficient antimicrobials[279].

1.3.4.8 Protein Delivery

Due to the natural ability of the Tat and penetratin peptides to transport the Tat and pAntp proteins into cells, CPPs are obvious candidates for delivery of various proteins. Many studies employ recombinantly expressed fusion proteins with the 11-amino acid Tat peptide. An early example of this is a cyclin-dependent kinase inhibitor protein ($p27^{Kip1}$) that could induce cell motility after delivery in cell culture[280]. The enzyme β-galactosidase was also expressed as a Tat fusion and could be delivered to cells *in vitro* and in a mouse model[281]. Cre recombinase is a DNA-editing enzyme that can carry out site-specific recombination events and has been a useful tool in research[282]. Fusions of Tat to cre recombinase were initially ineffective in gene editing, but this could be improved upon by adding a fusogenic HA2 peptide (derived from the influenza virus) to the fusion protein[198]. Further research into the delivery of a Tat-cre fusion showed that the protein was overwhelmingly confined to cytoplasmic vesicles, while fusions of Tat to a fluorophore were broadly distributed in the cytosol and nucleus[283]. This finding led to the conclusion that fusions of CPPs to large peptides or proteins are generally taken up via active transport and confined to endosomes, which was confirmed in several additional studies[151,284].

The chemical conjugation of CPPs to proteins allows the usage of CPPs with unnatural building blocks and the attachment via different linkages and different ratios of peptide to protein. Through chemical crosslinking of antibody fragments to Tat, they could be delivered into cells and had some inhibitory activity[285]. In another study, the chemical conjugation of transportan to several proteins of sizes between 30-150 kDa could be used to transport them into cells[286]. As noted previously, however, most of the delivered protein was confined to vesicular structures. One study used disulfide-linked conjugates of isotopically labelled proteins with the Tat CPP in conjunction with pyrenebutyrate[287]. This additive has been shown to assist in the cytosolic delivery of CPP-bearing cargoes[288]. The authors could then record NMR spectra of the isotopically labelled proteins within living cells. Recently, the conjugation of an arginine-rich CPP to the DNA editing enzyme Cas9 has been used for site-specific genome engineering *in vitro*[289]. In an attempt to achieve energy-independent uptake of a protein, a cyclic derivative of the tat peptide was conjugated to EGFP[290]. The cyclization of Tat had previously been shown to greatly increase the kinetics of energy-independent uptake (see section 1.3.4.3)[182]. Indeed, the conjugate of the cyclic tat with EGFP showed cytosolic localization and could enter cells at 4°C, while a conjugate of EGFP with a linear CPP could not.

1.3.5 Other Methods of Protein Delivery

One rather laborious option to improve the cellular uptake of a given protein is cationic protein resurfacing i.e. increasing the number of positively charged amino acids on the surface of a protein. Initially, it could be shown that replacing five surface-exposed acidic amino acids on GFP with arginines conferred some cellular uptake to the protein[291], although the protein was mostly localized to punctae within the cell, suggesting endosomal uptake without reaching the cytosol. In a second approach, GFP was resurfaced again to generate a mutant with a net +36 charge. This “supercharged” GFP could be used to transport fusion proteins into a variety of cell types[292]. A similar resurfacing strategy could then later also be applied to a single-domain antibody (nanobody)[293]. The process of resurfacing a protein is however very laborious, and generally seems to lead to endosomal entrapment, for the most part.

Generally, to improve passive membrane crossing of small molecule drugs, adding hydrophobicity is a viable option[294]. A very common approach in the design of small molecule

drugs is the esterification of alcohols and carboxylic acids to mask these hydrophilic groups[295]. Esters can be removed when the drugs are internalized into cells by unspecific esterases, making the modification bio-reversible and restoring the drug to its original state. Only very recently has this now been applied to proteins as well[296]. Chemoselective esterification in aqueous solvents is not easy, but with a sophisticated diazo-reagent it was possible to efficiently modify most solvent-exposed aspartic and glutamic acids on EGFP. Through this modification, the protein could then pass through cell membranes at 37°C and 4°C, indicating that transport through the membrane does indeed occur in an energy-independent process. The esters were also removed after internalisation on the protein level, returning the protein to its native state[296]. In a first follow-up study, the authors could also modify and deliver RNAse 1, which efficiently killed cells after delivery, showing that the enzyme was still active[297]. While this is a highly promising approach, it has only been demonstrated on two proteins so far, and more research is needed into the wider applicability of the method.

1.4 Synthesis of CPPs and CPP-Protein conjugates

As the recombinant expression of proteins fused to cell-penetrating peptides can be difficult[284] and as more complex (e.g. cyclic) peptides can generally not be obtained through recombinant expression at all, synthetic approaches are required.

1.4.1 Peptide Synthesis

For over 100 years, the chemical synthesis of peptides has been an important subject in organic synthesis, protein chemistry and in many research and clinical applications. Originally, peptide synthesis was done in solution and, by protecting the amine functionality and deprotecting it after attaching an unprotected amino acid to the carboxylic acid, small, functional peptides could be produced[298]. Pioneered by Bruce Merrifield, solid-phase peptide synthesis, in which the growing peptide chain is immobilized on an insoluble resin, would change the field forever and won the Nobel prize in 1984[299,300]. The main advantages of synthesizing peptides on a solid support is the ease of purification by filtration, as well as the simplicity of performing all reaction steps in the same reaction vessel. Many advances have

succeeded in improving yield, purity, and scalability of the method, such as microwave-assisted peptide synthesis[301]. Nevertheless, the basic process of peptide synthesis on the solid phase remains the same. Peptides are synthesized from the *C*-terminus to the *N*-terminus. The first amino acid is loaded on the resin with a protecting group on the amine functionality. The protecting group is removed, the next protected amino acid is coupled, and these last two steps are repeated until the peptide synthesis is completed, after which the peptide is cleaved from the resin (figure 8).

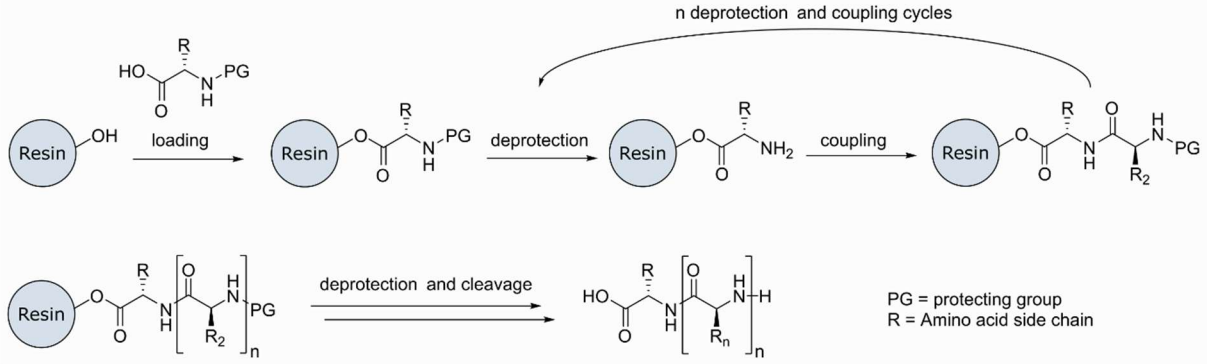

Figure 8. Peptide synthesis on the solid phase. The resin is first loaded by coupling the first amino acid to the solid support (resin). Cleavage of the protecting group is followed by coupling of the next amino acid, and these two steps are repeated until the peptide is complete. After deprotection and cleavage from the resin, the mature, unprotected peptide is obtained.

The tert-butoxy-carbonyl (Boc) and fluoren-9-ylmethyloxycarbonyl (Fmoc) groups are the most widely used protecting groups for *N*-terminal amines[300,302]. The side-chain functionalities of amino acids must also be protected during synthesis, and this protection must be orthogonal to the protection on the *N*-terminus i.e. the side chain protecting groups should not be removed under the same conditions as the *N*-terminal protection[303].

The great advantage of peptide synthesis over recombinant production of peptides and proteins is the ability to produce many unnatural peptide structures and incorporate unnatural building blocks, within the limitations of acidic deprotection. The incorporation of post-translational modifications from proteins into synthetic peptides has been given much attention, and lipidation[304], glycosylation[305,306] and phosphorylation[307-309] can all be achieved on synthetic peptides. It is also possible to use D-amino acids[161], peptidomimetics such as depsipeptides[310] and even nucleic acid analogues in peptide-nucleic acids[311]. Chemical handles for further functionalization, as well as fluorescent or other chemical probes can be easily

incorporated[303,312,313]. It is also possible to synthesize cyclic peptides, which is much more difficult using recombinant expression[314,315].

A major limitation of peptide synthesis is still the length of peptides that can be synthesized. The consequence of yields under 100% means that with an increasing number of steps, the amount of truncation products increases and consequentially the maximum length of a peptide synthesized by standard SPPS is around 60 amino acids[298,316]. For that reason, ligation strategies have been developed to enable the synthesis of peptides beyond this limitation.

1.4.1.1 Peptide Ligation

To facilitate the synthesis of large peptides, several strategies for the assembly of individual peptide fragments have been developed. The most prominent example of these is the native chemical ligation (NCL). In NCL, a peptide with an *N*-terminal cysteine reacts with another peptide that contains a C-terminal thioester (figure 9). The cysteine thiol generates a new thioester in the trans-thioesterification reaction, which results in a native amide bond after the S,N-acyl shift. The advantage of NCL is that due to the reversibility of the thioester formation, but irreversibility of the final amide-bond forming step it can be used on unprotected peptides and in the presence of other thiols[317]. Cysteine is now no longer required at the ligation site, serine and threonine can also be used in ligations[318]. Through desulfurization reactions, cysteine can also be converted to alanine after the ligation[319], and desulfurization can also be applied in ligations using unnatural, thiol-containing amino acids to convert them back into natural building blocks[320]. Several NCL steps can also be done sequentially to assemble even larger fragments[321], and NCL can also be done on solid support[322].

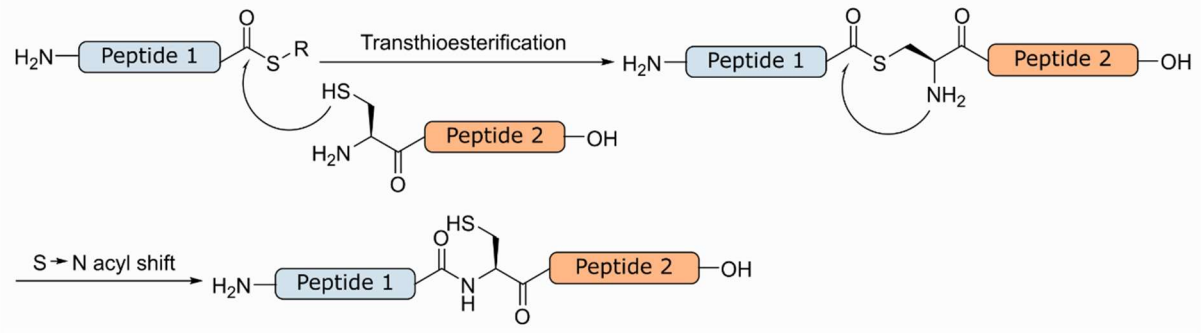

Figure 9. The native chemical ligation (NCL) reaction begins with the transthioesterification step in which a peptide with a C-terminal thioester (peptide 1) reacts with a second peptide

containing an N-terminal cysteine (peptide 2) to generate a new thioester. In the S,N-acyl shift the peptides rearrange to form a native amide bond.

An alternative ligation strategy to NCL exists in the traceless staudinger ligation. It allows the assembly of a native peptide bond from a C-terminal thioester and an N-terminal azide[323]. While the Staudinger ligation is promising and has been used in the assembly of entire unprotected proteins[324], it has not yet found widespread use in peptide assembly. If a native peptide bond is not required at the ligation site, other chemistries such as click reactions can also be used to assemble peptides[325].

1.4.2 Protein Conjugation Techniques

The conjugation of peptides to proteins can still be more challenging than of two peptides, as proteins generally are only folded correctly in aqueous conditions, and so water-free organic solvents cannot be used. Nevertheless, many techniques for the modification of proteins have been developed[326-329] and most can be applied to the ligation of peptides and proteins.

1.4.2.1 Expressed Protein Ligation and Protein Trans-splicing

Applying native chemical ligation to proteins requires the generation of an N-terminal cysteine or C-terminal thioester. N-terminal cysteine residues can be generated by expressing the protein recombinantly with a cleavage site for a specific protease that tolerates a cysteine in the P1 position immediately after the cleaved bond[330,331]. Other methods for the generation of N-terminal cysteines have also been developed[332-334]. By using a peptide with a C-terminal thioester, the two fragments can then be ligated via an NCL reaction.

For the generation of C-terminal thioesters on proteins, the natural protein-splicing mechanism of inteins can be used. During protein-splicing, an internal protein domain excises itself out of a polypeptide, resulting in an amide bond between the flanking peptide sequences (figure 10a)[335]. During this process, the intein enzymes proceed through a thioester stage. By using mutated inteins, it is possible to express proteins in which the intein is not spliced out, but can be used to generate a reactive thioester on the C-terminus of the protein[336]. This can then be

followed up with a native chemical ligation reaction in which any peptide containing an N-terminal cysteine can be ligated (figure 10b). This process is known as expressed protein ligation (EPL).

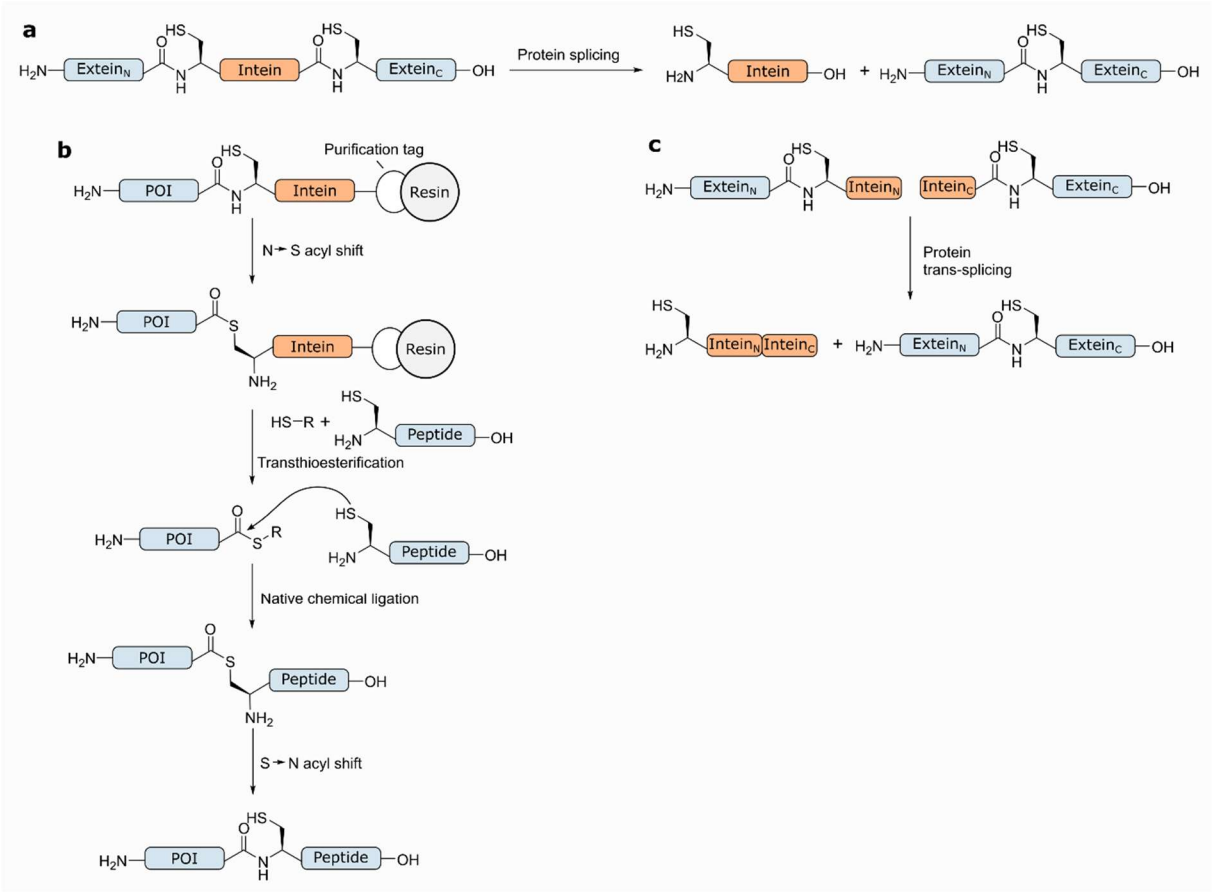

Figure 10. **a**, In protein splicing, the enzymatic activity of an intein causes it to be cleaved out, leaving behind ligated N- and C-extein fragments. **b**, In expressed protein ligation, a protein of interest (POI) is expressed with a mutated intein, and often a purification tag. The construct can be immobilized on a solid support, and the intein is then cleaved off by an excess of thiol, followed by transthioesterification with a synthetic peptide. After native chemical ligation, the protein of interest and peptide are connected via a native amide bond. **c**, In intein trans-splicing, two fragments of an intein recombine in solution to form a native bond between connected exteins.

To make this process more efficient, a purification tag can be appended on the C-terminus of the intein in these constructs (often a chitin-binding domain as in a commercially available kit)[337]. Thereby, intein cleavage and NCL can then be done on the resin, which will free up the reaction product after the reaction while the cleaved intein will remain bound to the solid support (figure 10b).

Alternatively, if generating a thioester is not desired, protein trans-splicing can also be used. In this methodology a split intein, with one part on each of the two fragments to be ligated, recombines upon mixing of the two parts, and splices itself out, leaving behind a ligated peptide (figure 10c). There are naturally occurring split inteins[338,339], but also inteins that were split artificially[340]. Very small split-intein constructs exist for both the N-intein and C-intein parts[341,342], which are easily accessible by SPPS or recombinant expression.

1.4.2.2 Chemoenzymatic Methods

Enzymes are a popular choice for the modification of proteins as they naturally have a high substrate specificity and thus promise a homogenously modified product[343,344]. Subtiligase is an enzyme that catalyses the formation of an amide bond starting from a C-terminal activated thioester together with the N-terminus of a given protein or peptide[345]. The thioesters can also be generated on proteins using inteins (see 1.4.2.1), but subtiligase labelling suffers from low specificity on the amino termini that it accepts.

Sortase A is a transpeptidase originally found in *Staphylococcus aureus*. The enzyme recognizes an LPXTG (X = any amino acid) peptide motif, cleaves the peptide after threonine and forms a thioester which can then be displaced by an amine nucleophile, typically an N-terminal polyglycine sequence[346]. The enzyme can be used to modify proteins on either terminus, and synthesizing a counterpart by SPPS is trivial because of the small size of the recognition motif. While the "sortagging" can suffer from poor yield, much work has been done to make more reliable and efficient sortase mutants[347].

Transglutaminase enzymes catalyse the formation of an isopeptide bond between lysine and glutamic acid side chains[348]. Initially, because of the low specificity of this reaction, the enzyme could not be used for site-specific modification of proteins, but several recognition peptides were developed that can provide additional specificity for a certain glutamic acid[349]. Some variants of the enzyme even have naturally higher specificity for certain peptide sequences[350].

Other enzymes can be used to generate handles that can then be addressed using biorthogonal chemistry. The tubulin-tyrosine ligase, for instance, appends a tyrosine residue to the C-terminus of a peptide tag. The enzyme also accepts tyrosine derivatives that contain

various chemical handles that can be functionalized in a second step[351]. The enzyme can even be used to append some small modifications in a single step[352]. Similarly, the lipoic acid ligase recognises a peptide tag and can conjugate derivatives of lipoic acid containing biorthogonal reaction handles[353]. A special case is the formylglycine-generating enzyme (FGE) that can oxidize a specific cysteine within a peptide motif, generating formylglycine. This aldehyde can then also be functionalized in a second step[354].

1.4.2.3 Chemoselective Reactions for Protein Modification

Chemoenzymatic methods and expressed protein ligation mostly require expression of the protein with a peptide tag and can often leave a scar after labelling. These methods are also mostly able to modify the termini of the protein. Reactions that use the reactivity of naturally occurring amino acids[355] or biorthogonal handles[356] can get around these limitations.

1.4.2.3.1 Reactions on Natural Amino Acids

Reactions on naturally occurring amino acids in proteins typically rely on the specific reactivity of a certain type of amino acid side chain. The ε-amine of lysine residues is nucleophilic, and can be addressed with activated esters to form stable amide linkages[357]. Other types of amine-specific reactions for protein labelling also exist, such as reductive amination[358] or isothiocyanates[359]. The N-termini of proteins have a slightly lower p*K*a and so they can in theory be addressed specifically. Lysine has a high abundance in proteins (~6%[360]), which is a double-edged sword, as it means lysine-reactive chemistry can be used to reliably label most proteins, but usually not site-specifically.

To achieve more selective protein modification, cysteine-specific labelling can be employed instead. Cysteines are the most nucleophilic amino acid and can be addressed with a variety of reagents[361]. Cysteines are less abundant than lysines, and many cysteines are also inaccessible because they are oxidized in disulfide bonds. This means that the labelling of cysteines will usually be more selective but can require reduction of disulfides. The labelling of cysteine residues that are naturally in disulfides can mean disruption of protein fold and function[362]. For this reason, introducing an additional cysteine via protein engineering can be

an option, although introducing additional cysteines can itself have detrimental effects on protein stability[363]. Maleimides are the archetypical cysteine-selective probes. They react with thiols in thio-michael additions and have been used in a variety of applications (figure 11a)[364]. Maleimide-cysteine linkages have recently been shown to have problematic stability in presence of other thiols, prompting several investigations into improving their stability[365,366]. Alternatively, reagents can be used that form more stable bonds (figure 11b)[367,368]. For the modification of disulfides, rebridging agents have been developed that can react with two thiols and can improve stability of the conjugates[369].

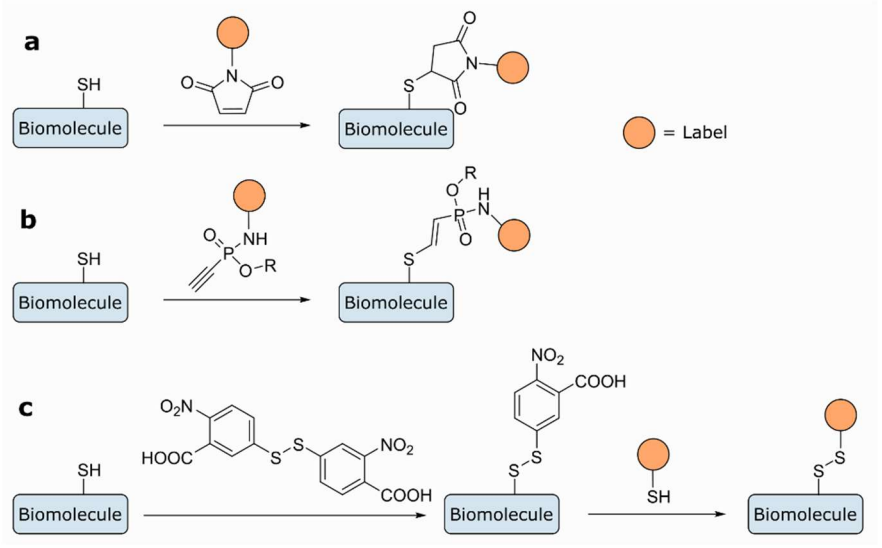

Figure 11. Select cysteine-selective reactions. **a**, Labelling of a cysteine residue with a maleimide. **b**, Labelling of a cysteine residue with an alkyne phosphonamidite, leading to a more stable bond. **c**, Labelling of a cysteine residue with a disulfide in two steps by first activating the nucleophilic thiol by converting it into an electrophilic disulfide using Ellman's reagent.

A special type of cysteine-selective reactions are reactions that will generate a disulfide bond between label and protein[370]. This is typically accomplished by first activating one of the two thiols (on the label or on the protein) with a reagent to form an electrophilic disulfide that will subsequently react with any free thiol (figure 11c). Activated thiols include sulfenyl halides[371] and pyridyl disulfides[372]. These disulfide conjugates are reversible in presence of thiols, which also means that they are cleavable within cells, as the cellular interior is a reducing environment[373,374].

Reactions selective for other amino acid side chains including methionines[375], tyrosines[376], histidines[377] and acidic amino acids[296] have also been developed and are still a topic of current research, but are less commonly used so far.

1.4.2.3.2 Bioorthogonal Reactions

Site-specificity in the modification of proteins can be achieved by using bioorthogonal reaction handles incorporated into the protein. Aside from the enzymatic methods (see 1.4.2.2), these handles can also be introduced in the form of unnatural amino acids. The simplest way to incorporate unnatural amino acids is through metabolic labelling, by replacing a naturally occurring amino acid with a structural analogue. For example, methionine can be replaced in growth medium by azidohomoalanine to introduce an azide handle at positions where methionine normally occurs in proteins[378]. As methionine is a particularly rare amino acid, this can sometimes be enough for the labelling to be site-specific. For more control of incorporation of unnatural amino acids, genetic code expansion can also be used. In amber suppression, the amber stop codon (UAG) is overridden by the overexpression of a tRNA/tRNA synthetase pair that recognizes the codon and incorporates an unnatural amino acid[379]. tRNA synthetases have been evolved to incorporate a large variety of amino acids with many biorthogonal handles such as azides[380], strained alkynes[381] and trans-cyclooctenes[382].

To address these handles specifically, biorthogonal reactions have been developed that do not react with naturally occurring moieties in proteins or biological environments[383]. The Staudinger ligation is a modification of the Staudinger reduction of azides by triphenylphosphine. By employing triarylphosphine derivatives with ester groups, the azide is reduced and forms an amide bond under hydrolysis of the ester[323]. Special phosphines can also undergo the “traceless” Staudinger ligation in which the phosphine is removed after the reaction[323,384]. On peptides, the ligation can also be triggered by using a protected phosphine, which has been used to generate *N*- to *C*- cyclized peptides chemoselectively[385].

Alternatively, azides can also react bioorthogonally with alkyne derivaties. The reaction between azides and alkynes is normally slow but can be sped up using copper catalysis (copper catalyzed azide-alkyne cycloaddition (CuAAC, mechanism in figure 12)) or by using more reactive, strained alkynes (strain promoted azide-alkyne cycloaddition (SPAAC)). The copper catalyzed click reaction is very quick, and can be further accelerated in water by the

usage of ligands that stabilize the reactive Cu(I) species[386], but copper is toxic and generally not compatible with living systems[387]. The strain-promoted reaction requires bulky alkynes, but can be used in living systems[388].

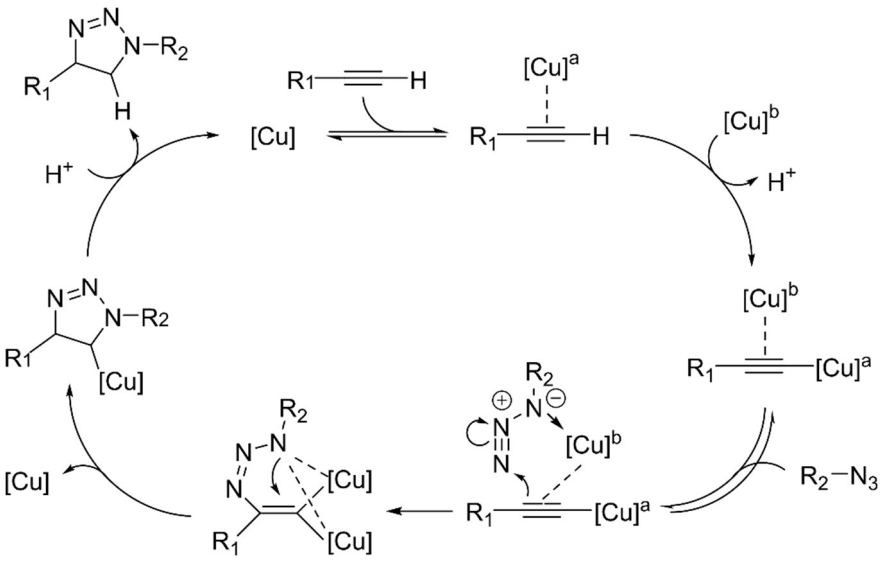

Figure 12. The proposed mechanism of the copper catalysed click reaction.

Aldehydes are another chemical entity that do not occur naturally on proteins. They can be addressed selectively with aldehydes under acidic conditions[389]. The reaction can also be performed at neutral pH using aniline or aniline derivatives as catalysts[390]. The inverse-eletron demand Diels-Alder (IEDDA) reaction between a tetrazine and a trans-cyclooctene is also biorthogonal and has been used to label proteins[391]. The IEDDA reaction has the potential to be the fastest biorthogonal reaction to date, which makes it a good candidate for reactions at very low concentrations[392]. It also does not use toxic metal species and can be used in living cells[393] and *in vivo*[394]. Reactions using cross-metathesis[395], and photoclick reactions using tetrazoles[396] have also found their way into protein labelling, amongst others.

1.5 Antigen-Binding Proteins and their cellular delivery

1.5.1 Antibodies

Antibodies are large glycoproteins secreted by B cells and a major part of the adaptive immune system[397]. The immunoglobulin G (IgG) type of antibody is the most common type and makes up over 10% of plasma protein in humans (figure 13)[398]. IgG antibodies consist of four amino acid chains, two heavy (~50 kDa) and two light (~25 kDa) that are interlinked by disulfide bonds. The antigen binding (Fab) fragment of the antibody is joined to the other fragment (Fc, with no antigen-binding activity) through a hinge region. The amino-terminal regions of all chains make up the variable regions that are responsible for antigen binding (V_H and V_L).In the adaptive immune response, this "hypervariable region" of an antibody is mutated through random recombination events, generating antibodies against pathogens[399,400]. The large diversity in sequences leads to a wide variety of antigens that can be bound by antibodies. Because antibodies can be generated against virtually any antigen, they have been important tools in cell biology for decades[401]. Modern applications often employ conjugates of the antibodies with enzymes or small molecules for highly sensitive detection of antigens[402,403]. It is important to note that the conjugation of these molecules to antibodies can severely disturb the function of the antibody, which must be taken into consideration when generating novel conjugates[404,405]. The function of antibodies has also been shown to be dependent on their glycosylation, which can make the production of antibodies in large scales difficult[406].

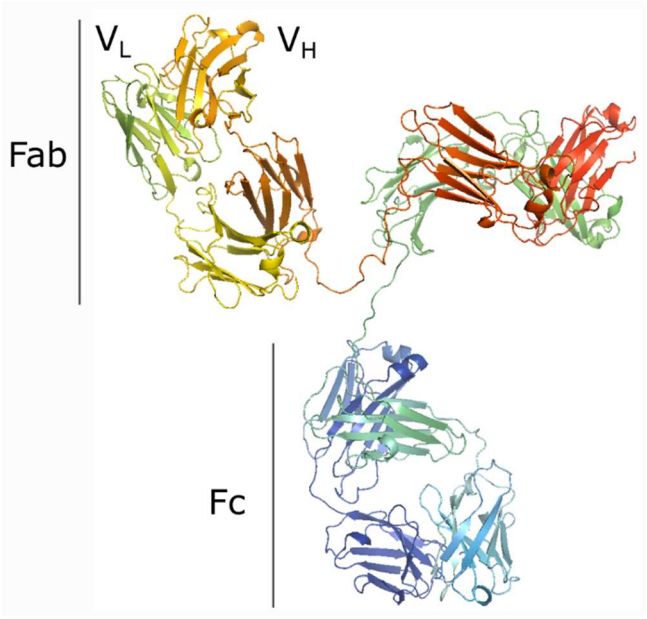

Figure 13. Crystal structure of an IgG antibody. Labelled are the Fc and Fab regions, as well as the antigen binding VL and VH domains. PDB: 1IGT

Because antibodies are large and bulky, they are often natural inhibitors of their antigens. They can also often inhibit interactions of proteins with large binding interfaces, which small molecule drugs cannot. This means that antibodies have inherent therapeutic potential, and many antibody-based therapeutics have already been approved[407]. Classically, however, antibodies are limited to extracellular applications, which greatly limits their potential and highlights the need for antibody delivery methods[408].

As antibodies are complex, large, and sensitive to modification, their intracellular delivery is challenging[9]. In the past, successful antibody delivery was often done through microinjection, which is simple but low in throughput[409,410]. More recently, other physical methods such as electroporation[411] and microfluidics[46] have also been successfully used in the delivery of antibodies. As an alternative, antibodies can also be expressed directly in the cell, which are then called intrabodies[412]. This can even be applied *in vivo*[413], but comes with the typical downsides of transfections such as cytotoxicity and low efficiency, and, when using viral vectors, the danger of genome integration of viral DNA[414].

Many conjugates of antibodies with cell-penetrating peptides have been generated. They have been used in live-cell immunofluorescence[415,416], and as inhibitors of their intracellular antigens[417,418]. A major limitation of CPP-based antibody delivery is endosomal entrapment of the antibody. For antibodies specifically, this has been improved upon using light-triggered endosomal lysis[419], and with an endosomolytic peptide[97].

Conjugates of antibodies with nanocarriers have also been generated, for example using cationic polymers[420], cationic lipids[421], virus-like particles[82], or silica nanoparticles[422]. Like the approaches with cell-penetrating peptides however, the nanocarrier-mediated antibody delivery is often inefficient as antibodies can be trapped in endosomes.

1.5.2 Other Antigen-Binding Proteins

The sometimes-problematic complexity and size (~150 kDa) of antibodies have led to the development of smaller alternatives (figure 14a)[423]. Fragments of IgG antibodies such as Fab (~50 kDa), or the scFv (~25 kDa), unnatural fusion of the two variable regions of an antibody) promise to deliver higher expression yields and lower complexity, but they still contain complex disulfides like full length antibodies[424]. Also, the assembly of the two domains required for

antigen binding is usually mediated only by hydrophobic, non-covalent interactions, which can be problematic when isolated[425]. These problems can be even more severe when only a single antigen-binding domain of a conventional IgG antibody is expressed by itself (V_H or V_L, ~13 kDa), as the hydrophobic amino acids are then solvent exposed[426].

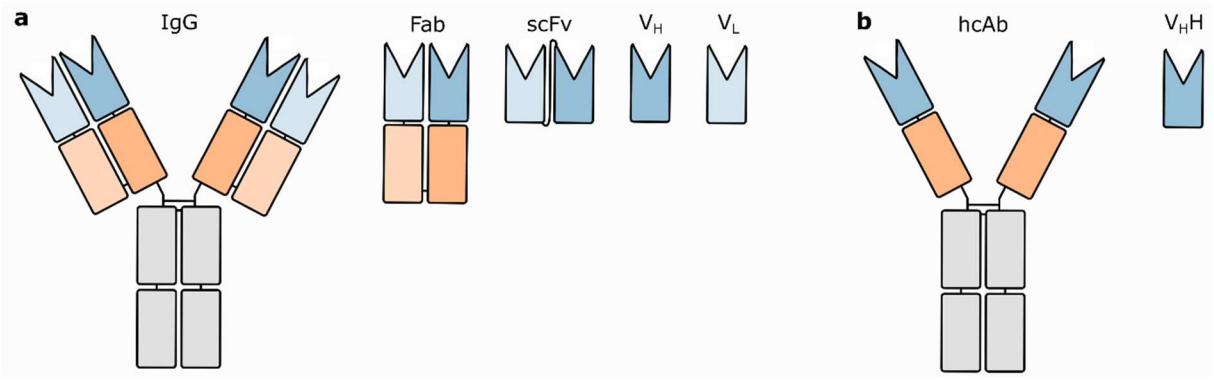

Figure 14. **a**, Schematic showing the structure of an IgG antibody and of commonly used IgG-derived fragments. **b**, Heavy chain antibody and the hcAb derived V_HH (nanobody).

An interesting solution to these problems comes from a special class of antibody called heavy-chain antibodies (hcAb), which only occur in few species and do not contain a light chain (figure 14b)[427]. The functional consequence of this is that these antibodies bind their antigen with a single domain. By isolating this domain, a nanobody (or V_HH, ~13 kDa) is obtained. Compared to isolated antigen-binding domains from conventional IgG antibodies (V_H or V_L), nanobodies have enlarged antigen-binding CDR loops[428] and are more hydrophilic and thus easier to express recombinantly[429,430]. Because of their advantageous properties, several nanobody candidates are being evaluated for their therapeutic potential[431].

Aside from antibody-derived proteins, binders can also come in the form of designed ankyrin repeat proteins (DARPins), which consist of ankyrin repeats, a naturally-occuring protein motif important in mediating protein-protein interactions[432]. DARPins are an engineered variant of ankyrin repeats consisting of 4-5 repeats (~14-18 kDa) and are usually generated through display methods such as ribosome[433] or phage display[434]. Monobodies are binders designed on the human fibronectin type III domain (~10 kDa), which has an immunoglobulin-like fold but lacks disulfide bonds, making it easier to use[435]. New monobodies are typically generated against novel antigens using display methods such as phage or yeast display[436]. Affibodies are similarly generated from display methods, but based on the scaffold of the B-domain of the

Staphylococcus aureus protein A[437]. With only ~60 amino acids they are some of the smallest recombinant binders (~6 kDa)[423].

Functionalization of these proteins is often easier than with full-length antibodies[438]. For instance, nanobodies can be expressed with an additional unpaired cysteine, which can then be addressed using cysteine-selective chemistry[439]. Because of the easier recombinant expression of these binders, chemoenzymatic labelling methods are also commonly used in their modification[351,440,441].

Delivery of recombinant antigen-binding proteins is promising, as through their high stability and lower complexity they may be better suited for intracellular applications than full length antibodies. Antibody fragments can, like full-length antibodies, be delivered through physical methods such as electroporation[442] and cell-squeezing[443]. Nanobodies have also been delivered into cells by cationic resurfacing, which entails exchanging surface-exposed amino acids to basic residues. Nanobodies with net +14 and +15 charges could thus be delivered into cells and could still bind their antigen (GFP)[293]. Cationic resurfacing is laborious however, and the high net charge could in principle affect properties of the protein. Alternatively, mesoporous silica nanoparticles have been used to deliver a chromobody (fusion of a nanobody with a fluorescent protein) into cells[422]. The delivery resulted mostly in endosomal entrapment, however. A delivery approach using a cationic polymer was more effective, but endosomal entrapment was still a bottleneck[444]. Using the anthrax lethal factor, a monobody, an affibody, and a DARPin could be delivered into cells[92], showing the versatility of the method. Delivery using the lethal factor does, however, require unfolding and subsequent refolding of the protein cargo while passing through the generated pore into the cytosol.

2 Research Objective

Protein delivery into mammalian cells has been a long-standing research objective. Many methods are very potent in specific applications, but the ideal method of protein delivery for every situation does not exist. The main weaknesses of existing methods lie in their limited applicability (e.g. physical methods) or in their inefficiency, often because of endosomal entrapment (in the case of nanocarrier or cell-penetrating peptide-based methods). While cell-penetrating peptides have been applied in various settings, it is still not completely clear why some reports show energy-independent uptake into the cytosol while others report endosomal uptake. Especially protein delivery (in contrast to small molecule or peptide cargoes) with cell-penetrating peptides is still relatively poorly studied and understood.

The research objective of this work is the delivery of a variety of protein cargoes using cell-penetrating peptides to both improve understanding of the underlying mechanisms as well as enhancing the delivery method thus enabling delivery of entirely new, functional cargoes that can then be used for cell-based assays. This overarching goal can be divided into three separate objectives.

Objective 1: Cytosolic Delivery of Antigen-Binding Proteins

As highlighted in section 1.5, antigen-binding proteins are of tremendous importance for nearly all areas of biomedical research. Aside from few previous examples their usage is generally restricted to *in vitro* and extracellular applications. The modification and cellular delivery of full-length IgG antibodies is challenging. Antibody fragments can be modified more easily, and it is much more achievable to generate highly defined protein conjugates that allow detailed characterization of cellular uptake. Some examples of cytosolic delivery of antibody fragments exist, but they require laborious protein engineering or suffer from low efficiency. A major objective is thus the generation of a nanobody fused to a potent cell-penetrating peptide and the subsequent detailed characterization of the conjugate and its uptake into cells.

Objective 2: Targeting of Proteins to Subcellular Compartments

As the fate of cargoes delivered with cell-penetrating peptides is not completely clear, it is interesting to investigate whether it is possible to not only deliver a protein to the cytosol, but to discreet locations within the cell. This may be achieved using naturally occurring peptidic

targeting sequences in combination with the CPP-mediated delivery. For this, it is required to efficiently produce fusion proteins containing mammalian targeting sequences recombinantly. It is also important to distinguish attachment of the cell-penetrating peptide via a non-cleavable or cleavable linker to the protein, as this may greatly influence the intracellular fate of the cargo.

Objective 3: Improving Cell-Penetrating Peptide-Mediated Delivery to Allow Delivery of Large Cargoes

The mode of cellular entry of cargoes using cell-penetrating peptides is thought to depend on the attached cargo. Past literature suggests that the delivery of large cargoes can be inefficient or even impossible. This is perhaps the key limitation in the CPP-based delivery of large protein cargoes. To overcome the problem of endosomal entrapment, it is important to first understand why the issues occurs. A strategy can then be developed to overcome or circumvent the issue. This could then be applied to the delivery of larger, and more complex cargoes, with one goal being the cytosolic delivery of IgG antibodies using cell-penetrating peptides.

3 RESULTS AND DISCUSSION

3.1 Cellular Delivery of Semi-Synthetic Antigen-Binding Domains and Applications Thereof

This chapter was published as follows:

H. D. Herce*, D. Schumacher*, A. F. L. Schneider, A. K. Ludwig, F. A. Mann, M. Fillies, M. A. Kasper, S. Reinke, E. Krause, H. Leonhardt, M. C. Cardoso*, and C. P. R. Hackenberger* Cell-permeable nanobodies for targeted immunolabelling and antigen manipulation in living cells. *Nat. Chem.*, **2017**, 9, 762-771.

https://doi.org/10.1038/nchem.2811

Abstract:

The previously developed cyclic cell-penetrating peptides cTat and cR10 were applied to the delivery of nanobodies into mammalian cells. A key difficulty was the efficient generation of recombinant nanobodies, site-specifically modified with a single CPP to avoid disturbing folding and binding to their antigen. Two different GFP-binding nanobodies were modified with the cyclic peptides using expressed protein ligation, which required some protein engineering. Purification of the CPP-conjugated nanobodies was possible using immobilized heparin, an anionic polysaccharide. The nanobodies could then be applied to cells. After cellular uptake, they could relocalize GFP-fusion proteins to the nucleoli, which CPPs have an affinity for. This relocalization could be used to quantify cellular uptake and allowed the detection of protein-protein interactions within cells.

Responsibility assignment

H. D. Herce and D. Schumacher contributed equally. M. C. Cardoso, H. Leonhardt and C. P. R. Hackenberger designed and conceived the project. H.D.H. conceived and performed the cellular uptake experiments, the relocalization-based visualization assay, the uptake of recombinant GFP and Mecp2–GFP, PCNA relocalization and the modified F3H assay and microscale thermophoresis measurements to determine the binding constant of functionalized nanobodies. D.S. designed and optimized the cell-permeable nanobody synthesis, cloned and expressed GBP–intein–CBD fusions, established the refolding protocol, performed the EPL and analysed all the constructs (MS, CD, binding to GFP), synthesized the linear, cyclic and cleavable CPPs, generated double-functionalized nanobodies and performed eGFP expression and purification. A. F. L. Schneider generated the GBP11-117A3–intein–CBD fusion, established a purification strategy, performed EPLs and synthesized cCPPs. A. K. Ludwig

purified recombinant proteins and performed some cellular uptake experiments as well as RNA isolation and RNA-binding assays. F. A. Mann optimized the EPL conditions and synthesized cCPPs. M. Filies generated and characterized the cell lines with the permanent expression of GFP and its fusions. M.-A. Kasper synthesized Cy5. S. Reinke performed the cloning and initial testing of the GBP–intein–CBD fusions. E. Krause contributed to the matrix-assisted laser desorption ionization measurements. H. Leonhardt provided the nanobodies. H. D. H. and D. S. wrote the manuscript supported by M. C. C., C. P. R. H., F. A. M., A. F. L. S., and A. K. L.

Summary of author contribution

A previously published GFP-binding nanobody that had previously been published, GBP1, was used in the attempt to generate cell-penetrating peptide conjugates[445]. The nanobody has very stable binding to GFP and can be expressed recombinantly in bacteria, making it a good candidate for this approach. As cell-penetrating peptides, previously employed cyclic variants of the commonly used Tat and R10 peptides (cTat and cR10) were to be used[182,290]. Using cyclic peptides, the nanobody-CPP fusions could not be generated through recombinant expression, and so a semi-synthetic strategy had to be employed. Expressed protein ligation was chosen as a strategy to generate the constructs. For this, cysteine-modified versions of the CPPs were first synthesized. Cyclization was accomplished by using orthogonal protecting groups on a lysine and glutamic acid residue, which could be removed, and cyclization was then done using a simple amide coupling. Optimization of the EPL conditions was required in order to obtain the nanobody-CPP conjugates in high yield, especially as purification of the conjugates from the unconjugated protein was difficult. After optimization, yields of up to 73% were achieved. A purification strategy for CPP-conjugates using the anionic polymer heparin was devised. The purification yielded very pure proteins in moderate yields.

Summary of content provided by other authors

As an alternative nanobody, the GFP-binding nanobody GBP4 was also used to generate nanobody-CPP conjugates. The conjugates were analysed using high resolution mass spectrometry and circular dichroism to ensure proper conjugation of the peptide without compromising the structure of the protein. Additionally, binding to GFP was also tested for the CPP conjugates to ensure they could still bind their antigen after modification.

The cellular uptake of the conjugates was first tested on a HeLa cell line expressing a fusion protein of the DNA repair protein PCNA (proliferating cell nuclear antigen) with GFP (GFP-PCNA). Arginine-rich Cell-penetrating peptides localize to the nucleoli after cellular uptake[244],

and this property can be used by observing the relocalization of the GFP fusion protein from the nucleus to the nucleolus upon binding of the nanobody. Using this property, cellular uptake could be easily quantified for all the synthesized conjugates. For the best conjugate, the nanobody GBP1 as a fusion with the cylic R10 peptide, more than 95% of cells showed relocalization of GFP after application of 10 µM of the nanobody. The cyclic peptides proved to be more effective than their linear counterparts, and the R10 peptide was more effective than the Tat peptide. The cellular uptake was also temperature independent and could be done at 4°C, suggesting that energy-dependent uptake is not required. Other proteins could also be relocalized by the nanobody, and it was even possible to co-transport the nanobody and a GFP-fusion of the Mecp2 protein into cells together. The nanobody-CPP conjugate could be used in a cell-based assay to detect protein-protein interactions by observing if the interaction partner would show the CPP-based relocalization to the nucleoli or not.

In many cases relocalization of the nanobody-CPP conjugate or the antigen may not be wanted, for example in immunofluorescence experiments. For this case, a fluorescent peptide was attached to the nanobody in the EPL reaction instead of the CPP. In a second conjugation, the nanobody can then first be activated with Ellman's reagent before addition of the cysteine-modified cyclic R10 peptide. This led to the formation of a disulfide bond between the fluorescent nanobody and the CPP, which could be cleaved by the addition of reducing agents. As the cellular interior is a reductive environment, the CPP should be cleavable after cellular uptake. Indeed, incubation of cells with the cleavable nanobody-CPP conjugate led to colocalization of the nanobody with GFP-PCNA without relocalization to the nucleolus, making this a useful tool for live-cell immunofluorescence of GFP fusion proteins.

Outlook

This work shows the potential of cell-penetrating peptides in the delivery of antibody fragments. The delivery of nanobodies has applications in immunofluorescence microscopy and other cellular assays. The delivery at 4°C implies that entire proteins can be delivered into cells in an energy-independent manner. More research is still required into the general applicability of CPP-mediated protein delivery and the intracellular fate of the CPP-conjugates.

3.2 Subcellular Targeting of Cleavable and Uncleavable Cell-Penetrating Peptide Conjugates

This chapter was published as follows:

A. F. L. Schneider, A. L. D. Wallabregue, L. Franz, and C. P. R. Hackenberger*

Targeted Subcellular Protein Delivery Using Cleavable Cyclic Cell-Penetrating Peptides.

Bioconj. Chem., **2019**, 30, 400-404.

https://doi.org/10.1021/acs.bioconjchem.8b00855

Abstract:

With the fluorescent protein mCherry as a model cargo, the targeting of delivered proteins to different subcellular compartments is evaluated. mCherry is generated recombinantly with an additional cysteine that can be modified with cyclic R10 peptides either via a cleavable disulphide bond or via an uncleavable thioether. The two different constructs show markedly different localization within cells as the uncleavable conjugate drives localization of the protein to nucleoli. By appending peptidic targeting sequences to the recombinant protein, it is possible to achieve localization of the proteins to nuclei or to the actin cytoskeleton after delivery. However, flawless localization to the target compartment is only achieved with the cleavable cell-penetrating peptide.

Responsibility assignment

A. F. L. Schneider and C. P. R. Hackenberger conceived the experiments and wrote the manuscript. A.F.L.S. cloned, expressed, purified, and characterized proteins, synthesized and characterized peptides and protein-peptide conjugates and performed uptake and microscopy experiments. A. L. D. Wallabregue performed uptake experiments. L. Franz cloned, expressed, and purified the Lifeact-mCherry construct.

Summary of content

To evaluate successful delivery of a protein to subcellular compartments, mCherry was chosen as the protein candidate. Because it is a fluorescent protein, mCherry fluorescence indicates that the protein is still intact. mCherry also does not contain any cysteines, which makes it easy to introduce an additional cysteine that can later be used as a handle to attach the cell-penetrating peptide. The fluorescence of the protein is also less dependent on the pH value than in the case of GFP, which may help distinguish endosomal entrapment from cytosolic delivery. To establish the method, an mCherry construct with an additional cysteine on the C-terminus was cloned and expressed in bacteria. After purification, the protein could be

modified with a cell-penetrating peptide. Two peptides were synthesized for this purpose: a maleimide-functionalized cyclic R10[446] peptide which would generate an uncleavable bond, and a cysteine-functionalized equivalent that can be used to furnish a disulfide-conjugate. Both peptides could be used to make mCherry-CPP conjugates, which could be analyzed by high resolution mass spectrometry and gel electrophoresis. The disulfide-linked CPP could be removed under reducing conditions as expected.

In the cellular uptake experiment, several concentrations of the mCherry-CPP conjugates were tested on HeLa cells. Low concentrations seemed to lead to endosomal entrapment, but the protein could be successfully delivered into the cytosol at 50 µM. When comparing the maleimide and disulfide constructs, the non-cleavable maleimide showed clear mCherry signal in the nucleoli, whereas the cleavable construct was excluded.

As a first peptidic targeting sequence the nuclear localization signal (NLS) from the human c-Myc protein[447] was used, which had previously been shown to be highly effective at nuclear import[79]. Recombinant expression of the NLS-mCherry with the C-terminal cysteine worked as before, as did the modification with the cyclic cell-penetrating peptides. Delivery was also effective only at 50 µM. Again, the maleimide-construct showed very clear nucleolar staining while the cleavable construct was broadly distributed throughout the nucleus.

To challenge the system further, an actin-targeting sequence was employed next. Lifeact is a well-established, non-toxic actin targeting sequence[448]. However, the sequence is also relatively hydrophobic. To compensate, the lifeact-mCherry fusion was expressed with maltose-binding protein (MBP) as a solubility tag, which was removed after purification. Conjugation and delivery of the cell-penetrating peptide could be achieved as before. The construct with the cleavable cell-penetrating peptide showed actin staining, which could be confirmed through colocalization with a known actin marker (SiR-actin).

Outlook

This study demonstrates that after delivery, conjugates of proteins with cell-penetrating peptides can reach subcellular compartments effectively, but only when the attached peptide can be cleaved off. The high required concentration to achieve successful uptake also highlights the biggest flaw of this method. Applying high concentrations of conjugates to cells can be difficult and potentially toxic, and this needs to be improved further.

3.2.1 Attempted Mitochondrial Targeting of mCherry after Delivery using Cell-Penetrating Peptides

Introduction:

Mitochondria are a membrane-bound cellular compartment involved in many cellular processes such as energy metabolism and regulation of the cell cycle[449]. Mitochondria contain their own genome, and proteins encoded in the mitochondrial DNA can be translated within mitochondria[450]. However, most proteins that are important for the function of mitochondria are encoded within the nuclear DNA and are imported into mitochondria[451]. Import of proteins into mitochondria membrane is a complex, regulated process and is generally accomplished through protein translocases on the outer and inner membranes[452]. Some proteins have been shown to be imported into mitochondria post-translationally, although co-translational import may also exist[453]. Proteins do seem to be unfolded while passing through the membrane however[454].

Delivering cargoes into mitochondria is interesting because it may allow alteration of mitochondrial functions. There are also many diseases associated with mitochondrial dysfunction[455], which could potentially be treated through mitochondrial delivery approaches[456]. Because mitochondrial import may require unfolding, the delivery of exogenously folded proteins into mitochondria may be difficult. Nevertheless, it is an important goal to pursue.

Results and Discussion:

As before, the fluorescent protein mCherry was the cargo of choice to be delivered. As a mitochondrial targeting sequence, the signal sequence of the cytochrome c oxidase, subunit 8a (COX8A) was chosen. At first, a plasmid for the expression of a histidine-tagged version of the mCherry protein with the mitochondrial targeting sequence was cloned. Recombinant expression in *e. coli* did not yield any protein (data not shown). The mitochondrial targeting sequence is hydrophobic, which may result in an insoluble protein after expression. To overcome this, the construct was cloned into an expression vector with maltose-binding protein (MBP) as a solubility tag. Expression in *e. coli* then yielded protein which could also be purified (Supplementary figure 1, in section 6, appendix). After removal of the MBP through cleavage with the TEV protease, protein aggregation was observed. This suggests that the protein can still aggregate even after folding. Nevertheless, several milligrams of pure protein could be isolated.

The conjugation of the cyclic R10 CPP was done as before[457], either by incubating the protein with a maleimide-functionalized cR10 peptide or by activating the protein with an excess of Ellman's reagent, removing the excess by dialysis, and then incubating the protein with the cysteine-containing cR10 (figure 1a). Conjugation was successful in both cases as confirmed by gel electrophoresis (figure 1b).

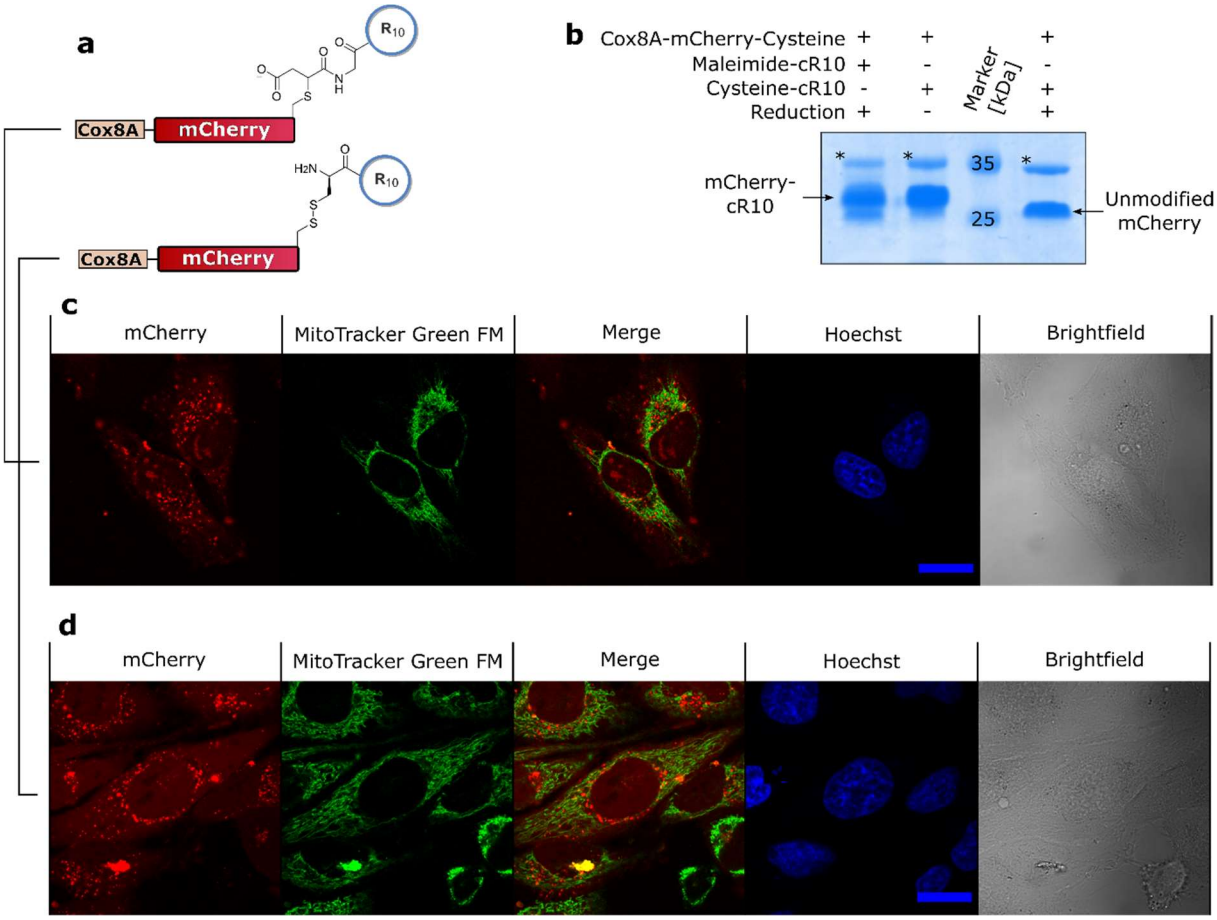

Figure 1. **a**, Schematic showing the semi-synthetic mCherry constructs bearing the mitochondrial localization signal of Cox8A as well as cR10 CPPs. **b**, Coomassie-stained SDS-PAGE gel showing the successful conjugation of mCherry to the CPPs and reduction of the disulfide. * = remaining maltose binding protein after purification. **c,d,** Confocal microscopy images of the maleimide- and disulfide linked mCherry-CPP conjugates after cellular uptake. Both constructs show localization within the cell, but no colocalization with the mitochondrial marker.

Cellular delivery was then tested in HeLa cells. 50 µM of either conjugate was added to the cells in HEPES buffer for 1 hour at 37°C. Colocalization was tested by co-treating the cells with

a mitochondrial marker (MitoTracker green FM). Unfortunately, while some of the fluorescence signal originating from the mCherry looked colocalized with mitochondria, the majority by far was not colocalized for either of the constructs (figure 1c-d). While much of the protein shows punctate staining indicating endosomal entrapment, a substantial amount of the disulfide-linked mCherry is also broadly distributed in the cytosol and should be able to be recruited to the mitochondria.

It is not completely clear why mitochondrial localization does not occur, as the targeting sequence can lead to mitochondrial localization of fluorescent proteins expressed within the cell[458]. One possible explanation is that mitochondrial import fails, as it may require unfolding of the mCherry protein. This constitutes a major hurdle which will have to be addressed if highly efficient mitochondrial delivery of proteins is desired.

Materials and Methods:

Cloning:

The previously published MBP-TEV-Lifeact-mCherry plasmid was used as a template. The Cox8A mitochondrial targeting sequence was amplified via PCR along with the backbone and they were combined using Gibson assembly.

Protein expression and purification:

The MBP-Cox8A-mCherry-Cysteine construct was expressed by inoculating a 5 mL starter culture in LB medium with a single colony from an agar plate of BL21 DE3 Lemo cells transformed with the corresponding plasmid DNA. The starter culture was incubated overnight at 37°C. 1 mL of the starter culture was used to inoculate a 250 mL culture in LB medium containing Kanamycin. The culture was incubated for ~6 hours at 37°C until it reached an OD600 value of 0.6. Expression was induced with 0.5 mM isopropyl-b-D-1-thiogalactopyranoside (IPTG) and incubated at 18 °C for 18 h.

Cells were spun down at 8000xg for 15 minutes. The cell pellets were washed once with PBS. The pellets were then resuspended in PBS containing, then lysed using sonication (3x 2 min, 30% Amplitude), followed by debris centrifugation at 25.000xg for 30 min. The proteins were purified on amylose resin, eluting with 100 mM maltose in PBS.

The MBP-Cox8A-mCherry-Cysteine construct was treated with TEV protease (1:20 w/w) while dialyzing against PBS at room temperature overnight for 18 hours. The protein was then

passed through the amylose resin again to remove the maltose-binding protein. The protein was further purified using size-exclusion chromatography.

Conjugation of the cell-penetrating peptide:

The previously published maleimide- and cysteine-functionalized cR10 peptides were used[457]. For the maleimide, 10 equivalents of peptide were added to the protein and it was incubated overnight at room temperature. For the disulfide-linkage, the protein was incubated with 10 equivalents of Ellman's reagent (5,5′-Dithiobis(2-nitrobenzoic acid)) for 1 hour at room temperature. The excess reagent was removed by dialysis overnight against 5 mM HEPES at pH 9.0, 140 mM NaCl, 2.5 mM KCL, 5 mM Glycine. The next day, 10 equivalents of the cysteine-modified cR10 peptide were added to the protein and it was incubated overnight. For both peptides, the excess peptide was removed by desalting in a spin column into hepes buffer (5 mM HEPES at pH 7.5, 140 mM NaCl, 2.5 mM KCL, 5 mM Glycin).

Cellular uptake and microscopy:

The day before the experiment, 30'000 HeLa cells were seeded in each well of an 8-well glass bottom microscopy slide. The cells were left to adhere overnight at 37°C and 5% CO_2. The next day, the cells were washed twice with HEPES buffer (5 mM HEPES at pH 7.5, 140 mM NaCl, 2.5 mM KCL, 5 mM Glycin). The buffer was then replaced with 50 µM protein in Hepes buffer, also containing 200 nM mitotracker green FM, and the cells were incubated for 1 hour at 37°C. The cells were then washed with cell medium containing 10% FCS with 5 µg/mL Hoechst 33342 and left in the medium for imaging.

Confocal microscopy images were acquired on a Zeiss laser scanning microscope. All images shown in this work were acquired using a PlanApo 100x oil objective (Zeiss). Brightfield images were aquired along with fluorescence images. Standard laser, a quad Dicroic (400-410,486-491, 560-570, AHF) and Emission filters were used in the acquisition of confocal fluorescence images (Hoechst 33342, ex.: 405 nm em.:450/50:, MitoTracker Green FM, ex.: 488 em.: 525/50, mCherry, ex.: 561 em.: 600/50 nm.

3.2.2 Membrane Targeting of mCherry after Delivery using Cell-Penetrating Peptides

Introduction:

Proteins are the component of membranes that are responsible for most of the specific functions of cell membranes. The association of proteins with membranes can happen in various ways. Proteins can be integral membrane proteins that contain transmembrane sequences that are integrated into the plasma membrane[459]. Peripheral membrane proteins are temporarily attached to the membrane either by amphipathic helices that associate with the membrane[460], or they can be modified co- or post-translationally with fatty acid chains or prenyl groups that will integrate into the membrane[461].

Lipid-anchored proteins can be attached to the cell membrane via various types of anchors including palmitoylation, myristoylation, farnesylation, geranylgeranylation and modification with cholesterol[462]. Protein lipidation occurs at specific motifs within the protein sequence and is a tightly regulated process[463]. Because it occurs on many disease-relevant proteins, it is also itself implicated in many diseases, from cardiovascular disease[462] to cancer[464]. The process of lipidation can be difficult to study, and exogenously delivered proteins that are lipidated within the cell can be an additional avenue for research into this type of modification.

Results and Discussion:

Different lipidation motifs were explored in the context of this approach. The palmitoylation motif of the Lyn tyrosine kinase protein was chosen, alongside the CaaX (where a = aliphatic amino acid and X = one of several amino acids) motifs of two GTPases, HRas and KRas. Interestingly, as all three sequences contain a cysteine that is later lapidated, this cysteine could also be used in the reversible modification of the protein with the cell-penetrating peptide for delivery. The peptide would then be removed inside of the cell, restoring the cysteine, and the lipid anchor could then be attached. The fluorescent protein mCherry was used as a model cargo. Plasmids encoding mCherry with the targeting sequences were cloned (plasmid schematics in figure 1a). The proteins were then recombinantly expressed in *E. coli* and purified using immobilized metal affinity chromatography (Supplementary figure 2, in section 6, appendix).

As the CPP has to be removed inside the cell to allow attachment of the lipid anchor, only disulfide conjugates of the cyclic R10 CPP were generated. This was accomplished as

published previously[457], by activating the protein with an excess of ellman's reagent, removing the excess by dialysis, and then incubating the protein with the cysteine-containing cR10. The attachment of the CPP was successful for all three fusion proteins, as confirmed by gel electrophoresis and high-resolution mass spectrometry (figure 1b and supplementary figure 3).

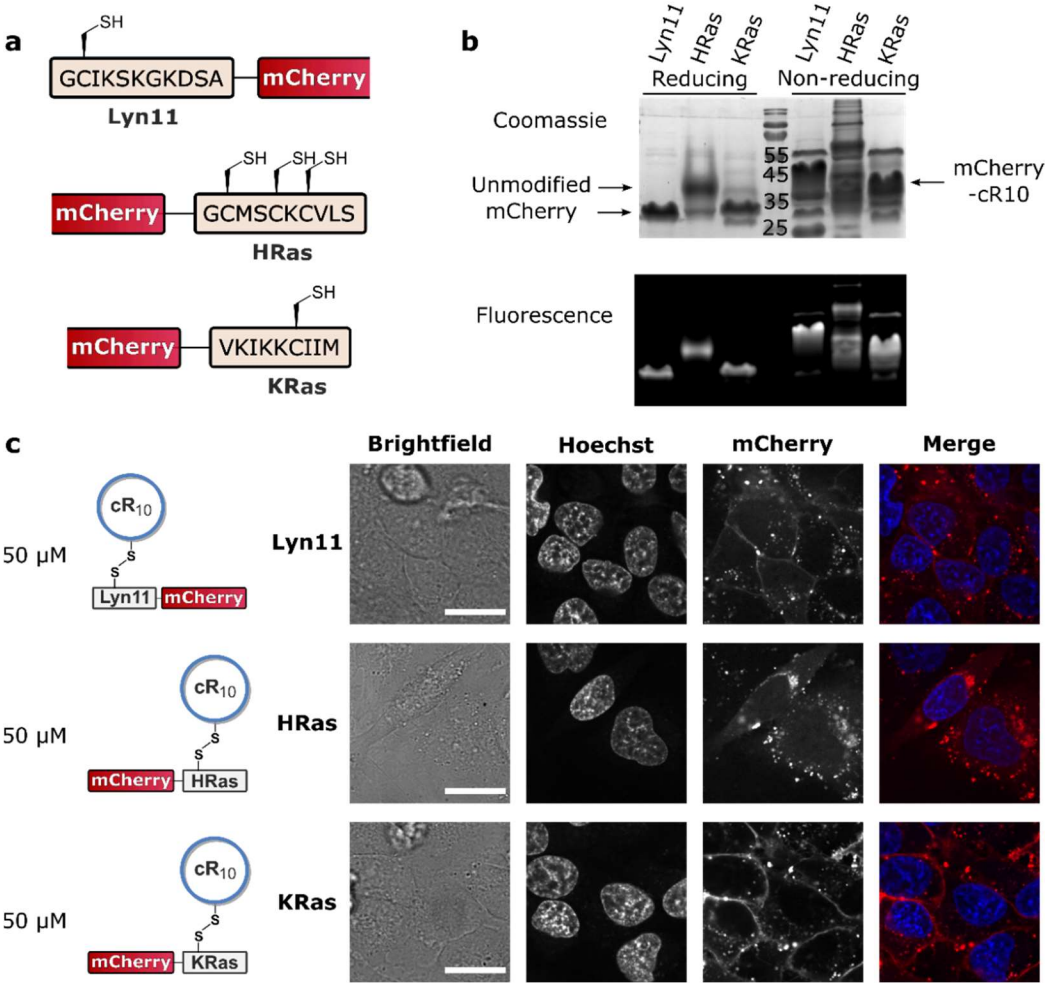

Figure 1. **a**, Schematic showing the fusion protein sequences of mCherry fused to the Lyn, HRas and KRas membrane localization sequences. **b**, Coomassie-stain and in-gel fluorescence of an SDS-PAGE gel showing the successful conversion of the mCherry constructs to the CPP-conjugates. Note that because the HRas construct contains several cysteines it leads to a complex disulfide bonding pattern. Nevertheless, conversion can be seen especially on the fluorescence image. **c,** Confocal microscopy images of the disulfide linked mCherry-CPP conjugates after cellular uptake. All constructs show fluorescence within the cell, with the lyn11 and KRas constructs showing membrane staining.

Cellular delivery was then tested in HeLa Kyoto cells using 50 μM of the conjugates in cell medium. The cytosolic delivery of all conjugates was successful, although some endosomal entrapment is also apparent. However, only two of the conjugates, the Lyn11 and KRas constructs show membrane staining (figure 1c, top and bottom rows). The HRas construct does not show membrane staining despite being delivered into the cytosol.

A possible reason for the unsuccessful plasma membrane localization of the HRas-fusion protein is that the intracellular localization of HRas changes between endomembranes and the plasma membrane depending on the number and character of the lipid modifications, as HRas (in contrast to the other two constructs) can be farnesylated and palmitoylated multiple times[465]. Nevertheless, the Lyn- and KRas constructs containing the cR10 peptide can be useful models to study regulation of membrane anchoring and could be used in conjunction with small molecule inhibitors of these processes to gain further understanding into the matter.

Materials and Methods:

Cloning:

The previously published mCherry-cysteine plasmid was used as a template. The Lyn palmitoylation motif (the 11 N-terminal amino acids (Lyn11)) was amplified via PCR along with the backbone and was introduced on the N-terminal side of the protein using Gibson assembly. The HRas and KRas CaaX motifs were also amplified via PCR and introduced on the C-terminus of the mCherry protein using Gibson assembly.

Protein expression and purification:

The protein constructs were expressed by inoculating a 5 mL starter culture in LB medium with a single colony from an agar plate of BL21 DE3 cells transformed with the corresponding plasmid DNA. The starter cultures were incubated overnight at 37°C. 1 mL of each starter culture was used to inoculate a 250 mL culture in LB medium containing Kanamycin. The cultures were incubated for ~6 hours at 37°C until they reached an OD600 value of 0.6. Expression was induced with 0.5 mM isopropyl-b-D-1-thiogalactopyranoside (IPTG) and incubated at 18 °C for 18 h.

Cells were spun down at 8000xg for 15 minutes. The cell pellets were washed once with PBS. The pellets were then resuspended in PBS containing 25 mM imidazole, then lysed using sonication (3x 2 min, 30% Amplitude), followed by debris centrifugation at 25.000xg for 30 min.

The proteins were purified on Nickel-NTA agarose and eluted with 500 mM imidazole in PBS. The proteins were then further purified using size-exclusion chromatography.

Conjugation of the cell-penetrating peptide:

The previously published cysteine-functionalized cR10 peptides was used[457]. To generate a disulfide-linkage, the proteins were incubated with 10 equivalents of ellman's reagent (5,5′-Dithiobis(2-nitrobenzoic acid)) for 1 hour at room temperature. The excess reagent was removed by dialysis overnight against 5 mM HEPES at pH 9.0, 140 mM NaCl, 2.5 mM KCL, 5 mM Glycine. The next day, 10 equivalents of the cysteine-modified cR10 peptide were added to the protein and it was incubated overnight. Excess peptide was removed by desalting in a spin column into hepes buffer (5 mM HEPES at pH 7.5, 140 mM NaCl, 2.5 mM KCL, 5 mM Glycin).

Cellular uptake and microscopy:

The day before the experiment, 10'000 HeLa Kyoto cells were seeded in each well of a 96-well glass bottom black plate. The cells were left to adhere overnight at 37°C and 5% CO_2. The next day, the cells were washed twice with HEPES buffer (5 mM HEPES at pH 7.5, 140 mM NaCl, 2.5 mM KCL, 5 mM Glycin). The buffer was then replaced with 50 µM protein in Hepes buffer and the cells were incubated for 1 hour at 37°C. The cells were then washed with cell medium containing 10% FCS with 5 µg/mL Hoechst 33342 and left in the medium for imaging.

Confocal microscopy images were acquired on a Nikon-CSU spinning disc microscope with an CSU-X1 (Andor) and a live cell incubation chamber (OKOlab). All images shown in this work were acquired using a PlanApo 60x NA 1.4 oil objective (Nikon) and an EMCCD (AU888, Andor). Brightfield images were aquired along with fluorescence images. Standard laser, a quad Dicroic (400-410,486-491, 560-570, 633-647, AHF) and Emission filters were used in the acquisition of confocal fluorescence images (BFP(Hoechst 33342), ex.: 405 nm em.:450/50: and RFP (mCherry) ex.: 561 em.:600/50 nm.

3.3 Improving Cell-Penetrating Peptide-Mediated Delivery to Allow Delivery of Large Cargoes

This chapter was accepted for publication as follows:

A. F. L. Schneider, M. Kithil, M. C. Cardoso, M. Lehmann and C. P. R. Hackenberger*
Cellular uptake of Large Biomolecules Enabled by Cell-Surface-Reactive Cell-Penetrating Peptide Additives. *Nat. Chem.*, **2021**, accepted. DOI-link not yet available.

Abstract:

A major bottleneck of the delivery of proteins using cell-penetrating peptides are the high concentrations that need to be applied to cells to achieve cytosolic delivery instead of endosomal entrapment. To circumvent this issue, a low µM concentration of cargo-CPP conjugate is applied to the cells along with low µM free CPP. Different CPP-additives are evaluated, and the most effective additives are CPPs that can react with the cell-surface through cysteine-selective chemistry. This delivery approach is effective for several different proteins at low concentrations and also works at 4°C, where active transport should not occur. The protocol can also be applied to the delivery of full-length IgG antibodies, which then colocalize with their antigen inside living cells.

Responsibility assignment

A. F. L. Schneider, M. Lehmann, M. C. Cardoso and C. P. R. Hackenberger conceived the experiments and wrote the manuscript. A.F.L.S. cloned, expressed, purified and characterized proteins, synthesized and characterized peptides and protein-peptide conjugates, performed uptake, cell viability, microscopy and flow cytometry experiments. M.L. performed microscopy experiments and wrote the quantification script together with A.F.L.S.. M. K. performed the Calcein AM staining.

Summary of content

To address the high concentrations required to achieve cytosolic delivery of cargoes with cell-penetrating peptides, several model cargoes were synthesized. A small molecule fluorophore (~500 Da), a fluorescent nanobody (~13 kDa) and the fluorescent protein mCherry (~30 kDa) were all connected to a cyclic R10 peptide. The constructs were then applied to HeLa cells at various concentrations (1-50 µM) and confocal microscopy images were recorded. Uptake experiments revealed that while the fluorophore could reach the cytosol even at 1 µM concentration, the other cargoes were trapped in endosomes unless much higher

concentrations were used (10 μM and 50 μM for the nanobody and mCherry, respectively). As a potential solution to this, the protein-CPP conjugates were applied to the cells at a 1 μM concentration in combination with 5 μM of free, unbound cell-penetrating peptide. It was expected that this could rescue the cytosolic delivery with the combined effect of the CPPs. Indeed, the application of 1 μM of either of the two proteins with 5 μM of the previously published cysteine-functionalized cyclic R10 peptide led to cytosolic delivery in both cases. The total concentration of cell-penetrating peptide was only 6 μM, much lower than the previously required amounts. Interestingly, the same effect could be achieved when a linear R10 peptide was used as the unbound additive, implying that the more challenging synthesis of the cyclic variant is not necessarily required.

To further characterize the mode of delivery, several other CPPs were synthesized, with a focus on the N-terminal cysteine residue that was initially included serendipitously. The cysteine thiol proved to be very important for the observed effect, since blocking it by alkylation with iodoacetamide strongly reduced the efficiency of the protocol. Interestingly, activating the thiol using Ellman's reagent, thereby making it more prone to form disulfide bonds, strongly increased the efficiency of delivery. Fluorescent versions of the cysteine-containing R10 peptides were then synthesized and the cellular uptake of these peptides was monitored in time-lapse confocal microscopy experiments. The Ellman's reagent activated fluorescent R10 peptide showed very quick cellular uptake, with nucleolar staining occurring in all cells within 90 seconds after addition. The peptide also showed very prominent "nucleation zones", i.e. very brightly fluorescent spots on the surface of the cell appearing immediately before uptake. The peptide with the blocked thiol showed no uptake at all under the same timeframe. We hypothesized that cysteine-selective chemistry can be used to covalently label certain spots on the membrane through which cellular uptake then occurs. To put this to the test, a maleimide-functionalized, fluorescent R10 peptide was synthesized. The maleimide-containing peptide also showed very rapid uptake comparable to the Ellman's reagent-activated peptide. The two peptides labelled the same regions on the cell membrane when added to cells together. Finally, through co-incubation of cells with the fluorescent maleimide-R10 peptide and an mCherry-CPP conjugate it was possible to observe the transduction of mCherry into the cell, which indeed seemed to occur through areas of the membrane that the maleimide-R10 peptide had previously labelled.

As an alternative way to anchor a CPP on the surface of cells, a chloroalkane-containing R10 peptide was synthesized. A plasmid was cloned that would lead to the expression of a halotag

protein on the cell-surface along with an EGFP reporter within the cell. After transfection of the plasmid into HeLa cells, the chloroalkane-R10 was added to the cells along with an mCherry-CPP conjugate, and cytosolic delivery could be observed predominantly into cells that expressed the halotag. This suggests that CPP-anchoring on the cell membrane is a generally applicable way to efficiently deliver proteins into cells.

The protocol was also successful in four other cancer cell lines of different tissue origin and could be applied in presence of low concentrations of serum. It was also possible to deliver the DNA editing enzyme cre recombinase. The best additive in the delivery protocol, the Ellman's reagent-activated R10 peptide, could also be used to deliver a cysteine-containing mCherry by simple co-incubation with an excess of peptide.

Lastly, the delivery of full-length IgG antibodies was tested using the new additive protocol. The antibodies first had to be thiolated using Traut's reagent, as they contain no unpaired cysteines. When the antibodies were then mixed with an excess of the Ellman's reagent-activated R10 peptide, they could be delivered into the cytosol of HeLa cells, and showed colocalization with their antigen. For example, an antibody against the Tomm20 mitochondrial receptor showed colocalization with a mitochondrial marker.

Outlook

The newly developed CPP-additive protocol in the delivery of proteins allowed the delivery of various protein conjugates into several cell lines. The labelling of cell membranes with CPPs and subsequent delivery could allow cell-specific delivery using CPPs, if one can only label a certain kind of cell. This is a long-sought goal in the field of CPP research. The delivery of full-length IgG antibodies also has much potential and can, in future work, be applied to the delivery of inhibitory antibodies for cell-based assays.

Cellular uptake of Large Biomolecules Enabled by Cell-surface-reactive Cell-penetrating Peptide Additives

Anselm F. L. Schneider[1,2], Marina Kithil[3], M. Cristina Cardoso[3], Martin Lehmann[1] and Christian P. R. Hackenberger*[1,4]

[1] Leibniz-Forschungsinstitut für Molekulare Pharmakologie (FMP), Robert-Rössle-Strasse 10, 13125 Berlin, Germany

[2] Institute of Chemistry and Biochemistry, Freie Universität Berlin, Takustrasse 3, 14189 Berlin, Germany

[3] Technische Universität Darmstadt, Schnittspahnstr. 10, 64287 Darmstadt, Germany

[4] Department of Chemistry, Humboldt-Universität zu Berlin, Brook-Taylor-Strasse 2, 12489 Berlin, Germany

*Corresponding author

Abstract

Enabling the cellular delivery and cytosolic bioavailability of functional proteins constitutes a major challenge for the life sciences. The conjugation with cell-penetrating peptides (CPPs) is frequently used to mediate the cellular uptake of various protein cargoes. At low µM-concentrations, protein-CPP conjugates can undergo endosomal uptake, which necessitates endosomal escape to avoid entrapment in endosomes, whereas at higher concentrations they can cross cell membranes directly and reach the cytosol via a non-endosomal delivery pathway.

In the current study, we demonstrate that thiol-reactive arginine-rich peptide additives can enhance the cellular uptake of protein-CPP conjugates in a non-endocytic mode even at low µM concentration. We show that such thiol- or halotag-reactive additives can result in covalently-anchored CPPs on the cell surface, which are highly effective at co-delivering protein cargoes. Taking advantage of the thiol-reactivity of our most effective CPP-additive we show that Cys-containing proteins can be readily delivered into the cytosol by simple co-

addition of a slight excess of this CPP. Furthermore, we demonstrate the application of our "CPP-additive technique" in the delivery of functional enzymes, nanobodies and full-length IgG antibodies. This new cellular uptake protocol greatly simplifies both the accessibility and efficiency of protein and antibody delivery with minimal chemical or genetic engineering.

Introduction

Proteins offer a tremendous structural and functional diversity, which makes them indispensable tools for biological and pharmacological applications. However, proteins are large and hydrophilic, and thus usually not cell-permeable, which severely limits their potential in both research and therapy. Consequently, the intracellular delivery of functional proteins remains one of the biggest challenges in the molecular life sciences, although considerable progress has been made recently[1,2]. Amongst other methods, cell-penetrating peptides (CPPs) have established themselves as potent tools in the delivery of a variety of cargoes[3].

The first cell-penetrating peptides or "protein transduction domains" (PTDs) have been discovered about 30 years ago originating from the transactivator of transcription (TAT) protein of the human immunodeficiency virus (HIV)[4] and the Drosophila antennapedia homeodomain (penetratin)[5,6]. Since then, many CPPs have been described, both from natural and synthetic origin. Several studies have investigated their mechanism of action and used them in various applications in biology[7,8]; nevertheless, how exactly CPPs enter cells is still often controversially discussed. Much effort has been devoted to cationic CPPs, which can bind to cell membranes through ionic interactions before being endocytosed.[9,10] Equally, many reports describe CPP-mediated uptake at cold temperatures, where active uptake processes should not occur, or in the presence of endocytosis inhibitors[11,12]. The latter process, commonly referred to as "transduction", is reported to be dependent on the concentration[13,14] and also on the cargo attached to the peptide[15]. This can be seen when using linear CPPs to transport small cargoes such as fluorophores and peptides, which typically leads to localization in the cytosol, whereas larger protein cargoes are often trapped in endosomes[16,17].

To further improve the delivery of CPP-linked cargoes researchers have implemented additional modules into uptake protocols. For instance, the addition of the enzyme sphingomyelinase resulted in an increased uptake of cationic CPPs by generating ceramide on the cell surface[18]. Alternatively, the addition of pyrenebutyrate as a hydrophobic counterion to cells before adding the CPP-conjugate led to an improved uptake[19]. Finally, the addition of peptides or small molecules has been pursued to mediate endosomal leakage for the release of cargoes into the cytosol [20-24].

An important element in the design of effective CPPs for the transport of cargo to the cytosol is cyclization[25,26]. It was demonstrated that cyclization leads to a remarkable increase in both efficiency and speed of membrane transduction[27], which likely stems from the presentation of the positive charges on the peptide. We have previously shown that cyclization and subsequent conjugation of a single TAT-peptide can be used to transport GFP into the cytosol of cells, which was impossible with the linear variant[28]. Since then, we have been able to apply this methodology to the cytosolic transport of nanobodies as well as the intracellular targeting of fluorescent proteins[29,30]. Still, to achieve transduction of proteins into the cytosol, rather high concentrations of the cargo protein must be applied, ranging from 10 µM of a small antibody fragment (nanobody) to up to over 100 µM of EGFP. These concentrations are much higher than required for the transduction of small cargoes[27] and suggest that there is a size-dependence of the cargo on transduction. Consequently, it might not be possible at all to deliver even larger molecules in an energy-independent manner.

Encouraged by previous findings, which report the cooperative interaction of arginine-rich CPPs with physiological membranes in a concentration-dependent manner[31-34], we probed the impact of CPPs that were added to cells in addition to protein-CPP cargoes. Starting with simple cysteine-containing, unbound CPPs as additives, we find that thiol-reactivity plays an important role in this additive-approach, which is consistent with previous reports using thiol-reactive cargoes[35,36]. In particular, we show that electrophilic thiol-reactive CPP-additives are highly effective at creating nucleation zones on the cell-surface, which enable efficient

transduction of protein-CPP conjugates. Our protocol proves to be highly effective, simple, and not harmful to the cell. Importantly, we show that we enable the transduction of recombinant CPP-containing proteins as well as a 150 kDa IgG antibody into living cells via a non-endosomal uptake mechanism.

Results

Improved cellular uptake of cargoes mediated by cell-penetrating peptide additives

To evaluate the concentration, temperature and cargo-size dependency of added arginine-rich peptides to mediate cytosolic delivery, we chose three distinct cargoes to transport: the organic fluorophore Tetramethylrhodamine (TAMRA, ~450 Da), the camelid-derived anti-GFP nanobody GBP1 (~14 kDa) and the fluorescent protein mCherry with a nuclear localization signal (NLS-mCherry, ~28 kDa). We attached each of the cargoes to a synthetic cyclic R10 (cR10) peptide yielding an intracellularly non-cleavable conjugate, either via an amide bond in the case of TAMRA or using maleimide chemistry for the proteins (analytical data for peptides in SI Fig.1, characterization of GBP1 and mCherry and their CPP conjugates in SI Figs. 2-3), following our previous reports[29,30]. In all cases, successful cytosolic delivery would lead to staining of the cytosol and of the nucleolus, an RNA-rich membrane-less compartment inside the nucleus (red area in the nucleus, Fig. 1a), for which cationic CPPs have an affinity[29,37,38].The cR10 peptide, consisting of ten arginines with alternating L- and D-configurations, has previously been shown to be effective in the delivery of functional proteins, albeit only at relatively high concentrations[29,30]. We then applied all of the synthesized cargoes to HeLa Kyoto cells (expressing nuclear GFP-PCNA[39,40] as antigen for the nanobody), at both 37 and 4°C (Figs. 1b-d and individual channels in SI Fig. 4). At 37°C, the CPP-bearing cargoes can reach the cytosol either via endocytosis and endosomal escape (Fig. 1 a) or directly transduce the membrane, circumventing the energy-dependent transport. At 4°C however, active transport should not occur, and cellular fluorescence would be the result of transduction[41,42].

Upon incubation of the cells with TAMRA-cR10 for 1 hour in cell culture medium, we found cytosolic (and nucleolar) localization of the red fluorophore at only 1 μM both when the incubation was done at 4 and 37°C (Fig. 1b). These experiments show that successful cytosolic delivery for this small fluorophore can be achieved under conditions without endosomal uptake.

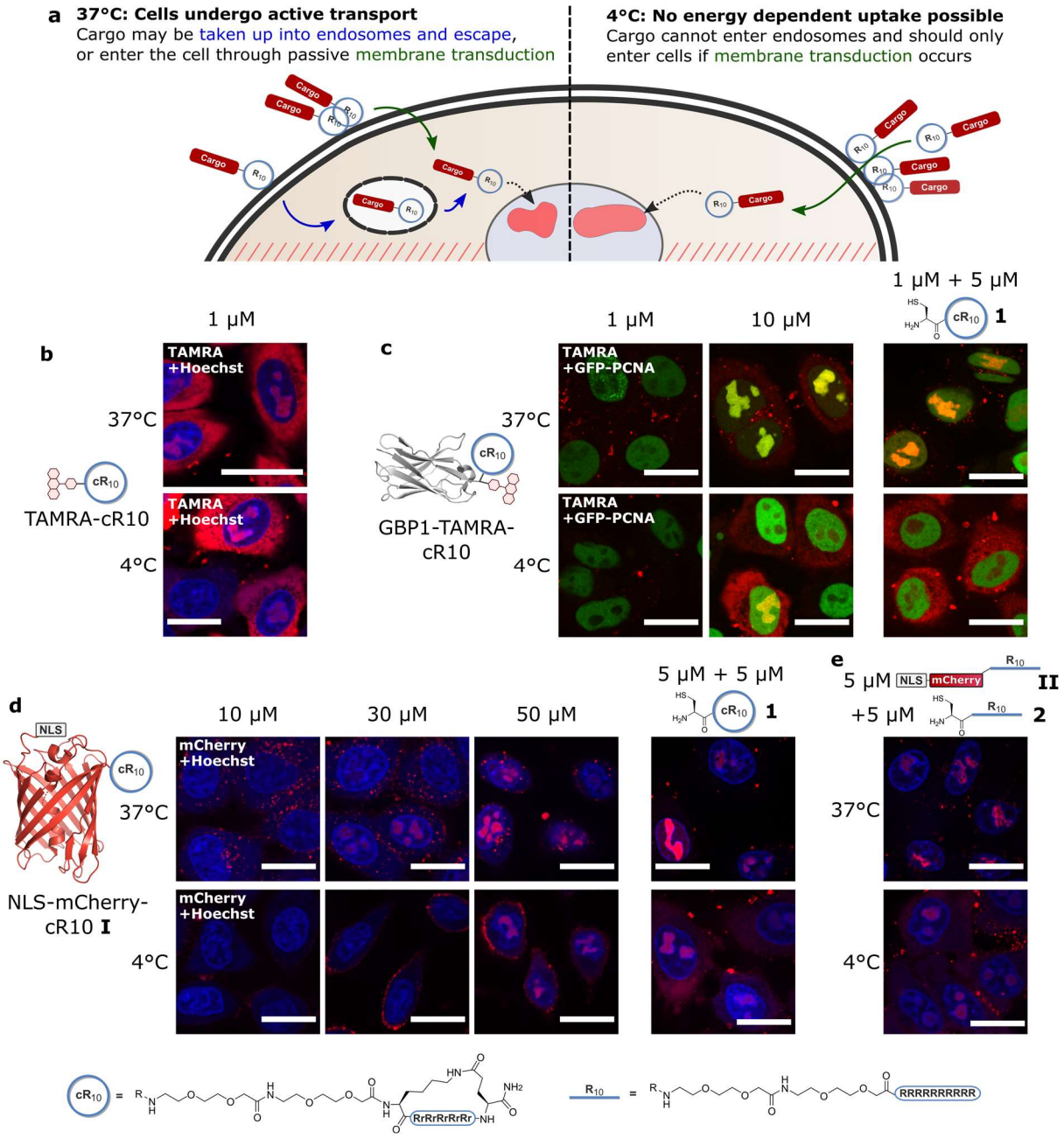

Fig. 1 Concentration dependent delivery of CPP-bearing red fluorescent cargoes into HeLa Kyoto cells at 37 and 4°C. a, Different modes of uptake at 37 and 4°C. **b**, Cellular uptake of TAMRA-cR10 at 37 and 4°C and 1 μM concentration. **c**, Cellular uptake of fluorescently-labelled GBP1 nanobody (Structure: 3K1K) with cR10 peptide at 37 and 4°C and 1 and 10 μM concentration, and at 1 μM concentration with 5 μM additional cR10 **1**. Here, the nuclear GFP fluorescence of the GFP-PCNA fusion

protein is shown instead of the Hoechst staining. **d**, Cellular uptake of cR10-modified NLS-mCherry **I** (Structure: 2H5Q) at 37 and 4°C and 10, 30 and 50 μM concentration, and at 5 μM concentration with 5 μM additional cR10. **e**, Cellular uptake of linear R10-modified NLS-mCherry **II** with added 5 μM linear R10 **2**. Scale bars 20 μm. Uppercase R is L-arginine while lower case R is D-arginine. Split channel images and additional concentrations in SI Fig. 4.

For the nanobody-CPP conjugate, 1 μM concentration results in predominantly punctate endosomal fluorescence at 37°C while at 4°C the nanobody is excluded from the cell (Fig. 1c). At 5 μM concentration, endosomal uptake is less prominent, and uptake also works to some extent at the cold temperature (SI Fig. 4b). At 10 μM concentration, all cells show cytosolic (and nucleolar) staining at 37°C and 4°C (Fig. 1c) Interestingly, for all proteins we tested the nucleolar staining is more evident at 37°C whereas cytosolic staining is more pronounced at 4°C, which may be because active nuclear import is also an energy independent process[43].

Following our proposal, we thought it may be possible to rescue the cytosolic delivery of the protein at low concentrations by addition of unbound CPP. Indeed, when we co-incubated 5 μM of a cysteine-containing cR10 peptide (Cys-cR10, **1**), which we previously used for the semi-synthesis of nanobodies by expressed protein ligation[30], with 1 μM of the nanobody-cR10 conjugate for 1 hour on HeLa cells, the nanobody showed efficient cytosolic and nucleolar staining at both temperatures (Fig. 1c and SI Fig. 4b).

For the NLS-mCherry-cR10 conjugate (**I**), the required concentration to achieve cytosolic uptake is even more restrictive, with anything below 50 μM leading to dominant endosomal uptake without nucleolar localization at 37°C and no uptake at all at 4°C (Fig. 1d). Analogous to the nanobody experiments, the addition of 5 μM peptide **1** allowed energy-independent transduction of mCherry at a low concentration of 5 μM (Fig. 1d). Delivery could even be achieved at 1 μM protein and 5 μM peptide (SI Fig. 4c), although under these conditions the fluorescence of the mCherry was faint and difficult to detect.

Encouraged by these findings, we subsequently probed the performance of linear CPP sequences in the cargo-conjugates and additives. Although CPP cyclization is known to improve cell permeability,[27,28] we now also observed efficient nucleolar delivery of 5 μM NLS-mCherry linked to a linear R10-peptide (conjugate **II**) with 5 μM of a linear CPP-additive (Cys-R10 **2**), in which both sequences consist of ten L-arginine residues. (Fig. 1e). With the CPP-additive **2**, nucleolar red fluorescence could be detected in more than 90% of cells, but in less than 5% without the additive (SI Fig. 5b). As comparison, we tested the delivery of mCherry-R10 **II** in presence of 10 or 150 μM of the endosomolytic peptide ppTG21[44,45]. Neither concentration led to efficient endosomal release, but instead to the formation of large, fluorescent aggregates in cells (SI Fig. 5c).

Finally, we performed uptake at 37°C with NLS-mCherry-R10 **II** and the CPP-additive **2** in presence of Alexa647-labelled Transferrin (which undergoes receptor-mediated endocytosis[46,47]) and endocytosis inhibitors (sodium azide, dynasore and pitstop 2). While we could see inhibition of the endocytosis of transferrin, we could detect nucleolar mCherry regardless of the inhibitor used (SI Fig. 6).

A thiol-reactive deca-arginine is a highly effective additive for delivering CPP-conjugated proteins

To further evaluate the high efficiency of the CPP-peptide additives **1** and **2** in our additive protocol and to probe the impact of the *N*-terminal thiol functionality, we synthesized additional linear CPPs **3**-**5** with different thiol derivatives (Fig. 2a). We then co-delivered 5 μM of CPP-conjugates of mCherry either linked to a linear (**II**) or cyclic R10 (**I**) (as above in Fig. 1 d-e) together with the newly synthesized peptides **1**-**5** into HeLa Kyoto cells and used microscopy to measure both nuclear and total fluorescence (representative pictures for all tested conditions in SI Fig. 7). Thereby, we quantified the desirable delivery to the nucleus and nucleoli (Fig. 2a), and also the amount of unwanted endosomal entrapment (SI Fig. 8, see

methods for details). Using unconjugated mCherry as a cargo did not result into any detectable intracellular florescence, while using mCherry-R10 conjugate **II** in combination with additive R10 peptide **2** led to nuclear/nucleolar staining as before (Fig. 2a, first two bars).

To exclude thiol-based interactions of the peptide, we capped the N-terminal Cys-residue with iodoacetamide in CPP **3**. Using **3**, we observed a sharp decrease in efficiency of the nuclear protein delivery in comparison to additive **2**, (Fig. 2a, grey and mint bars). To probe a potential dimerization of the CPP, following the previous observation of using disulfide-linked TAT dimers[21], we employed the dimer of Cys-R10 (**4**, red bar); however, no increase in efficiency over using the monomer **2** was visible in our case.

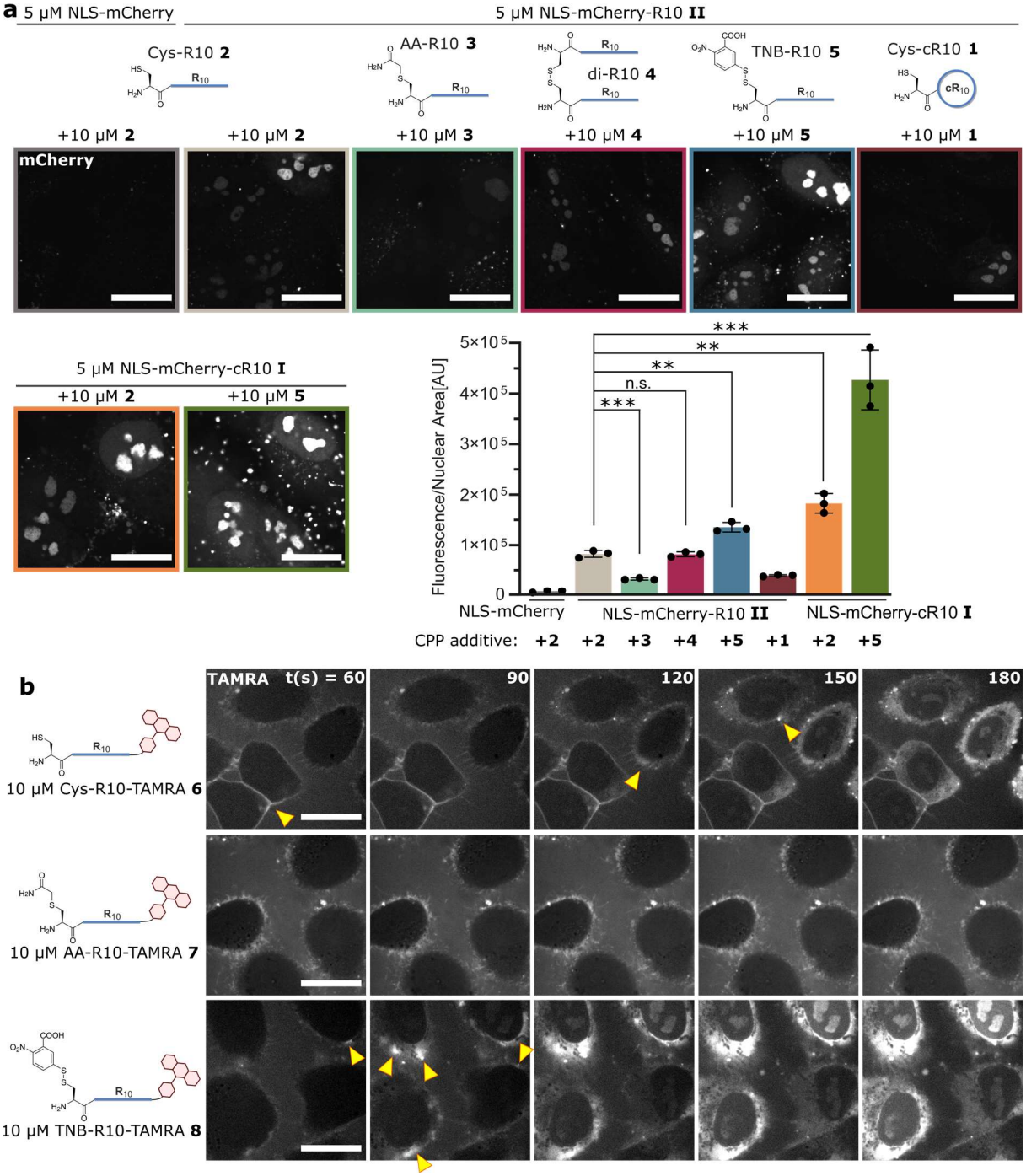

Fig. 2 TNB-R10 and its performance in delivering CPP-bearing cargoes into cells. a, Quantitative microscopy data showing the mean fluorescence intensity in the nucleus of mCherry-R10 conjugates **I** and **II** with R10-peptides **1**-**5** with representative microscopy images (pictures of at least 150 cells were taken in triplicates for each condition). Shown are individual values and mean ± standard deviation. Unpaired t-test, *** = P<0.0005, ** = P< 0.005, n.s. = not significant. **b**, Time-lapse experiments showing the cellular uptake of fluorescent R10 peptides with different head groups. Yellow arrowheads indicate nucleation zones where fluorescence is enriched before uptake into the cell. Scale bars 20 µm.

Based on these observations we hypothesized that the better delivery using peptide-additive **2** is due to the formation of disulfide bridges on the cell-surface.[48,49] Therefore, we synthesized a thio-nitro-benzoic acid activated R10-peptide (TNB-R10, **5**), which carries an electrophilic disulfide to accelerate the disulfide formation. Indeed, we observed more than 50% increase in nuclear mCherry fluorescence intensity as compared to the Cys-variant **2** (blue bar, Fig. 2a), and a significant increase in the fraction of nuclear fluorescence (SI Fig. 8).

Using the cyclic R10-peptide **1** as co-delivery agent decreased the uptake efficiency (Fig. 2a, brown bar), but using the mCherry-conjugate with the cyclic-R10 (**I**) made the delivery with additive **2** even more efficient (Fig. 2a, orange bar).

By far the highest nuclear fluorescence was observed with conjugate (**I**) in combination with the electrophilic disulfide additive **5** (Fig. 2a, green bar), although endosomal fluorescence was also increased under these conditions (SI Fig. 8).

Another clear advantage of using an additive to control the cytosolic delivery of cargoes is that it may allow more control over the delivered cargo concentration. To test this proposal, we added various amounts of NLS-mCherry-R10 to cells together with a constant concentration of peptide additive **5**. We could see a linear relationship between the amount of mCherry added to the cells and the resulting nucleolar fluorescence, indicating that it is possible to titrate a cargo into cells precisely (SI Fig. 9).

To obtain a better understanding of how the cysteine- and TNB-containing peptide additives perform better in cargo delivery, we synthesized fluorescent variants **6**-**8** of peptides **2**, **3** and **5**. We performed time-lapse uptake experiments of the peptides alone at 5, 10 and 20 µM concentration (Fig. 2b and complete data set in SI Fig. 10). All peptides showed rapid uptake into cells at 20 µM concentration, immediately after the appearance of bright spots on the membrane, which were previously described as “nucleation zones”[13,50]. At 10 µM

concentration, the acetylated peptide **7** did not show any uptake during the first 3 minutes, whereas the uptake was already complete for **6** and **8** (Fig. 2b). Notably, the TNB-modified peptide **8** (Fig 2b, bottom row) showed very quick uptake and very frequent formation of nucleation zones (yellow arrowheads, enlarged insets in SI Fig. 10). Similar observations could also be made with 5 µM peptide, although uptake was slower (SI Fig. 10). These findings suggest that the thiol-reactive head groups assist the peptide in forming these zones and crossing the membrane.

To ensure that this effect is due to the thiol-reactivity of the TNB-group, we pre-treated cells with a thiol-reactive maleimide that should at least partially block accessible cell-surface thiols. After this pre-treatment, the uptake of the TNB-R10 **8** was indeed slowed down considerably (SI Fig. 11b). The peptide was also not taken up at all in presence of the anionic polysaccharide heparin (SI Fig. 11c), showing that the electrostatic interactions between the polyarginine and cell are also crucial for uptake. We also investigated the addition of free, reduced cysteine into the cell medium during uptake[51]. Addition of cysteine neither sped up the uptake of the acetylated peptide **7** (SI Fig. 12) nor slowed down the uptake of the cysteine containing peptide **6** (SI Fig. 13).

To verify that these effects are independent of the position of the cysteine within the peptide, we also synthesized two additional cysteine-containing, fluorescent R10 peptides in which the cysteine was in a different position (within the polyarginine sequence or at the C-terminus). These peptides showed comparable rates of uptake to the previous peptide and they were also much faster than their acetylated counterparts (peptides **9**-**12**, SI Fig. 14).

Covalent immobilization of CPPs on the cell-surface allows delivery of large cargoes through the membrane

Next, we wanted to explore other cysteine-selective reactions in this context. Maleimides are also thiol-selective and form more stable bonds (under biological conditions) than disulfides,

which makes characterization easier. We first wanted to confirm that there are addressable, surface-exposed thiols on cells. To that end, we labelled cells with a cell-impermeable, maleimide-functionalized fluorophore (SI Fig. 15). The fluorophore showed effective membrane staining, which could be strongly reduced by first blocking thiols on the cells with Ellman's reagent (SI Fig. 15).

We then synthesized a fluorescent, maleimide-functionalized linear R10 (Maleimide-R10-Cy5) **13**, which can be traced separately by fluorescent microscopy. First, we wanted to confirm that this peptide shows similar uptake behavior as the fluorescent TAMRA-labeled TNB-activated R10 peptide **8**. Indeed, when the two fluorescent peptides are incubated with cells simultaneously, they stain the same nucleation zones and are taken up at similar rates (Fig. 3a and SI Fig. 16a), and peptide **13** also shows staining of nucleation zones alone (SI Fig. 16b).

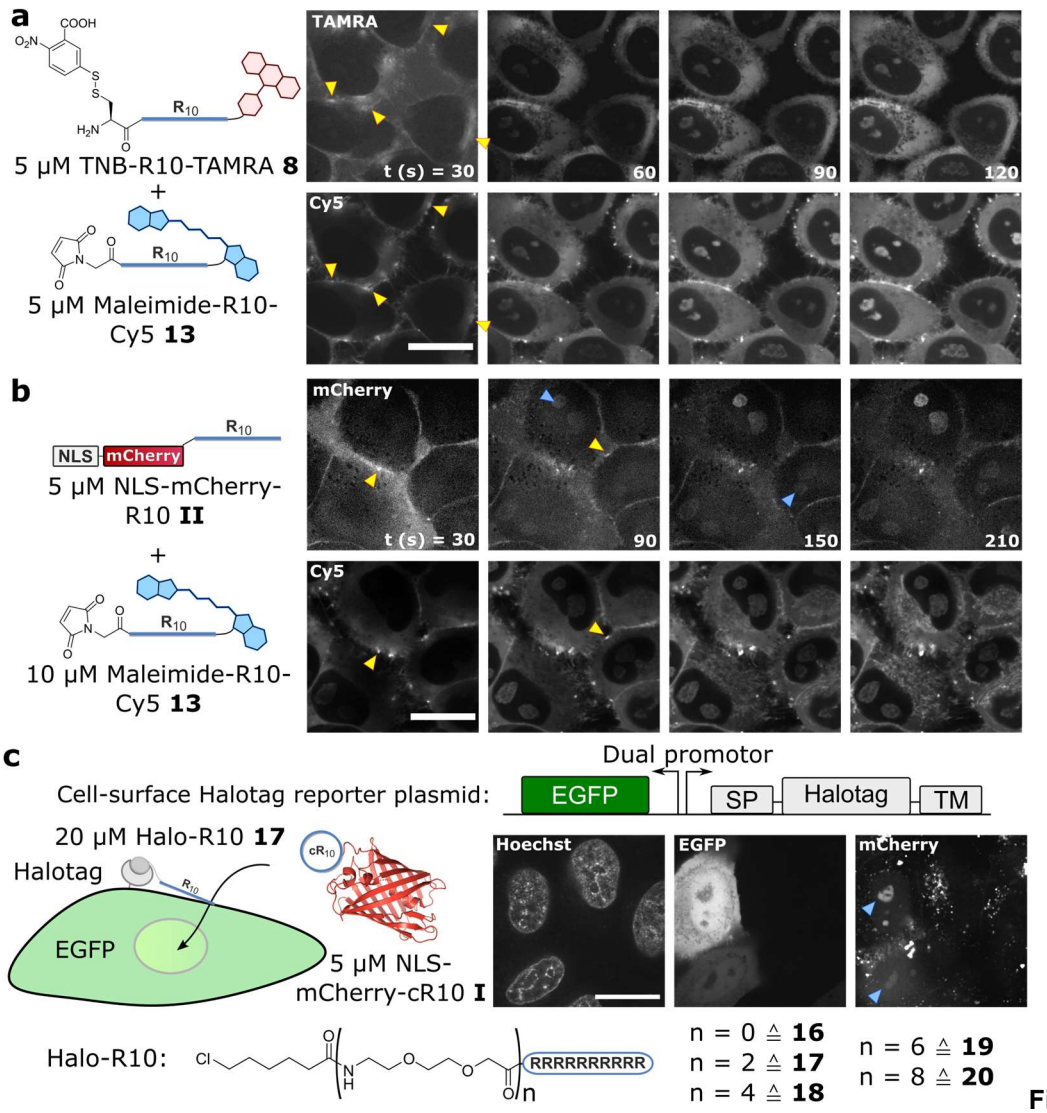

Fig. 3 Protein transduction into cells through CPP-labelled cell membranes. a, Time-lapse experiment of the simultaneous uptake of the TNB-R10-TAMRA **8** and Maleimide-R10-Cy5 **13** peptides into cells in cell medium. Yellow arrowheads indicate nucleation zones stained by both peptides. **b**, Time-lapse of the co-delivery of NLS-mCherry-R10 **II** together with the Maleimide-R10-Cy5 peptide **13** on HeLa Kyoto cells in cell medium. Yellow arrowheads indicate nucleation zones and blue arrowheads the appearance of nucleolar staining of the mCherry. **c**, Cellular uptake of NLS-mCherry-cR10 **I** in presence of chloroalkane-modified "Halo-R10" **17** on HeLa Kyoto cells transfected with EGFP-transmembrane-Halotag plasmid, 1 hour at 37°C in cell medium. SP: Signal peptide, TM: transmembrane sequence. Blue arrowheads show mCherry in the nucleoli of EGFP-positive cells. Uptake experiments with peptides **16** and **18-20** in SI Fig. 21. Scale bars 20 µm.

We then co-delivered R10-modified mCherry **II** together with the newly synthesized Maleimide-R10-Cy5 peptide **13** (Fig. 3b and SI Fig. 16c). We observed that the protein was localized at the same nucleation zones and is subsequently taken up into cells, although the protein requires more time to reach the nucleolus (note the longer steps in the time-lapse experiment). This observation supports the assumption that the protein crosses nucleation zones, which are "pre-labelled" by the reactive peptide additives.

As additional evidence for the covalent modification of a membrane component with **13**, we treated cells with the peptide and subsequently washed the cells with either medium or 50 µM Triton X-100 to remove unbound peptide. The peptide stained membranes even after washing with the detergent (SI Fig. 17). We also treated cells with **13** and delivered NLS-mCherry-R10 **II** into these cells after washing with 25 µg/mL heparin (SI Fig. 18). Washing with heparin should remove cell-penetrating peptides that are non-covalently bound to the cell membrane[20]. The successful delivery of mCherry **II** suggests that the covalently bound peptide can be sufficient for protein delivery.

To explore this concept further, we treated cells with peptides **2**, **3**, **5** or with a non-fluorescent maleimide-R10 peptide **14** in a first step. After certain time points, we removed the peptide solution and added the R10-conjugated mCherry **II** (SI Fig. 19). For the maleimide- and TNB-R10 peptides 5 and 12, we could still observe nuclear delivery after 5 minutes of "pre-labelling" with the peptide, and successful, albeit reduced, delivery of mCherry **II** after 30 minutes.

To identify potential reaction partners of the cysteine-reactive peptides, we synthesized a biotinylated version of the maleimide-R10 peptide (**15**) and applied it to cells followed by a streptavidin pulldown, tryptic digestion, and protein identification by mass spectrometry. Label-free-quantification of identified proteins revealed several membrane proteins enriched by the R10-peptide over untreated cells and a biotin-maleimide control (SI Fig. 20). This suggests that there is no single target but rather several proteins that the peptides can react with.

To investigate changes in the membrane at nucleation zones, we performed uptake of CPPs in the presence of the phosphatidylserine-binding protein annexin V. It had previously been suggested that the accumulation of CPPs at nucleation zones leads to a local membrane inversion, facilitating cargo uptake[52]. We could not detect any enrichment of phosphatidylserine (SI Fig. 21); however, we employed Flipper-TR, a fluorescent membrane tension probe[53] and could observe a reduction of membrane tension at nucleation zones, which points to a local deformation of the membrane (SI Fig. 22).

Taken together, our results support that thiol-reactive CPPs increase cellular delivery of cargoes through the covalent linking of peptides to the cell membrane. To elaborate this further we generated a plasmid that would lead to expression of an EGFP reporter inside transfected cells along with a Halotag[54] on the cell surface (simplified plasmid map in Fig. 3c, validation of the plasmid and additional controls in SI Fig. 23). We then synthesized a series of chloroalkane-modified R10 peptides **16-20** with varying polyethylene glycol linker lengths for covalent labeling of the expressed halotag. We then added the "Halo-R10" peptides **16-20** to the cells together with NLS-mCherry-cR10 **I**. We observed no nucleolar staining for the peptide with no ethylene glycol between the chloroalkane and the R10 peptide (SI Fig. 23c). For all peptides containing a linker, we saw nucleolar mCherry staining in transfected cells (Fig. 3c, blue arrows, cells showing EGFP signal and SI Fig. 23c peptides **18-20**), but not in untransfected cells. However, all cells showed significant endosomal uptake and 20 µM of the Halo-R10 were needed to achieve nucleolar staining. This lower efficiency may be due to the limited amount and reactivity of the halotag protein on the cell surface.

Cargo delivery using TNB-R10 is robust in various cell lines and accepts recombinant CPPs and cysteine-containing proteins

To test if membrane transduction of proteins can be achieved in different cell lines, we tested our protocol in four additional cancer cell lines from different tissue origin (A549, MDCK2, SJSA-1 and SKBR3). We recorded uptake and nucleolar staining of 5 µM mCherry-R10 **II** in

presence of 10 μM TNB-R10 **5** in all tested cell lines at 37°C (Fig. 4a-b and SI Fig. 24) and 4°C (SI Fig. 25).

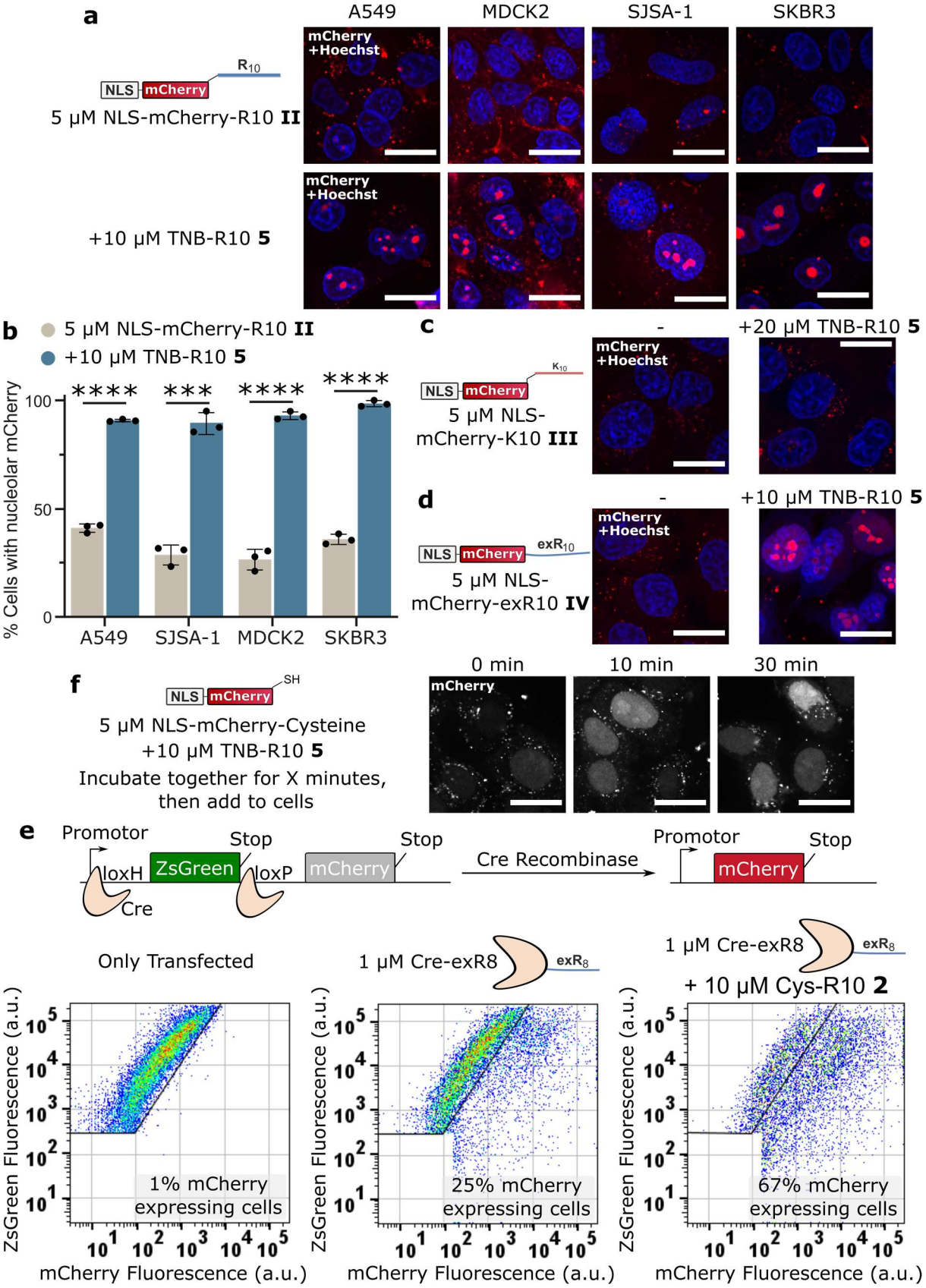

Fig. 4 Co-delivery with cysteine-reactive R10 peptides in different cell lines and with different

cargoes. a, Confocal microscopy images of four cancer cell lines treated with mCherry-R10 **II** and TNB-R10 **5**, for 1 hour at 37°C. **b**, Quantification of cells showing nucleolar fluorescence. At least 150 cells were counted over three biological replicates. Unpaired t-test, **** = P<0.0001, *** = P< 0.0005. **c**, Cellular uptake of K10-modified mCherry with or without TNB-R10 **5** at 37°C leads to endosomal staining and no nucleolar fluorescence. **d**, Cellular uptake of mCherry with recombinant R10 (exR10) shows endosomal or nucleolar staining in absence and presence of TNB-R10 **5**, respectively. **e**, Scheme showing the cre stoplight reporter plasmid and flow cytometry data of HeLa CCL-2 cells transfected with it and subsequently treated with Cre-exR8 with or without Cys-R10 (**2**). **f**, Disulfide CPP modification of mCherry and in situ cellular uptake. Scale bars 20 µm.

Most of our findings point to an energy-independent mode of uptake, but to probe whether TNB-R10 **5** can also lead to endosomal leakage of an entrapped cargo, we used peptide **5** on cells in combination with an mCherry variant (NLS-mCherry-K10 **III**) that had been modified with a K10 peptide (via maleimide chemistry, see SI Fig. 3). The K10 peptide should be sufficient to bring the protein in contact to the cell membrane and deliver it into endosomes through active transport, but should not transduce, as lysine-rich peptides do not share the crucial characteristics of arginine-rich peptides in membrane interaction[33,55]. Indeed, incubation of 5 µM mCherry-K10 alone or in combination with 20 µM peptide **5** did not lead to nuclear localization but only punctate fluorescence indicative of endosomal entrapment (Fig. 4c and SI Fig. 26).

Additionally, peptide **5** showed no signs of cytotoxicity or decreased cell viability up to 50 µM peptide (SI Fig. 27a). Cells that took up mCherry with or without **5** showed staining with Calcein AM, a cell-permeable caged fluorophore that shows intracellular fluorescence in cells with active metabolism (SI Fig. 27b). Performing the uptake in presence of the dead cell stain Sytox blue did also not lead to nuclear staining with the dye (SI Fig. 27c). Taken together, these experiments suggest that TNB-R10 peptide **5** does not lead to disruption of the endosomal or cellular membrane.

Methods of cargo delivery that rely on endosomal escape are often susceptible to the presence of serum, as they require effective endocytosis of both the cargo and the endosomolytic agent[21]. We hypothesized that peptide **5** would likely react with thiols in the serum, but the co-delivery with **2** (Cys-R10) should still function. While the presence of serum did lead to reduced efficiency at 10% serum, 5% serum or lower had a negligible effect on uptake (SI Figs. 28a, b). Interestingly, even in presence of serum the thiol-containing peptide **2** performed significantly better than the alkylated variant **3** (SI Fig 28a, b). Reduction in efficiency in presence of large amounts of serum may be due to the thiols in serum or the unspecific binding of CPPs to serum proteins[27].

We also tested if recombinantly expressed CPP-fusion proteins can be delivered, as these require much less equipment and effort to produce. To test this, we expressed and purified mCherry with a C-terminal R10 peptide (NLS-mCherry-exR10 **IV**, characterization in SI Fig. 29). mCherry-exR10 showed similar behavior to the semi-synthetic variant, showing predominantly endosomal uptake alone at a low, 5 µM concentration, which can be efficiently rescued by addition of peptide **5** (Fig. 4d and SI Fig. 30). This mCherry variant does not contain any cysteines, meaning it cannot form a disulfide with **5**, thus demonstrating that the recombinant polyarginine is enough for co-transport.

In the same vein, we also made mCherry variants modified with R5 and R8 peptides and co-delivered them into cells with TNB-R10 **5** (SI Figs. 31-32). The R8 peptide showed comparable results to the R10 peptide, while we saw a clear drop in efficiency with the R5 peptide.

Since peptide **5** can readily react with thiols, we tested if applying a labeling mixture of a protein containing a free thiol and CPP-additive **5** without intermediate work-up would facilitate the uptake protocol. Upon mixing 5 µM mCherry with a free cysteine were mixed with 15 µM peptide **5**, cell-permeability of the mCherry was already visible after ten minutes, which further improved after a 30-minute incubation (Fig. 4e). This same protocol also worked well for a

cysteine containing fluorescent nanobody (SI Fig. 33). It should be noted that here, the CPP is linked to both protein cargoes via an intracellularly cleavable disulfide, which results in broad nuclear staining (because of a nuclear antigen for the nanobody) as opposed to the nucleolar localization observed before[29,30].

To challenge our delivery protocol, we expressed and purified Cre recombinase fused to a C-terminal R8 peptide (Cre-exR8, characterization in SI Fig. 34). Fusions of Cre recombinase with the arginine-rich HIV TAT peptide have been previously reported to aid in cell uptake[56]. We transfected HeLa cells with a Cre activity reporter plasmid (Cre Stoplight 2.4[57]) that leads to a change in fluorescence from green to red when the enzyme is present within cells (Fig. 4f). We then treated cells with 1 μM Cre-exR8 alone or with added 10 μM Cys-R10 **2** in presence of 5% serum and then monitored expression of the reporter gene by flow cytometry and microscopy. As expected, the addition of peptide led to a strong increase in expression of the Cre reporter, indicating successful delivery of active Cre into the nucleus (Fig. 4f and microscopy in SI Fig. 35).

The TNB-R10 CPP-additive allows cytosolic delivery of functional IgG-antibodies

Antibodies are exceptionally useful proteins in molecular biology and pharmacology, targeting most of the human proteome. Nevertheless, the cellular delivery of full-length antibodies is particularly challenging due to the complex and quite large architecture with a molecular weight of 150 kDa and a length of 15 nanometers, approximately. Some methods to deliver full length antibodies into cells already exist, although they mostly rely on endosomal escape[21,23]. To test whether we can deliver a full-length IgG antibody into cells at 4°C, we first used the fluorescently labeled therapeutic antibody Brentuximab. Thiolation was performed with 2-iminothiolane[58]. As before, by addition of peptide **5**, the antibody can be modified with the cell-penetrating peptide via a disulfide bond, while the excess cell-penetrating peptide should simultaneously aid in the cellular uptake (Fig. 5a). Indeed, treatment of cells with the antibody led to cellular delivery at 37°C, but not in the absence of CPP-additive **5** (Fig. 5b). A fluorescent

signal could not be observed in the nucleus (counterstained with Hoechst), which is likely due to the size of the antibody excluding it from permeation through nuclear pores. Even at 4°C, antibody uptake could also be observed in most cells demonstrating energy-independent membrane transduction of an antibody (Fig. 5b).

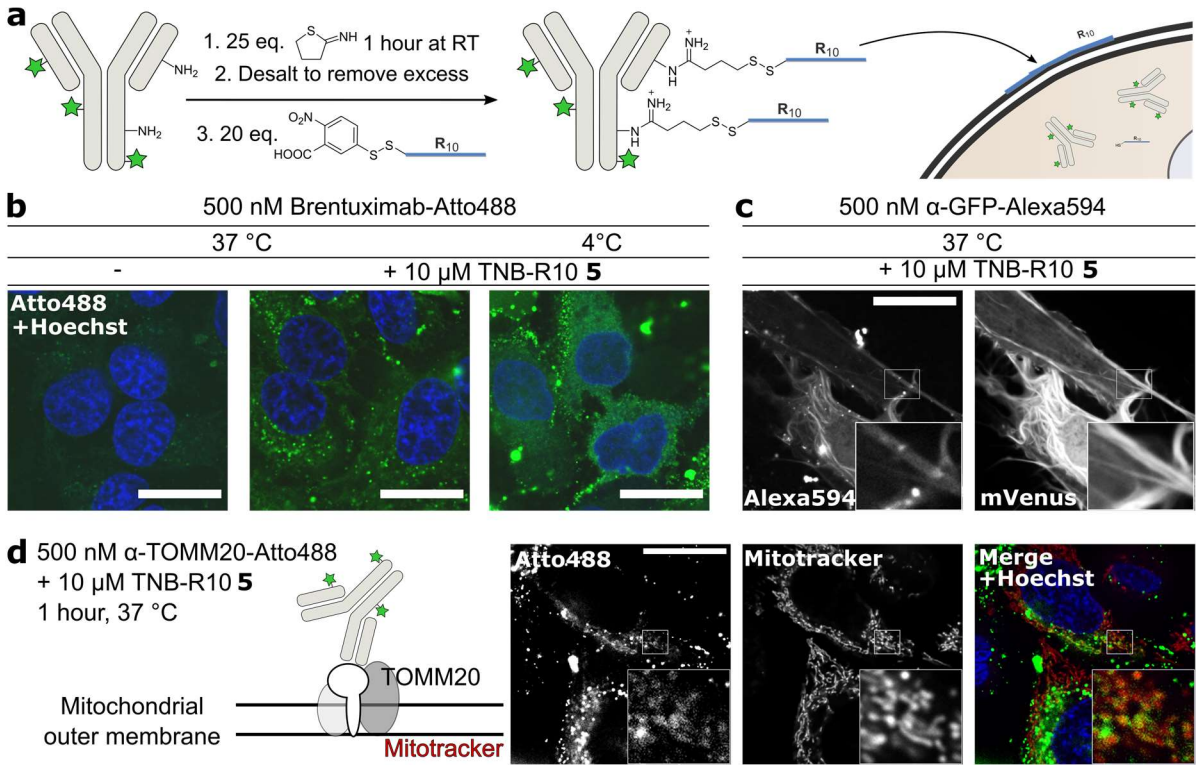

Fig. 5 The application of TNB-R10 in IgG antibody delivery. a, Method of delivering antibodies into cells using TNB-R10. **b**, Cellular uptake of 500 nM Atto488-labelled Brentuximab into HeLa CCL-2 cells in presence and absence of TNB-R10 **5** and at 37 and 4°C. Cells counterstained with Hoechst 33342 to demonstrate exclusion of the antibody from the nucleus. **c**, Cellular uptake of 500 nM Alexa594-labelled anti-GFP antibody into HeLa CCL-2 cells transfected with Lifeact-mVenus. **d**, Cellular uptake of 500 nM Atto488-labelled anti-TOMM20 antibody into HeLa CCL-2 cells, simultaneously treated with MitoTracker Red CMXROS. Scale bars 20 μm.

To validate that the delivered antibodies are still intact and functional after cellular uptake, we subsequently tested two additional commercial antibodies in our protocols. Here, we first transfected a plasmid encoding a GFP mutant (Lifeact-mVenus) into HeLa cells and functionalized a fluorescently labelled (Alexa 594) anti-GFP antibody as before. Incubation of

cells with the antibody showed uptake of the antibody into cells and colocalization of the antibody and mVenus signals within the cell (Fig. 5c, pearson correlation coefficient (PCC) in shown inset = 0.80).

Finally, we also tested an antibody against the endogenous mitochondrial receptor TOMM20. As with Brentuximab, we first fluorescently labelled the antibody, followed by thiolation and mixing with CPP-additive **5**. Incubation of HeLa cells with the mixture and a mitochondrial marker (MitoTracker Red CMXRos) led to noticeable endosomal entrapment, but also visible colocalization of the two components (Fig. 5d, PCC in shown inset = 0.58).

Discussion

Over the past years, a diverse array of methods for the delivery of biomolecules into cells has been developed[2]. Still, we believe that cell-penetrating-peptide-mediated delivery is among the top methodologies, particularly with respect to synthetic flexibility. Nevertheless, advancing the delivery of CPP-protein and –antibody conjugates with even better uptake properties remains challenging and requires often laborious chemical protein engineering.

Through our work, we have shown delivery of various cargoes with both synthetic and recombinant CPPs using thiol-reactive R10 peptides. This uptake seems to be independent of active transport and is not harmful to the cell. Cysteine, as well as thiol-reactive species have been described in the context of cellular uptake before[35,36]. The thiol-reactivity of the CPPs we describe seems to be a crucial factor in our additive protocol and in investigating it further we find that we can co-valently label cell-surfaces through which we can then deliver cargoes. We believe that this may develop into a valuable tool in achieving cell-specific delivery of cargoes, if one can only modify cells of a certain type. This could have great therapeutic potential, for example in gene editing, and should be pursued further.

As the TNB-R10 **5** also quickly reacts with thiol residues on biomolecules to form bio-reversible disulfide bonds, it allows a “covalent transfection” that is immediately applicable to many protein substrates. Importantly, no purification is required after addition of the peptide, since the excess directly acts as the CPP-additive, thereby strongly enhancing uptake of the protein cargo. Furthermore, we show that even IgG antibodies without any free cysteines can be thiolated to allow usage of peptide **5**, whereas the thiolation could, in principle, also be done in a reversible manner.

An essential benefit in our protocol is the possibility to perform uptake at 4°C. Thereby, no active endosomal uptake occurs, which allows the delivery of compounds that are sensitive to endosomal degradation or toxic for the cell upon prolonged exposure. Another key advantage in our findings is the ability to employ proteins from standard recombinant expression, in which the protein cargo is genetically fused to an oligo-Arg tag, and use them in non-endocytic uptake. Using these, our protocol allows a straightforward evaluation of CPP-additives to enhance uptake. Using this co-delivery strategy, we could deliver active Cre recombinase into cells without any necessary conjugation chemistry. We achieve efficient gene editing, which could easily be applied to the delivery of other functional enzymes. We have demonstrated the cytosolic delivery of three different antibodies using CPP-additives, resulting in the expected intracellular localization. Because of their high efficiency and lack of measurable cellular toxicity, we envision our CPP-additives to become important tools in cell biology.

This work is an important step in advancing the field biomolecule delivery with applications ranging from the intracellular immunostaining demonstrated here to the design of next generation biopharmaceuticals. Our future work will be directed at making use of this technique in going beyond cell culture to tissue culture and even simple model organisms.

Data Availability

Additional data and methodologies are found in the supplementary information. All plasmids used in this study and their sequence information are available from the authors upon request.

References

1 Fu, A., Tang, R., Hardie, J., Farkas, M. E. & Rotello, V. M. Promises and pitfalls of intracellular delivery of proteins. *Bioconjug Chem* **25**, 1602-1608, doi:10.1021/bc500320j (2014).

2 Du, S., Liew, S. S., Li, L. & Yao, S. Q. Bypassing Endocytosis: Direct Cytosolic Delivery of Proteins. *J Am Chem Soc*, doi:10.1021/jacs.8b06584 (2018).

3 Wang, F. *et al.* Recent progress of cell-penetrating peptides as new carriers for intracellular cargo delivery. *J Control Release* **174**, 126-136, doi:10.1016/j.jconrel.2013.11.020 (2014).

4 Viscidi, R. P., Mayur, K., Lederman, H. M. & Frankel, A. D. Inhibition of antigen-induced lymphocyte proliferation by Tat protein from HIV-1. *Science* **246**, 1606-1608, doi:10.1126/science.2556795 (1989).

5 Joliot, A. H., Triller, A., Volovitch, M., Pernelle, C. & Prochiantz, A. alpha-2,8-Polysialic acid is the neuronal surface receptor of antennapedia homeobox peptide. *New Biol* **3**, 1121-1134 (1991).

6 Derossi, D., Joliot, A. H., Chassaing, G. & Prochiantz, A. The third helix of the Antennapedia homeodomain translocates through biological membranes. *J Biol Chem* **269**, 10444-10450 (1994).

7 Borrelli, A., Tornesello, A. L., Tornesello, M. L. & Buonaguro, F. M. Cell Penetrating Peptides as Molecular Carriers for Anti-Cancer Agents. *Molecules* **23**, doi:10.3390/molecules23020295 (2018).

8 Guidotti, G., Brambilla, L. & Rossi, D. Cell-Penetrating Peptides: From Basic Research to Clinics. *Trends Pharmacol Sci* **38**, 406-424, doi:10.1016/j.tips.2017.01.003 (2017).

9 Richard, J. P. *et al.* Cellular uptake of unconjugated TAT peptide involves clathrin-dependent endocytosis and heparan sulfate receptors. *J Biol Chem* **280**, 15300-15306, doi:10.1074/jbc.M401604200 (2005).

10 Fittipaldi, A. *et al.* Cell membrane lipid rafts mediate caveolar endocytosis of HIV-1 Tat fusion proteins. *J Biol Chem* **278**, 34141-34149, doi:10.1074/jbc.M303045200 (2003).

11 Ben-Dov, N. & Korenstein, R. The uptake of HIV Tat peptide proceeds via two pathways which differ from macropinocytosis. *Biochim Biophys Acta* **1848**, 869-877, doi:10.1016/j.bbamem.2014.12.015 (2015).

12 Herce, H. D., Garcia, A. E. & Cardoso, M. C. Fundamental molecular mechanism for the cellular uptake of guanidinium-rich molecules. *J. Am. Chem. Soc.* **136**, 17459-17467, doi:10.1021/ja507790z (2014).

13 Duchardt, F., Fotin-Mleczek, M., Schwarz, H., Fischer, R. & Brock, R. A comprehensive model for the cellular uptake of cationic cell-penetrating peptides. *Traffic* **8**, 848-866, doi:10.1111/j.1600-0854.2007.00572.x (2007).

14 Futaki, S. & Nakase, I. Cell-Surface Interactions on Arginine-Rich Cell-Penetrating Peptides Allow for Multiplex Modes of Internalization. *Acc Chem Res* **50**, 2449-2456, doi:10.1021/acs.accounts.7b00221 (2017).

15 He, L., Sayers, E. J., Watson, P. & Jones, A. T. Contrasting roles for actin in the cellular uptake of cell penetrating peptide conjugates. *Sci Rep* **8**, 7318, doi:10.1038/s41598-018-25600-8 (2018).

16 Patel, S. G. *et al.* Cell-penetrating peptide sequence and modification dependent uptake and subcellular distribution of green florescent protein in different cell lines. *Sci Rep* **9**, 6298, doi:10.1038/s41598-019-42456-8 (2019).

17 Tunnemann, G. *et al.* Cargo-dependent mode of uptake and bioavailability of TAT-containing proteins and peptides in living cells. *FASEB J.* **20**, 1775-1784, doi:10.1096/fj.05-5523com (2006).

18 Verdurmen, W. P., Thanos, M., Ruttekolk, I. R., Gulbins, E. & Brock, R. Cationic cell-penetrating peptides induce ceramide formation via acid sphingomyelinase: implications for uptake. *J Control Release* **147**, 171-179, doi:10.1016/j.jconrel.2010.06.030 (2010).

19 Takeuchi, T. *et al.* Direct and rapid cytosolic delivery using cell-penetrating peptides mediated by pyrenebutyrate. *ACS Chem Biol* **1**, 299-303, doi:10.1021/cb600127m (2006).
20 Wadia, J. S., Stan, R. V. & Dowdy, S. F. Transducible TAT-HA fusogenic peptide enhances escape of TAT-fusion proteins after lipid raft macropinocytosis. *Nat Med* **10**, 310-315, doi:10.1038/nm996 (2004).
21 Erazo-Oliveras, A. *et al.* Protein delivery into live cells by incubation with an endosomolytic agent. *Nat Methods* **11**, 861-867, doi:10.1038/nmeth.2998 (2014).
22 Allen, J. *et al.* Cytosolic Delivery of Macromolecules in Live Human Cells Using the Combined Endosomal Escape Activities of a Small Molecule and Cell Penetrating Peptides. *ACS Chem Biol*, doi:10.1021/acschembio.9b00585 (2019).
23 Akishiba, M. *et al.* Cytosolic antibody delivery by lipid-sensitive endosomolytic peptide. *Nature Chemistry*, doi:10.1038/nchem.2779 (2017).
24 Morris, M. C., Depollier, J., Mery, J., Heitz, F. & Divita, G. A peptide carrier for the delivery of biologically active proteins into mammalian cells. *Nat Biotechnol* **19**, 1173-1176, doi:10.1038/nbt1201-1173 (2001).
25 Reichart, F., Horn, M. & Neundorf, I. Cyclization of a cell-penetrating peptide via click-chemistry increases proteolytic resistance and improves drug delivery. *J Pept Sci* **22**, 421-426, doi:10.1002/psc.2885 (2016).
26 Dougherty, P. G., Sahni, A. & Pei, D. Understanding Cell Penetration of Cyclic Peptides. *Chem Rev* **119**, 10241-10287, doi:10.1021/acs.chemrev.9b00008 (2019).
27 Lattig-Tunnemann, G. *et al.* Backbone rigidity and static presentation of guanidinium groups increases cellular uptake of arginine-rich cell-penetrating peptides. *Nat Commun* **2**, 453, doi:10.1038/ncomms1459 (2011).
28 Nischan, N. *et al.* Covalent attachment of cyclic TAT peptides to GFP results in protein delivery into live cells with immediate bioavailability. *Angewandte Chemie* **54**, 1950-1953, doi:10.1002/anie.201410006 (2015).
29 Schneider, A. F. L., Wallabregue, A. L. D., Franz, L. & Hackenberger, C. P. R. Targeted Subcellular Protein Delivery Using Cleavable Cyclic Cell-Penetrating Peptides. *Bioconjug Chem* **30**, 400-404, doi:10.1021/acs.bioconjchem.8b00855 (2019).
30 Herce, H. D. *et al.* Cell-permeable nanobodies for targeted immunolabelling and antigen manipulation in living cells. *Nat Chem* **9**, 762-771, doi:10.1038/nchem.2811 (2017).
31 Medina, S. H. *et al.* An Intrinsically Disordered Peptide Facilitates Non-Endosomal Cell Entry. *Angewandte Chemie* **55**, 3369-3372, doi:10.1002/anie.201510518 (2016).
32 Jones, A. T. & Sayers, E. J. Cell entry of cell penetrating peptides: tales of tails wagging dogs. *J Control Release* **161**, 582-591, doi:10.1016/j.jconrel.2012.04.003 (2012).
33 Robison, A. D. *et al.* Polyarginine Interacts More Strongly and Cooperatively than Polylysine with Phospholipid Bilayers. *J Phys Chem B* **120**, 9287-9296, doi:10.1021/acs.jpcb.6b05604 (2016).
34 Shi, J. & Schneider, J. P. De novo Design of Selective Membrane-Active Peptides by Enzymatic Control of Their Conformational Bias on the Cell Surface. *Angewandte Chemie* **58**, 13706-13710, doi:10.1002/anie.201902470 (2019).
35 Aubry, S. *et al.* Cell-surface thiols affect cell entry of disulfide-conjugated peptides. *FASEB J* **23**, 2956-2967, doi:10.1096/fj.08-127563 (2009).
36 Gasparini, G., Sargsyan, G., Bang, E. K., Sakai, N. & Matile, S. Ring Tension Applied to Thiol-Mediated Cellular Uptake. *Angewandte Chemie* **54**, 7328-7331, doi:10.1002/anie.201502358 (2015).
37 Martin, R. M., Herce, H. D., Ludwig, A. K. & Cardoso, M. C. Visualization of the Nucleolus in Living Cells with Cell-Penetrating Fluorescent Peptides. *Methods Mol Biol* **1455**, 71-82, doi:10.1007/978-1-4939-3792-9_6 (2016).
38 Martin, R. M., Tunnemann, G., Leonhardt, H. & Cardoso, M. C. Nucleolar marker for living cells. *Histochem Cell Biol* **127**, 243-251, doi:10.1007/s00418-006-0256-4 (2007).
39 Leonhardt, H. *et al.* Dynamics of DNA replication factories in living cells. *J Cell Biol* **149**, 271-280, doi:10.1083/jcb.149.2.271 (2000).
40 Chagin, V. O. *et al.* 4D Visualization of replication foci in mammalian cells corresponding to individual replicons. *Nat Commun* **7**, 11231, doi:10.1038/ncomms11231 (2016).
41 Hunt, L. *et al.* Low-temperature pausing of cultivated mammalian cells. *Biotechnol Bioeng* **89**, 157-163, doi:10.1002/bit.20320 (2005).
42 Goldenthal, K. L., Pastan, I. & Willingham, M. C. Initial steps in receptor-mediated endocytosis. The influence of temperature on the shape and distribution of plasma membrane clathrin-coated pits in cultured mammalian cells. *Exp Cell Res* **152**, 558-564, doi:10.1016/0014-4827(84)90658-x (1984).

43 Melchior, F., Guan, T., Yokoyama, N., Nishimoto, T. & Gerace, L. GTP hydrolysis by Ran occurs at the nuclear pore complex in an early step of protein import. *J Cell Biol* **131**, 571-581, doi:10.1083/jcb.131.3.571 (1995).
44 Rittner, K. *et al.* New basic membrane-destabilizing peptides for plasmid-based gene delivery in vitro and in vivo. *Mol Ther* **5**, 104-114, doi:10.1006/mthe.2002.0523 (2002).
45 Rouet, R. *et al.* Receptor-Mediated Delivery of CRISPR-Cas9 Endonuclease for Cell-Type-Specific Gene Editing. *J Am Chem Soc* **140**, 6596-6603, doi:10.1021/jacs.8b01551 (2018).
46 Mayle, K. M., Le, A. M. & Kamei, D. T. The intracellular trafficking pathway of transferrin. *Biochim Biophys Acta* **1820**, 264-281, doi:10.1016/j.bbagen.2011.09.009 (2012).
47 Ter-Avetisyan, G. *et al.* Cell entry of arginine-rich peptides is independent of endocytosis. *J. Biol. Chem.* **284**, 3370-3378, doi:10.1074/jbc.M805550200 (2009).
48 Gasparini, G. *et al.* Cellular uptake of substrate-initiated cell-penetrating poly(disulfide)s. *J Am Chem Soc* **136**, 6069-6074, doi:10.1021/ja501581b (2014).
49 Fu, J., Yu, C., Li, L. & Yao, S. Q. Intracellular Delivery of Functional Proteins and Native Drugs by Cell-Penetrating Poly(disulfide)s. *J Am Chem Soc* **137**, 12153-12160, doi:10.1021/jacs.5b08130 (2015).
50 Wallbrecher, R. *et al.* Membrane permeation of arginine-rich cell-penetrating peptides independent of transmembrane potential as a function of lipid composition and membrane fluidity. *J Control Release* **256**, 68-78, doi:10.1016/j.jconrel.2017.04.013 (2017).
51 Wei, Y., Tang, T. & Pang, H. B. Cellular internalization of bystander nanomaterial induced by TAT-nanoparticles and regulated by extracellular cysteine. *Nat Commun* **10**, 3646, doi:10.1038/s41467-019-11631-w (2019).
52 Hirose, H. *et al.* Transient focal membrane deformation induced by arginine-rich peptides leads to their direct penetration into cells. *Mol Ther* **20**, 984-993, doi:10.1038/mt.2011.313 (2012).
53 Colom, A. *et al.* A fluorescent membrane tension probe. *Nat Chem* **10**, 1118-1125, doi:10.1038/s41557-018-0127-3 (2018).
54 England, C. G., Luo, H. & Cai, W. HaloTag technology: a versatile platform for biomedical applications. *Bioconjug Chem* **26**, 975-986, doi:10.1021/acs.bioconjchem.5b00191 (2015).
55 Tesei, G. *et al.* Self-association of a highly charged arginine-rich cell-penetrating peptide. *Proc Natl Acad Sci U S A* **114**, 11428-11433, doi:10.1073/pnas.1712078114 (2017).
56 Peitz, M., Pfannkuche, K., Rajewsky, K. & Edenhofer, F. Ability of the hydrophobic FGF and basic TAT peptides to promote cellular uptake of recombinant Cre recombinase: a tool for efficient genetic engineering of mammalian genomes. *Proc Natl Acad Sci U S A* **99**, 4489-4494, doi:10.1073/pnas.032068699 (2002).
57 Yang, Y. S. & Hughes, T. E. Cre stoplight: a red/green fluorescent reporter of Cre recombinase expression in living cells. *Biotechniques* **31**, 1036, 1038, 1040-1031, doi:10.2144/01315st03 (2001).
58 Jue, R., Lambert, J. M., Pierce, L. R. & Traut, R. R. Addition of sulfhydryl groups to Escherichia coli ribosomes by protein modification with 2-iminothiolane (methyl 4-mercaptobutyrimidate). *Biochemistry* **17**, 5399-5406, doi:10.1021/bi00618a013 (1978).

Acknowledgements

The authors thank members of the Hackenberger lab for comments and discussion and Kristin Kemnitz-Hassanin and Ines Kretzschmar for technical support. The authors thank Dominik Schumacher and Heinrich Leonhardt for providing the Brentuximab antibody. This work was supported by grants from the Deutsche Forschungsgemeinschaft (SPP1623) to C.P.R.H. (HA 4468/9-1) and M.C.C. (CA 198/8-2), the Einstein Foundation Berlin (Leibniz-Humboldt Professorship) and the Boehringer-Ingelheim Foundation (Plus 3 award) to C.P.R.H., the Fonds der Chemischen Industrie (FCI) to C.P.R.H. and A.F.L.S. (Chemiefonds fellowship).

Author contributions

A.F.L.S., M.L., M.C.C. and C.P.R.H. conceived the experiments and wrote the manuscript. A.F.L.S. cloned, expressed, purified and characterized proteins, synthesized and characterized peptides and protein-peptide conjugates, performed uptake, cell viability, microscopy and flow cytometry experiments. M.L. performed microscopy experiments and wrote the quantification script together with A.F.L.S.. M. K. performed the Calcein AM staining.

Competing interests

The technology described in this manuscript is part of a patent application by A.F.L.S., M.L., and C.P.R.H..

Additional information

-

Cellular uptake of Large Biomolecules Enabled by Cell-surface-reactive Cell-penetrating Peptide Additives

Anselm F. L. Schneider[1,2], Marina Kithil[3], M. Cristina Cardoso[3], Martin Lehmann[1] and Christian P. R. Hackenberger*[1,4]

[1] Leibniz-Forschungsinstitut für Molekulare Pharmakologie (FMP), Robert-Rössle-Strasse 10, 13125 Berlin, Germany

[2] Institute of Chemistry and Biochemistry, Freie Universität Berlin, Takustrasse 3, 14189 Berlin, Germany

[3] Technische Universität Darmstadt, Schnittspahnstr. 10, 64287 Darmstadt, Germany

[4] Department of Chemistry, Humboldt-Universität zu Berlin, Brook-Taylor-Strasse 2, 12489 Berlin, Germany

*Corresponding author

Supporting Information

Table of Contents

Supporting Figures

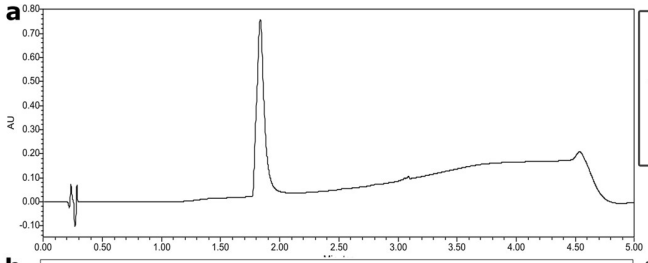

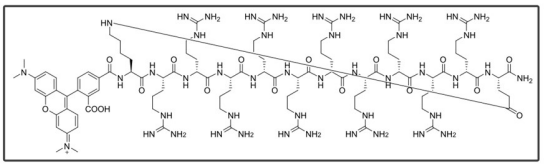

TAMRA-cR10

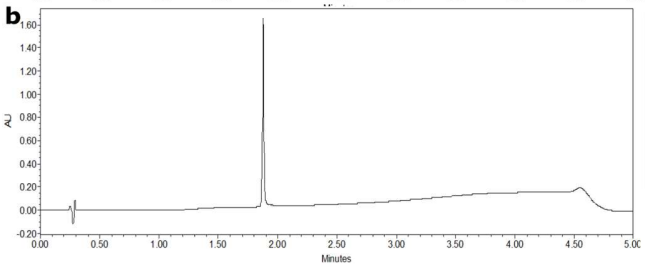

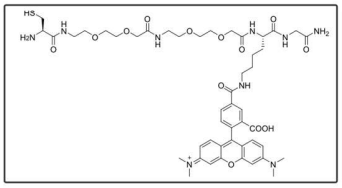

Cys-TAMRA (for EPL)

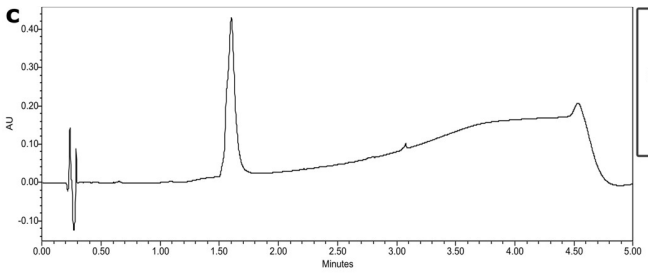

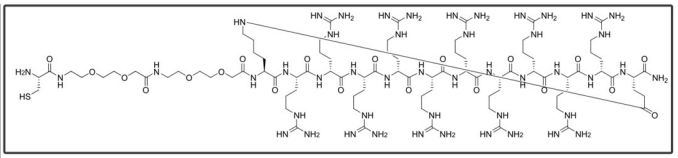

Cys-cR10 **1**

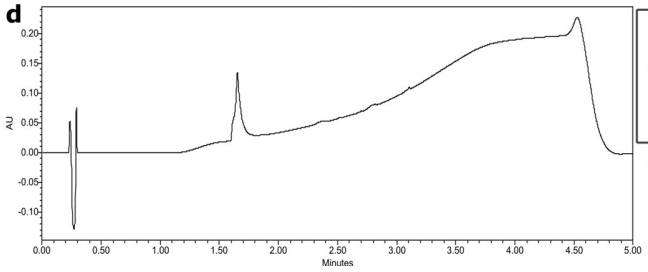

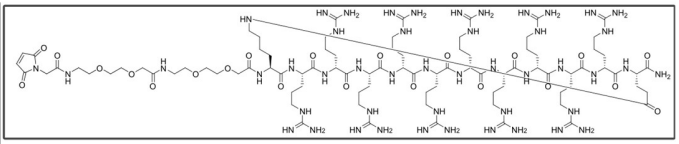

Maleimide-cR10

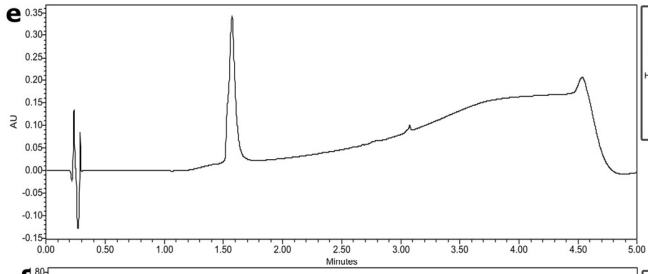

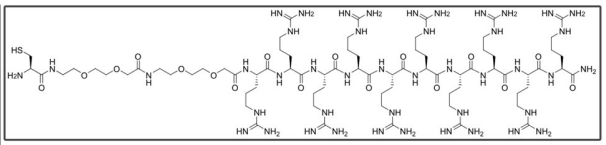

Cys-R10 **2**

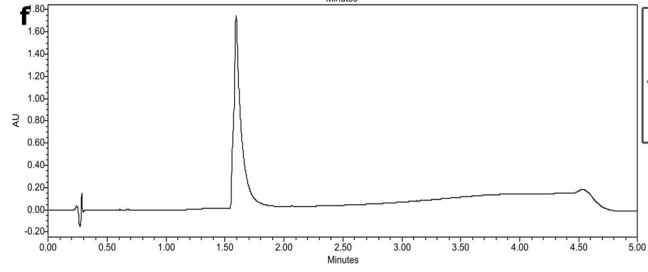

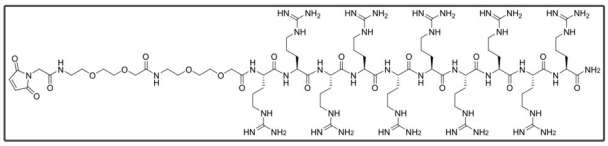

Maleimide-R10 **14**

g

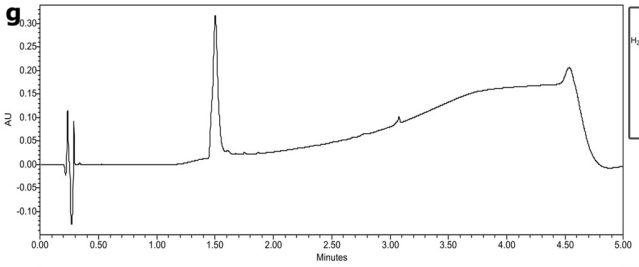

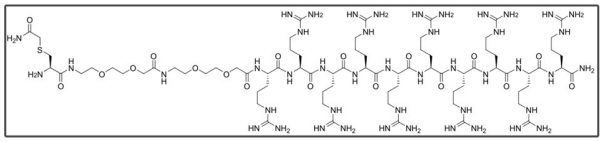

AA-R10 **3**

h

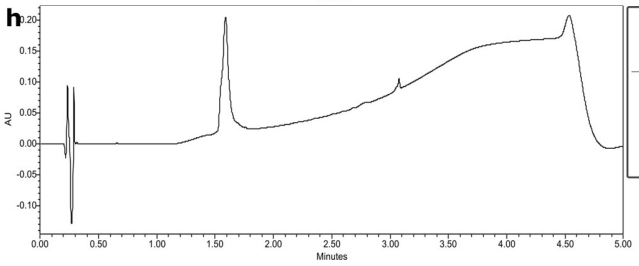

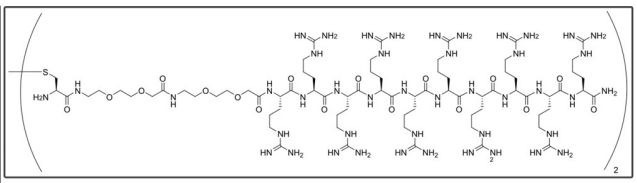

di-R10 **4**

i

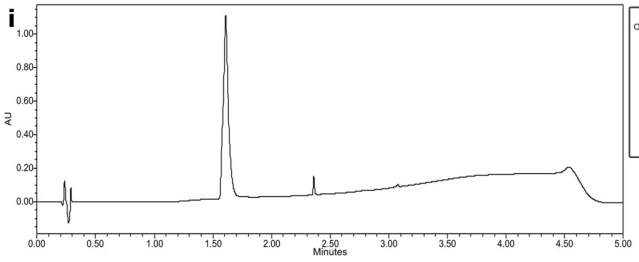

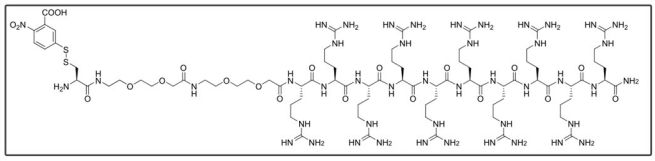

TNB-R10 **5**

j

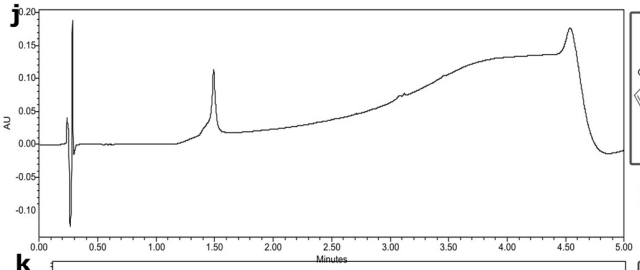

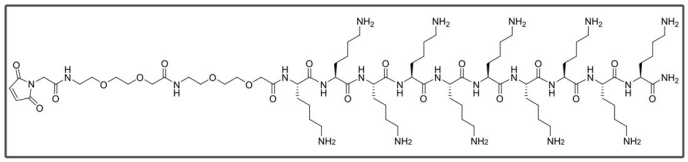

Maleimide-K10

k

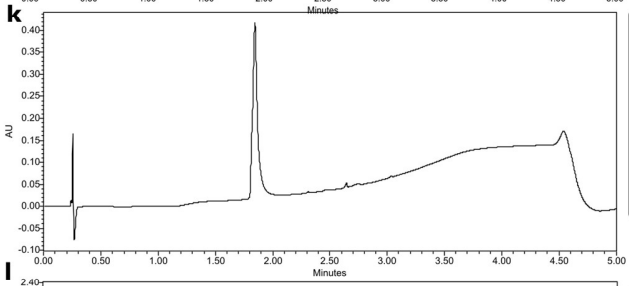

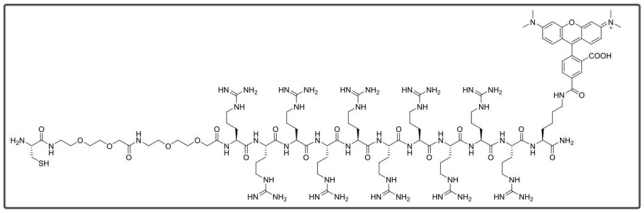

Cys-R10-TAMRA **6**

l

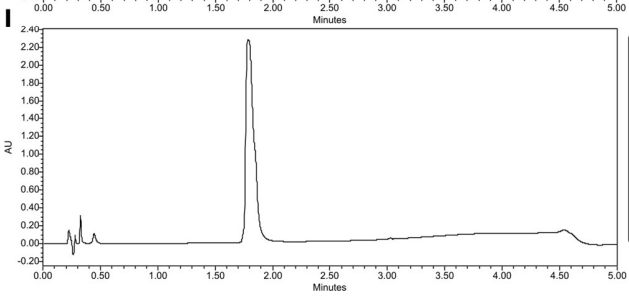

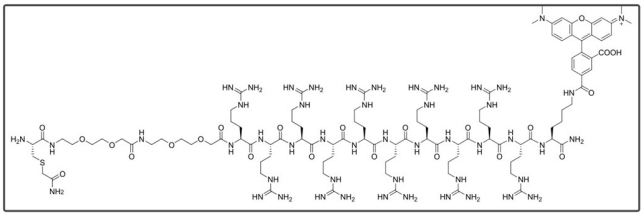

AA-R10-TAMRA **7**

m

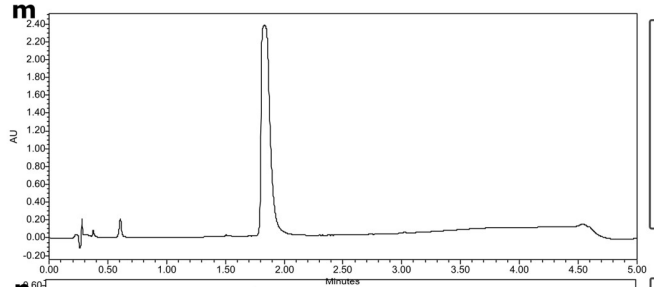

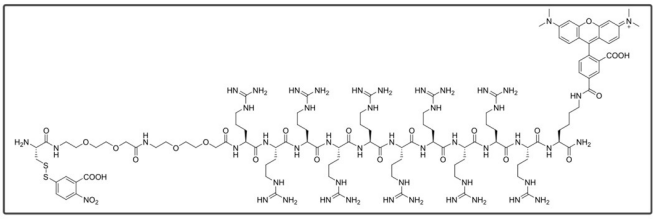

TNB-R10-TAMRA **8**

n

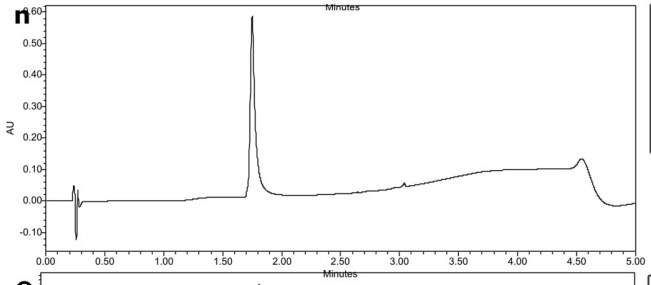

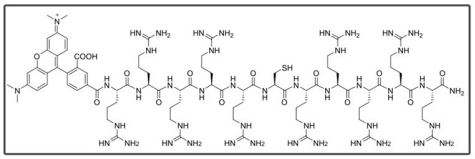

TAMRA-R5-Cys-R5 **9**

o

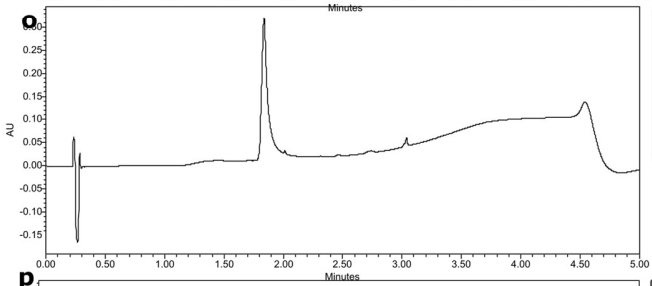

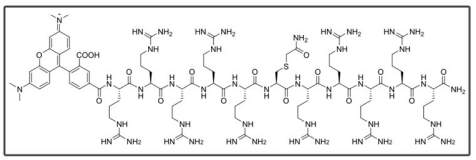

TAMRA-R5-AA-R5 **10**

p

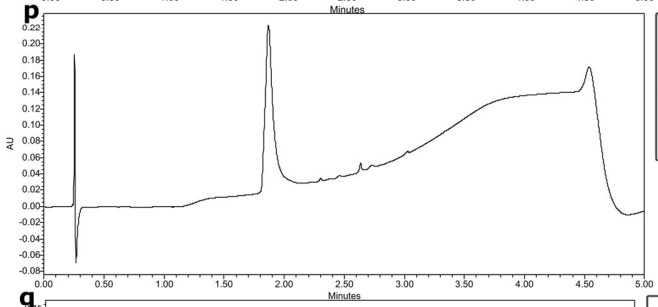

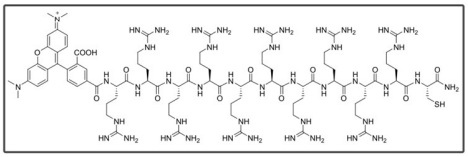

TAMRA-R10-Cys **11**

q

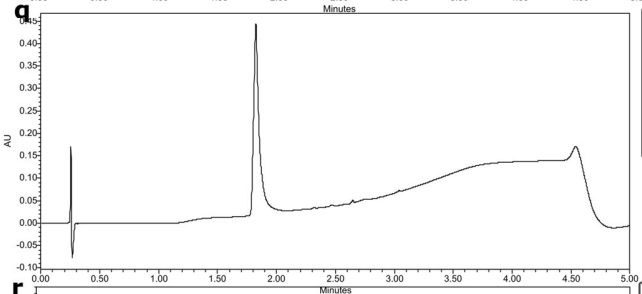

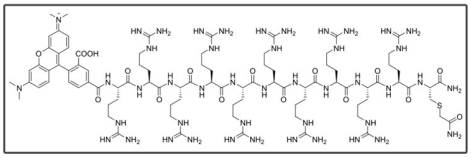

TAMRA-R10-AA **12**

r

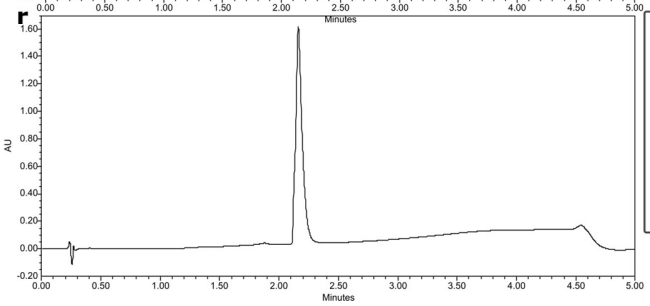

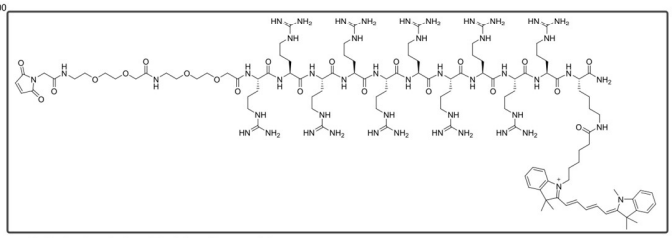

Maleimide-R10-Cy5 **13**

s

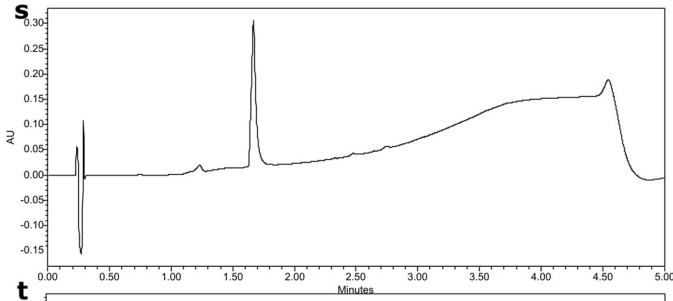

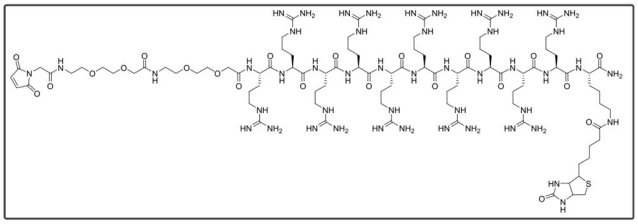

Maleimide-R10-Biotin **15**

t

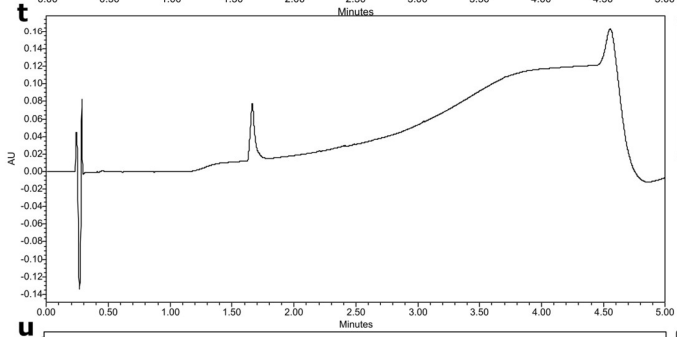

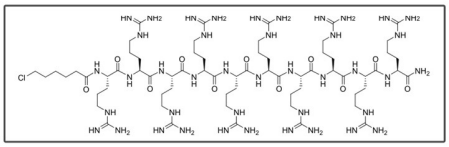

Halo-R10 **16**

u

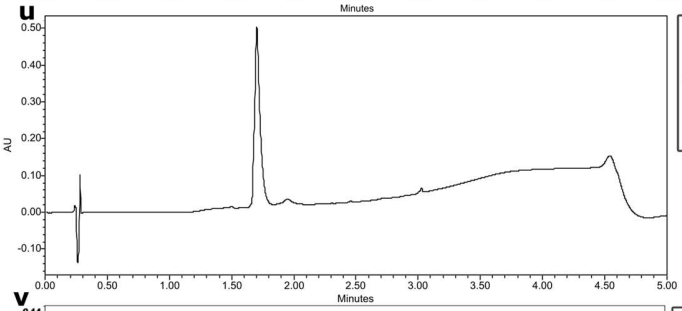

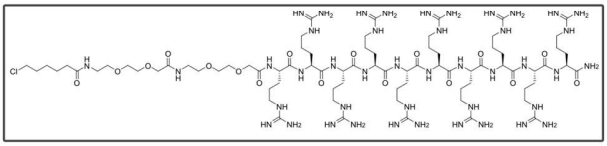

Halo-R10 **17**

v

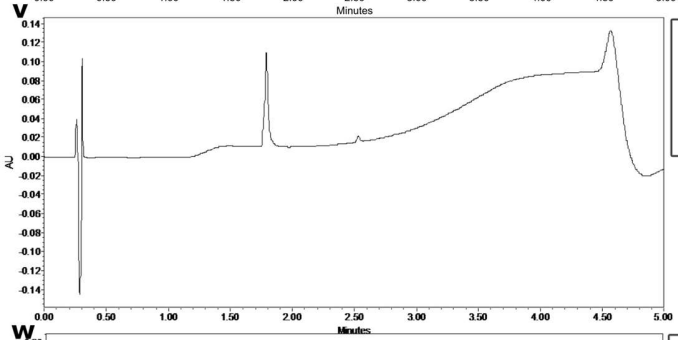

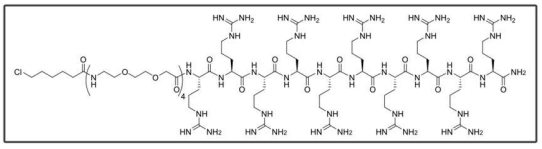

Halo-R10 **18**

w

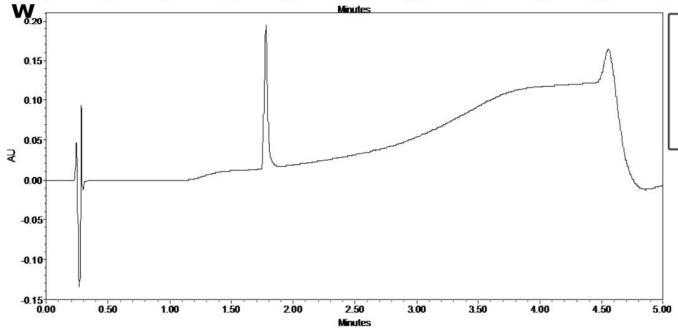

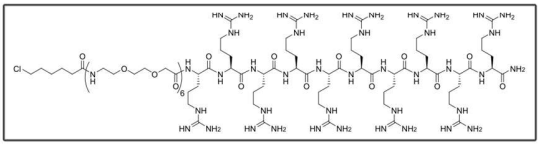

Halo-R10 **19**

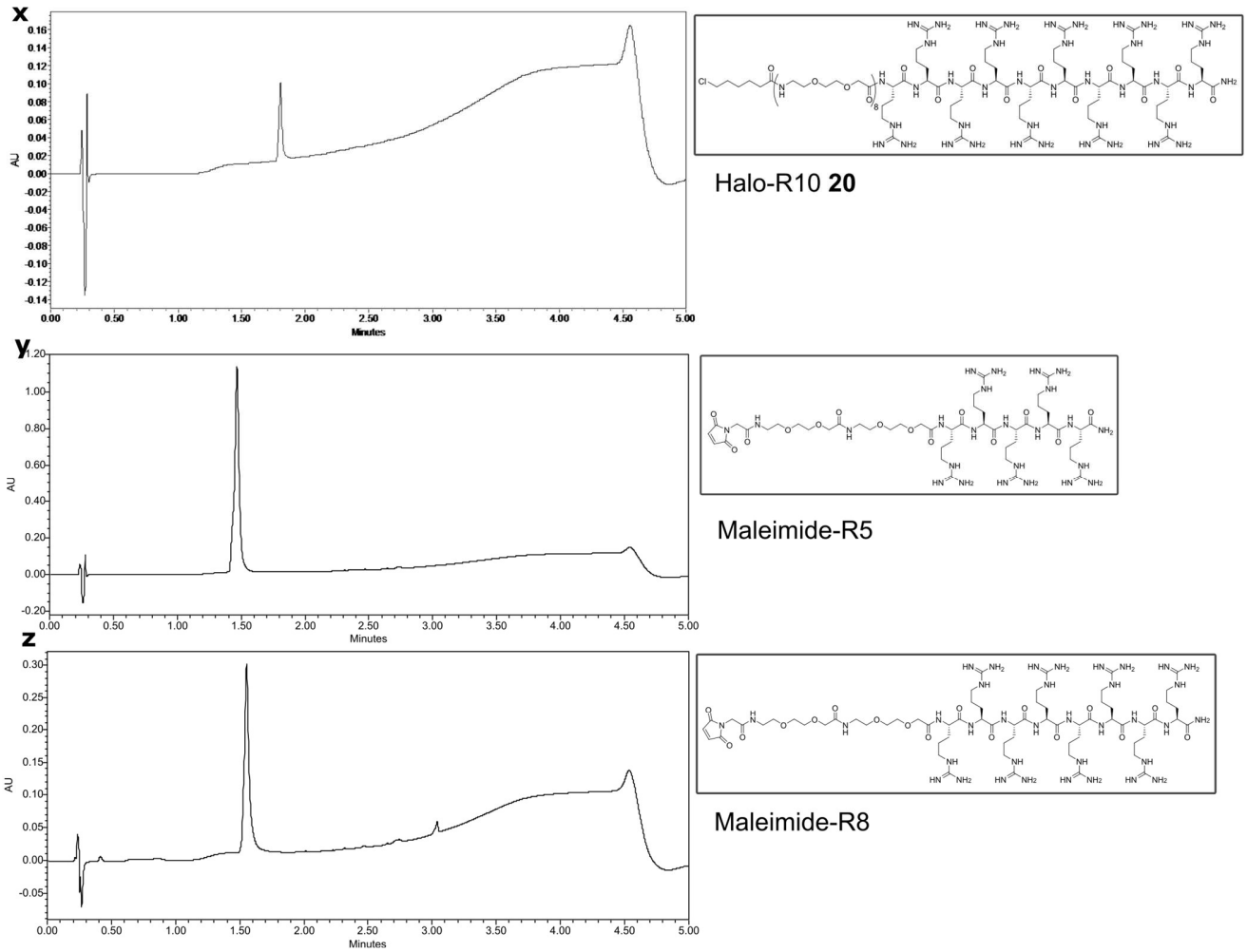

SI Fig. 1 Structures and UV-purity of peptides used in this study. a, TAMRA-cR10, HRMS: Calc.: 372.7257 [M+5H]. exp.: 372.7282. **b**, Cys-TAMRA, HRMS: Calc.: 504.7284 [M+2H], exp.: 504.7448. **c**, Cys-cR10 **1**, HRMS: Calc.: 553.8385 [M+4H], exp.: 553.9105. **d**, Maleimide-cR10, HRMS: Calc.: 449.8720 [M+5H], exp.: 449.8819. **e**, Cys-R10 **2**, HRMS: Calc.: 494.0568[M+4H], exp.: 494.0788. **f**, Maleimide-R10 (**14**), HRMS: Calc.: 402.2473 [M+5H], exp.: 402.2525. **g**, AA-R10 **3**, HRMS: Calc.: 508.3121 [M+4H], exp.: 508.3181. **h**, di-R10 **4**, HRMS: Calc.: 395.2453 [M+10H], exp.: 395.2491. **i**, TNB-R10 **5**, HRMS: Calc.: 543.3013 [M+4H], exp.: 543.3025. **j**, Maleimide-K10, HRMS: Calc.: 346.0343 [M+5H], exp.: 346.0502. **k**, Cys-R10-TAMRA **6**, HRMS: Calc.: 419.7465 [M+5H], exp.: 419.7466. **l**, AA-R10-TAMRA **7**, HRMS: Calc.: 367.9292 [M+6H], exp.: 367.9271. **m**, TNB-R10-TAMRA **8**, HRMS: Calc.: 452.5769 [M+6H], exp.: 452.5703. **n**, TAMRA-R5-Cys-R5 **9**, HRMS: Calc.: 419.8458 [M+5H], exp.: 419.8387. **o**, TAMRA-R5-AA-R5 **10**, HRMS: Calc.: 431.2501 [M+5H], exp.: 431.2468. **p**, TAMRA-R10-Cys **11**, HRMS: Calc.: 419.6451 [M+5H], exp.: 419.6376. **q**, TAMRA-R10-AA **12**, HRMS: Calc.: 431.2501 [M+5H], exp.: 431.2383. **r**, Maleimide-R10-Cy5 **13**, HRMS: Calc.: 434.1036 [M+6H], exp.: 434.0886. **s**, Maleimide-R10-Biotin **15**, HRMS: Calc.: 472.8811 [M+5H], exp.: 472.8772. **t**, Halo-R10 **16**, HRMS: Calc.: 428.5252 [M+4H], exp.: 428.5278. **u**, Halo-R10 **17**, HRMS: Calc.: 334.5444 [M+6H], exp.: 334.5357. **v**, Halo-R10 **18**, HRMS: Calc.: 573.8500 [M+4H], exp.: 573.8497. **w**, Halo-R10 **19**, HRMS: Calc.: 646.3869 [M+4H], exp.: 646.3752. **x**, Halo-R10 **20**, HRMS: Calc.: 718.9239 [M+4H], exp.: 718.9248. **y**, Maleimide-R5, HRMS: Calc.: 613.8546 [M+2H], exp.: 613.8481. **z**, Maleimide-R8, HRMS: Calc.: 424.2559 [M+4H], exp.: 424.2505.

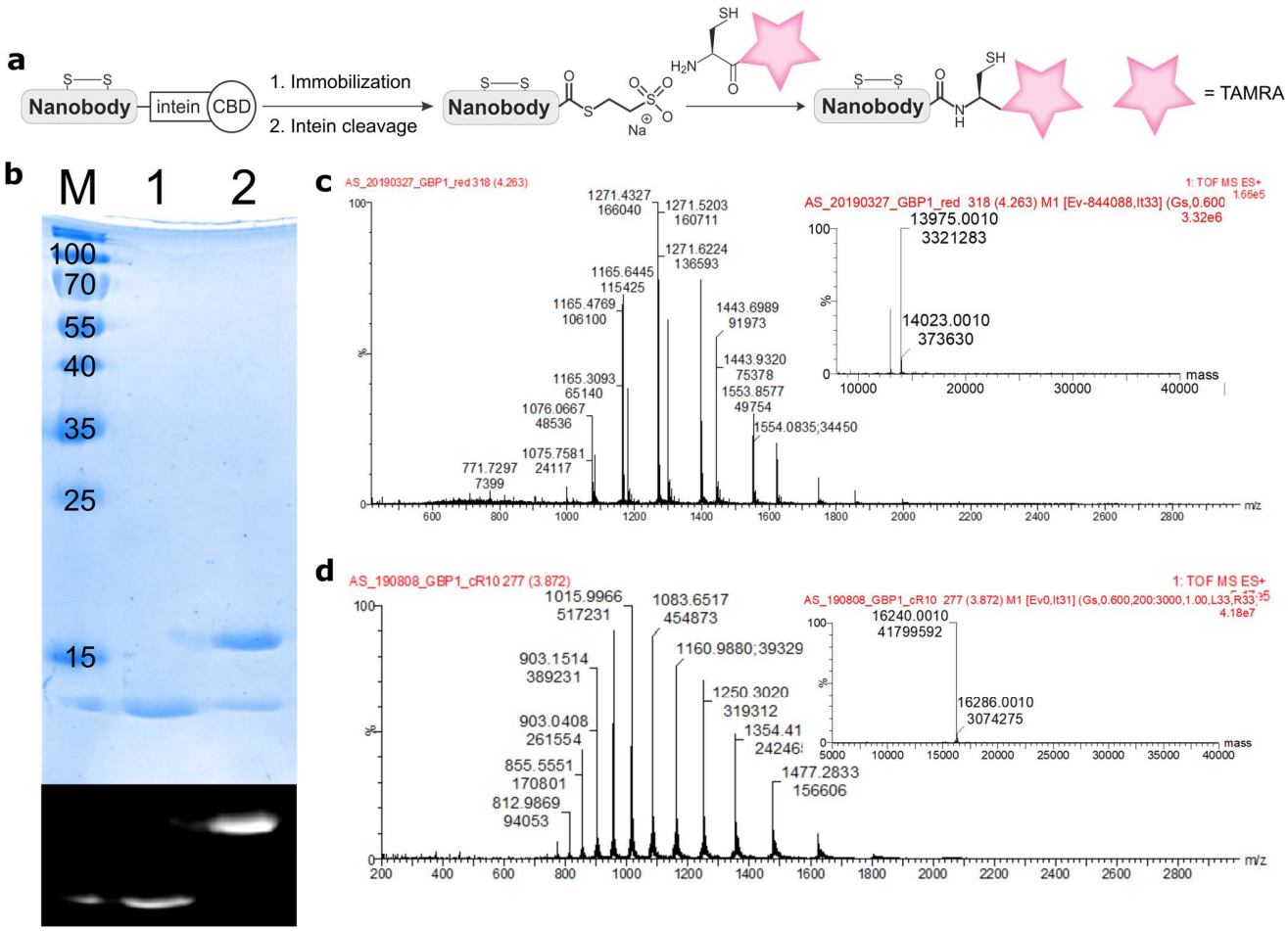

SI Fig. 2 Characterization of anti-GFP-nanobody GBP1 and its CPP conjugate. a, Strategy for the semi-synthesis of thiol- and fluorophore modified GBP1 nanobody via expressed protein ligation. **b**, SDS-PAGE gel, stained with Coomassie and fluorescence imaging of TAMRA on the bottom, of GBP1-TAMRA after expressed protein ligation (1) and after conjugation to the Maleimide-cR10 (2). Synthetic details in supplementary methods. **c**, High resolution mass spectrum of GBP1-TAMRA after EPL. Calc.: 13977 [M+H]; Exp.: 13975. **d**, High resolution mass spectrum of GBP1-TAMRA-cR10, Calc.: 16222 [M+H], 16240 [M+H2O+H] (Maleimide ring opening hydrolysis); Exp.: 16240.

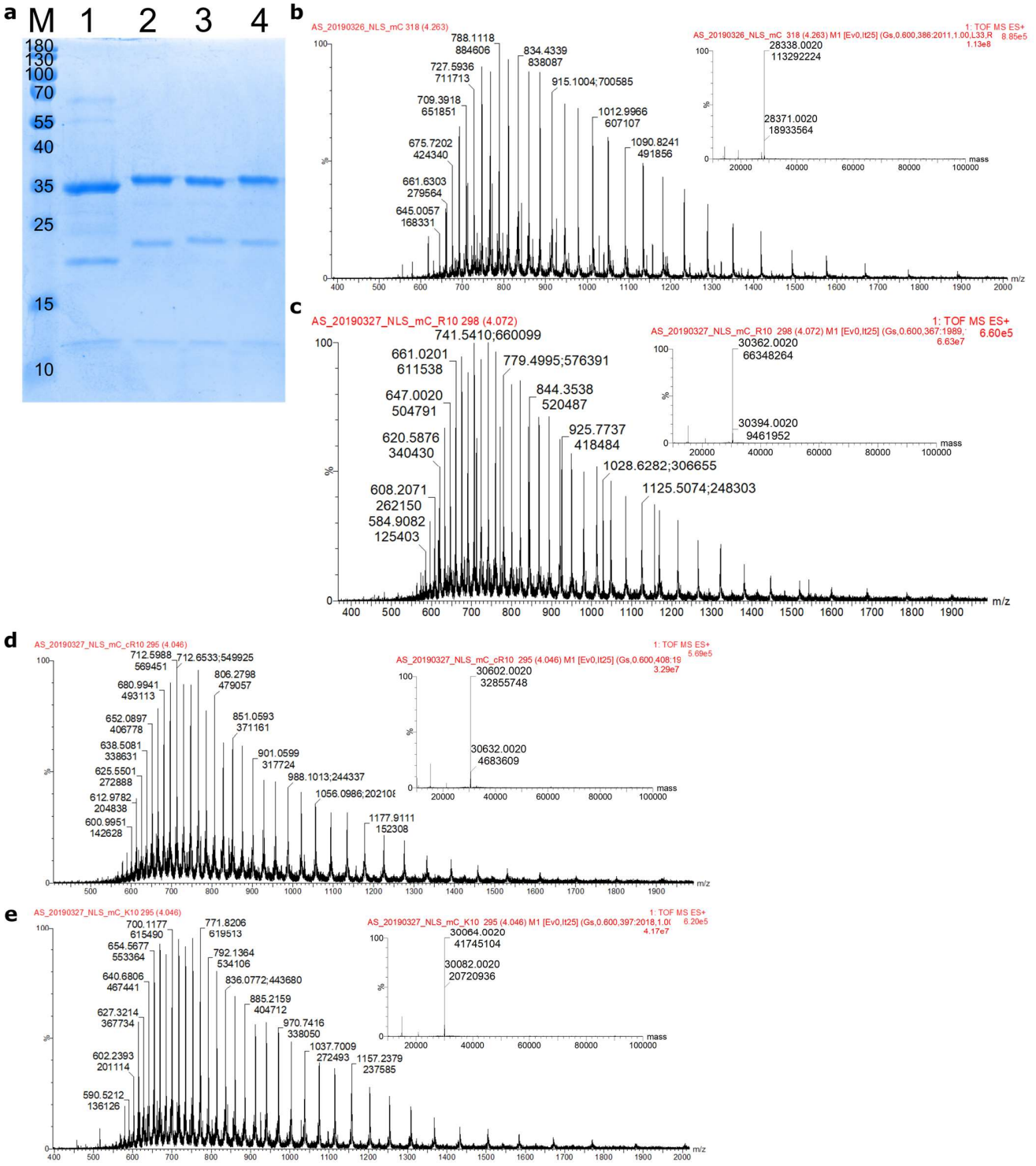

SI Fig. 3 Characterization of NLS-mCherry and its CPP conjugates. For synthetic details, see Protein-CPP conjugation section in the supplementary methods. **a**, SDS-PAGE gel showing the purity and conversion of NLS-mCherry (lane 1) and the linear R10, cyclic R10 and K10 peptide conjugates (lanes 2-4). The protein shows two lower molecular weight bands, which are an artefact of the sample preparation (boiling) for SDS-PAGE[1]. **b**, High resolution mass spectrum of NLS-mCherry, Calc.: 28339 [M+H]; Exp.: 28338. **c**, High resolution mass spectrum of NLS-mCherry-R10 **II**, Calc.: 30344 [M+H], 30362 [M+H2O+H]; Exp.: 30362. **d**, High resolution mass spectrum of NLS-mCherry-cR10 **I**, Calc.: 30583 [M+H], 30601 [M+H2O+H]; Exp.: 30602. **e**, High resolution mass spectrum of NLS-mCherry-K10 **III**, Calc.: 30064 [M+H], 30082 [M+H2O+H]; Exp.: 30064, 30082.

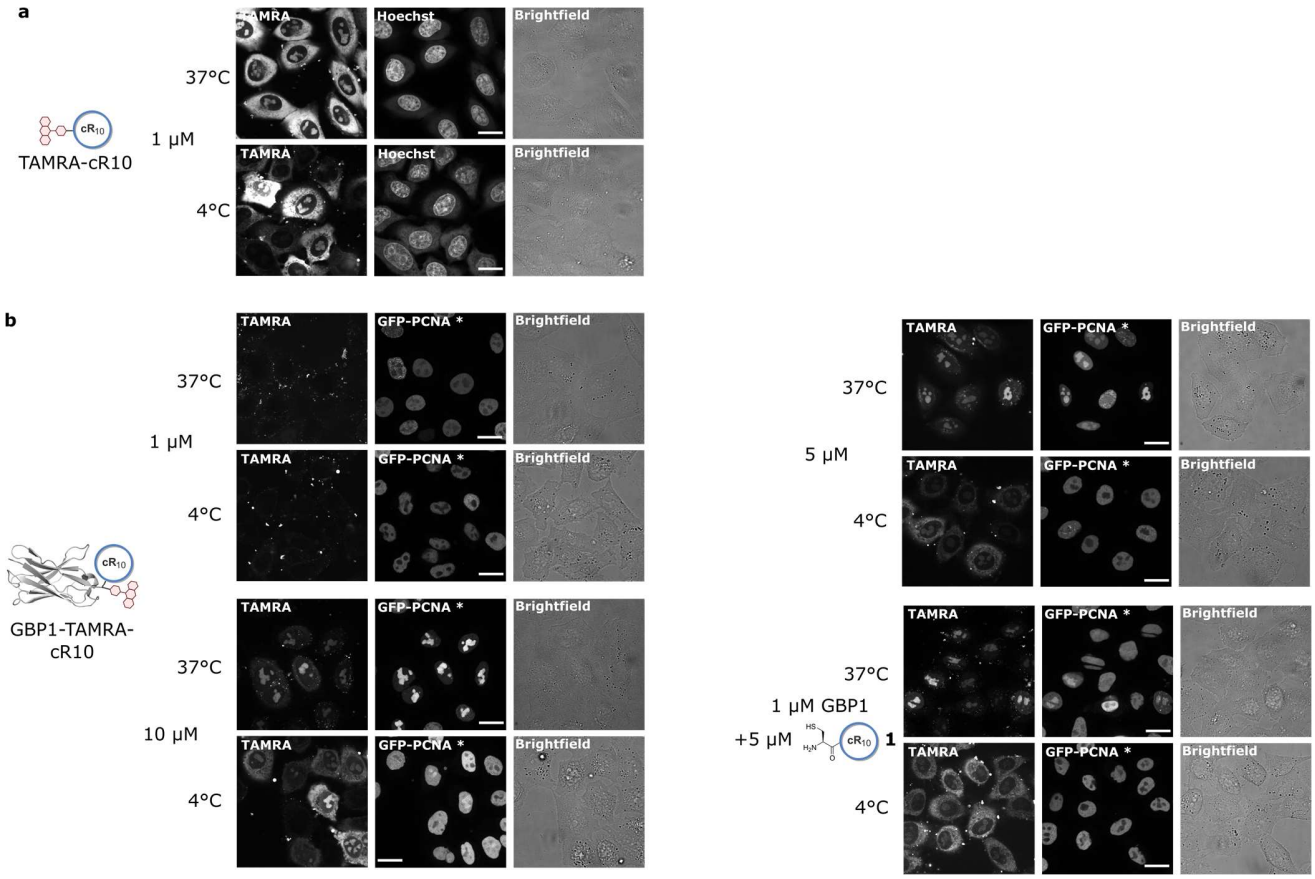
a
TAMRA-cR10
37°C
1 µM
4°C
TAMRA
Hoechst
Brightfield
b
GBP1-TAMRA-cR10
37°C
1 µM
4°C
10 µM
4°C
TAMRA
GFP-PCNA *
Brightfield
37°C
5 µM
4°C
37°C
1 µM GBP1
+5 µM
1
4°C

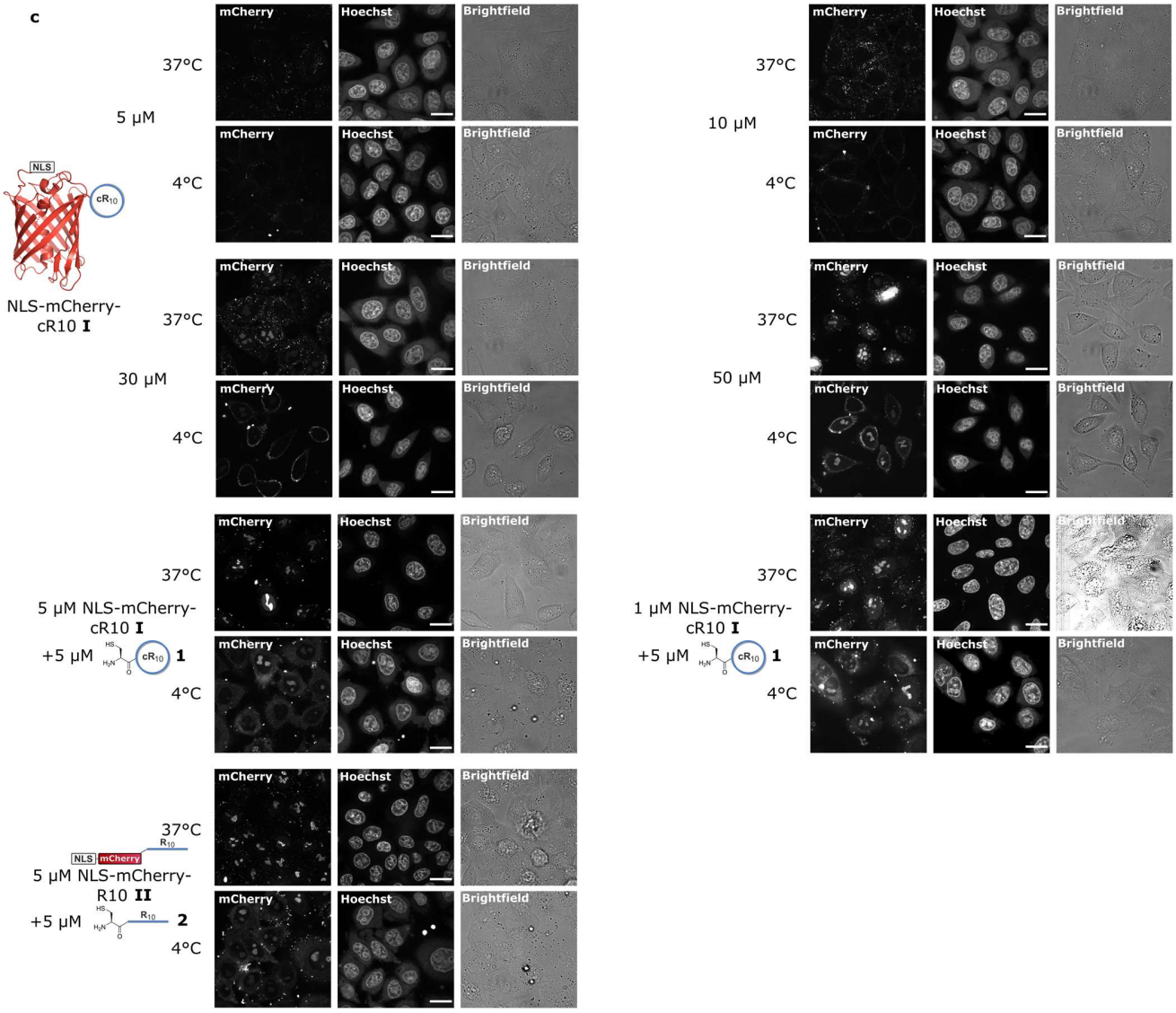

SI Fig. 4 Full set of confocal microscopy pictures after cellular uptake of R10-bearing cargoes into HeLa cells at 37 and 4°C. a, Uptake of TAMRA-cR10 at 1 µM, at 37 and 4°C. **b**, Uptake of 1-10 µM GBP1-TAMRA-cR10 (with additional Cys-cR10 **1**) at 37 and 4°C. **c**, Uptake of 1-50 µM NLS-mCherry-cR10 **I** and NLS-mCherry-R10 **II** (with additional Cys-cR10 **1** or Cys-R10 **2**) at 37 and 4°C. Scale bars 20 µm.

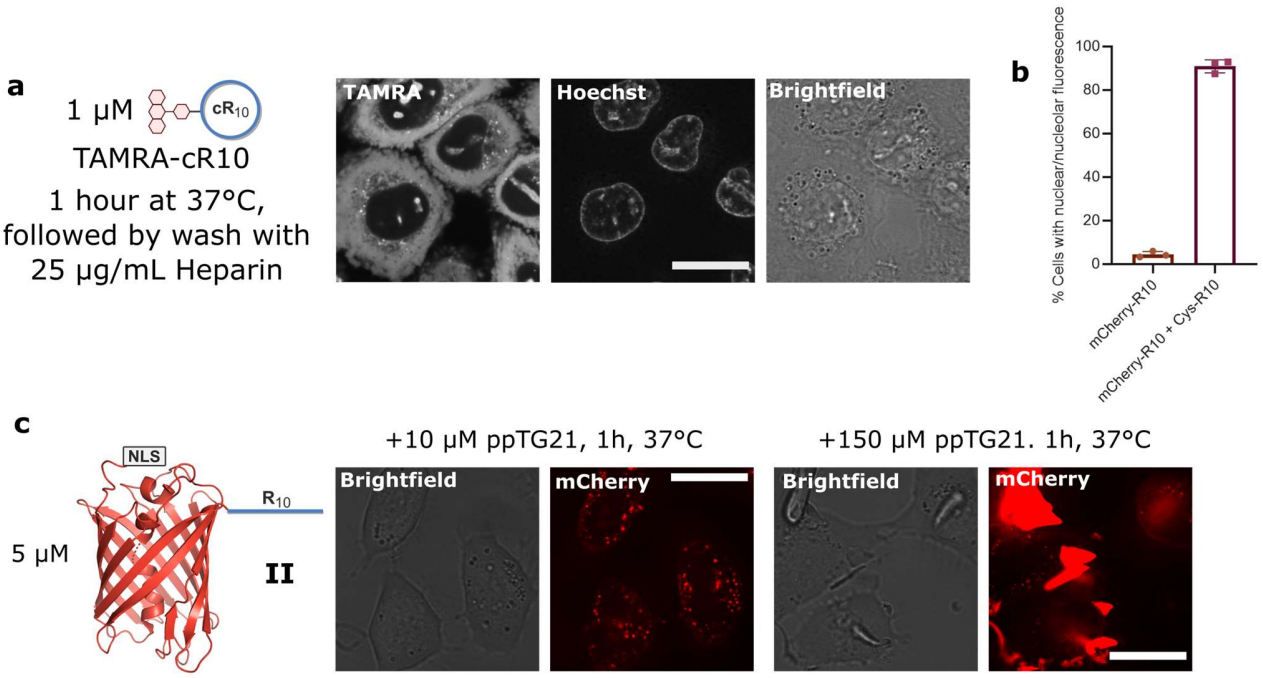

SI Fig. 5 Additional experiments in the uptake of TAMRA-cR10 and NLS-mCherry. a, Uptake of 1 µM TAMRA-cR10 at 37°C, followed by washing with 25 µg/mL heparin to remove residual CPP bound to the cell membrane. **b**, Counted cells with nuclear or nucleolar fluorescence after uptake of 5 µM NLS-mCherry-R10 **II** with added Cys-R10 CPP **2**. Over 150 cells were counted manually in three independent replicates. Shown are individual values with mean and standard deviation. **c**, Uptake of 5 µM NLS-mCherry-R10 **II** with added endosomolytic peptide ppTG21 at 37°C for 1 hour. At the higher concentration, large aggregates are formed that persist after washing and are highly fluorescent. Scale bars 20 µm.

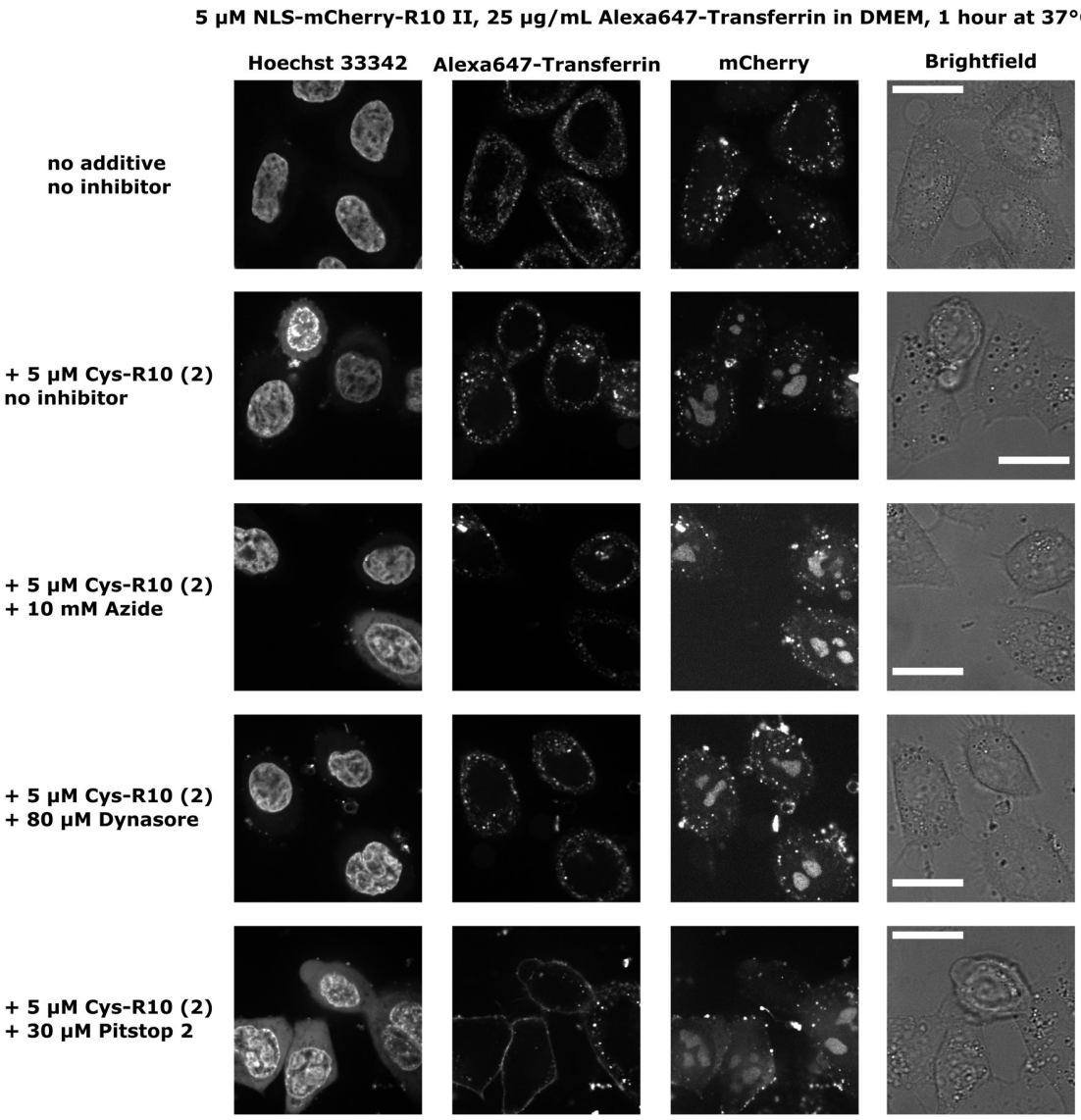

SI Fig. 6 Uptake of NLS-mCherry-R10 and Alexa647-Transferrin with endocytosis inhibitors. NLS-mCherry-R10 **II** at a 5 µM concentration was added to cells in combination with 25 µg/mL Alexa647-Transferrin (Invitrogen) as endocytosis control. Where indicated, 5 µM of the Cys-R10 peptide **2** were added to induce nucleolar delivery of the mCherry. For the incubation with sodium azide and Dynasore, the cells were pre-incubated with the inhibitors for 30 minutes, for pitstop 2 for 15 minutes, the inhibitors were then also added to the solution of mCherry and Transferrin. Nucleolar mCherry was seen anytime the Cys-R10 was present. In contrast, uptake of transferrin was strongly reduced in presence of azide and almost completely blocked in presence of pitstop 2, indicating that the inhibitors block endocytic uptake. Scale bars 20 µm.

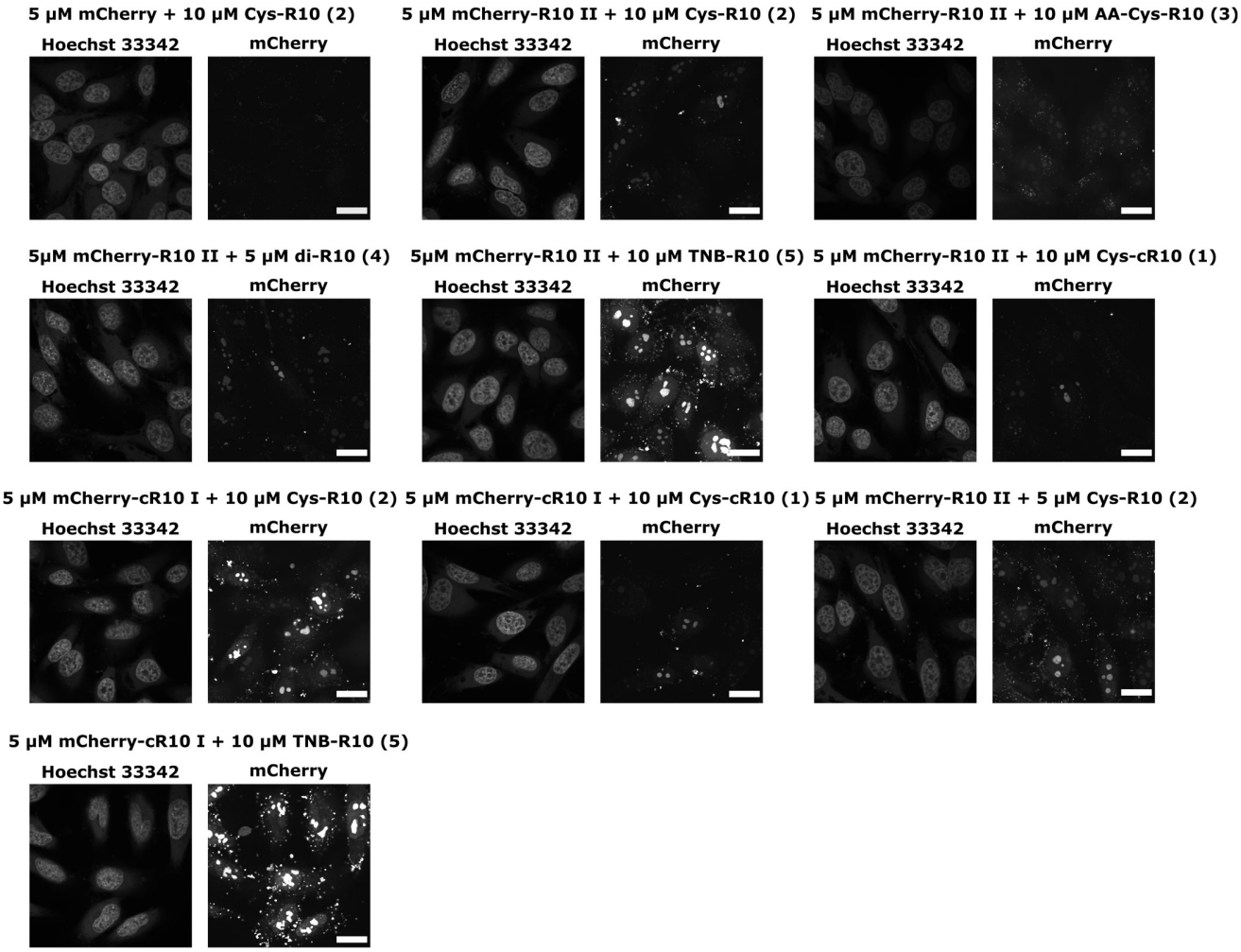

SI Fig. 7 Representative images used in quantitative microscopy experiments. NLS-mCherry derivatives were added in the indicated concentration and with the indicated CPPs to HeLa CCL-2 cells for 1 hour at 37°C, and they were counterstained with Hoechst 33342. The cells were fixed after thorough washing to prevent an effect of the long microscopy time required. Confocal microscopy pictures were then taken, of at least 100 cells in independent triplicates at a 60x magnification to allow proper spatial separation of the nuclei and the endosomes. Scale bars 20 µm.

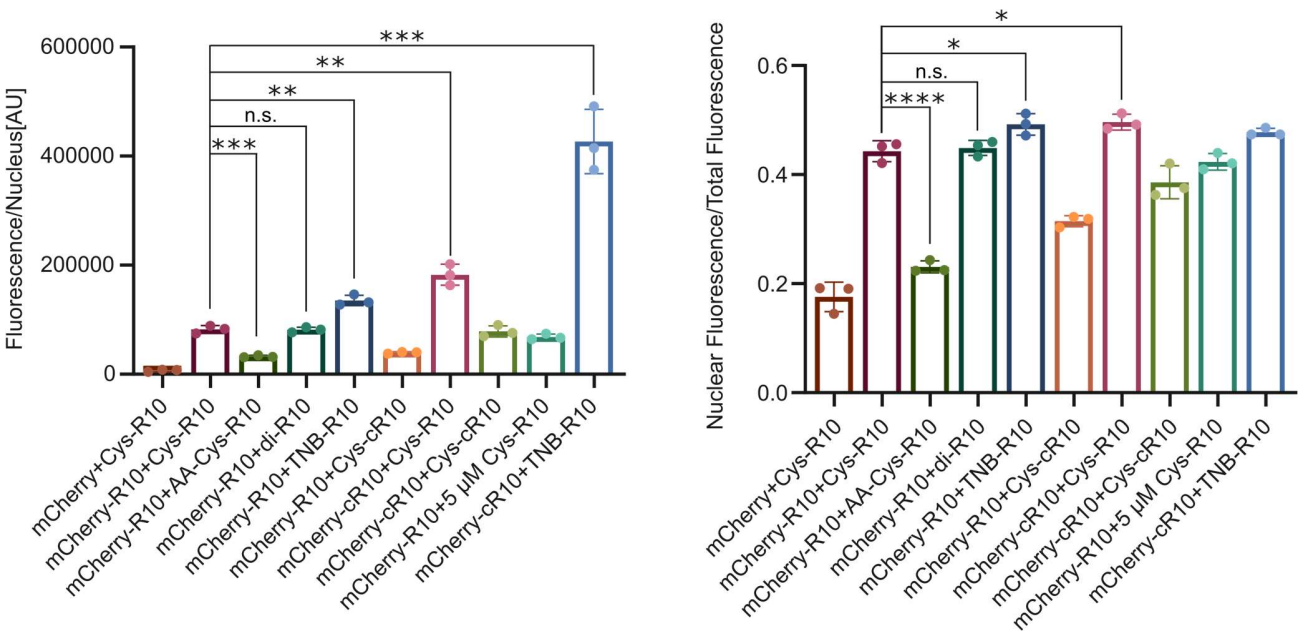

SI Fig. 8 Full graphs of relative and absolute quantification of cellular uptake. a, Absolute quantification of red fluorescence originating from the mCherry protein within the nucleus of HeLa cells. Images of at least 100 cells were taken in independent triplicates. Shown are individual values and mean ± sd. **b**, Ratio of red fluorescence in the nucleus of cells divided by the total measured fluorescence in each frame. This is a measure of the efficiency of delivery to the nucleus and nucleolus relative to mCherry outside of the nucleus, predominantly a result of endosomal entrapment. Individual values and mean ± sd. n.s. = not significant, * = P < 0.05, ** = P < 0.005, *** = P < 0.0005, **** = P < 0.0001.

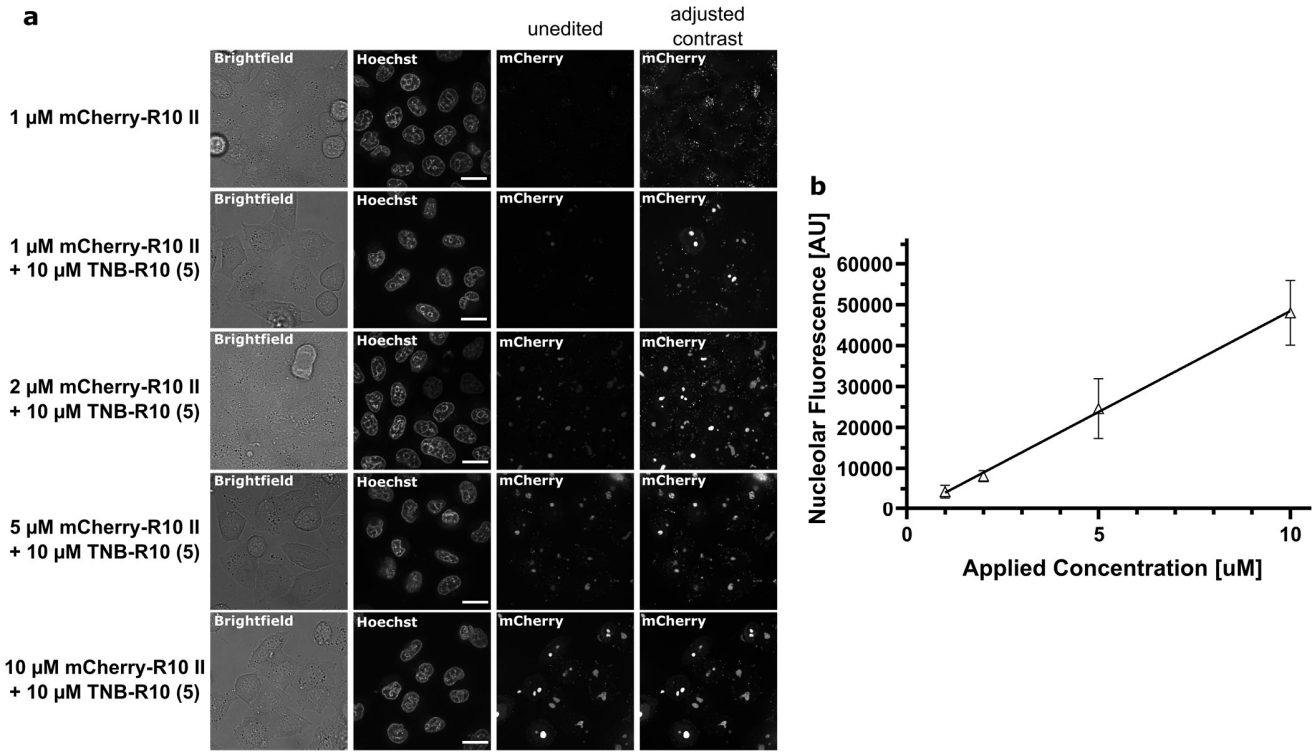

SI Fig. 9 Titration of NLS-mCherry-R10 II into cells with constant concentration of additive CPP. a, Microscopy pictures of the uptake of different concentrations of NLS-mCherry-R10 **II** in presence of constant 10 µM TNB-R10 (**5**). **b**, Quantification of the fluorescence intensity of a 20x20 pixel ROI in the nucleoli of 10 different cells per condition. Shown is the mean ± SD for each concentration. A linear fit shows the linear relationship between applied concentration and resulting fluorescence (R^2 = 0.92.)

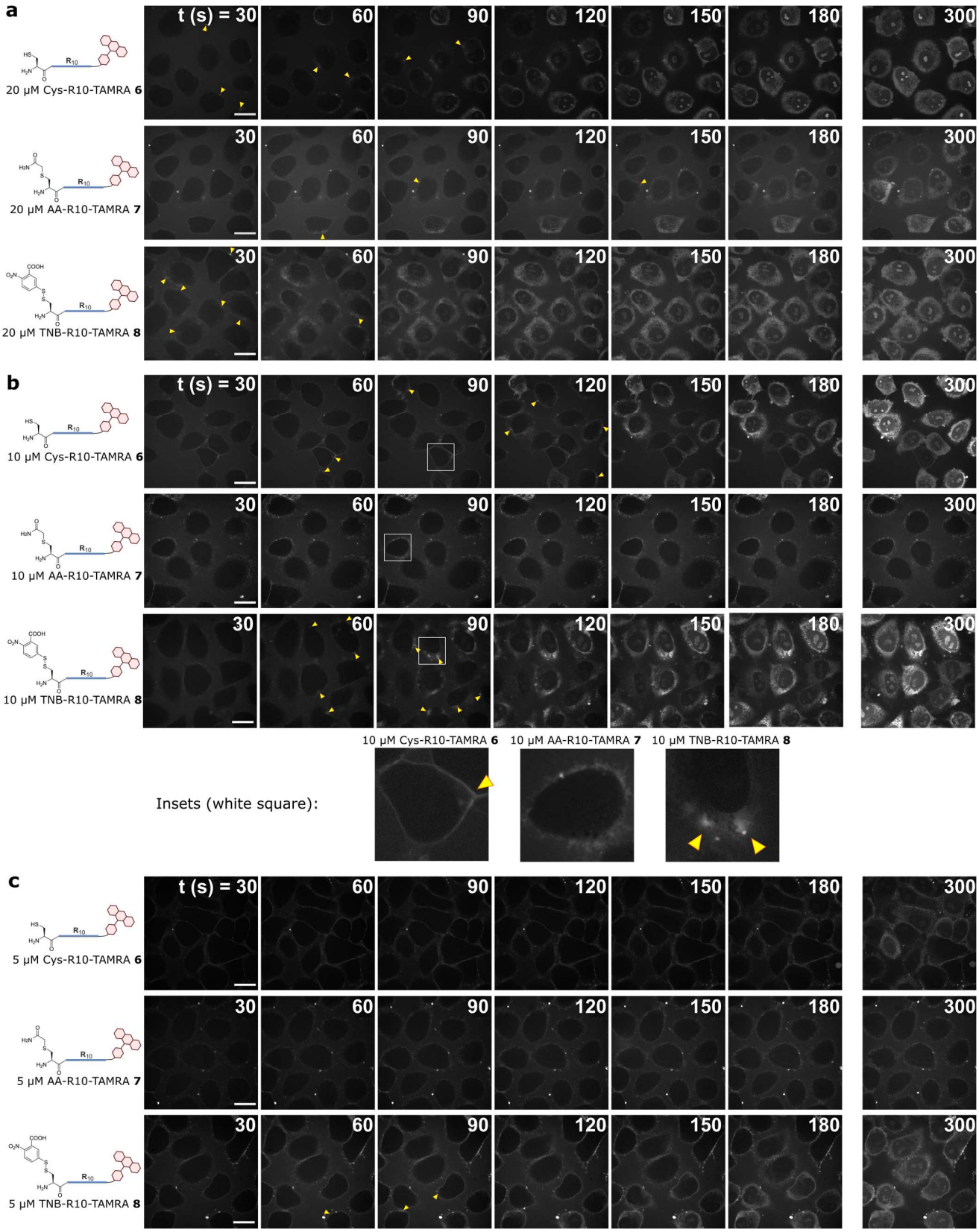

SI Fig. 10 Montage of timelapse experiments of the cellular uptake of TAMRA-labelled R10 peptides with different N-terminal head groups. a, Uptake at 20 μM concentration. **b**, Uptake at 10 μM concentration. Insets show the appearance of nucleation zones (bright spots, immediately followed by uptake). **c**, Uptake at 5 μM concentration. Yellow arrowheads show nucleation zones. Scale bars 20 μm.

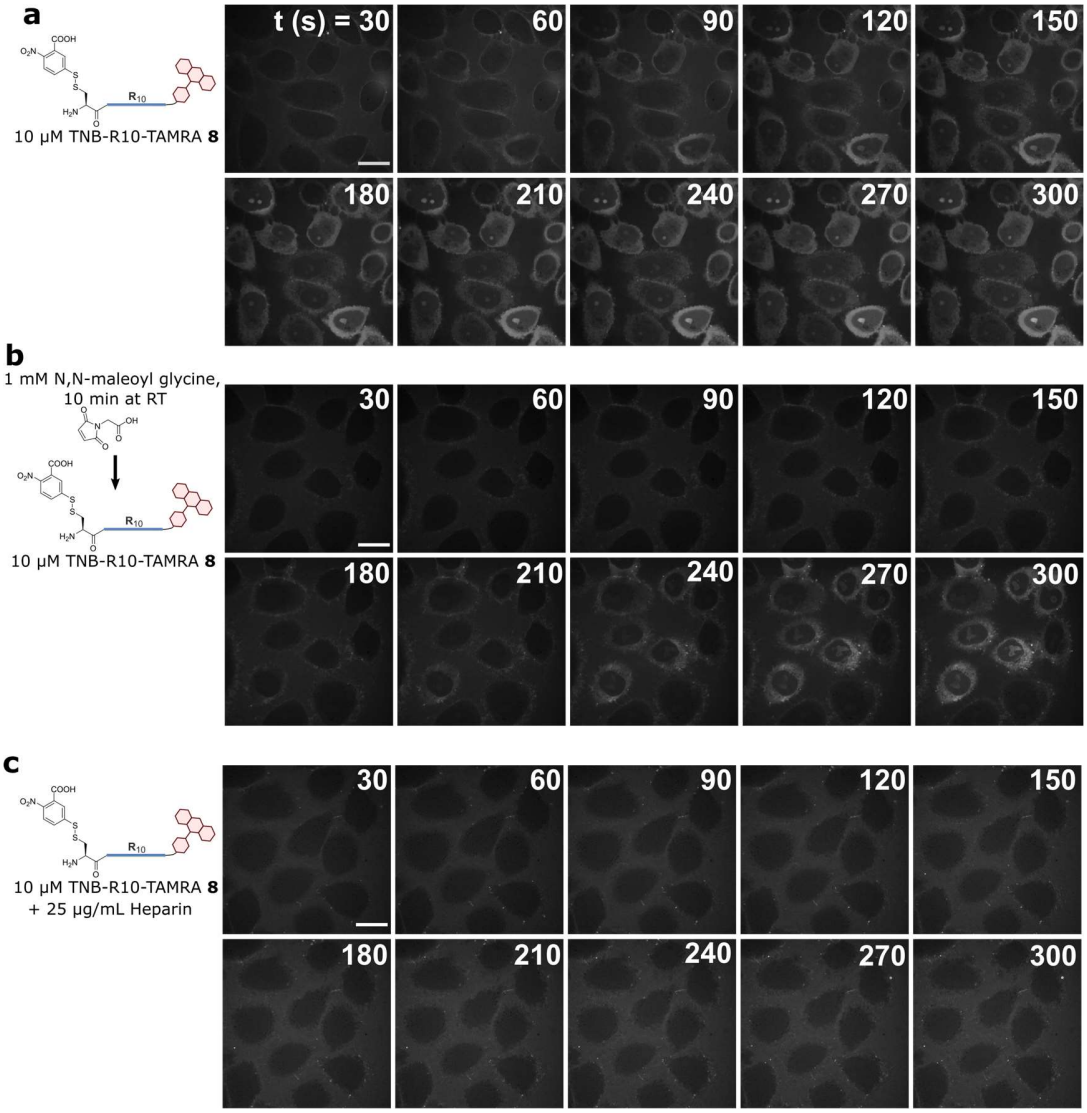

SI Fig. 11 Montage of timelapse experiments of the cellular uptake of TNB-R10-TAMRA 8 in cells pre-treated with a small-molecule maleimide. a, Control uptake of the peptide without pre-treatment at 10 μM concentration. **b**, Uptake into cells that were treated first for 10 minutes with 1 mM of N,N-maleoyl glycine, followed by removal of the maleimide solution and addition of the peptide. **c**, Uptake into cells in presence of the anionic polysaccharide heparin. Scale bars 20 μm.

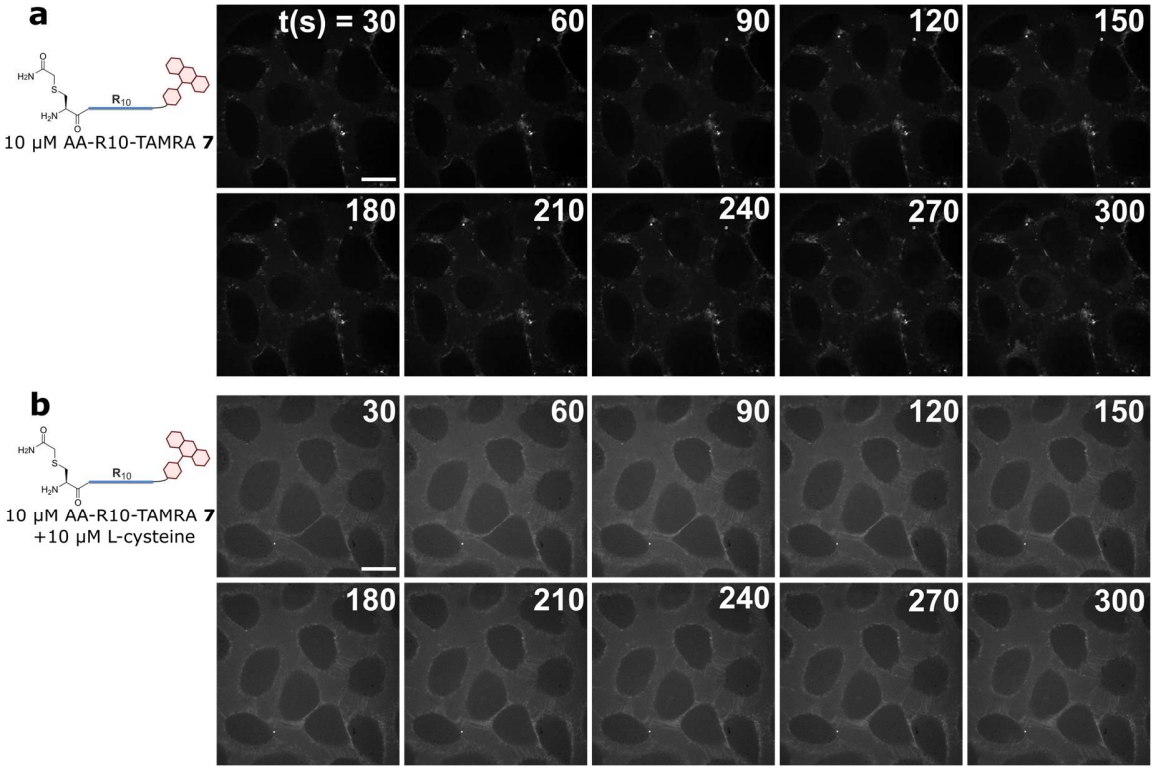

SI Fig. 12 Montage of timelapse experiments of the cellular uptake of AA-R10-TAMRA in cells co-incubated with cysteine. a, Control uptake of the peptide without cysteine at 10 μM concentration. **b**, Uptake into cells in presence of 10 μM L-cysteine. Scale bars 20 μm.

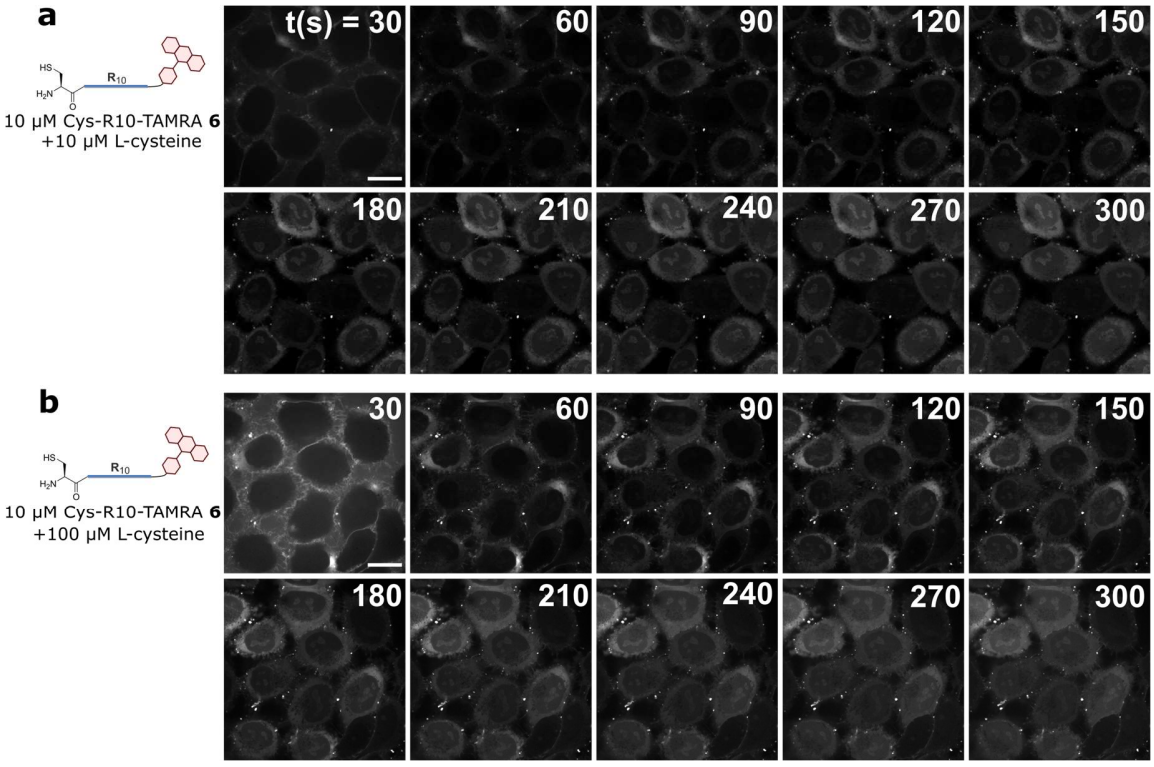

SI Fig. 13 Montage of timelapse experiments of the cellular uptake of Cys-R10-TAMRA with competition with free cysteine. a,**b**, Cellular uptake of the peptide with 10 (**a**) or 100 (**b**) μM L-cysteine. Scale bars 20 μm.

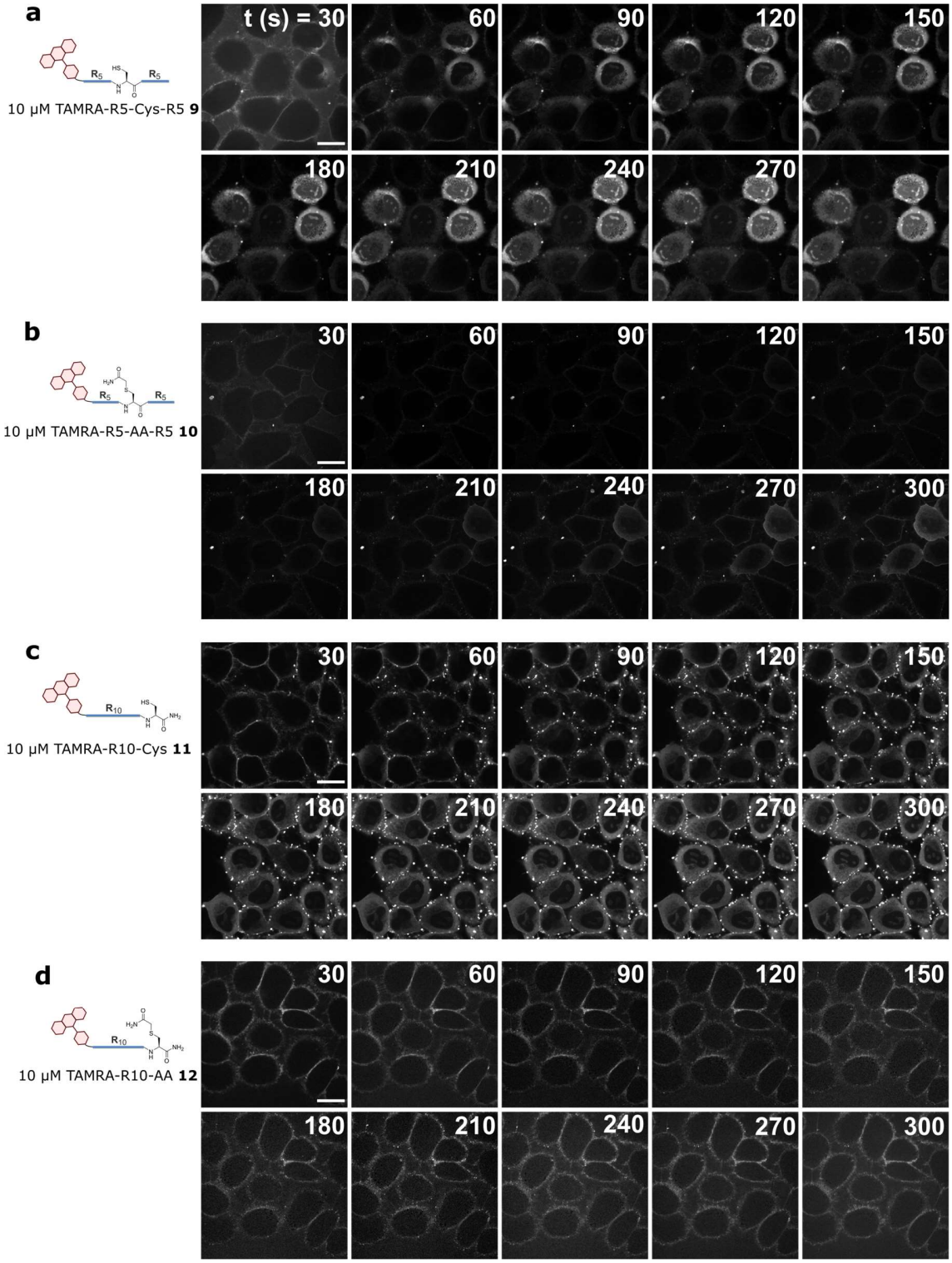

SI Fig. 14 Montage of timelapse experiments of the cellular uptake of R10-TAMRA peptides with cysteine at different positions, in comparison with acetylated variants. a, Cellular uptake of 10 µM cysteine-containing TAMRA-R5-Cys-R5 peptide. **b**, Uptake of the acetylated variant of **a**. **c**, Uptake of the cysteine containing TAMRA-R10-Cys peptide. **d**, Uptake of the acetylated variant of **c**. Scale bars 20 µm.

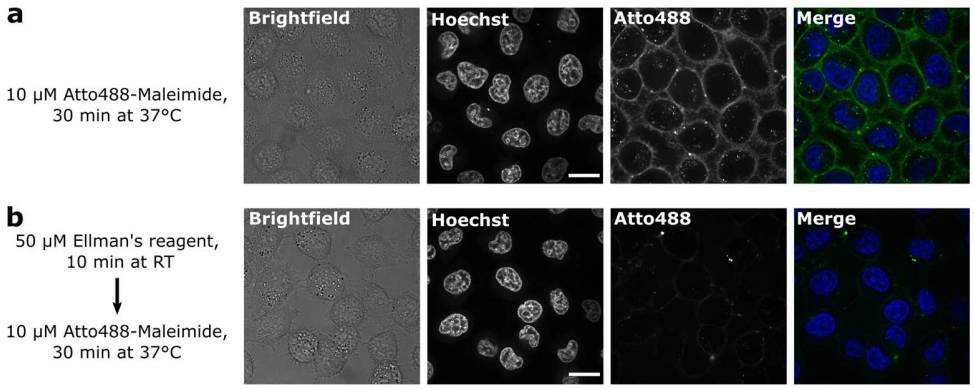

SI Fig. 15. Fluorescent labelling of accessible cell-surface thiols using cell-impermeable fluorophore. a, Labelling of accessible cell surface thiols with 10 µM of the membrane impermeant (sulfated) fluorophore atto 488[2] functionalized with a maleimide. **b**, To confirm that Ellman's reagent and the fluorophore label the same thiols, cells were first treated with 50 µM Ellman's reagent for 10 minutes, then washed once and then treated with 10 µM of the fluorophore. Labelling is dramatically reduced. Scale bars 20 µm.

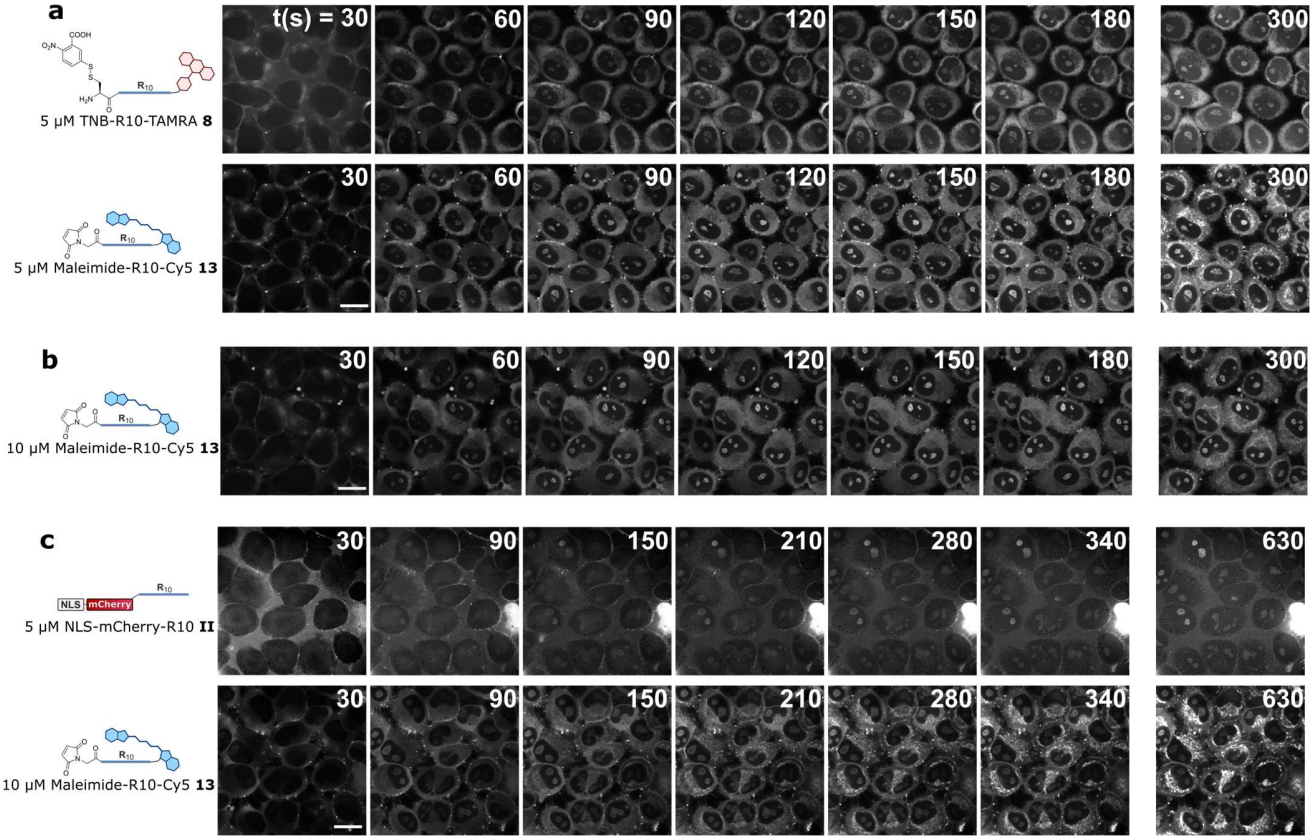

SI Fig. 16 Montage of timelapse experiments of the cellular uptake of the Maleimide-R10-Cy5 peptide 13 alone or in combination with TNB-R10-TAMRA 8 and NLS-mCherry-R10 II. a, Full dataset of uptake of 5 µM TNB-R10-TAMRA **8** with 5 µM Maleimide-R10-Cy5 **13**. **b**, Uptake of 10 µM Maleimide-R10-Cy5 **13**. **c**, Uptake of 5 µM NLS-mCherry-R10 **II** into cells in presence of 10 µM Maleimide-R10-Cy5 **13**. Scale bars 20 µm.

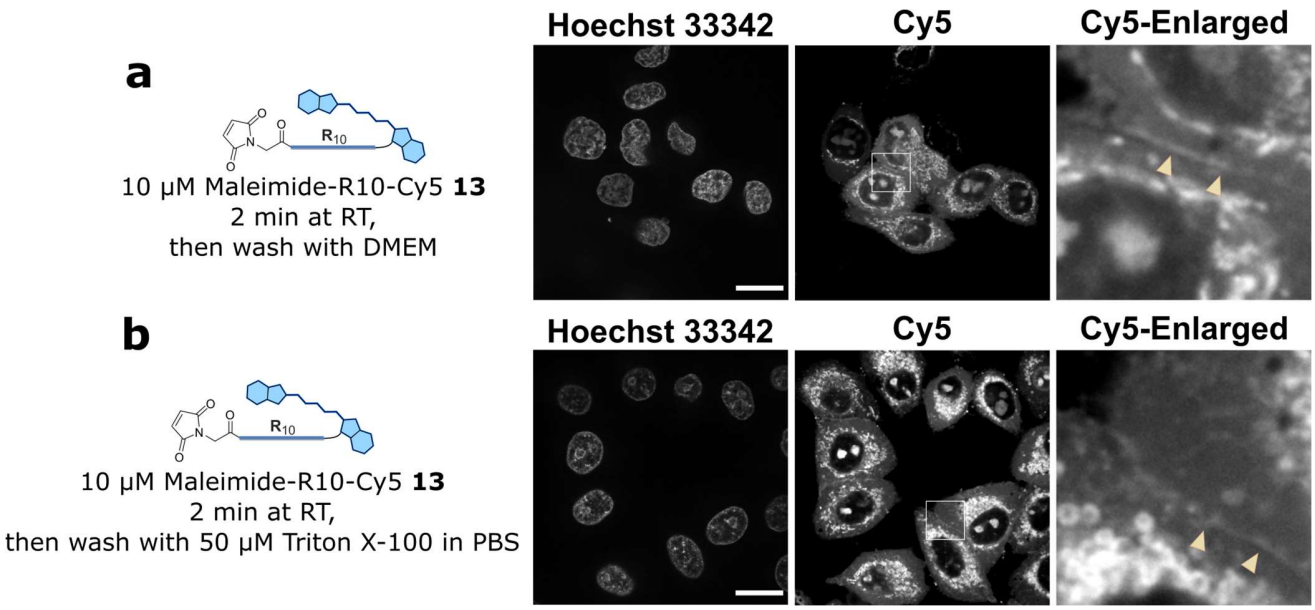

SI Fig. 17 Treatment of cells with maleimide-R10-Cy5 peptide 13 followed by washing reveals membrane bound peptide. a, Washing with cell medium. **b**, Washing with 50 μM Triton X-100 in PBS[3]. In both cases, cells also show mitochondrial staining of the Cy5. Cy5 has an affinity for mitochondria[4], and the labelling of mitochondria may indicate partial degradation of the peptide. Proteolytic degradation of CPPs can occur within minutes[5]. Enlarged are areas where two cells are in contact. The membrane staining is more apparent at these interfaces due to the nature of the confocal images. Scale bars 20 μm.

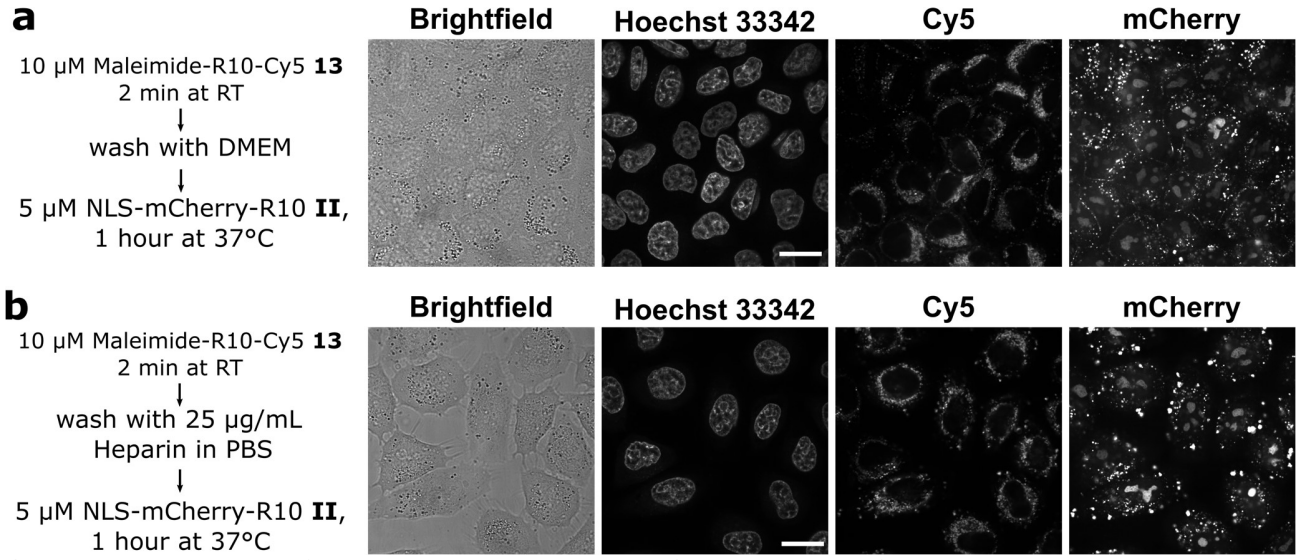

SI Fig. 18 Treatment of cells with maleimide-R10-Cy5 peptide 13 followed by washing and subsequent delivery of mCherry. a, Washing with cell medium. **b**, Washing with 25 μg/mL heparin in PBS. In both cases, cells show nucleolar mCherry fluorescence. As shown in SI Fig. 19a, an unreactive CPP additive does not deliver mCherry into nucleoli even without washing with heparin. Scale bars 20 μm.

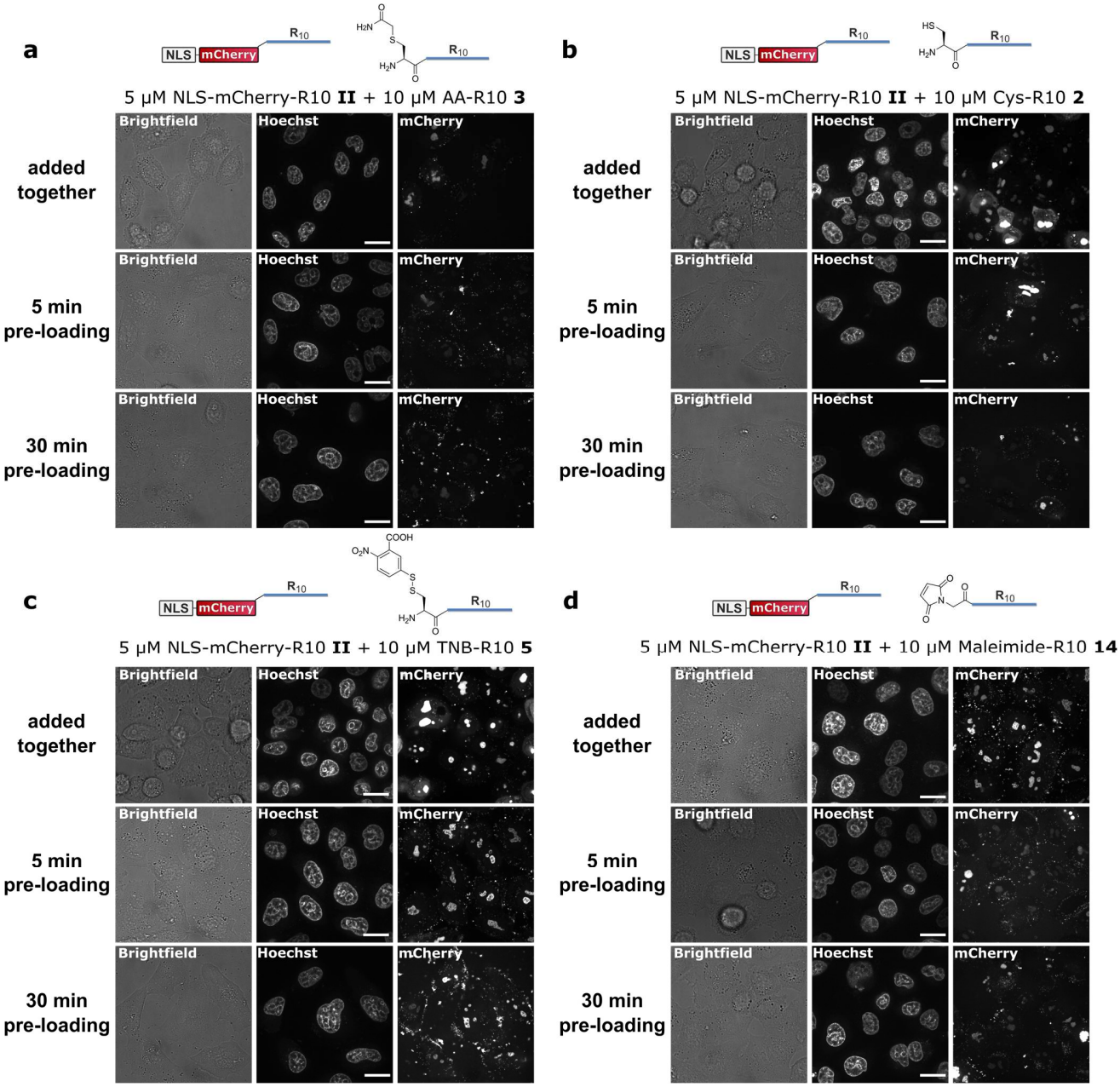

SI Fig. 19 ”Pre-loading” of CPPs on cells followed by cellular uptake of NLS-mCherry-R10 II. a, 5 µM NLS-mCherry-R10 **II** together with 10 µM AA-R10 (**3**). **b**, 5 µM NLS-mCherry-R10 **II** together with 10 µM Cys-R10 (**3**). **c**, 5 µM NLS-mCherry-R10 **II** together with 10 µM TNB-R10 (**2**). **d**, 5 µM NLS-mCherry-R10 together with 10 µM Maleimide-R10. Scale bars 20 µm.

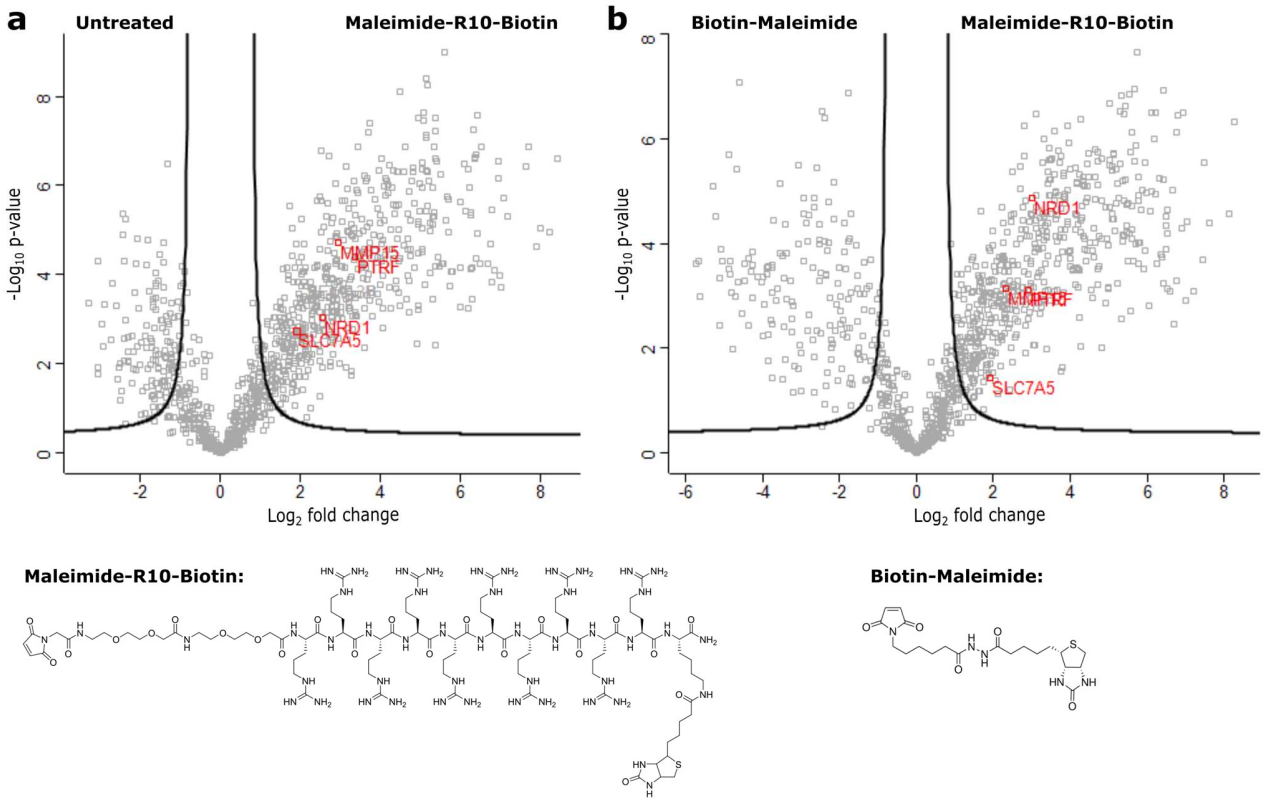

SI Fig. 20 Volcano plots of label-free quantification after protein identification of streptavidin pull-down samples by mass spectrometry. a, Cells were either untreated or treated with 20 µM of the Maleimide-R10-Biotin peptide. **b**, Cells were treated either with 20 µM of commercially available Biotin-Maleimide or with the Maleimide-R10-Biotin peptide. In both cases, several membrane bound proteins were highly enriched by the cell-penetrating peptide. Amongst those are two membrane-bound metallo-proteases (NRD1 and MMP15), an amino acid transporter (SLC7A5) and a caveolae-associated protein (PTRF). See Methods section for experimental details.

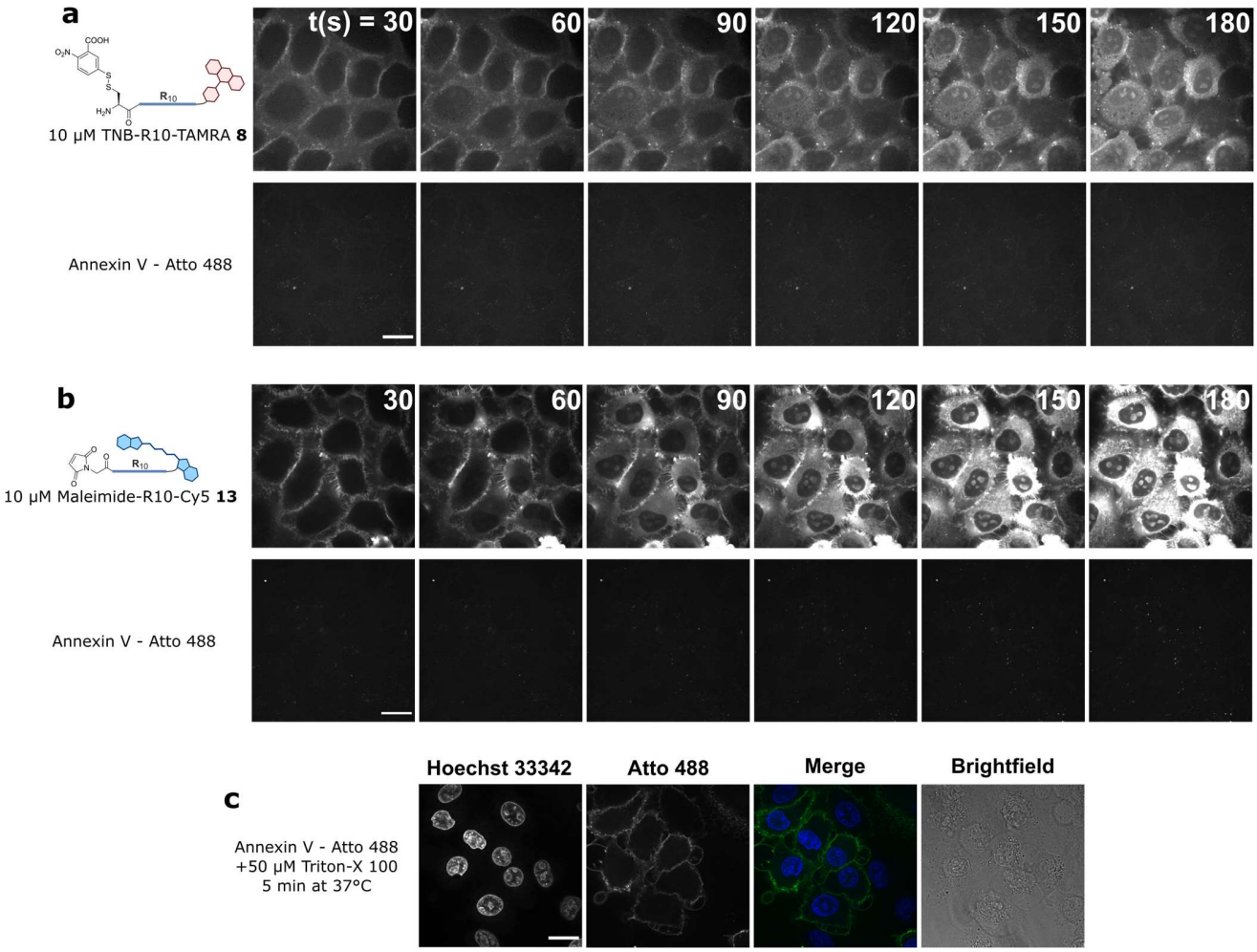

SI Fig. 21 Cellular uptake of thiol-reactive CPPs in presence of Annexin V. a, HeLa Kyoto cells were treated with 10 µM TNB-R10-TAMRA **8** in presence of Annexin V – Atto 488 conjugate (1:50) in annexin V buffer (10 mM Hepes (pH 7.4), 140 mM NaCl, 2.5 mM $CaCl_2$). **b**, HeLa Kyoto cells were treated with 10 µM Maleimide-R10-Cy5 **13** in presence of Annexin V – Atto 488 conjugate (1:50) in annexin V buffer (10 mM Hepes (pH 7.4), 140 mM NaCl, 2.5 mM $CaCl_2$). **c**, As a positive control for binding of annexin V to apoptotic cells under the same conditions, HeLa Kyoto cells were incubated for 5 minutes at 37°C with Annexin V – Atto 488 in annexin V buffer with 50 µM Triton-X 100. Scale bars 20 µm.

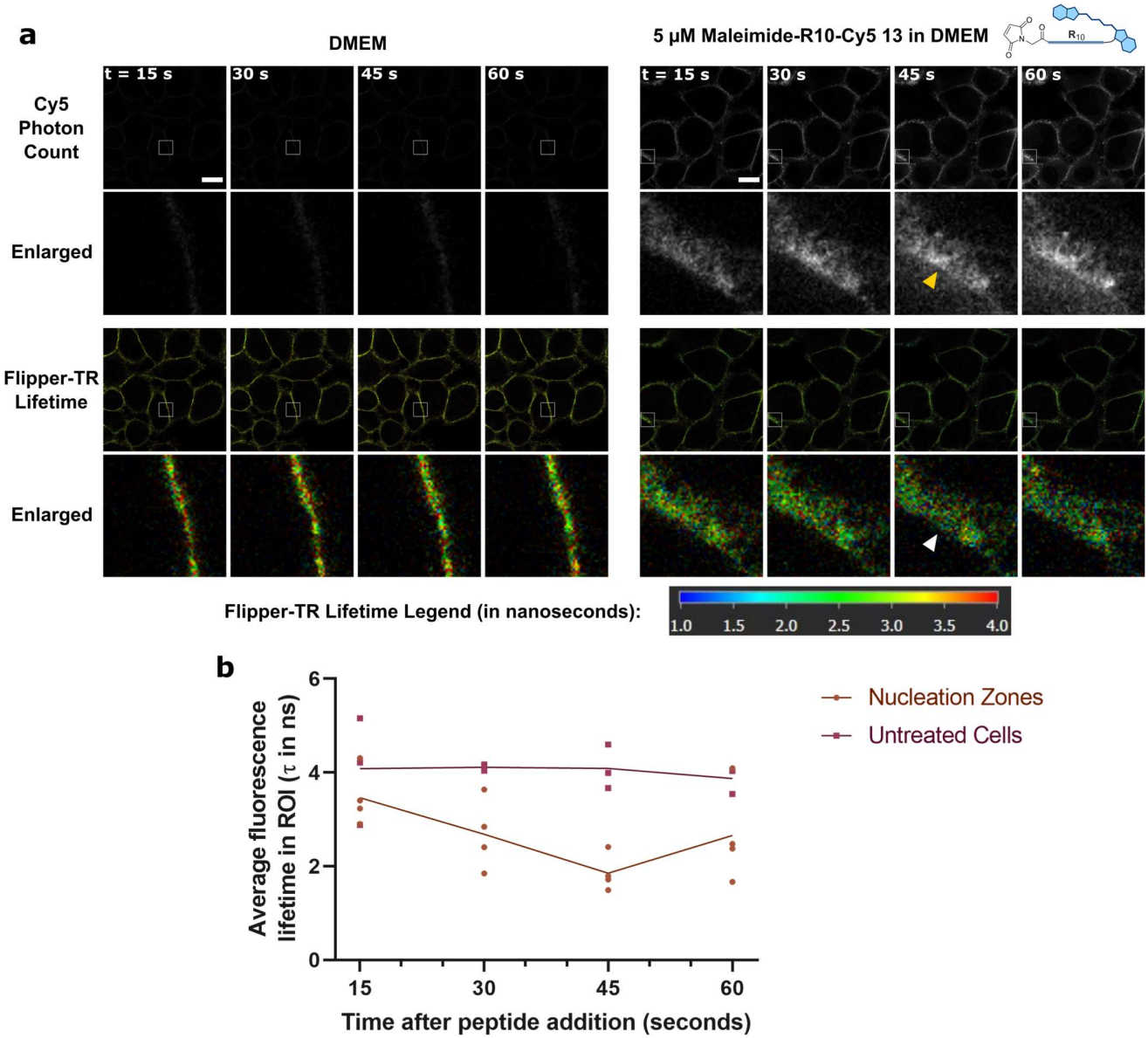

SI Fig. 22 Cellular uptake of Maleimide-R10-Cy5 peptide 13 in presence of Flipper-TR membrane tension probe. a, HeLa Kyoto cells were pre-incubated in DMEM with 2 µM Flipper-TR (Spirochrome). Afterwards, DMEM or 10 µM Maleimide-R10-Cy5 **13** in DMEM were added to the cells. Fluorescence lifetime images were acquired every 15 seconds for 60 seconds. Shown are the Cy5 photon count and the FastFLIM images. The arrows indicate a site where the CPP is enriched (Cy5 channel) and where the lifetime of the Flipper-TR probe decreases. **c**, Four ROIs in membrane regions for each time-lapse were chosen. A double exponential fit was applied to the fluorescence decay, and the weighted average lifetime was calculated for each ROI. This value was then plotted over time. Shown are individual values and the mean as a line. At nucleation zones, the membrane tension decreases throughout the experiment. Scale bars 20 µm.

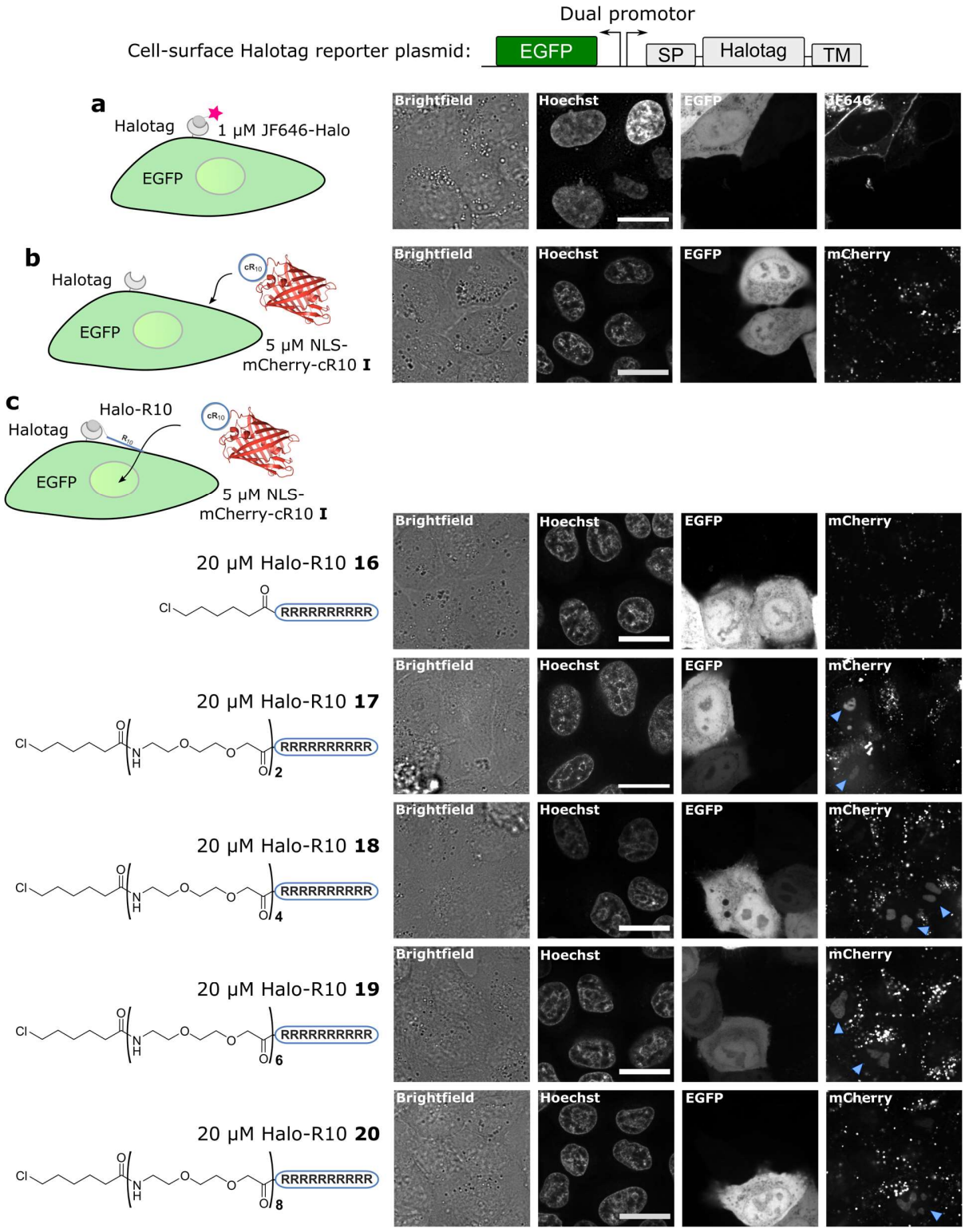

SI Fig. 23 Halotag-tethering of CPP and delivery of NLS-mCherry-cR10 I into Halotag-expressing cells. a, Cells transfected with the Halotag-EGFP reporter plasmid express EGFP inside the cell and Halotag on the cell surface. Transfected cells were treated with 1 μM JF646-Halotag-ligand (Promega). The fluorophore shows staining of the cell membrane (and secretory pathway) in EGFP-expressing cells only. **b**, Delivery of 5 μM NLS-mCherry-cR10 **I** on cells transfected with the reporter plasmid. **c**, Delivery of 5 μM NLS-mCherry-cR10 **I** in presence of 20 μM "Halo-R10" variants on cells transfected with the reporter plasmid. Blue arrowheads show nucleoli with mCherry fluorescence. See also main text figure 3. Scale bars 20 μm.

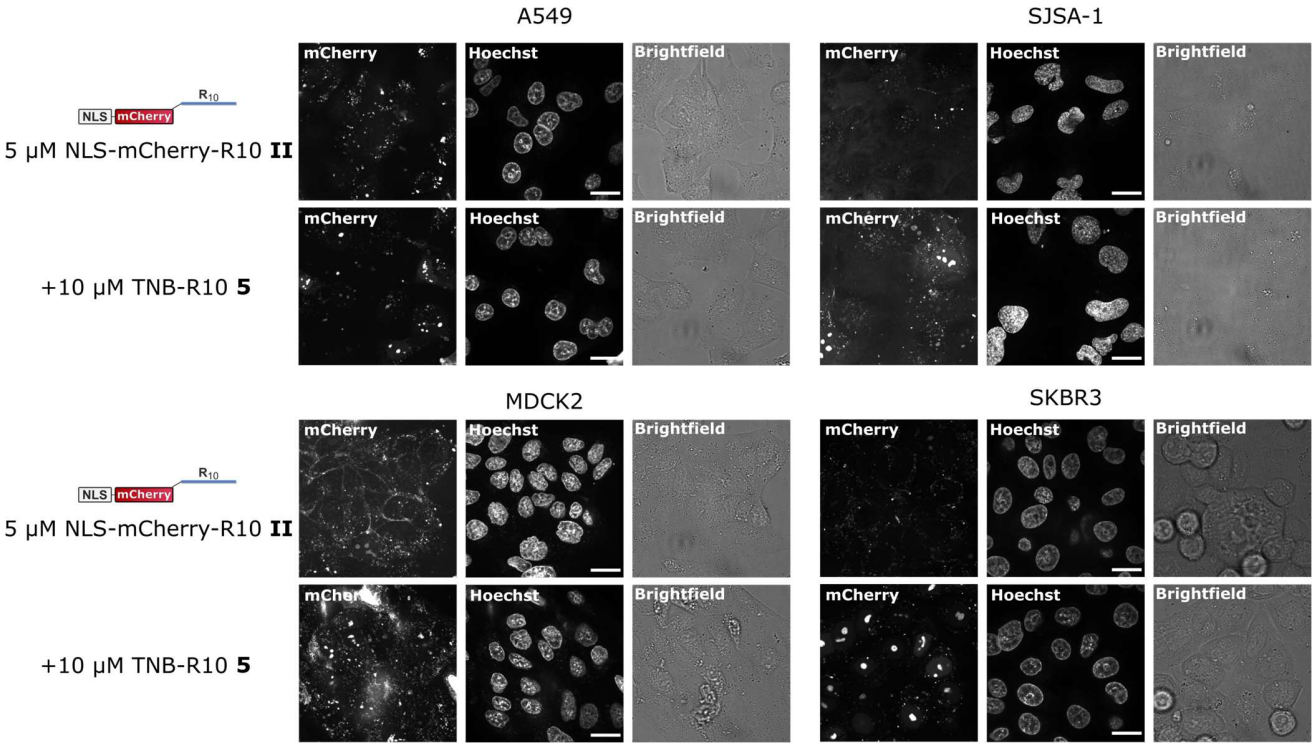

SI Fig. 24 Confocal microscopy images from all channels from the screen of different cell lines in the co-delivery of NLS-mCherry-R10 II with TNB-R10 5. Scale bars 20 μm.

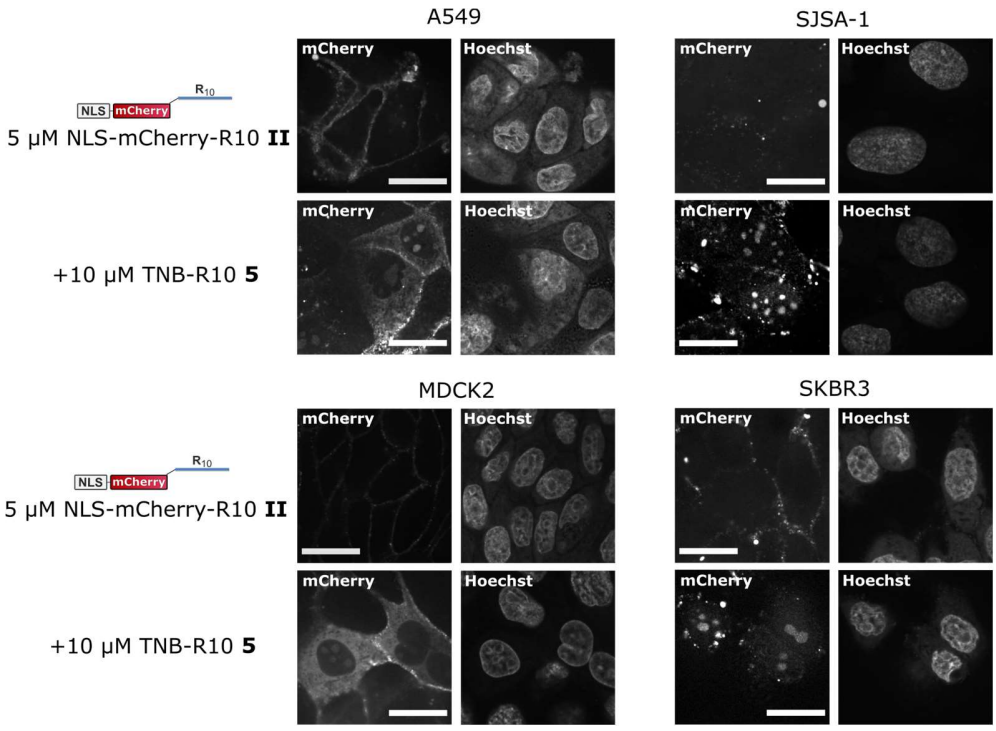

SI Fig. 25 Cellular uptake of NLS-mCherry-R10 II with or without added TNB-R10 5 at 4°C in various cell lines. Scale bars 20 μm.

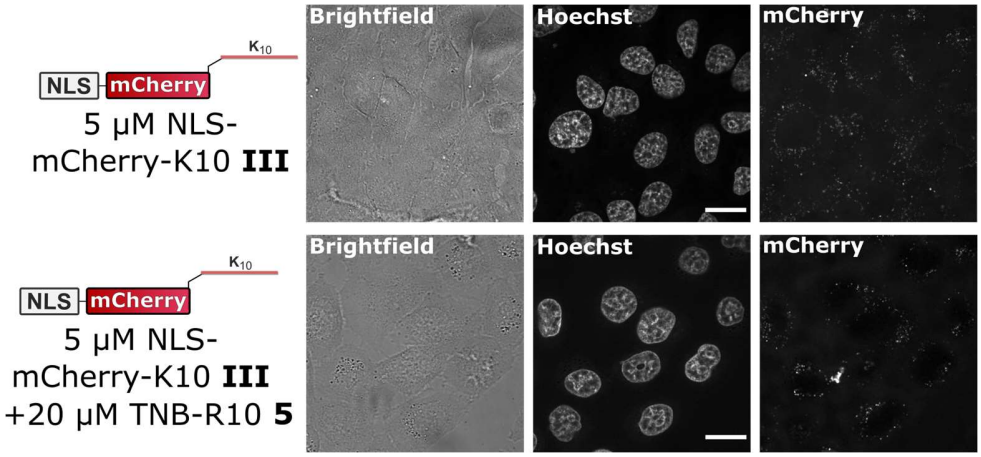

SI Fig. 26 Confocal microscopy images of cellular uptake of NLS-mCherry-K10 III with or without TNB-R10 5. Scale bars 20 μm.

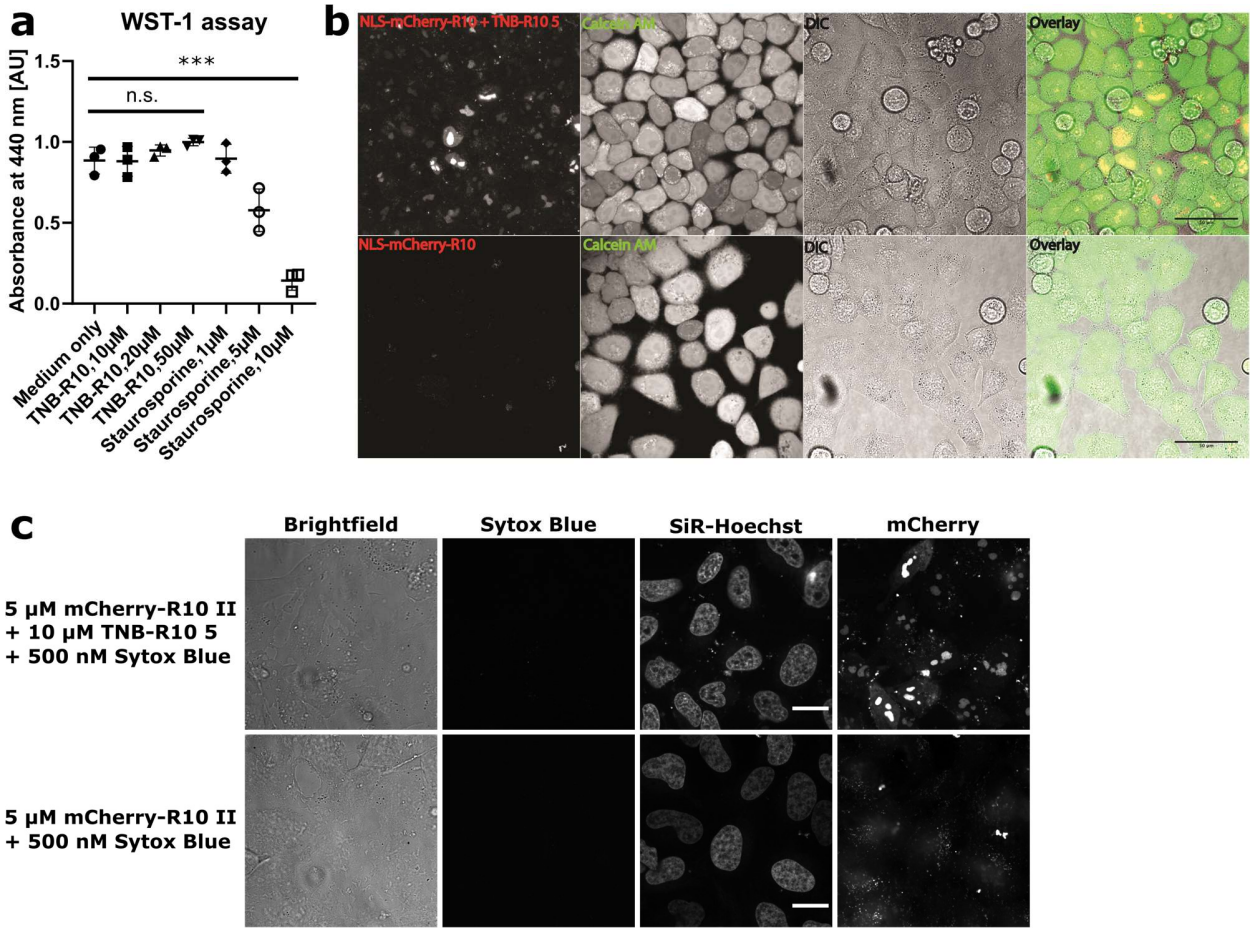

SI Fig. 27 Cell viability assays of cells treated with TNB-R10 5. a, WST-1 assay of HeLa CLL-2 cells. Absorbance at 440 nm is indicative of cellular metabolic activity in the processing of WST-1 to the absorbing Formazan. TNB-R10 had no effect on metabolism up to 50 μM peptide, while the positive control staurosporine had a significant, detrimental effect at a 10 μM concentration under the same treatment conditions. n.s. = not significant, *** = P<0.0005. **b**, Calcein AM cell viability assay of HeLa Kyoto cells. The cells were treated with either 5 μM NLS-mCherry-R10 **II** in DMEM alone (lower panel) or with 10 μM TNB-R10 **5** in DMEM (upper panel). After one-hour incubation, cells were washed again in DMEM and

treated with 5 µM Calcein AM in DMEM. The morphology of the cells as shown in the differential interference contrast (DIC) images is also unaffected. Scale bars 50 µm. **c**, Co-delivery of NLS-mCherry-R10 **II** in presence of Sytox Blue dead cell stain with or without added TNB-R10 **5**. Scale bars 20 µm.

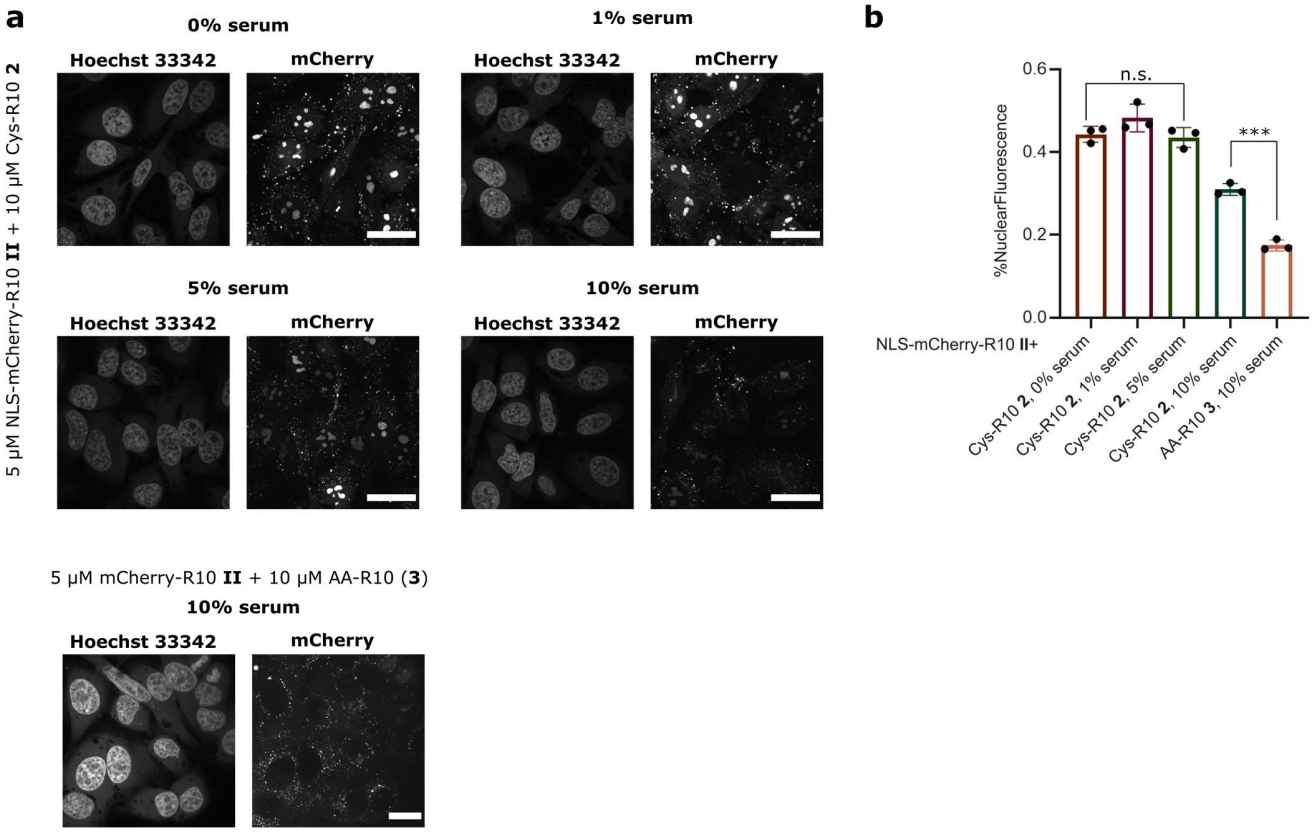

SI Fig. 28 Uptake of NLS-mCherry-R10 II in presence of additional Cys-R10 2 or AA-R10 3 and serum. a, Microscopy pictures showing the fluorescence of NLS-mCherry-R10 **II** after uptake with additional CPP in varying amounts of serum, at 37°C. Scale bars 20 µm. **b**, Quantification of relative nuclear fluorescence intensities from microscopy pictures. n.s. = not significant, *** = P<0.0005.

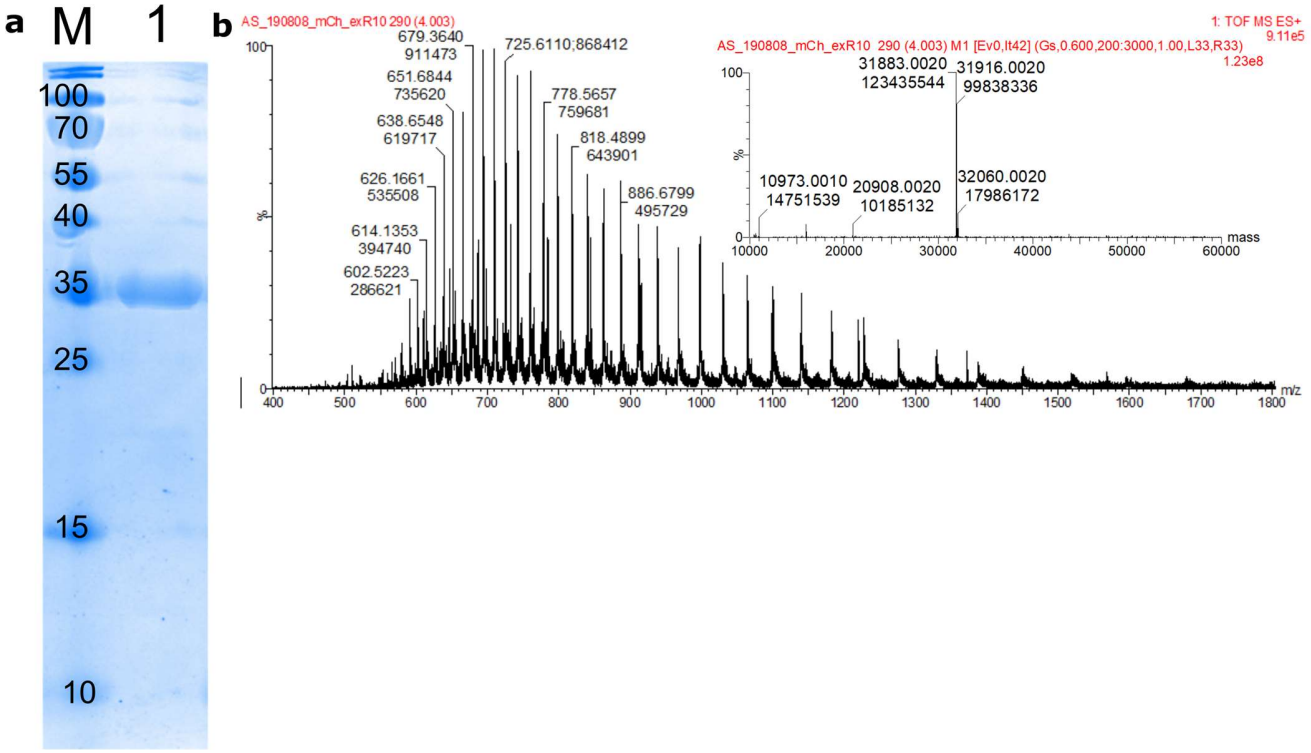

SI Fig. 29 Characterization of NLS-mCherry-exR10 IV. a, SDS-PAGE gel showing the purity of mCherry-exR10 **IV**. **b**, High resolution mass spectrum of NLS-mCherry-exR10 **IV**, Calc.: 31883 [M+H], 32060 [M+Gluconoylation+H][6]; Exp.: 31883, 32060.

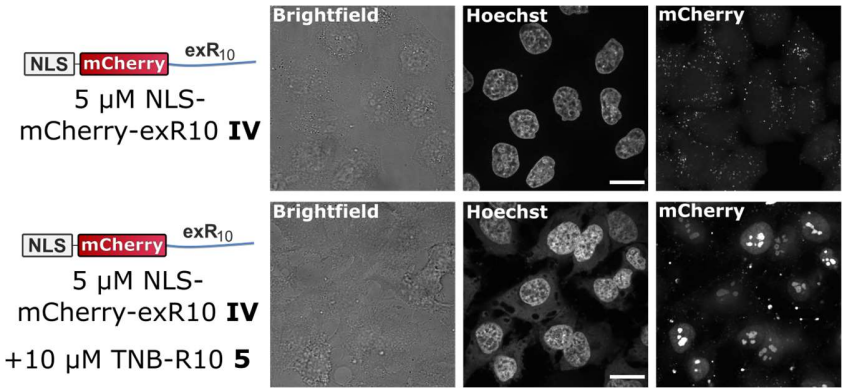

SI Fig. 30 Confocal microscopy images of cellular uptake of NLS-mCherry-exR10 IV with or without TNB-R10 5. Scale bars 20 µm.

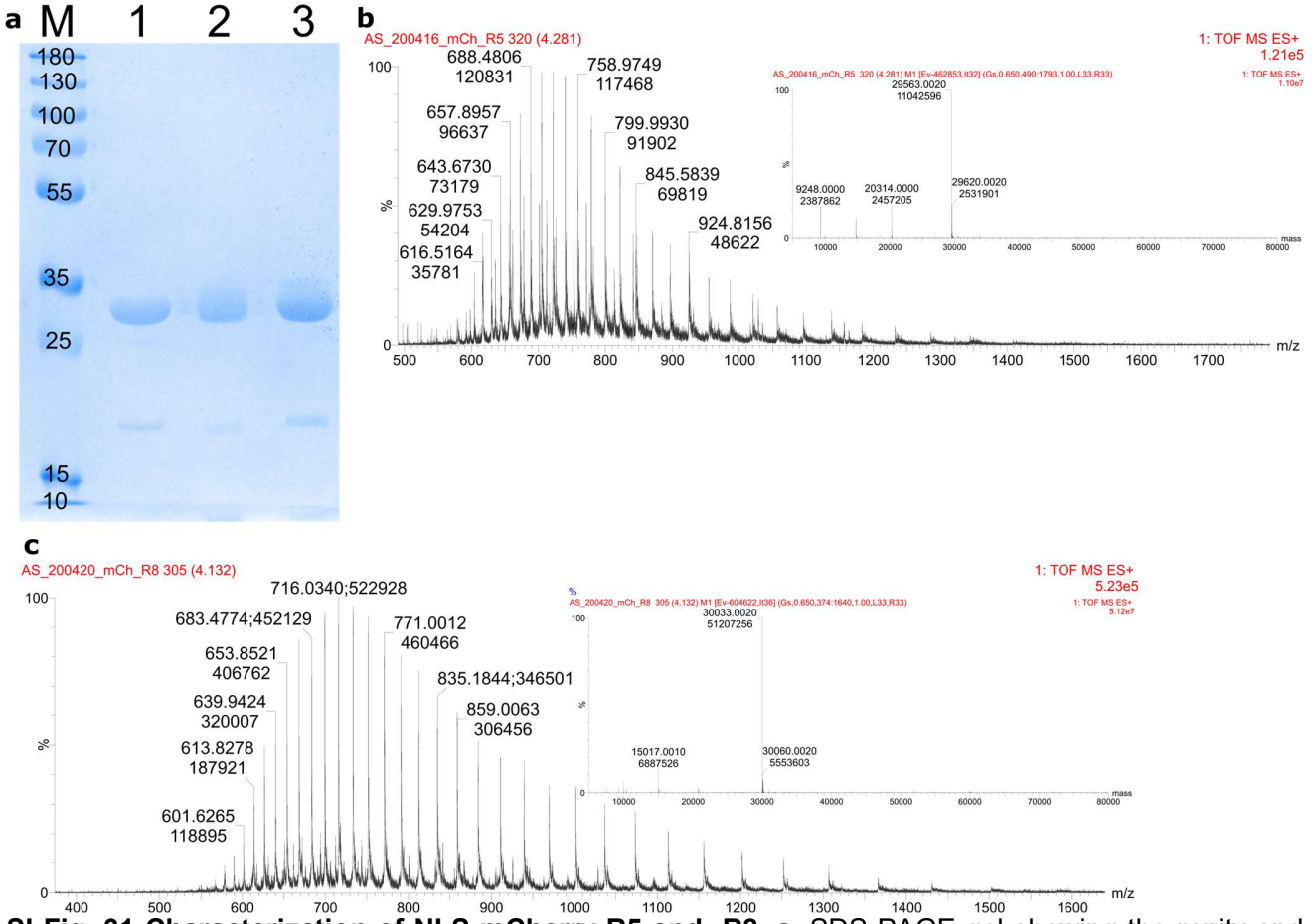

SI Fig. 31 Characterization of NLS-mCherry-R5 and -R8. a, SDS-PAGE gel showing the purity and conversion of NLS-mCherry (lane 1) to the R5 and R8 conjugates (lanes 2-3). **b**, High resolution mass spectrum of NLS-mCherry-5, Calc.: 29564 [M+H]; Exp.: 29563. **c**, High resolution mass spectrum of NLS-mCherry-R8, Calc.: 30033 [M+H]; Exp.: 30033.

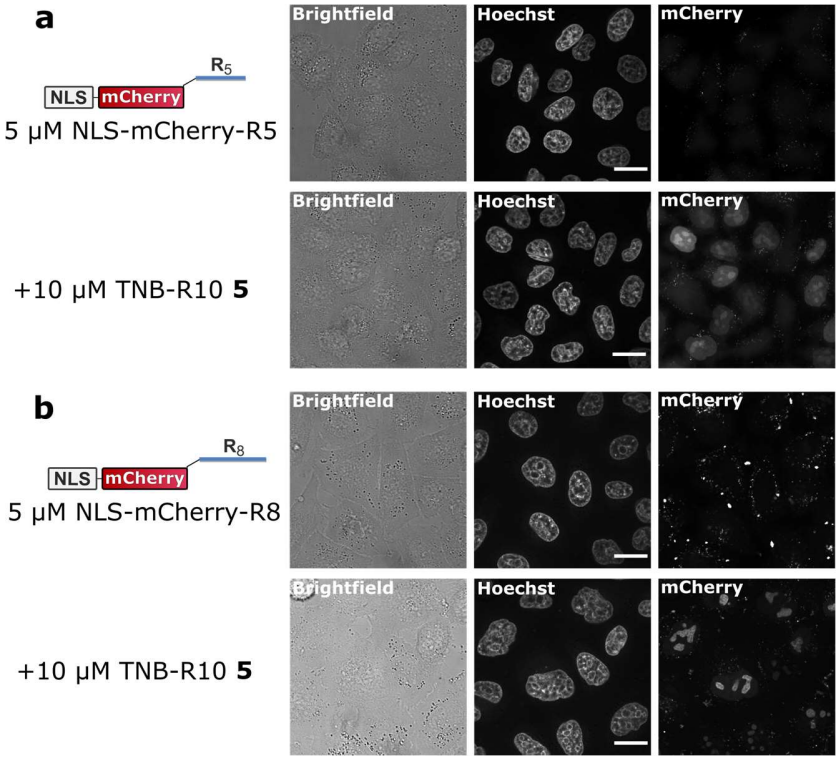

SI Fig. 32 Confocal microscopy images of cellular uptake of NLS-mCherry-R5 and -R8. a, Cellular uptake of NLS-mCherry-R5 with or without additive TNB-R10 **5**. **b**, Cellular uptake of NLS-mCherry-R8 with or without additive TNB-R10 **5**. Scale bars 20 µm.

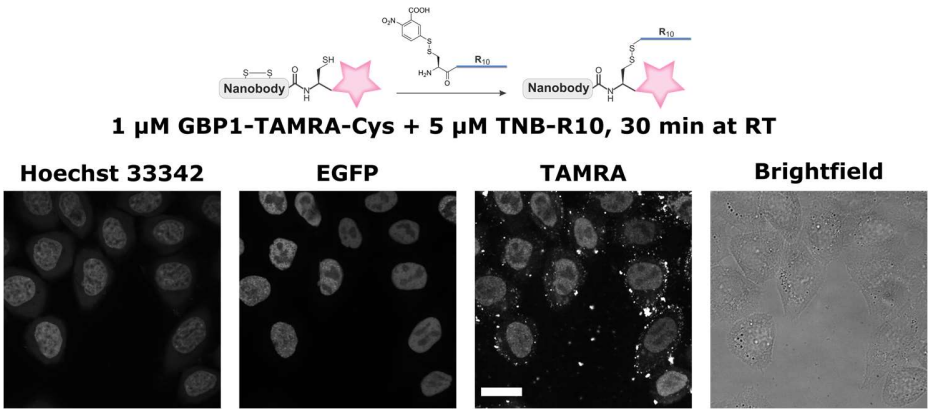

SI Fig. 33 *In situ* uptake of TAMRA-labelled GBP1 nanobody after 30-minute incubation with TNB-R10. The GBP1 nanobody with a free cysteine (after expressed protein ligation and size-exclusion chromatography (see supplementary methods and scheme in SI Fig. 2) was incubated with TNB-R10 (**5**) for 30 minutes at room temperature. The mixture was then added to HeLa Kyoto cells expressing GFP-PCNA. After 1 hour at 37°C, the cells were washed, counterstained with Hoechst 33342 and imaged. Scale bar 20 µm.

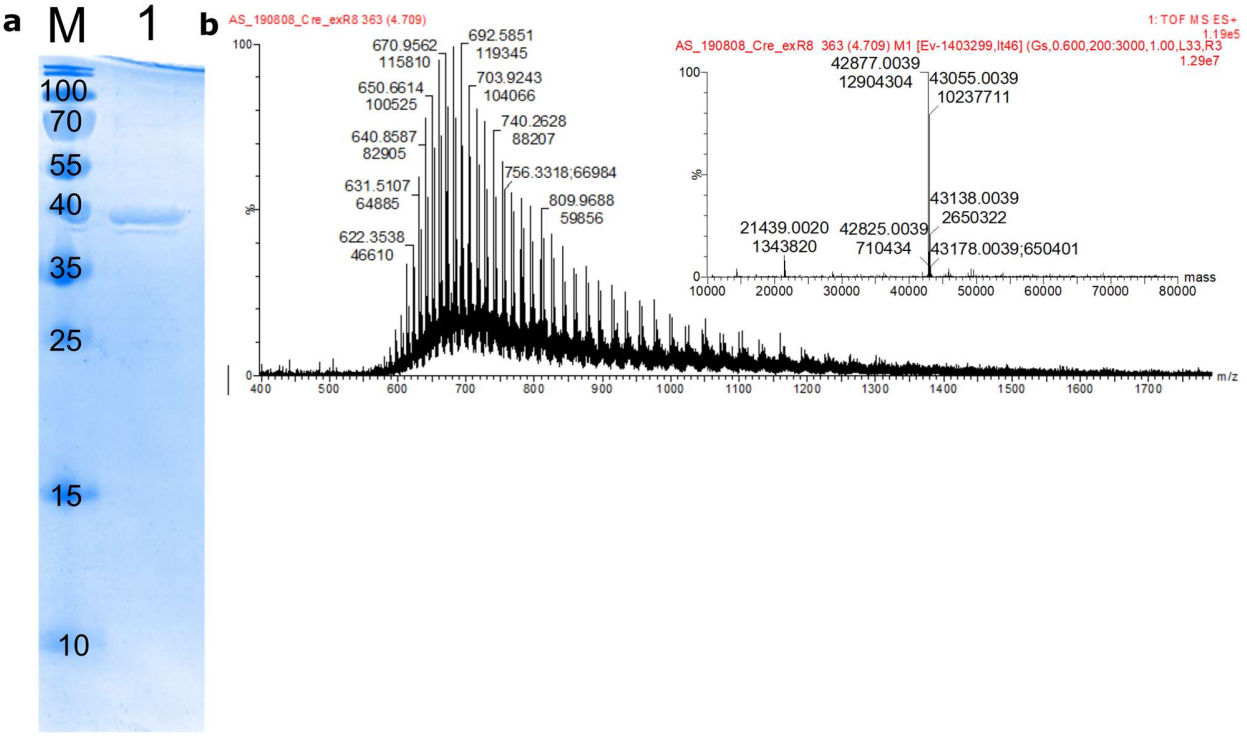

SI Fig. 34 Characterization of Cre-exR8. a, SDS-PAGE gel showing the purity of Cre-exR8. **b**, High resolution mass spectrum of Cre-exR8, Calc.: 42876 [M+H], 43054 [M+Gluconoylation+H]; Exp.: 42877, 43055.

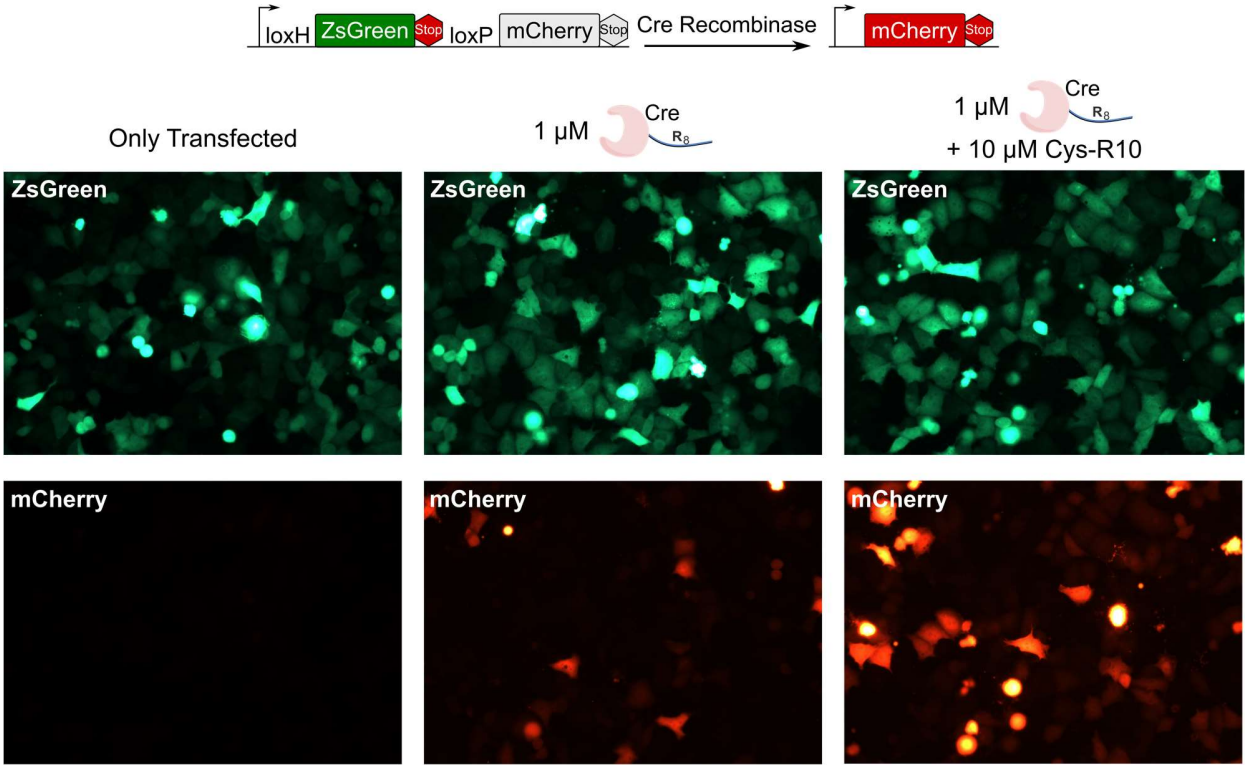

SI Fig. 35 Epifluorescence microscopy pictures of HeLa CCL-2 cells transiently transfected with Cre-Stoplight 2.4 and treatment with Cre-exR8. Cells treated with Cre-exR8 in presence of additional Cys-R10 show higher incidence of red fluorescence.

Supporting Methods

General materials and methods

Solvents and chemicals

Solvents (DMF, DCM) were purchased from Thermo Fisher Scientific (USA). Amino acids, rink amide resin and coupling reagents were purchased from Iris Biotech (Germany). 5(6)-Carboxytetramethylrhodamine (TAMRA) was purchased from Merck (Germany). HATU was purchased from Bachem (Switzerland). DIEA and TFA were purchased from Carl Roth (Germany).

Salts, LB medium, antibiotics and other buffer components were purchased from Carl Roth (Germany).

Mammalian cell culture media and fetal bovine serum were purchased from VWR (USA).

Analytical UPLC-MS

UPLC-UV traces were obtained on a Waters H-class instrument equipped with a Quaternary Solvent Manager, a Waters autosampler and a Waters TUV detector with an Acquity UPLC-BEH C18 1.7 µm, 2.1x 50 mm RP column. The following gradient was used: A = H_2O + 0.1% TFA, B = MeCN + 0.1% TFA 5-95% B 0-5 min, flow rate 0.6 mL/min. UPLC-UV chromatograms were recorded at 220 nm.

Preparative HPLC

Preparative HPLC of peptides was done on a Gilson PLC 2020 system using a Nucleodur C18 Htec Spum column (Macherey-Nagel, 100 A, 5 m, 250 mm x 32 mm, 30 mL/min). The following gradient was used in all purifications: A = H_2O + 0.1% TFA, B = MeCN + 0.1% TFA 5% B 0-10 min, 5-50% B 10-60 min, 50-99% 60-80 min.

High resolution mass spectrometry (HRMS)

High resolution mass spectra were measured on a Xevo G2-XS QTof (Waters) mass spectrometer coupled to an acquity UPLC system running on water and acetonitrile, both with 0.01% formic acid. Protein spectra were devonvoluted using the MaxEnt 1 tool.

Size exclusion chromatography of proteins

Size exclusion chromatography was done on an AKTA Purifier system (GE Healthcare) on a Superdex S75 increase 16/600 column (GE Healthcare) for all proteins except antibodies, which were purified after fluorescent labelling on a Superose 6 16/600 column (GE Healthcare).

SDS-PAGE

Proteins were mixed with 4x reducing Laemmli buffer (Bio-Rad) and boiled at 95° C for 5 minutes before separation on 15% SDS-PAGE gels. In-gel fluorescence was imaged first, followed by Coomassie staining and imaging. Gels were imaged on a ChemiDoc XRS+ system (Bio-Rad).

Software

Microscopy pictures were processed with ImageJ including the FIJI package. Graphing and statistics were done using Graphpad Prism 8. Flow cytometry data was processed and analyzed using FlowJo.

Peptide synthesis

All peptides were synthesized by standard Fluorenylmethoxycarbonyl (Fmoc)-solid-phase peptide synthesis (SPPS) on Rink amide resin (0.05 mmol scale, 0.22 mmol/g). Amino acid couplings were done using five equivalents of amino acid with five equivalents of HCTU (O-(1H-6-Chlorobenzotriazole-1-yl)-1,1,3,3-tetramethyluronium hexafluorophosphate) and four equivalents of Oxyma (Ethyl cyanohydroxyiminoacetate) with ten equivalents of DIEA (N,N-Diisopropylethylamine) in DMF (Dimethylformamide). Fmoc removal was accomplished by incubating the resin three times for five minutes with a 20% solution of piperidine in DMF.

Cyclization of the cyclic R10 peptides was done by incorporation of a lysine and glutamic acid residue flanking the CPP sequence, orthogonally protected by N-Allyloxycarbonyl (Alloc) and allyl, respectively. The orthogonal protecting groups were removed using palladium tetrakis ($Pd(PPh_3)_4$ (0.1 equivalents) with phenylsilane (25 equivalents) in dry dichloromethane (DCM) for 30 min at ambient temperature under argon atmosphere. To remove the Pd catalyst afterwards, the resin was washed additionally with 0.2 M DIEA in DMF. Cyclization followed with one equivalent of 1-[Bis(dimethylamino)methylene]-1H-1,2,3-triazolo[4,5-b]pyridinium 3-oxid hexafluorophosphate (HATU) and two equivalents of DIEA in DMF for two hours at room temperature.

Arginine was incorporated with Pbf protection, cysteine was incorporated on the N-termini with Boc and Trityl protection. In the K10 peptide, Lysine with Boc protection on the side chain was used.

In the synthesis of the fluorescent peptides bearing a TAMRA- or Cy5- fluorophore on the side-chain of a lysine, the linear synthesis was completed first with a lysine that was orthogonally protected with N-methyltrityl (Mtt). After completion of the linear synthesis, Mtt was removed using 2% TFA with 2% TIS in DCM, five times for two minutes and the fluorophore was subsequently coupled with one equivalent of fluorophore and one equivalent of HATU and four equivalents of DIEA.

For the synthesis of the peptides with an N-terminal TAMRA fluorophore, the N-terminal Fmoc protection was removed as above and the fluorophore was coupled using one equivalent of the fluorophore with one equivalent of HATU and four equivalents of DIEA.

The linear sequences of all peptides used in this study is found in supplementary table 1, the final structure and analytical data in supplementary figure 1.

Supplementary table 1 Linear sequences of peptides used in this study. PEG* corresponds to two consecutively coupled units of 8-amino-3,6-dioxaoctanoic acid. Uppercase letters are L-amino acids while lower case letters are D-amino acids.

Peptide	Sequence
TAMRA-cR10	TAMRA-K(Alloc)RrRrRrRrRrE(Allyl)-Amide
Cys-TAMRA	C-PEG*-K(Mtt)-G-Amide
Maleimide-cR10	Maleimidoacetic acid-PEG*-K(Alloc)RrRrRrRrRrE(Allyl)-Amide
Cys-cR10	C-PEG*-K(Alloc)RrRrRrRrRrE(Allyl)-Amide
Maleimide-R10	Maleimidoacetic acid-PEG*-RRRRRRRRRR-Amide
Cys-R10	C-PEG*-RRRRRRRRRR-Amide
Maleimide-K10	Maleimidoacetic acid-PEG*-KKKKKKKKKK-Amide
Cys-R10-TAMRA	C-PEG*-RRRRRRRRRR-K(Mtt)-Amide
TAMRA-R5-Cys-R5	RRRRRCRRRRR-Amide

TAMRA-R10-Cys	RRRRRRRRRRC-Amide
Maleimide-R10-Cy5/Biotin	Maleimidoacetic acid-PEG*-RRRRRRRRRRK(Mtt)-Amide
Halo-R10	6-chlorohexanoic acid-PEG*-RRRRRRRRRR-Amide
Maleimide-R5	Maleimidoacetic acid-PEG*-RRRRR-Amide
Maleimide-R8	Maleimidoacetic acid-PEG*-RRRRRRRR-Amide

For the synthesis of the alkylated peptides in which the cysteine is modified with iodoacetamide, the cysteine equivalent was taken up in water at a 5 mM concentration and 5 equivalents of iodoacetamide were added for 1 hour at RT. The resulting peptide was immediately purified using reverse phase HPLC to prevent overalkylation. The di-R10 dimer was generated by incubating the Cys-R10 peptide in oxygenated 5 mM HEPES buffer at pH 7.5 for 3 days at room temperature. The Ellman's reagent (thionitrobenzoic acid, TNB) peptides were generated by reacting the cysteine variants at a 5 mM concentration with 10 equivalents of Ellman's reagent (5,5'-dithiobis-(2-nitrobenzoic acid)) and the resulting peptides were purified by reverse phase HPLC.

Protein-CPP conjugation

To conjugate the maleimide-functionalized R10, cR10 and K10 peptides to the thiol containing proteins, the proteins were diluted to 50 µM concentration in 5 mM HEPES at pH 7.5, 140 mM NaCl, 2.5 mM KCL, 5 mM Glycin. 5 equivalents of the maleimide-peptide were added, and the solution was incubated overnight at room temperature. Excess cell-penetrating peptide was removed by desalting in a spin column.

For the *in situ* CPP conjugation and cell uptake, proteins were diluted to 5 or 25 µM in HEPES buffer (5 mM HEPES at pH 7.5, 140 mM NaCl, 2.5 mM KCL, 5 mM Glycin) and 25 or 75 µM TNB-R10 (for the nanobody and mCherry, respectively) were added for the indicated times. The proteins were then diluted to 1 or 5 µM with DMEM and immediately used in cell experiments.

Cellular uptake experiments

Cell culturing is described in the supplementary methods, along with a list of cell lines used in this study. For microscopy experiments, 20´000 cells (10´000 in the case of the GFP-PCNA HeLa Kyoto cell line[7]) were seeded into the wells of a 96-well glass bottom plate. The cells were left to adhere and grow for 24 hours at 37°C with 5% CO_2. For 37°C experiments, the cells were washed once with DMEM before addition of the protein samples in DMEM. The cells were incubated for 1 hour at 37°C. The cells were then washed three times with DMEM with 10% fetal bovine serum (FBS). Cells were generally imaged live with incubation at 37°C and 5% CO_2. For the quantitative microscopy experiments, the cells were fixed using 4% PFA in PBS for 30 minutes at room temperature after washing.

For 4°C experiments, the cells were pre-chilled at 4°C for 1 hour. The cells were then washed with cold DMEM and the proteins were added in cold DMEM to the cells. The cells were incubated at 4°C for 1 hour. Afterwards, the cells were washed thrice with cold DMEM with 10% FBS, before fixation with 4% PFA in PBS for 30 minutes at room temperature.

For uptake experiments with live data acquisition, cells on a 96-well plate (seeded as above) were placed into the microscope covered with 100 µl DMEM containing Hoechst stain. The nuclear stain was used to find the center of the nuclei. The autofocus was then turned on and 100 µl of the peptide solution at twice the final concentration were added to the well (to give the final concentration on the cells). Recording of images was started 30 seconds after addition of the peptide solution.

For the experiment with the anti-GFP antibody, cells were seeded as above and after 24 hours the cells were transfected with the GFP-mutant-plasmid (Lifeact-mVenus), using Lipofectamine 2000. The cells were then incubated for another 24 hours before treatment with the CPP-conjugate. For the TOMM20 antibody uptake, 200 nM MitoTracker were added to the antibody-CPP mixture before addition to the cells.

Microscopy

Confocal microscopy images were acquired on a Nikon-CSU spinning disc microscope with an CSU-X1 (Andor) and a live cell incubation chamber (OKOlab). All images shown in this work were acquired using a PlanApo 60x NA 1.4 oil objective (Nikon) and an EMCCD (AU888, Andor). Brightfield images were aquired along with fluorescence images. Standard laser, a quad Dicroic (400-410,486-491, 560-570, 633-647, AHF) and Emission filters were used in the acquisition of confocal fluorescence images (BFP (Hoechst 33342), ex.: 405 nm em.:450/50:, GFP (Atto488, mVenus), ex.: 488 em.:525/50, RFP (TAMRA, mCherry, Alexa 594, MitoTracker Red CMXRos), ex.: 561 em.:600/50 nm and iRFP (Cy5, SiR-Hoechst), ex.: 640 em.:685/50 nm. The microscopy images of cells treated with Cre recombinase were acquired on a Nikon Eclipse Ti2 epifluorescence microscope using the GFP and RFP filter sets. The microscopy pictures of the anti-TOMM20 antibody uptake were taken using an additional 1.5x optical magnification.

Quantification of cellular uptake was done using a script for FIJI, see section “Quantification Script”. Briefly, the Hoechst stain was used as a mask for the nuclei. The red fluorescence channel was background subtracted and the red fluorescence within the nuclear mask and outside of it was quantified. Nuclear fluorescence was either normalized to the nuclear area (absolute fluorescence graph in Fig. 2) or to the sum of nuclear and outside fluorescence (relative fluorescence graph in SI Fig. 6). Pearson’s correlation coefficient was calculated using the Coloc2 tool in Fiji.

Antibody modification and uptake

A list of antibodies can be found in table 2. Antibodies were used at a 0.5 mg/mL concentration (~6.7 µM). The anti-GFP antibody was purchased as a fluorophore conjugate. The Brentuximab and anti-TOMM20 antibody were first labelled fluorescently using 8 equivalents of NHS-Atto488 (Atto-Tec GmbH) for 1 hour at room temperature before purification via gel filtration on a superpose 6 column. All antibodies were then modified with 25 equivalents of Traut’s reagent (2-Iminothiolane) for 1 hour at room temperature. Excess reagent was removed using a desalting column. Then, 20 equivalents of TNB-R10 were added immediately and the antibodies were incubated in the fridge until use. The antibodies were diluted to 500 nM in DMEM before cell experiments.

Table 2 Antibodies used in this study.

Antibody	Source
Brentuximab	Ludwig-Maximilians-Universität (LMU) München, Germany
Alexa Fluor 594 anti-GFP Antibody, Clone 1GFP63	BioLegend (USA)
Anti-Tom20/Tomm20, clone 2F8.1	Merck (Germany)

Cloning, protein expression and purification

GBP1 Nanobody:

The GBP1 nanobody was expressed and labelled through expressed protein ligation (EPL), similarly to a previously published protocol[8]. Briefly, the nanobody was expressed in BL21 DE3 cells as a fusion protein with the DnaE intein and a chitin binding domain (pTXB1 vector system). Protein sequence (Nanobody sequence after intein cleavage underlined):

MADVQLVESGGALVQPGGSLRLSCAASGFPVNRYSMRWYRQAPGKEREWVAGMSSAGDRSSYED
SVKGRFTISRDDARNTVYLQMNSLKPEDTAVYYCNVNVGFEYWGQGTQVTVSSAAACITGDALVALP
EGESVRIADIVPGARPNSDNAIDLKVLDRHGNPVLADRLFHSGEHPVYTVRTVEGLRVTGTANHPLLCL
VDVAGVPTLLWKLIDEIKPGDYAVIQRSAFSVDCAGFARGKPEFAPTTYTVGVPGLVRFLEAHHRDPDA
QAIADELTDGRFYYAKVASVTDAGVQPVYSLRVDTADHAFITNGFVSHATGLTGLNSGLTTNPGVSAW
QVNTAYTAGQLVTYNGKTYKCLQPHTSLAGWEPSNVPALWQLQ*

For the expression, T7 express cells (New England Biolabs) were transformed with the plasmid and grown overnight at 37°C in 5 mL of LB medium with 100 µg/mL ampicillin. The next day, the expression culture in 250 mL LB medium with ampicillin was inoculated with 1 mL of the starter culture. The culture was incubated at 37°C until it reached an OD600 of 0.6. Protein expression was then induced using 1 mM IPTG and the culture was incubated for 16 hours at 18°C. Cells were collected by centrifugation at 4000xg for 15 minutes. The cells were washed once in PBS, then resuspended in lysis buffer (20 mM Tris-HCl, pH 8.5, 500 mM NaCl, 1 mM EDTA, 0.1% Triton X-100, 100 µg/mL lysozyme and 25 µg/mL DNAse I), lysed using sonication (3x 2 min, 30% Amplitude), followed by debris centrifugation at 25'000xg for 30 min.

For the purification, the clear lysate was loaded on 2 mL of chitin-agarose, equilibrated in EPL buffer (20 mM Tris-HCl pH 8.5, 500 mM NaCl). The agarose beads were washed with 20 column volumes of EPL buffer. Then, a TAMRA- and cysteine-functionalized peptide (see SI Fig. 1b) was coupled to the C-terminus of the protein using EPL. For this, the protein was reacted on the chitin column with 1 mM peptide in 20 mM Tris-HCl pH 8.5, 500 mM NaCl and 100 mM sodium 2-mercaptoethanesulfonate for 16 hours while shaking at room temperature. The next day, the protein was washed off the column using 5 mL of EPL buffer. The protein was further purified from the reaction mixture using size exclusion chromatography on a Superdex 75 16/60 column in 5 mM HEPES at pH 7.5, 140 mM NaCl, 2.5 mM KCL, 5 mM Glycin. Peak fractions were pooled, and protein aliquots were shock-frozen and stored at -80 °C.

NLS-mCherry-Cysteine:

The protein was expressed as published previously[9]. Protein sequence (Sequence after thrombin cleavage underlined, chromophore in red, cysteine in blue):

MGSSHHHHHHSSGLVPRGSHMPAAKRVKLDMVSKGEEDNMAIIKEFMRFKVHMEGSVNGHEFEIEG
EGEGRPYEGTQTAKLKVTKGGPLPFAWDILSPQFMYGSKAYVKHPADIPDYLKLSFPEGFKWERVMN
FEDGGVVTVTQDSSLQDGEFIYKVKLRGTNFPSDGPVMQKKTMGWEASSERMYPEDGALKGEIKQRL
KLKDGGHYDAEVKTTYKAKKPVQLPGAYNVNIKLDITSHNEDYTIVEQYERAEGRHSTGGMDELYKAC
A*

For the expression, BL21 DE3 cells were transformed with the plasmid. A single colony from an agar plate was picked and grown for 24 hours at 37°C in 250 mL of LB medium with 40 µg/mL Kanamycin. Induction was not necessary. Cells were collected by centrifugation at 4000xg for 15 minutes. The cells were washed once in PBS, then resuspended in lysis buffer and lysed using sonication (3x 2 min, 30% Amplitude), followed by debris centrifugation at 25'000xg for 30 min.

For the purification, the clear lysate was loaded on 2 mL of Ni-NTA agarose. The beads were washed with 20 column volumes of PBS with 20 mM imidazole. The protein was then eluted using 2 mL of PBS containing 500 mM imidazole. The purification tag was removed by the addition of thrombin (1:1000 v/v), overnight at 37°C for 18 hours. The protein was further purified by size exclusion chromatography using

a Superdex 75 16/60 column in 5 mM HEPES at pH 7.5, 140 mM NaCl, 2.5 mM KCL, 5 mM Glycine. Peak fractions were pooled, and protein aliquots were shock-frozen and stored at -80 °C.

NLS-mCherry-exR10 **IV**:

The NLS-mCherry-exR10 construct was cloned from the NLS-mCherry plasmid using Gibson assembly[10]. A 7 amino acid long linker and 10 arginines were introduced at the C-terminus using overlap extension PCR, and the thrombin cleavage site was exchanged for a TEV protease cleavage site in the same PCR reaction. The construct was cloned back into the pET28a(+) bacterial expression plasmid in the assembly reaction.

Protein sequence (NLS in green, Chromophore in red, R10 sequence in blue):

MGSSHHHHHHSSGENLYFQGPAAKRVKLDMVSKGEEDNMAIIKEFMRFKVHMEGSVNGHEFEIEGE
GEGRPYEGTQTAKLKVTKGGPLPFAWDILSPQFMYGSKAYVKHPADIPDYLKLSFPEGFKWERVMNF
EDGGVVTVTQDSSLQDGEFIYKVKLRGTNFPSDGPVMQKKTMGWEASSERMYPEDGALKGEIKQRL
KLKDGGHYDAEVKTTYKAKKPVQLPGAYNVNIKLDITSHNEDYTIVEQYERAEGRHSTGGMDELYKAS
GSGSGRRRRRRRRRR*

NLS-mCherry-exR10 was expressed in BL21 DE3 cells transformed with the plasmid. The cells were grown overnight at 37°C in 5 mL of LB medium with 40 µg/mL kanamycin. The next day, the expression culture in 250 mL LB medium with kanamycin was inoculated with 1 mL of the starter culture. After incubation at 37°C, when the culture reached an OD600 of 0.6, expression was induced with 0.5 mM IPTG, and the culture was incubated for 16 hours at 18°C. The cells were first harvested by centrifugation at 4000xg for 15 minutes, washed once with PBS, then resuspended in lysis buffer and lysed using sonication (3x 2 min, 30% Amplitude), followed by debris centrifugation at 25'000xg for 30 min.

For the purification, the clear lysate was loaded on 2 mL of Ni-NTA agarose. The beads were washed with 20 column volumes of PBS with 20 mM imidazole. The protein was then eluted with 2 mL of PBS containing 500 mM imidazole. The purification tag was not removed as it led to unexpected degradation, possibly of the C-terminal R10 peptide. The protein was further purified by size exclusion chromatography using a Superdex 75 16/60 column in 5 mM HEPES at pH 7.5, 140 mM NaCl, 2.5 mM KCL, 5 mM Glycine. Peak fractions were pooled, and protein aliquots were shock-frozen and stored at -80 °C.

NLS-Cre-exR8:

A plasmid encoding NLS-Cre recombinase was obtained from addgene (Plasmid #62730). The Cre-exR8 construct was cloned using overlap extension PCR from the original plasmid by appending 8 arginines to the C-terminus of the protein and by appending a TEV protease cleavage site on the N-terminus of the protein. The PCR product was inserted into the pET28a vector using Gibson assembly.

Protein sequence (NLS in green, R8 peptide in blue):

MGSSHHHHHHSSGENLYFQGPKKKRKVSNLLTVHQNLPALPVDATSDEVRKNLMDMFRDRQAFSEH
TWKMLLSVCRSWAAWCKLNNRKWFPAEPEDVRDYLLYLQARGLAVKTIQQHLGQLNMLHRRSGLPR
PSDSNAVSLVMRRIRKENVDAGERAKQALAFERTDFDQVRSLMENSDRCQDIRNLAFLGIAYNTLLRIA
EIARIRVKDISRTDGGRMLIHIGRTKTLVSTAGVEKALSLGVTKLVERWISVSGVADDPNNYLFCRVRKN
GVAAPSATSQLSTRALEGIFEATHRLIYGAKDDSGQRYLAWSGHSARVGAARDMARAGVSIPEIMQAG
GWTNVNIVMNYIRNLDSETGAMVRLLEDGDASGRRRRRRRR*

NLS-Cre-exR8 was expressed by transforming the corresponding plasmid into BL21 DE3 cells, which were grown overnight at 37°C in 5mL of LB medium with 40 µg/mL kanamycin. The next day, a culture in 250 mL LB medium containing kanamycin was inoculated with 1 mL of the starter culture and grown

at 37°C until the OD600 reached 0.6. Expression was induced with 0.5 mM IPTG and the cells were incubated for another 16 hours at 18°C. The cells were harvested using centrifugation at 4000xg for 15 minutes, washed with PBS once, then taken up in 100 mM NaH_2PO_4 with 10 mM Tris pH 8.0, 300 mM NaCl, 10 mM imidazole and lysed using sonication (3x 2 min, 30% Amplitude), followed by debris centrifugation at 25'000xg for 30 min.

For the purification, the clear lysate was loaded on 2 mL of Ni-NTA agarose equilibrated in phosphate buffer (100 mM NaH_2PO_4 with 10 mM Tris pH 8.0, 300 mM NaCl, 10 mM imidazole). The protein was washed with 20 column volumes of the same buffer and subsequently eluted with the same buffer containing 250 mM imidazole. The protein was further purified on a Superdex 75 16/60 column in 100 mM NaH_2PO_4 with 10 mM Tris pH 8.0, 300 mM NaCl. Peak fractions were combined, frozen in liquid nitrogen and stored at -80°C until use.

Cloning of plasmids for transfection:

The Cre Stoplight 2.4 plasmid[11] was obtained from addgene (Plasmid #37402).

For the cell-surface halotag-reporter plasmid, a dual cytomegalovirus (CMV)-reporter plasmid that led to expression of EGFP within the cell along with a peroxidase on the cell surface (addgene plasmid #31156) was used as a starting point. A sequence encoding the halotag was generated by PCR from the pHTN vector (Promega). The peroxidase sequence was then replaced with the halotag sequence using Gibson cloning.

Mammalian cell culture

Cell lines were grown at 37° C in a humidified atmosphere with 5% CO_2. A list of cell lines with their corresponding media can be found in supplementary table 1.

Supplementary Table 1 Cell lines used in this study.

Cell line	Medium
HeLa CCL-2	DMEM 4.5 g/L Glucose + 10% fetal bovine serum (FBS), 1% Penicillin-Streptomycin (PS)
HeLa Kyoto	DMEM 4.5 g/L Glucose + 10% FBS, 1% PS
HeLa Kyoto GFP-PCNA[7,12]	DMEM 4.5 g/L Glucose + 10% FBS, 1% PS
SKBR-3	DMEM/Ham's F-12 + 10% FBS, 1% PS
A549	DMEM/Ham's F-12 + 10% FBS, 1% PS
MDCK-2	DMEM 1 g/L Glucose + 10% FBS, 1% PS
SJSA-1	RPMI 1640 + 10% FBS, 1% PS

For the Calcein AM cell viability assay, 20´000 HeLa Kyoto cells were seeded on ibidi slides. The cells were left to adhere and grow for 24 hours at 37 °C and 5% CO2. The cells were washed once with DMEM before addition of either 5 µM NLS-mCherry-R10 in DMEM alone or 5 µM NLS-mCherry-R10 with 10 µM TNB-R10 in DMEM. After one hour incubation at 37 °C and 5% CO2 cells were washed three times with DMEM before treatment with 5 µM Calcein AM (Sigma; diluted from a 500 mM stock solution of Calcein AM in dimethyl sulfoxide (DMSO)) in DMEM. Microscopy images were collected three and six hours after

addition of Calcein AM. Confocal microscopic images were acquired on a Leica SP5II equipped with an oil immersion ACS APO 63x / 1.3 NA objective with laser line at 561 nm and 488 nm using similar settings for the same fluorophores.

On-cell biotinylation, pulldown and proteomics

Each treatment and pulldown was performed in quadruplicate to obtain reliable label-free quantification (LFQ) data. 500‘000 HeLa Kyoto cells were seeded in each well of a 6-well plate. The cells were incubated for 48 hours at 37°C and 5% CO2 to adhere and grow to near-confluency. The cells were then washed three times with PBS, then incubated for 30 minutes at room temperature with either PBS only, or 20 µM of commercially available Biotin-Maleimide (Sigma-Aldrich) or the Maleimide-R10-biotin peptide. Cells were then washed twice with PBS.

For cell lysis 500 µl of lysis buffer (2% NP-40, 1% Triton X-100, 10% glycerol, EDTA free protease inhibitor tablet in PBS) was added to the cells. Cells were scraped off the plates and transferred to a reaction tube followed by incubation on ice on a shaker for 30 min. The cell extracts were centrifuged for 20 min (20800×g, at 4°C) to pellet the insoluble material.

The supernatants were mixed with 100 µl of Streptavidin-agarose beads and the beads were incubated for 1 hour at 4°C. Beads were washed twice with lysis buffer, then another two times times with 300 mM NaCl in lysis buffer.

Then, 50 µl of 4x Laemmli buffer containing beta-mercaptoethanol were added to the beads and they were boiled at 75°C for 15 minutes to denature proteins and disturb the streptavidin-biotin interaction.

20 µl for each condition were loaded on a 10% SDS-PAGE gel. The samples were only run until approximately 1 cm into the separating gel. This part was cut out and used for the in-gel tryptic digest. Samples in the gel were reduced, alkylated and digested with trypsin followed by extraction from the gel as described previously[13].

MS-spectra were input into MaxQuant to identify proteins from the Uniprot Homo Sapiens database. All cysteines were specified with a static modification for carbamidomethylation (+57.02146). Perseus was used to process the data (two-tailed t-tests, false discovery rate = 0.1) and generate the sample matrix and volcano plots.

Flow Cytometry

For the Cre recombinase experiments, 200’000 cells were seeded in each well of a 12-well plate. The cells were incubated for 24 hours at 37°C to settle, then transfected with the reporter plasmid (Cre Stoplight 2.4) using Lipofectamine 2000. The cells were incubated for another 24 hours, then treated with Cre recombinase (or medium) in DMEM with 5% FCS and incubated for 24 more hours. Microscopy pictures were then taken, and the cells were detached with accutase, dead cells stained with DAPI and all cells measured on a LSRFortessa (BD Biosciences, USA) flow cytometer. Dead cells and multiplets were removed in the analysis through gating, followed by untransfected cells that showed no fluorescence in either the green or red channel. At least 10’000 cells were counted for each condition. The gating strategy is illustrated in supplementary figure 36.

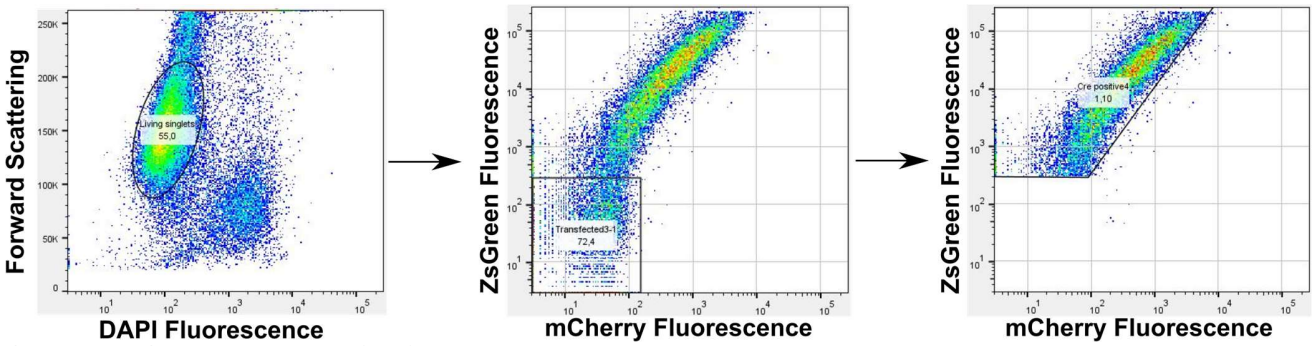

SI Fig. 36 Gating strategy for flow cytometry data.

Quantification script

The following quantification macro for FIJI opens files in a chosen directory, then identifies nuclei in the Hoechst channel (channel 1) through thresholding, fills holes and erodes once to ensure separation of nuclear from endosomal fluorescence. After that, the selected nuclear area is set as a region of interest (ROI) together with the inverse selection (area outside of the nuclei) and, after background subtraction, the fluorescence of the mCherry (in channel 2) is quantified in both ROIs.

```
//this Macro analyses NLS-mCherry in aquired images on Nikon_CSU 60x oil
//ch1=Hoechst, ch2=NLS-mCherry uptake ch3-... not used

setBatchMode(true);
dir=getDirectory("Choose Source Directory ");
list = getFileList(dir);
for(i=0; i<list.length; i++) {
	file=list[i];
	run("Bio-Formats Importer", "open=["+dir+"/"+file+"] autoscale color_mode=Default concatenate_series open_all_series rois_import=[ROI manager] view=Hyperstack stack_order=XYCZT");
	getDimensions(width, height, channels, slices, frames);

	{
		run("Bio-Formats Importer", "open=["+dir+"/"+file+"] autoscale color_mode=Default rois_import=[ROI manager] view=Hyperstack stack_order=XYCZT");
		name=getTitle;
		print(name);
		run("Duplicate...", "duplicate channels=1");
		run("Median...", "radius=5");
		run("Auto Threshold", "method=Default white");
		run("Fill Holes");
		run("Erode");
		run("Invert");
		run("Create Selection");
		roiManager("Add");
		run("Create Selection");
		run("Make Inverse");
		roiManager("Add");

		run("Set Measurements...", "area mean modal integrated display redirect=None decimal=0");
		selectWindow(name);
		run("Duplicate...", "duplicate channels=2");
		run("Subtract Background...", "rolling=100");
		run("Subtract Background...", "rolling=100");
		roiManager("Select", 0);
```

```
        run("Measure");
        roiManager("Select", 1);
        run("Measure");
        roiManager("Deselect");
        roiManager("Delete");
        run("Close All");

}
}
```

Supporting References

1 Gross, L. A., Baird, G. S., Hoffman, R. C., Baldridge, K. K. & Tsien, R. Y. The structure of the chromophore within DsRed, a red fluorescent protein from coral. *Proc Natl Acad Sci U S A* **97**, 11990-11995, doi:10.1073/pnas.97.22.11990 (2000).

2 Zhang, M., Li, M., Zhang, W., Han, Y. & Zhang, Y. H. Simple and efficient delivery of cell-impermeable organic fluorescent probes into live cells for live-cell superresolution imaging. *Light Sci Appl* **8**, 73, doi:10.1038/s41377-019-0188-0 (2019).

3 van de Ven, A. L., Adler-Storthz, K. & Richards-Kortum, R. Delivery of optical contrast agents using Triton-X100, part 1: reversible permeabilization of live cells for intracellular labeling. *J Biomed Opt* **14**, 021012, doi:10.1117/1.3090448 (2009).

4 Lorenz, S., Tomcin, S. & Mailander, V. Staining of mitochondria with Cy5-labeled oligonucleotides for long-term microscopy studies. *Microsc Microanal* **17**, 440-445, doi:10.1017/S1431927611000249 (2011).

5 Palm, C., Jayamanne, M., Kjellander, M. & Hallbrink, M. Peptide degradation is a critical determinant for cell-penetrating peptide uptake. *Biochim Biophys Acta* **1768**, 1769-1776, doi:10.1016/j.bbamem.2007.03.029 (2007).

6 Geoghegan, K. F. *et al.* Spontaneous alpha-N-6-phosphogluconoylation of a "His tag" in Escherichia coli: the cause of extra mass of 258 or 178 Da in fusion proteins. *Anal Biochem* **267**, 169-184, doi:10.1006/abio.1998.2990 (1999).

7 Chagin, V. O. *et al.* 4D Visualization of replication foci in mammalian cells corresponding to individual replicons. *Nat Commun* **7**, 11231, doi:10.1038/ncomms11231 (2016).

8 Herce, H. D. *et al.* Cell-permeable nanobodies for targeted immunolabelling and antigen manipulation in living cells. *Nat Chem* **9**, 762-771, doi:10.1038/nchem.2811 (2017).

9 Sarabipour, S., King, C. & Hristova, K. Uninduced high-yield bacterial expression of fluorescent proteins. *Anal Biochem* **449**, 155-157, doi:10.1016/j.ab.2013.12.027 (2014).

10 Gibson, D. G. Enzymatic assembly of overlapping DNA fragments. *Methods Enzymol* **498**, 349-361, doi:10.1016/B978-0-12-385120-8.00015-2 (2011).

11 Yang, Y. S. & Hughes, T. E. Cre stoplight: a red/green fluorescent reporter of Cre recombinase expression in living cells. *Biotechniques* **31**, 1036, 1038, 1040-1031, doi:10.2144/01315st03 (2001).

12 Leonhardt, H. *et al.* Dynamics of DNA replication factories in living cells. *J Cell Biol* **149**, 271-280, doi:10.1083/jcb.149.2.271 (2000).

13 Shevchenko, A., Tomas, H., Havlis, J., Olsen, J. V. & Mann, M. In-gel digestion for mass spectrometric characterization of proteins and proteomes. *Nat Protoc* **1**, 2856-2860, doi:10.1038/nprot.2006.468 (2006).

4 Summary

Since their first discovery a little over 30 years ago, cell-penetrating peptides have been the subject of intensive research. Nevertheless, there is much less work, and much more controversy, when it comes to the delivery of entire proteins using CPPs. Early reports claim that while small molecules and peptides can be taken up in a non-endocytic manner, protein-CPP conjugates would enter cells exclusively through endocytosis – and often remain trapped in endosomes. In this thesis, the delivery of proteins using cell-penetrating peptides is at the centre-stage. In several different contexts, protein delivery could in fact be achieved in an energy-independent manner.

Initially, a pair of GFP-nanobodies were chosen as an easily applicable cargo. The small antibody fragments were engineered to allow modification of at the *C*-termini using expressed protein ligation. Cyclic CPPs (Tat and R10) were attached, and the conjugates could be purified by affinity chromatography using an immobilized form of the anionic polymer heparin. The conjugates could then enter cells and could be used in downstream intracellular applications.

To explore the intracellular fate and targetability of CPP conjugates, the fluorescent protein mCherry was recombinantly expressed as a fusion protein with several peptidic targeting sequences and conjugated to a cyclic R10 CPP through either a cleavable disulfide, or non-cleavable thioether linkage. The cytosolic delivery of the protein was successful in either case, though it required elevated concentrations. Interestingly, the non-cleavable conjugate showed accumulation in the nucleoli due to the CPP, while the disulfide-linked conjugate showed clean localization to the target structure or compartment. Localization of the protein to mitochondria after delivery could not be achieved.

Finally, it was possible to devise a methodology that allows circumventing the harsh concentration dependence of CPP-mediated transport of large protein cargoes. Through usage of a low µM concentration of both the protein-CPP conjugate along with unbound, free CPP, highly efficient delivery can be achieved. The best CPP additives proved to be thiol-reactive peptides, that can label specific loci on the cell membrane through which the protein cargo can transduce. This was effective in several cell lines, as well as with many protein cargoes, amongst others full-length IgG antibodies. In future research, these findings could be used in cell-type specific delivery approaches, by labelling only specific cells with CPPs, and in applications with functional antibodies.

5 Zusammenfassung

Seit ihrer ersten Entdeckung vor etwas mehr als 30 Jahren waren zellpenetrierende Peptide bereits im Fokus zahlreicher Forschungsarbeiten. Der zelluläre Import ganzer Proteine mit Hilfe von CPPs ist hingegen noch weitaus weniger erforscht. Frühe Berichte behaupten, dass kleine Moleküle und Peptide zwar auf nicht-endozytotische Weise aufgenommen werden können, Protein-CPP-Konjugate jedoch ausschließlich durch Endozytose in die Zellen gelangen würden und oft in den Endosomen verbleiben. In dieser Arbeit steht die Einschleusung von Proteinen in das Cytosol mittels zellpenetrierender Peptide im Mittelpunkt. In verschiedenen Kontexten konnte der Import tatsächlich energieunabhängig erfolgen.

Ursprünglich wurde ein Paar GFP-Nanobodies als Modellsystem gewählt. Die kleinen Antikörperfragmente wurden so konstruiert, dass sie am C-Terminus durch die Expressed Protein Ligation modifiziert werden konnten. Zyklische CPPs (Tat und R10) wurden angehängt, und die Konjugate konnten durch Affinitätschromatographie unter Verwendung einer immobilisierten Form des anionischen Polymeres Heparin aufgereinigt werden. Die Konjugate konnten dann in die Zellen gelangen und in nachfolgenden intrazellulären Anwendungen verwendet werden.

Es wurde das intrazelluläre Schicksal von CPP-Konjugaten untersucht, auch um zu evaluieren, ob es möglich ist, ein CPP-Konjugat nach zellulärem Import in ein spezifisches Kompartiment zu leiten. Dafür wurde das fluoreszierende Protein mCherry rekombinant als Fusionsprotein mit mehreren peptidischen Zielsequenzen exprimiert. Das Protein wurde entweder über eine spaltbare Disulfid- oder eine nicht spaltbare Thioetherbindung an ein zyklisches R10-CPP konjugiert. Die Einschleusung des Proteins in das Cytosol war in beiden Fällen erfolgreich. Allerdings waren erhöhte Proteinkonzentrationen erforderlich. Interessanterweise zeigte das nicht spaltbare Konjugat aufgrund des CPP eine Akkumulation in den Nucleoli, während das disulfidgebundene Konjugat eine saubere Lokalisierung in der Zielstruktur oder dem Zielkompartiment zeigte. Eine Lokalisierung des Proteins in den Mitochondrien nach Import in die Zellen konnte nicht erreicht werden.

Schließlich war es möglich, eine neue Methodik zu entwickeln, die es erlaubt, die starke Konzentrationsabhängigkeit des CPP-vermittelten Transports großer Proteine zu umgehen. Durch die Verwendung einer niedrigen µM Konzentration sowohl des Protein-CPP-Konjugats als auch eines ungebundenen, freien CPP kann ein hocheffizienter Transport in das Cytosol erreicht werden. Die besten CPP-Additive erwiesen sich als thiolreaktive Peptide, die spezifische Loci auf der Zellmembran markieren können. Durch diese Loci können Protein-

CPP-Konjugate dann transduzieren. Dies war bei mehreren Zelllinien und einigen unterschiedlichen Proteinen, unter anderem bei IgG-Antikörpern wirksam. In zukünftiger Forschung könnten diese Erkenntnisse in CPP-basierten, zelltypspezifischen Transportansätzen genutzt werden, indem nur bestimmte Zellen mit CPPs markiert werden. Weiterhin sind auch Anwendungen mit funktionellen Antikörpern möglich.

6 Appendix

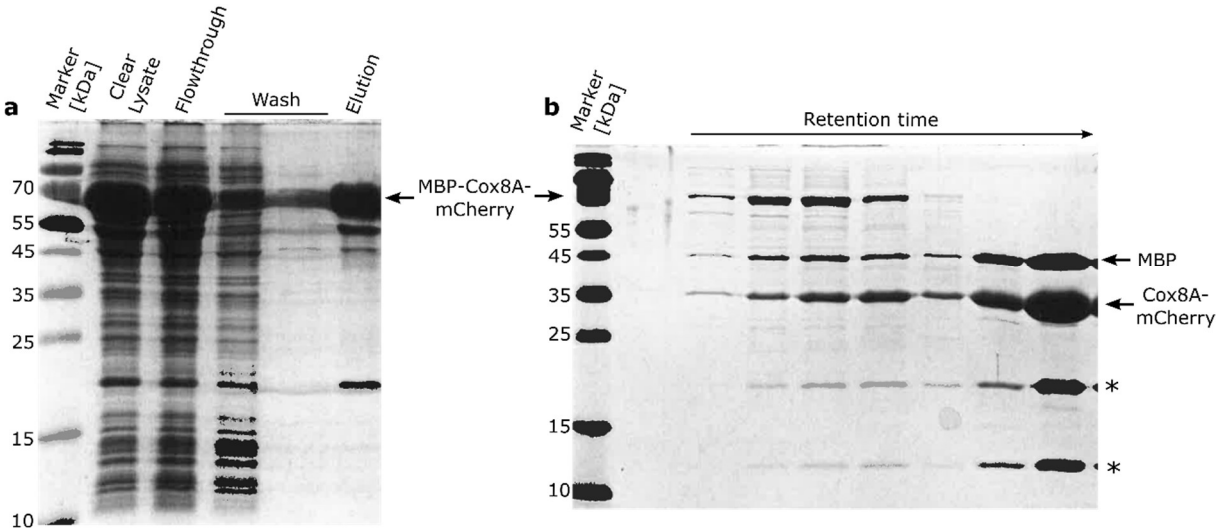

Supplementary Figure 1. **a**, Coomassie stained SDS-PAGE gel from the expression and purification of Cox8A-mCherry on amylose resin. **b**, Coomassie stained SDS-PAGE gel from the size-exclusion chromatography of the TEV-protease treated MBP-Cox8a-mCherry protein. Stars indicate cleavage products of the mCherry occurring during SDS-Page sample preparation[466].

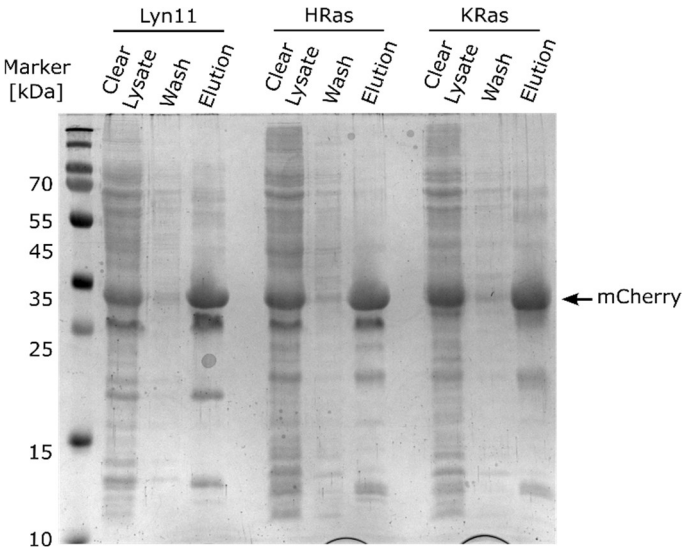

Supplementary Figure 2. Coomassie stained SDS-PAGE gel from the expression and purification of Lyn11, HRas and KRas membrane targeting sequences fused to mCherry. The purification was accomplished on nickel-NTA agarose resin.

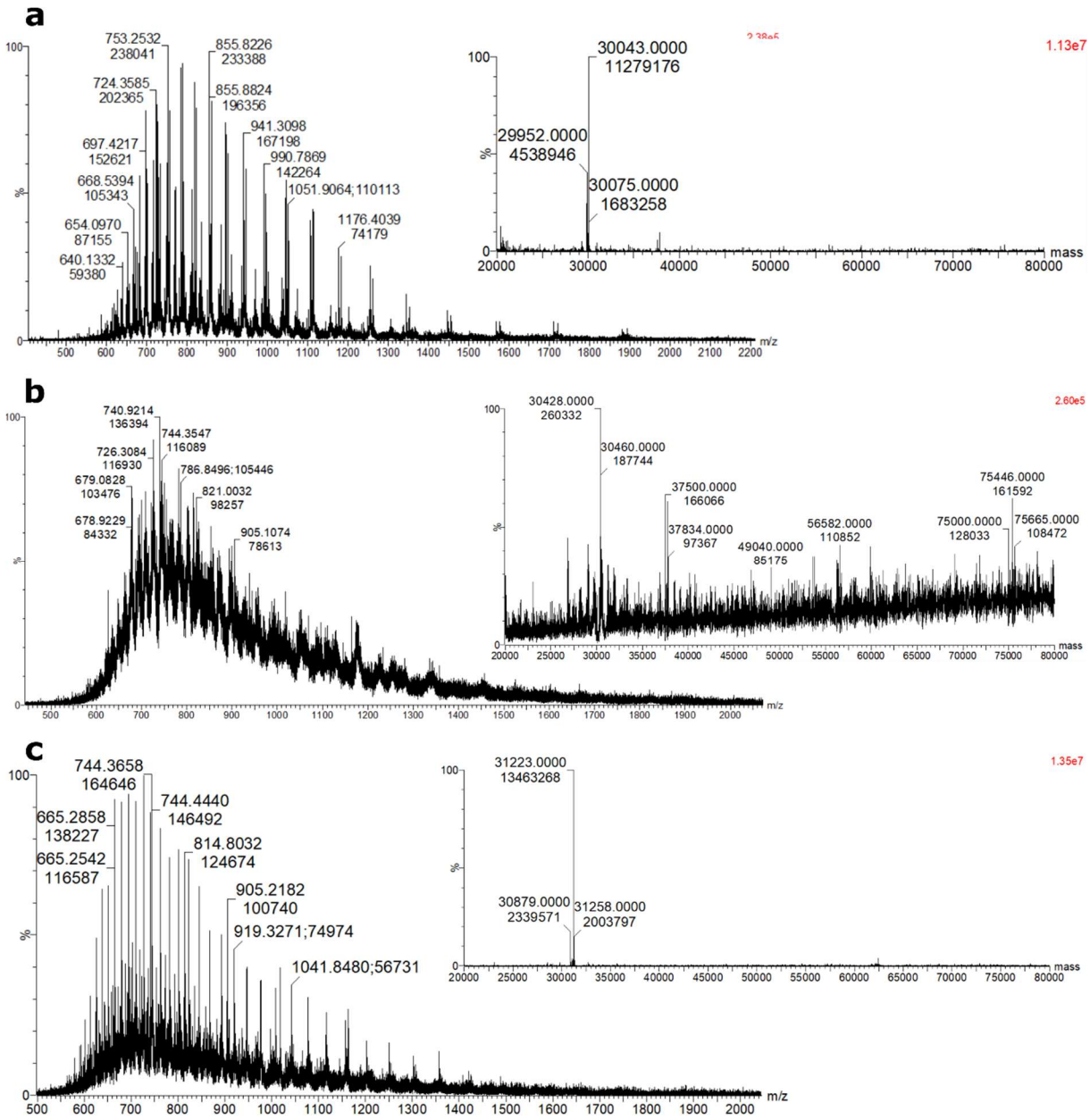

Supplementary Figure 3. High resolution mass spectra of mCherry proteins fused to membrane targeting sequences. Shown are raw spectra with deconvoluted spectra inset. **a**, Lyn11-mCherry: Calc.: 30048 [M+H]; Exp.: 30043. **b**, mCherry-HRas: Calc.: 30434 [M+H]; Exp.: 30428. **c**, mCherry-KRas: Calc.: 31228 [M+H]; Exp.: 31223.

7 References

1 Arnold, F. H. Directed Evolution: Bringing New Chemistry to Life. *Angewandte Chemie* **57**, 4143-4148, doi:10.1002/anie.201708408 (2018).

2 Mitragotri, S., Burke, P. A. & Langer, R. Overcoming the challenges in administering biopharmaceuticals: formulation and delivery strategies. *Nat Rev Drug Discov* **13**, 655-672, doi:10.1038/nrd4363 (2014).

3 Liyanage, V. R. & Rastegar, M. Rett syndrome and MeCP2. *Neuromolecular Med* **16**, 231-264, doi:10.1007/s12017-014-8295-9 (2014).

4 Pickar-Oliver, A. & Gersbach, C. A. The next generation of CRISPR-Cas technologies and applications. *Nat Rev Mol Cell Biol* **20**, 490-507, doi:10.1038/s41580-019-0131-5 (2019).

5 Wilbie, D., Walther, J. & Mastrobattista, E. Delivery Aspects of CRISPR/Cas for in Vivo Genome Editing. *Acc Chem Res* **52**, 1555-1564, doi:10.1021/acs.accounts.9b00106 (2019).

6 Lu, R. M. *et al.* Development of therapeutic antibodies for the treatment of diseases. *J Biomed Sci* **27**, 1, doi:10.1186/s12929-019-0592-z (2020).

7 Edwards, P. A. Some properties and applications of monoclonal antibodies. *Biochem J* **200**, 1-10, doi:10.1042/bj2000001 (1981).

8 Weiner, G. J. Building better monoclonal antibody-based therapeutics. *Nat Rev Cancer* **15**, 361-370, doi:10.1038/nrc3930 (2015).

9 Slastnikova, T. A., Ulasov, A. V., Rosenkranz, A. A. & Sobolev, A. S. Targeted Intracellular Delivery of Antibodies: The State of the Art. *Front Pharmacol* **9**, 1208, doi:10.3389/fphar.2018.01208 (2018).

10 Fu, A., Tang, R., Hardie, J., Farkas, M. E. & Rotello, V. M. Promises and pitfalls of intracellular delivery of proteins. *Bioconjug Chem* **25**, 1602-1608, doi:10.1021/bc500320j (2014).

11 Du, S., Liew, S. S., Li, L. & Yao, S. Q. Bypassing Endocytosis: Direct Cytosolic Delivery of Proteins. *J Am Chem Soc*, doi:10.1021/jacs.8b06584 (2018).

12 Mellert, K., Lamla, M., Scheffzek, K., Wittig, R. & Kaufmann, D. Enhancing endosomal escape of transduced proteins by photochemical internalisation. *PLoS One* **7**, e52473, doi:10.1371/journal.pone.0052473 (2012).

13 Stewart, M. P. *et al.* In vitro and ex vivo strategies for intracellular delivery. *Nature* **538**, 183-192, doi:10.1038/nature19764 (2016).

14 Lee, Y. W. *et al.* Protein Delivery into the Cell Cytosol using Non-Viral Nanocarriers. *Theranostics* **9**, 3280-3292, doi:10.7150/thno.34412 (2019).

15 Alberts, B. *Molecular biology of the cell*. Sixth edition. edn, (Garland Science, Taylor and Francis Group, 2015).

16 Nagle, J. F. & Tristram-Nagle, S. Structure of lipid bilayers. *Biochim Biophys Acta* **1469**, 159-195, doi:10.1016/s0304-4157(00)00016-2 (2000).

17 Singer, S. J. & Nicolson, G. L. The fluid mosaic model of the structure of cell membranes. *Science* **175**, 720-731, doi:10.1126/science.175.4023.720 (1972).

18 Goni, F. M. The basic structure and dynamics of cell membranes: an update of the Singer-Nicolson model. *Biochim Biophys Acta* **1838**, 1467-1476, doi:10.1016/j.bbamem.2014.01.006 (2014).

19 Di, L. *et al.* Evidence-based approach to assess passive diffusion and carrier-mediated drug transport. *Drug Discov Today* **17**, 905-912, doi:10.1016/j.drudis.2012.03.015 (2012).

20 Nicolson, G. L. Transmembrane control of the receptors on normal and tumor cells. I. Cytoplasmic influence over surface components. *Biochim Biophys Acta* **457**, 57-108, doi:10.1016/0304-4157(76)90014-9 (1976).

21 Lee, A. G. Lipid-protein interactions in biological membranes: a structural perspective. *Biochim Biophys Acta* **1612**, 1-40, doi:10.1016/s0005-2736(03)00056-7 (2003).

22 Yeagle, P. L. Non-covalent binding of membrane lipids to membrane proteins. *Biochim Biophys Acta* **1838**, 1548-1559, doi:10.1016/j.bbamem.2013.11.009 (2014).

23 Iozzo, R. V. & Schaefer, L. Proteoglycan form and function: A comprehensive nomenclature of proteoglycans. *Matrix Biol* **42**, 11-55, doi:10.1016/j.matbio.2015.02.003 (2015).

24 Brandley, B. K. & Schnaar, R. L. Cell-surface carbohydrates in cell recognition and response. *J Leukoc Biol* **40**, 97-111, doi:10.1002/jlb.40.1.97 (1986).

25 Mani, K. *et al.* HIV-Tat protein transduction domain specifically attenuates growth of polyamine deprived tumor cells. *Mol Cancer Ther* **6**, 782-788, doi:10.1158/1535-7163.MCT-06-0370 (2007).

26 Kopatz, I., Remy, J. S. & Behr, J. P. A model for non-viral gene delivery: through syndecan adhesion molecules and powered by actin. *J Gene Med* **6**, 769-776, doi:10.1002/jgm.558 (2004).

27 Fuchs, S. M. & Raines, R. T. Pathway for polyarginine entry into mammalian cells. *Biochemistry* **43**, 2438-2444, doi:10.1021/bi035933x (2004).

28 Yang, N. J. & Hinner, M. J. Getting across the cell membrane: an overview for small molecules, peptides, and proteins. *Methods Mol Biol* **1266**, 29-53, doi:10.1007/978-1-4939-2272-7_3 (2015).

29 Lipinski, C. A., Lombardo, F., Dominy, B. W. & Feeney, P. J. Experimental and computational approaches to estimate solubility and permeability in drug discovery and development settings. *Adv Drug Deliv Rev* **46**, 3-26 (2001).

30 Faller, B., Ottaviani, G., Ertl, P., Berellini, G. & Collis, A. Evolution of the physicochemical properties of marketed drugs: can history foretell the future? *Drug Discov Today* **16**, 976-984, doi:10.1016/j.drudis.2011.07.003 (2011).

31 Hediger, M. A., Clemencon, B., Burrier, R. E. & Bruford, E. A. The ABCs of membrane transporters in health and disease (SLC series): introduction. *Mol Aspects Med* **34**, 95-107, doi:10.1016/j.mam.2012.12.009 (2013).

32 Doherty, G. J. & McMahon, H. T. Mechanisms of endocytosis. *Annu Rev Biochem* **78**, 857-902, doi:10.1146/annurev.biochem.78.081307.110540 (2009).

33 Kaksonen, M. & Roux, A. Mechanisms of clathrin-mediated endocytosis. *Nat Rev Mol Cell Biol* **19**, 313-326, doi:10.1038/nrm.2017.132 (2018).

34 Mellman, I. Endocytosis and molecular sorting. *Annu Rev Cell Dev Biol* **12**, 575-625, doi:10.1146/annurev.cellbio.12.1.575 (1996).

35 Bruce, V. J. & McNaughton, B. R. Inside Job: Methods for Delivering Proteins to the Interior of Mammalian Cells. *Cell Chem Biol* **24**, 924-934, doi:10.1016/j.chembiol.2017.06.014 (2017).

36 Chiper, M., Niederreither, K. & Zuber, G. Transduction Methods for Cytosolic Delivery of Proteins and Bioconjugates into Living Cells. *Adv Healthc Mater* **7**, e1701040, doi:10.1002/adhm.201701040 (2018).

37 Du, X. *et al.* Advanced physical techniques for gene delivery based on membrane perforation. *Drug Deliv* **25**, 1516-1525, doi:10.1080/10717544.2018.1480674 (2018).

38 Barber, M. A. A technic for the inoculation of bacteria and other substances into living cells. *J. Infect. Dis.* **8**, 348–360 (1911).

39 Barber, M. A. The pipette method in the isolation of single microorganisms and the inoculation
of substances into living cells. *Philipp J Sci* **9**, 307–358 (1914).

40 Pepperkok, R. *et al.* Automatic microinjection system facilitates detection of growth inhibitory mRNA. *Proc Natl Acad Sci U S A* **85**, 6748-6752, doi:10.1073/pnas.85.18.6748 (1988).

41 Zhang, T., Fu, J. & Fang, Q. Improved high-speed capillary electrophoresis system using a short capillary and picoliter-scale translational spontaneous injection. *Electrophoresis* **35**, 2361-2369, doi:10.1002/elps.201400186 (2014).

42 Ansorge, W. Improved system for capillary microinjection into living cells. *Exp Cell Res* **140**, 31-37, doi:10.1016/0014-4827(82)90152-5 (1982).

43 Gehl, J. Electroporation: theory and methods, perspectives for drug delivery, gene therapy and research. *Acta Physiol Scand* **177**, 437-447, doi:10.1046/j.1365-201X.2003.01093.x (2003).

44 Yang, Z., Chang, L., Chiang, C. L. & Lee, L. J. Micro-/nano-electroporation for active gene delivery. *Curr Pharm Des* **21**, 6081-6088, doi:10.2174/1381612821666151027152121 (2015).

45 Geng, T. & Lu, C. Microfluidic electroporation for cellular analysis and delivery. *Lab Chip* **13**, 3803-3821, doi:10.1039/c3lc50566a (2013).

46 Sharei, A. *et al.* A vector-free microfluidic platform for intracellular delivery. *Proc Natl Acad Sci U S A* **110**, 2082-2087, doi:10.1073/pnas.1218705110 (2013).

47 Kollmannsperger, A. *et al.* Live-cell protein labelling with nanometre precision by cell squeezing. *Nat Commun* **7**, 10372, doi:10.1038/ncomms10372 (2016).

48 DiTommaso, T. *et al.* Cell engineering with microfluidic squeezing preserves functionality of primary immune cells in vivo. *Proc Natl Acad Sci U S A* **115**, E10907-E10914, doi:10.1073/pnas.1809671115 (2018).

49 McNeil, P. L. & Warder, E. Glass beads load macromolecules into living cells. *J Cell Sci* **88 (Pt 5)**, 669-678 (1987).

50 Lentacker, I., De Cock, I., Deckers, R., De Smedt, S. C. & Moonen, C. T. Understanding ultrasound induced sonoporation: definitions and underlying mechanisms. *Adv Drug Deliv Rev* **72**, 49-64, doi:10.1016/j.addr.2013.11.008 (2014).

51 Teng, K. W. *et al.* Labeling Proteins Inside Living Cells Using External Fluorophores for Fluorescence Microscopy. *Elife* **6**, doi:10.7554/eLife.25460 (2017).

52 Peer, D. *et al.* Nanocarriers as an emerging platform for cancer therapy. *Nat Nanotechnol* **2**, 751-760, doi:10.1038/nnano.2007.387 (2007).

53 Shi, J., Votruba, A. R., Farokhzad, O. C. & Langer, R. Nanotechnology in drug delivery and tissue engineering: from discovery to applications. *Nano Lett* **10**, 3223-3230, doi:10.1021/nl102184c (2010).

54 Ray, M., Lee, Y. W., Scaletti, F., Yu, R. & Rotello, V. M. Intracellular delivery of proteins by nanocarriers. *Nanomedicine (Lond)* **12**, 941-952, doi:10.2217/nnm-2016-0393 (2017).

55 Qin, X. *et al.* Rational Design of Nanocarriers for Intracellular Protein Delivery. *Adv Mater* **31**, e1902791, doi:10.1002/adma.201902791 (2019).

56 Sarker, S. R., Hokama, R. & Takeoka, S. Intracellular delivery of universal proteins using a lysine headgroup containing cationic liposomes: deciphering the uptake mechanism. *Mol Pharm* **11**, 164-174, doi:10.1021/mp400363z (2014).

57 Chatin, B. *et al.* Liposome-based Formulation for Intracellular Delivery of Functional Proteins. *Mol Ther Nucleic Acids* **4**, e244, doi:10.1038/mtna.2015.17 (2015).

58 Zuris, J. A. *et al.* Cationic lipid-mediated delivery of proteins enables efficient protein-based genome editing in vitro and in vivo. *Nat Biotechnol* **33**, 73-80, doi:10.1038/nbt.3081 (2015).

59 Wang, M. *et al.* Efficient delivery of genome-editing proteins using bioreducible lipid nanoparticles. *Proc Natl Acad Sci U S A* **113**, 2868-2873, doi:10.1073/pnas.1520244113 (2016).

60 Yuba, E., Harada, A., Sakanishi, Y., Watarai, S. & Kono, K. A liposome-based antigen delivery system using pH-sensitive fusogenic polymers for cancer immunotherapy. *Biomaterials* **34**, 3042-3052, doi:10.1016/j.biomaterials.2012.12.031 (2013).

61 Kube, S. *et al.* Fusogenic Liposomes as Nanocarriers for the Delivery of Intracellular Proteins. *Langmuir* **33**, 1051-1059, doi:10.1021/acs.langmuir.6b04304 (2017).

62 Yang, J., Tu, J., Lamers, G. E. M., Olsthoorn, R. C. L. & Kros, A. Membrane Fusion Mediated Intracellular Delivery of Lipid Bilayer Coated Mesoporous Silica Nanoparticles. *Adv Healthc Mater* **6**, doi:10.1002/adhm.201700759 (2017).

63 Armstrong, J. P., Holme, M. N. & Stevens, M. M. Re-Engineering Extracellular Vesicles as Smart Nanoscale Therapeutics. *ACS Nano* **11**, 69-83, doi:10.1021/acsnano.6b07607 (2017).

64 Hall, J. *et al.* Delivery of Therapeutic Proteins via Extracellular Vesicles: Review and Potential Treatments for Parkinson's Disease, Glioma, and Schwannoma. *Cell Mol Neurobiol* **36**, 417-427, doi:10.1007/s10571-015-0309-0 (2016).

65 Tan, A., De La Pena, H. & Seifalian, A. M. The application of exosomes as a nanoscale cancer vaccine. *Int J Nanomedicine* **5**, 889-900, doi:10.2147/IJN.S13402 (2010).

66 Gyorgy, B., Hung, M. E., Breakefield, X. O. & Leonard, J. N. Therapeutic applications of extracellular vesicles: clinical promise and open questions. *Annu Rev Pharmacol Toxicol* **55**, 439-464, doi:10.1146/annurev-pharmtox-010814-124630 (2015).

67 Yim, N. *et al.* Exosome engineering for efficient intracellular delivery of soluble proteins using optically reversible protein-protein interaction module. *Nat Commun* **7**, 12277, doi:10.1038/ncomms12277 (2016).

68 Li, S. P., Lin, Z. X., Jiang, X. Y. & Yu, X. Y. Exosomal cargo-loading and synthetic exosome-mimics as potential therapeutic tools. *Acta Pharmacol Sin* **39**, 542-551, doi:10.1038/aps.2017.178 (2018).

69 Ryu, J. H., Bickerton, S., Zhuang, J. & Thayumanavan, S. Ligand-decorated nanogels: fast one-pot synthesis and cellular targeting. *Biomacromolecules* **13**, 1515-1522, doi:10.1021/bm300201x (2012).

70 dos Santos, M. A. & Grenha, A. Polysaccharide nanoparticles for protein and Peptide delivery: exploring less-known materials. *Adv Protein Chem Struct Biol* **98**, 223-261, doi:10.1016/bs.apcsb.2014.11.003 (2015).

71 Ventura, J. *et al.* Reactive Self-Assembly of Polymers and Proteins to Reversibly Silence a Killer Protein. *Biomacromolecules* **16**, 3161-3171, doi:10.1021/acs.biomac.5b00779 (2015).

72 Gasparini, G. & Matile, S. Protein delivery with cell-penetrating poly(disulfide)s. *Chem Commun (Camb)* **51**, 17160-17162, doi:10.1039/c5cc07460f (2015).

73 Qian, L. *et al.* Intracellular Delivery of Native Proteins Facilitated by Cell-Penetrating Poly(disulfide)s. *Angewandte Chemie* **57**, 1532-1536, doi:10.1002/anie.201711651 (2018).

74 Pantarotto, D., Briand, J. P., Prato, M. & Bianco, A. Translocation of bioactive peptides across cell membranes by carbon nanotubes. *Chem Commun (Camb)*, 16-17, doi:10.1039/b311254c (2004).

75 Li, H., Fan, X. & Chen, X. Near-Infrared Light Activation of Proteins Inside Living Cells Enabled by Carbon Nanotube-Mediated Intracellular Delivery. *ACS Appl Mater Interfaces* **8**, 4500-4507, doi:10.1021/acsami.6b00323 (2016).

76 Han, G., Ghosh, P. & Rotello, V. M. Functionalized gold nanoparticles for drug delivery. *Nanomedicine (Lond)* **2**, 113-123, doi:10.2217/17435889.2.1.113 (2007).

77 Ghosh, P. *et al.* Intracellular delivery of a membrane-impermeable enzyme in active form using functionalized gold nanoparticles. *J Am Chem Soc* **132**, 2642-2645, doi:10.1021/ja907887z (2010).

78 Tang, R. *et al.* Direct delivery of functional proteins and enzymes to the cytosol using nanoparticle-stabilized nanocapsules. *ACS Nano* **7**, 6667-6673, doi:10.1021/nn402753y (2013).

79 Ray, M., Tang, R., Jiang, Z. & Rotello, V. M. Quantitative tracking of protein trafficking to the nucleus using cytosolic protein delivery by nanoparticle-stabilized nanocapsules. *Bioconjug Chem* **26**, 1004-1007, doi:10.1021/acs.bioconjchem.5b00141 (2015).

80 Abbing, A. *et al.* Efficient intracellular delivery of a protein and a low molecular weight substance via recombinant polyomavirus-like particles. *J Biol Chem* **279**, 27410-27421, doi:10.1074/jbc.M313612200 (2004).

81 Kaczmarczyk, S. J., Sitaraman, K., Young, H. A., Hughes, S. H. & Chatterjee, D. K. Protein delivery using engineered virus-like particles. *Proc Natl Acad Sci U S A* **108**, 16998-17003, doi:10.1073/pnas.1101874108 (2011).

82 Abraham, A. *et al.* Intracellular delivery of antibodies by chimeric Sesbania mosaic virus (SeMV) virus like particles. *Sci Rep* **6**, 21803, doi:10.1038/srep21803 (2016).

83 Galliani, M., Tremolanti, C. & Signore, G. Nanocarriers for Protein Delivery to the Cytosol: Assessing the Endosomal Escape of Poly(Lactide-co-Glycolide)-Poly(Ethylene Imine) Nanoparticles. *Nanomaterials (Basel)* **9**, doi:10.3390/nano9040652 (2019).

84 Varkouhi, A. K., Scholte, M., Storm, G. & Haisma, H. J. Endosomal escape pathways for delivery of biologicals. *J Control Release* **151**, 220-228, doi:10.1016/j.jconrel.2010.11.004 (2011).

85 Smith, B. D., Higgin, J. J. & Raines, R. T. Site-specific folate conjugation to a cytotoxic protein. *Bioorg Med Chem Lett* **21**, 5029-5032, doi:10.1016/j.bmcl.2011.04.081 (2011).

86 Authier, F., Posner, B. I. & Bergeron, J. J. Endosomal proteolysis of internalized proteins. *FEBS Lett* **389**, 55-60, doi:10.1016/0014-5793(96)00368-7 (1996).

87 Feld, G. K., Brown, M. J. & Krantz, B. A. Ratcheting up protein translocation with anthrax toxin. *Protein Sci* **21**, 606-624, doi:10.1002/pro.2052 (2012).

88 Bachran, C. & Leppla, S. H. Tumor Targeting and Drug Delivery by Anthrax Toxin. *Toxins (Basel)* **8**, doi:10.3390/toxins8070197 (2016).

89 Liu, S., Netzel-Arnett, S., Birkedal-Hansen, H. & Leppla, S. H. Tumor cell-selective cytotoxicity of matrix metalloproteinase-activated anthrax toxin. *Cancer Res* **60**, 6061-6067 (2000).

90 Arora, N. & Leppla, S. H. Residues 1-254 of anthrax toxin lethal factor are sufficient to cause cellular uptake of fused polypeptides. *J Biol Chem* **268**, 3334-3341 (1993).

91 Rabideau, A. E., Liao, X., Akcay, G. & Pentelute, B. L. Translocation of Non-Canonical Polypeptides into Cells Using Protective Antigen. *Sci Rep* **5**, 11944, doi:10.1038/srep11944 (2015).

92 Liao, X., Rabideau, A. E. & Pentelute, B. L. Delivery of antibody mimics into mammalian cells via anthrax toxin protective antigen. *Chembiochem* **15**, 2458-2466, doi:10.1002/cbic.201402290 (2014).

93 Li, W., Nicol, F. & Szoka, F. C., Jr. GALA: a designed synthetic pH-responsive amphipathic peptide with applications in drug and gene delivery. *Adv Drug Deliv Rev* **56**, 967-985, doi:10.1016/j.addr.2003.10.041 (2004).

94 Nakase, I., Kogure, K., Harashima, H. & Futaki, S. Application of a fusiogenic peptide GALA for intracellular delivery. *Methods Mol Biol* **683**, 525-533, doi:10.1007/978-1-60761-919-2_37 (2011).

95 Kobayashi, S. *et al.* Cytosolic targeting of macromolecules using a pH-dependent fusogenic peptide in combination with cationic liposomes. *Bioconjug Chem* **20**, 953-959, doi:10.1021/bc800530v (2009).

96 Li, M. *et al.* Discovery and characterization of a peptide that enhances endosomal escape of delivered proteins in vitro and in vivo. *J Am Chem Soc* **137**, 14084-14093, doi:10.1021/jacs.5b05694 (2015).

97 Akishiba, M. *et al.* Cytosolic antibody delivery by lipid-sensitive endosomolytic peptide. *Nat Chem* **9**, 751-761, doi:10.1038/nchem.2779 (2017).

98 Akishiba, M. & Futaki, S. Inducible Membrane Permeabilization by Attenuated Lytic Peptides: A New Concept for Accessing Cell Interiors through Ruffled Membranes. *Mol Pharm* **16**, 2540-2548, doi:10.1021/acs.molpharmaceut.9b00156 (2019).

99 Qian, Z. *et al.* Efficient delivery of cyclic peptides into mammalian cells with short sequence motifs. *ACS Chem Biol* **8**, 423-431, doi:10.1021/cb3005275 (2013).

100 Qian, Z. *et al.* Early endosomal escape of a cyclic cell-penetrating peptide allows effective cytosolic cargo delivery. *Biochemistry* **53**, 4034-4046, doi:10.1021/bi5004102 (2014).

101 Srinivasan, D. *et al.* Conjugation to the cell-penetrating peptide TAT potentiates the photodynamic effect of carboxytetramethylrhodamine. *PLoS One* **6**, e17732, doi:10.1371/journal.pone.0017732 (2011).

102 Erazo-Oliveras, A. *et al.* Protein delivery into live cells by incubation with an endosomolytic agent. *Nat Methods* **11**, 861-867, doi:10.1038/nmeth.2998 (2014).

103 Brock, D. J. *et al.* Efficient cell delivery mediated by lipid-specific endosomal escape of supercharged branched peptides. *Traffic* **19**, 421-435, doi:10.1111/tra.12566 (2018).

104 Lonn, P. *et al.* Enhancing Endosomal Escape for Intracellular Delivery of Macromolecular Biologic Therapeutics. *Sci Rep* **6**, 32301, doi:10.1038/srep32301 (2016).

105 Al-Bari, M. A. A. Targeting endosomal acidification by chloroquine analogs as a promising strategy for the treatment of emerging viral diseases. *Pharmacol Res Perspect* **5**, e00293, doi:10.1002/prp2.293 (2017).

106 Bus, T., Traeger, A. & Schubert, U. S. The great escape: how cationic polyplexes overcome the endosomal barrier. *J Mater Chem B* **6**, 6904-6918, doi:10.1039/c8tb00967h (2018).

107 Caron, N. J., Quenneville, S. P. & Tremblay, J. P. Endosome disruption enhances the functional nuclear delivery of Tat-fusion proteins. *Biochem Biophys Res Commun* **319**, 12-20, doi:10.1016/j.bbrc.2004.04.180 (2004).

108 Juliano, R. L. *et al.* Structure-activity relationships and cellular mechanism of action of small molecules that enhance the delivery of oligonucleotides. *Nucleic Acids Res* **46**, 1601-1613, doi:10.1093/nar/gkx1320 (2018).

109 Allen, J. *et al.* Cytosolic Delivery of Macromolecules in Live Human Cells Using the Combined Endosomal Escape Activities of a Small Molecule and Cell Penetrating Peptides. *ACS Chem Biol* **14**, 2641-2651, doi:10.1021/acschembio.9b00585 (2019).

110 LeCher, J. C., Nowak, S. J. & McMurry, J. L. Breaking in and busting out: cell-penetrating peptides and the endosomal escape problem. *Biomol Concepts* **8**, 131-141, doi:10.1515/bmc-2017-0023 (2017).

111 Frankel, A. D. & Pabo, C. O. Cellular uptake of the tat protein from human immunodeficiency virus. *Cell* **55**, 1189-1193, doi:10.1016/0092-8674(88)90263-2 (1988).

112 Campbell, G. R. *et al.* The glutamine-rich region of the HIV-1 Tat protein is involved in T-cell apoptosis. *J Biol Chem* **279**, 48197-48204, doi:10.1074/jbc.M406195200 (2004).

113 Xiao, H. *et al.* Selective CXCR4 antagonism by Tat: implications for in vivo expansion of coreceptor use by HIV-1. *Proc Natl Acad Sci U S A* **97**, 11466-11471, doi:10.1073/pnas.97.21.11466 (2000).

114 Green, M. & Loewenstein, P. M. Autonomous functional domains of chemically synthesized human immunodeficiency virus tat trans-activator protein. *Cell* **55**, 1179-1188, doi:10.1016/0092-8674(88)90262-0 (1988).

115 Vives, E., Brodin, P. & Lebleu, B. A truncated HIV-1 Tat protein basic domain rapidly translocates through the plasma membrane and accumulates in the cell nucleus. *J Biol Chem* **272**, 16010-16017, doi:10.1074/jbc.272.25.16010 (1997).

116 Qian, Y. Q. *et al.* The structure of the Antennapedia homeodomain determined by NMR spectroscopy in solution: comparison with prokaryotic repressors. *Cell* **59**, 573-580, doi:10.1016/0092-8674(89)90040-8 (1989).

117 Le Roux, I., Joliot, A. H., Bloch-Gallego, E., Prochiantz, A. & Volovitch, M. Neurotrophic activity of the Antennapedia homeodomain depends on its specific DNA-binding properties. *Proc Natl Acad Sci U S A* **90**, 9120-9124, doi:10.1073/pnas.90.19.9120 (1993).

118 Joliot, A., Pernelle, C., Deagostini-Bazin, H. & Prochiantz, A. Antennapedia homeobox peptide regulates neural morphogenesis. *Proc Natl Acad Sci U S A* **88**, 1864-1868, doi:10.1073/pnas.88.5.1864 (1991).

119 Derossi, D., Joliot, A. H., Chassaing, G. & Prochiantz, A. The third helix of the Antennapedia homeodomain translocates through biological membranes. *J Biol Chem* **269**, 10444-10450 (1994).

120 Derossi, D. *et al.* Cell internalization of the third helix of the Antennapedia homeodomain is receptor-independent. *J Biol Chem* **271**, 18188-18193, doi:10.1074/jbc.271.30.18188 (1996).

121 Agrawal, P. *et al.* CPPsite 2.0: a repository of experimentally validated cell-penetrating peptides. *Nucleic Acids Res* **44**, D1098-1103, doi:10.1093/nar/gkv1266 (2016).

122 Manavalan, B., Subramaniyam, S., Shin, T. H., Kim, M. O. & Lee, G. Machine-Learning-Based Prediction of Cell-Penetrating Peptides and Their Uptake Efficiency with Improved Accuracy. *J Proteome Res* **17**, 2715-2726, doi:10.1021/acs.jproteome.8b00148 (2018).

123 Wolfe, J. M. *et al.* Machine Learning To Predict Cell-Penetrating Peptides for Antisense Delivery. *ACS Cent Sci* **4**, 512-520, doi:10.1021/acscentsci.8b00098 (2018).

124 Pujals, S., Sabido, E., Tarrago, T. & Giralt, E. all-D proline-rich cell-penetrating peptides: a preliminary in vivo internalization study. *Biochem Soc Trans* **35**, 794-796, doi:10.1042/BST0350794 (2007).

125 Gao, C. *et al.* A cell-penetrating peptide from a novel pVII-pIX phage-displayed random peptide library. *Bioorg Med Chem* **10**, 4057-4065, doi:10.1016/s0968-0896(02)00340-1 (2002).

126 Martin, I., Teixido, M. & Giralt, E. Design, synthesis and characterization of a new anionic cell-penetrating peptide: SAP(E). *Chembiochem* **12**, 896-903, doi:10.1002/cbic.201000679 (2011).

127 Milletti, F. Cell-penetrating peptides: classes, origin, and current landscape. *Drug Discov Today* **17**, 850-860, doi:10.1016/j.drudis.2012.03.002 (2012).

128 Futaki, S. *et al.* Arginine-rich peptides. An abundant source of membrane-permeable peptides having potential as carriers for intracellular protein delivery. *J Biol Chem* **276**, 5836-5840, doi:10.1074/jbc.M007540200 (2001).

129 Wender, P. A. *et al.* The design, synthesis, and evaluation of molecules that enable or enhance cellular uptake: peptoid molecular transporters. *Proc Natl Acad Sci U S A* **97**, 13003-13008, doi:10.1073/pnas.97.24.13003 (2000).

130 Wang, H., Ma, J., Yang, Y., Zeng, F. & Liu, C. Highly Efficient Delivery of Functional Cargoes by a Novel Cell-Penetrating Peptide Derived from SP140-Like Protein. *Bioconjug Chem* **27**, 1373-1381, doi:10.1021/acs.bioconjchem.6b00161 (2016).

131 Nasrolahi Shirazi, A., Tiwari, R., Chhikara, B. S., Mandal, D. & Parang, K. Design and biological evaluation of cell-penetrating peptide-doxorubicin conjugates as prodrugs. *Mol Pharm* **10**, 488-499, doi:10.1021/mp3004034 (2013).

132 Fernandez-Carneado, J., Kogan, M. J., Castel, S. & Giralt, E. Potential peptide carriers: amphipathic proline-rich peptides derived from the N-terminal domain of gamma-zein. *Angewandte Chemie* **43**, 1811-1814, doi:10.1002/anie.200352540 (2004).

133 Wierzbicki, P. M. *et al.* Protein and siRNA delivery by transportan and transportan 10 into colorectal cancer cell lines. *Folia Histochem Cytobiol* **52**, 270-280, doi:10.5603/FHC.a2014.0035 (2014).

134 Almarwani, B. *et al.* Vesicles mimicking normal and cancer cell membranes exhibit differential responses to the cell-penetrating peptide Pep-1. *Biochim Biophys Acta Biomembr* **1860**, 1394-1402, doi:10.1016/j.bbamem.2018.03.022 (2018).

135 Oehlke, J. *et al.* Cellular uptake of an alpha-helical amphipathic model peptide with the potential to deliver polar compounds into the cell interior non-endocytically. *Biochim Biophys Acta* **1414**, 127-139, doi:10.1016/s0005-2736(98)00161-8 (1998).

136 Rhee, M. & Davis, P. Mechanism of uptake of C105Y, a novel cell-penetrating peptide. *J Biol Chem* **281**, 1233-1240, doi:10.1074/jbc.M509813200 (2006).

137 Yamada, T., Das Gupta, T. K. & Beattie, C. W. p28, an anionic cell-penetrating peptide, increases the activity of wild type and mutated p53 without altering its conformation. *Mol Pharm* **10**, 3375-3383, doi:10.1021/mp400221r (2013).

138 Poon, G. M. & Gariepy, J. Cell-surface proteoglycans as molecular portals for cationic peptide and polymer entry into cells. *Biochem Soc Trans* **35**, 788-793, doi:10.1042/BST0350788 (2007).

139 Persson, D., Thoren, P. E. & Norden, B. Penetratin-induced aggregation and subsequent dissociation of negatively charged phospholipid vesicles. *FEBS Lett* **505**, 307-312, doi:10.1016/s0014-5793(01)02843-5 (2001).

140 Fischer, P. M. *et al.* Structure-activity relationship of truncated and substituted analogues of the intracellular delivery vector Penetratin. *J Pept Res* **55**, 163-172, doi:10.1034/j.1399-3011.2000.00163.x (2000).

141 Goncalves, E., Kitas, E. & Seelig, J. Binding of oligoarginine to membrane lipids and heparan sulfate: structural and thermodynamic characterization of a cell-penetrating peptide. *Biochemistry* **44**, 2692-2702, doi:10.1021/bi048046i (2005).

142 Gelman, R. A., Glaser, D. N. & Blackwell, J. Interaction between chondroitin-6-sulfate and poly-L-arginine in aqueous solution. *Biopolymers* **12**, 1223-1232, doi:10.1002/bip.1973.360120603 (1973).

143 Robison, A. D. *et al.* Polyarginine Interacts More Strongly and Cooperatively than Polylysine with Phospholipid Bilayers. *J Phys Chem B* **120**, 9287-9296, doi:10.1021/acs.jpcb.6b05604 (2016).

144 Rothbard, J. B., Jessop, T. C., Lewis, R. S., Murray, B. A. & Wender, P. A. Role of membrane potential and hydrogen bonding in the mechanism of translocation of guanidinium-rich peptides into cells. *J Am Chem Soc* **126**, 9506-9507, doi:10.1021/ja0482536 (2004).

145 Li, J. H., Chiu, W. C., Yao, Y. C. & Cheng, R. P. Effect of arginine methylation on the RNA recognition and cellular uptake of Tat-derived peptides. *Bioorg Med Chem* **23**, 2281-2286, doi:10.1016/j.bmc.2015.01.051 (2015).

146 Zaro, J. L. & Shen, W. C. Quantitative comparison of membrane transduction and endocytosis of oligopeptides. *Biochem Biophys Res Commun* **307**, 241-247, doi:10.1016/s0006-291x(03)01167-7 (2003).

147 Dietrich, L. *et al.* Cell Permeable Stapled Peptide Inhibitor of Wnt Signaling that Targets beta-Catenin Protein-Protein Interactions. *Cell Chem Biol* **24**, 958-968 e955, doi:10.1016/j.chembiol.2017.06.013 (2017).

148 Takayama, K. *et al.* Enhanced intracellular delivery using arginine-rich peptides by the addition of penetration accelerating sequences (Pas). *J Control Release* **138**, 128-133, doi:10.1016/j.jconrel.2009.05.019 (2009).

149 Mishra, A. *et al.* Translocation of HIV TAT peptide and analogues induced by multiplexed membrane and cytoskeletal interactions. *Proc Natl Acad Sci U S A* **108**, 16883-16888, doi:10.1073/pnas.1108795108 (2011).

150 Magzoub, M., Eriksson, L. E. & Graslund, A. Comparison of the interaction, positioning, structure induction and membrane perturbation of cell-penetrating peptides and non-translocating variants with phospholipid vesicles. *Biophys Chem* **103**, 271-288, doi:10.1016/s0301-4622(02)00321-6 (2003).

151 Maiolo, J. R., Ferrer, M. & Ottinger, E. A. Effects of cargo molecules on the cellular uptake of arginine-rich cell-penetrating peptides. *Biochim Biophys Acta* **1712**, 161-172, doi:10.1016/j.bbamem.2005.04.010 (2005).

152 Bechara, C. *et al.* Tryptophan within basic peptide sequences triggers glycosaminoglycan-dependent endocytosis. *FASEB J* **27**, 738-749, doi:10.1096/fj.12-216176 (2013).

153 Amand, H. L. *et al.* Cell surface binding and uptake of arginine- and lysine-rich penetratin peptides in absence and presence of proteoglycans. *Biochim Biophys Acta* **1818**, 2669-2678, doi:10.1016/j.bbamem.2012.06.006 (2012).

154 Berlose, J. P., Convert, O., Derossi, D., Brunissen, A. & Chassaing, G. Conformational and associative behaviours of the third helix of antennapedia homeodomain in membrane-mimetic environments. *Eur J Biochem* **242**, 372-386, doi:10.1111/j.1432-1033.1996.0372r.x (1996).

155 Takechi, Y. *et al.* Physicochemical mechanism for the enhanced ability of lipid membrane penetration of polyarginine. *Langmuir* **27**, 7099-7107, doi:10.1021/la200917y (2011).

156 Caesar, C. E., Esbjorner, E. K., Lincoln, P. & Norden, B. Membrane interactions of cell-penetrating peptides probed by tryptophan fluorescence and dichroism techniques: correlations of structure to cellular uptake. *Biochemistry* **45**, 7682-7692, doi:10.1021/bi052095t (2006).

157 Christiaens, B. *et al.* Membrane interaction and cellular internalization of penetratin peptides. *Eur J Biochem* **271**, 1187-1197, doi:10.1111/j.1432-1033.2004.04022.x (2004).

158 Deshayes, S., Decaffmeyer, M., Brasseur, R. & Thomas, A. Structural polymorphism of two CPP: an important parameter of activity. *Biochim Biophys Acta* **1778**, 1197-1205, doi:10.1016/j.bbamem.2008.01.027 (2008).

159 Eiriksdottir, E., Konate, K., Langel, U., Divita, G. & Deshayes, S. Secondary structure of cell-penetrating peptides controls membrane interaction and insertion. *Biochim Biophys Acta* **1798**, 1119-1128, doi:10.1016/j.bbamem.2010.03.005 (2010).

160 Kalafatovic, D. & Giralt, E. Cell-Penetrating Peptides: Design Strategies beyond Primary Structure and Amphipathicity. *Molecules* **22**, doi:10.3390/molecules22111929 (2017).

161 Feng, Z. & Xu, B. Inspiration from the mirror: D-amino acid containing peptides in biomedical approaches. *Biomol Concepts* **7**, 179-187, doi:10.1515/bmc-2015-0035 (2016).

162 Tunnemann, G. *et al.* Live-cell analysis of cell penetration ability and toxicity of oligo-arginines. *J Pept Sci* **14**, 469-476, doi:10.1002/psc.968 (2008).

163 Verdurmen, W. P. *et al.* Preferential uptake of L- versus D-amino acid cell-penetrating peptides in a cell type-dependent manner. *Chem Biol* **18**, 1000-1010, doi:10.1016/j.chembiol.2011.06.006 (2011).

164 Kolmel, D. K. *et al.* Cell Penetrating Peptoids (CPPos): Synthesis of a Small Combinatorial Library by Using IRORI MiniKans. *Pharmaceuticals (Basel)* **5**, 1265-1281, doi:10.3390/ph5121265 (2012).

165 Kolmel, D. K. *et al.* Cell-penetrating peptoids: introduction of novel cationic side chains. *Eur J Med Chem* **79**, 231-243, doi:10.1016/j.ejmech.2014.03.078 (2014).

166 Fernandez-Carneado, J. *et al.* Fatty acyl moieties: improving Pro-rich peptide uptake inside HeLa cells. *J Pept Res* **65**, 580-590, doi:10.1111/j.1399-3011.2005.00253.x (2005).

167 Marullo, R., Kastantin, M., Drews, L. B. & Tirrell, M. Peptide contour length determines equilibrium secondary structure in protein-analogous micelles. *Biopolymers* **99**, 573-581, doi:10.1002/bip.22217 (2013).

168 Ma, W., Jin, G. W., Gehret, P. M., Chada, N. C. & Suh, W. H. A Novel Cell Penetrating Peptide for the Differentiation of Human Neural Stem Cells. *Biomolecules* **8**, doi:10.3390/biom8030048 (2018).

169 Song, J., Qian, Z., Sahni, A., Chen, K. & Pei, D. Cyclic Cell-Penetrating Peptides with Single Hydrophobic Groups. *Chembiochem* **20**, 2085-2088, doi:10.1002/cbic.201900370 (2019).

170 Karle, I. L. & Balaram, P. Structural characteristics of alpha-helical peptide molecules containing Aib residues. *Biochemistry* **29**, 6747-6756, doi:10.1021/bi00481a001 (1990).

171 Yamashita, H. *et al.* Amphipathic short helix-stabilized peptides with cell-membrane penetrating ability. *Bioorg Med Chem* **22**, 2403-2408, doi:10.1016/j.bmc.2014.03.005 (2014).

172 Yamashita, H. *et al.* A Helix-Stabilized Cell-Penetrating Peptide as an Intracellular Delivery Tool. *Chembiochem* **17**, 137-140, doi:10.1002/cbic.201500468 (2016).

173 Yamashita, H. *et al.* Development of a Cell-penetrating Peptide that Exhibits Responsive Changes in its Secondary Structure in the Cellular Environment. *Sci Rep* **6**, 33003, doi:10.1038/srep33003 (2016).

174 Nagel, Y. A., Raschle, P. S. & Wennemers, H. Effect of Preorganized Charge-Display on the Cell-Penetrating Properties of Cationic Peptides. *Angewandte Chemie* **56**, 122-126, doi:10.1002/anie.201607649 (2017).

175 Li, M., Puschmann, R., Herdlitschka, A., Fiedler, D. & Wennemers, H. Delivery of myo-Inositol Hexakisphosphate to the Cell Nucleus with a Proline-Based Cell-Penetrating Peptide. *Angewandte Chemie*, doi:10.1002/anie.202006770 (2020).

176 Joo, S. H. Cyclic peptides as therapeutic agents and biochemical tools. *Biomol Ther (Seoul)* **20**, 19-26, doi:10.4062/biomolther.2012.20.1.019 (2012).

177 Qian, Z., Dougherty, P. G. & Pei, D. Targeting intracellular protein-protein interactions with cell-permeable cyclic peptides. *Curr Opin Chem Biol* **38**, 80-86, doi:10.1016/j.cbpa.2017.03.011 (2017).

178 Dougherty, P. G., Sahni, A. & Pei, D. Understanding Cell Penetration of Cyclic Peptides. *Chem Rev* **119**, 10241-10287, doi:10.1021/acs.chemrev.9b00008 (2019).

179 Furukawa, A. *et al.* Passive Membrane Permeability in Cyclic Peptomer Scaffolds Is Robust to Extensive Variation in Side Chain Functionality and Backbone Geometry. *J Med Chem* **59**, 9503-9512, doi:10.1021/acs.jmedchem.6b01246 (2016).

180 Hewitt, W. M. *et al.* Cell-permeable cyclic peptides from synthetic libraries inspired by natural products. *J Am Chem Soc* **137**, 715-721, doi:10.1021/ja508766b (2015).

181 Park, S. E., Sajid, M. I., Parang, K. & Tiwari, R. K. Cyclic Cell-Penetrating Peptides as Efficient Intracellular Drug Delivery Tools. *Mol Pharm* **16**, 3727-3743, doi:10.1021/acs.molpharmaceut.9b00633 (2019).

182 Lattig-Tunnemann, G. *et al.* Backbone rigidity and static presentation of guanidinium groups increases cellular uptake of arginine-rich cell-penetrating peptides. *Nat Commun* **2**, 453, doi:10.1038/ncomms1459 (2011).

183 Mandal, D., Nasrolahi Shirazi, A. & Parang, K. Cell-penetrating homochiral cyclic peptides as nuclear-targeting molecular transporters. *Angewandte Chemie* **50**, 9633-9637, doi:10.1002/anie.201102572 (2011).

184 Traboulsi, H. *et al.* Macrocyclic cell penetrating peptides: a study of structure-penetration properties. *Bioconjug Chem* **26**, 405-411, doi:10.1021/acs.bioconjchem.5b00023 (2015).

185 Oh, D., Darwish, S. A., Shirazi, A. N., Tiwari, R. K. & Parang, K. Amphiphilic bicyclic peptides as cellular delivery agents. *ChemMedChem* **9**, 2449-2453, doi:10.1002/cmdc.201402230 (2014).

186 Wolfe, J. M. *et al.* Perfluoroaryl Bicyclic Cell-Penetrating Peptides for Delivery of Antisense Oligonucleotides. *Angewandte Chemie* **57**, 4756-4759, doi:10.1002/anie.201801167 (2018).

187 Qian, Z. *et al.* Intracellular Delivery of Peptidyl Ligands by Reversible Cyclization: Discovery of a PDZ Domain Inhibitor that Rescues CFTR Activity. *Angewandte Chemie* **54**, 5874-5878, doi:10.1002/anie.201411594 (2015).

188 Futaki, S. & Nakase, I. Cell-Surface Interactions on Arginine-Rich Cell-Penetrating Peptides Allow for Multiplex Modes of Internalization. *Acc Chem Res* **50**, 2449-2456, doi:10.1021/acs.accounts.7b00221 (2017).

189 He, L., Sayers, E. J., Watson, P. & Jones, A. T. Contrasting roles for actin in the cellular uptake of cell penetrating peptide conjugates. *Sci Rep* **8**, 7318, doi:10.1038/s41598-018-25600-8 (2018).

190 Bhosle, G. S. & Fernandes, M. (R-X-R)4 -Motif Peptides Containing Conformationally Constrained Cyclohexane-Derived Spacers: Effect on Cellular Uptake. *ChemMedChem* **12**, 1743-1747, doi:10.1002/cmdc.201700498 (2017).

191 Mueller, J., Kretzschmar, I., Volkmer, R. & Boisguerin, P. Comparison of cellular uptake using 22 CPPs in 4 different cell lines. *Bioconjug Chem* **19**, 2363-2374, doi:10.1021/bc800194e (2008).

192 Fretz, M. M. *et al.* Temperature-, concentration- and cholesterol-dependent translocation of L- and D-octa-arginine across the plasma and nuclear membrane of CD34+ leukaemia cells. *Biochem J* **403**, 335-342, doi:10.1042/BJ20061808 (2007).

193 Illien, F. *et al.* Quantitative fluorescence spectroscopy and flow cytometry analyses of cell-penetrating peptides internalization pathways: optimization, pitfalls, comparison with mass spectrometry quantification. *Sci Rep* **6**, 36938, doi:10.1038/srep36938 (2016).

194 Richard, J. P. *et al.* Cell-penetrating peptides. A reevaluation of the mechanism of cellular uptake. *J Biol Chem* **278**, 585-590, doi:10.1074/jbc.M209548200 (2003).

195 Qian, Z., Dougherty, P. G. & Pei, D. Monitoring the cytosolic entry of cell-penetrating peptides using a pH-sensitive fluorophore. *Chem Commun (Camb)* **51**, 2162-2165, doi:10.1039/c4cc09441g (2015).

196 Swiecicki, J. M. *et al.* How to unveil self-quenched fluorophores and subsequently map the subcellular distribution of exogenous peptides. *Sci Rep* **6**, 20237, doi:10.1038/srep20237 (2016).

197 Allolio, C. *et al.* Arginine-rich cell-penetrating peptides induce membrane multilamellarity and subsequently enter via formation of a fusion pore. *Proc Natl Acad Sci U S A* **115**, 11923-11928, doi:10.1073/pnas.1811520115 (2018).

198 Wadia, J. S., Stan, R. V. & Dowdy, S. F. Transducible TAT-HA fusogenic peptide enhances escape of TAT-fusion proteins after lipid raft macropinocytosis. *Nat Med* **10**, 310-315, doi:10.1038/nm996 (2004).

199 Karatas, H. *et al.* Real-Time Imaging and Quantification of Peptide Uptake in Vitro and in Vivo. *ACS Chem Biol* **14**, 2197-2205, doi:10.1021/acschembio.9b00439 (2019).

200 Aubry, S. *et al.* MALDI-TOF mass spectrometry: a powerful tool to study the internalization of cell-penetrating peptides. *Biochim Biophys Acta* **1798**, 2182-2189, doi:10.1016/j.bbamem.2009.11.011 (2010).

201 Iacopetta, B. J. & Morgan, E. H. The kinetics of transferrin endocytosis and iron uptake from transferrin in rabbit reticulocytes. *J Biol Chem* **258**, 9108-9115 (1983).

202 Vercauteren, D. *et al.* The use of inhibitors to study endocytic pathways of gene carriers: optimization and pitfalls. *Mol Ther* **18**, 561-569, doi:10.1038/mt.2009.281 (2010).

203 Ciobanasu, C., Siebrasse, J. P. & Kubitscheck, U. Cell-penetrating HIV1 TAT peptides can generate pores in model membranes. *Biophys J* **99**, 153-162, doi:10.1016/j.bpj.2010.03.065 (2010).

204 Crosio, M. A. *et al.* Interaction of a Polyarginine Peptide with Membranes of Different Mechanical Properties. *Biomolecules* **9**, doi:10.3390/biom9100625 (2019).

205 Grasso, G. *et al.* Cell penetrating peptide modulation of membrane biomechanics by Molecular dynamics. *J Biomech* **73**, 137-144, doi:10.1016/j.jbiomech.2018.03.036 (2018).

206 Herce, H. D. & Garcia, A. E. Molecular dynamics simulations suggest a mechanism for translocation of the HIV-1 TAT peptide across lipid membranes. *Proc Natl Acad Sci U S A* **104**, 20805-20810, doi:10.1073/pnas.0706574105 (2007).

207 Gao, X. *et al.* Membrane potential drives direct translocation of cell-penetrating peptides. *Nanoscale* **11**, 1949-1958, doi:10.1039/c8nr10447f (2019).

208 Wagstaff, K. M. & Jans, D. A. Protein transduction: cell penetrating peptides and their therapeutic applications. *Curr Med Chem* **13**, 1371-1387, doi:10.2174/092986706776872871 (2006).

209 Guidotti, G., Brambilla, L. & Rossi, D. Cell-Penetrating Peptides: From Basic Research to Clinics. *Trends Pharmacol Sci* **38**, 406-424, doi:10.1016/j.tips.2017.01.003 (2017).

210 Madani, F., Lindberg, S., Langel, U., Futaki, S. & Graslund, A. Mechanisms of cellular uptake of cell-penetrating peptides. *J Biophys* **2011**, 414729, doi:10.1155/2011/414729 (2011).

211 Gestin, M., Dowaidar, M. & Langel, U. Uptake Mechanism of Cell-Penetrating Peptides. *Adv Exp Med Biol* **1030**, 255-264, doi:10.1007/978-3-319-66095-0_11 (2017).

212 Pouny, Y., Rapaport, D., Mor, A., Nicolas, P. & Shai, Y. Interaction of antimicrobial dermaseptin and its fluorescently labeled analogues with phospholipid membranes. *Biochemistry* **31**, 12416-12423, doi:10.1021/bi00164a017 (1992).

213 Durzynska, J. *et al.* Viral and other cell-penetrating peptides as vectors of therapeutic agents in medicine. *J Pharmacol Exp Ther* **354**, 32-42, doi:10.1124/jpet.115.223305 (2015).

214 Herce, H. D. *et al.* Arginine-rich peptides destabilize the plasma membrane, consistent with a pore formation translocation mechanism of cell-penetrating peptides. *Biophys J* **97**, 1917-1925, doi:10.1016/j.bpj.2009.05.066 (2009).

215 Herce, H. D., Garcia, A. E. & Cardoso, M. C. Fundamental molecular mechanism for the cellular uptake of guanidinium-rich molecules. *J Am Chem Soc* **136**, 17459-17467, doi:10.1021/ja507790z (2014).

216 Vedovato, N. & Rispoli, G. A novel technique to study pore-forming peptides in a natural membrane. *Eur Biophys J* **36**, 771-778, doi:10.1007/s00249-007-0152-4 (2007).

217 Duchardt, F., Fotin-Mleczek, M., Schwarz, H., Fischer, R. & Brock, R. A comprehensive model for the cellular uptake of cationic cell-penetrating peptides. *Traffic* **8**, 848-866, doi:10.1111/j.1600-0854.2007.00572.x (2007).

218 Verdurmen, W. P., Thanos, M., Ruttekolk, I. R., Gulbins, E. & Brock, R. Cationic cell-penetrating peptides induce ceramide formation via acid sphingomyelinase: implications for uptake. *J Control Release* **147**, 171-179, doi:10.1016/j.jconrel.2010.06.030 (2010).

219 Kawamoto, S. *et al.* Inverted micelle formation of cell-penetrating peptide studied by coarse-grained simulation: importance of attractive force between cell-penetrating peptides and lipid head group. *J Chem Phys* **134**, 095103, doi:10.1063/1.3555531 (2011).

220 Rosales, C. & Uribe-Querol, E. Phagocytosis: A Fundamental Process in Immunity. *Biomed Res Int* **2017**, 9042851, doi:10.1155/2017/9042851 (2017).

221 Bitsikas, V., Correa, I. R., Jr. & Nichols, B. J. Clathrin-independent pathways do not contribute significantly to endocytic flux. *Elife* **3**, e03970, doi:10.7554/eLife.03970 (2014).

222 Antonny, B. *et al.* Membrane fission by dynamin: what we know and what we need to know. *EMBO J* **35**, 2270-2284, doi:10.15252/embj.201694613 (2016).

223 Kawaguchi, Y. *et al.* Syndecan-4 Is a Receptor for Clathrin-Mediated Endocytosis of Arginine-Rich Cell-Penetrating Peptides. *Bioconjug Chem* **27**, 1119-1130, doi:10.1021/acs.bioconjchem.6b00082 (2016).

224 Anderson, R. G. The caveolae membrane system. *Annu Rev Biochem* **67**, 199-225, doi:10.1146/annurev.biochem.67.1.199 (1998).

225 Pelkmans, L. Secrets of caveolae- and lipid raft-mediated endocytosis revealed by mammalian viruses. *Biochim Biophys Acta* **1746**, 295-304, doi:10.1016/j.bbamcr.2005.06.009 (2005).

226 Kovtun, O., Tillu, V. A., Ariotti, N., Parton, R. G. & Collins, B. M. Cavin family proteins and the assembly of caveolae. *J Cell Sci* **128**, 1269-1278, doi:10.1242/jcs.167866 (2015).

227 Ferrari, A. *et al.* Caveolae-mediated internalization of extracellular HIV-1 tat fusion proteins visualized in real time. *Mol Ther* **8**, 284-294, doi:10.1016/s1525-0016(03)00122-9 (2003).

228 Ter-Avetisyan, G. *et al.* Cell entry of arginine-rich peptides is independent of endocytosis. *J Biol Chem* **284**, 3370-3378, doi:10.1074/jbc.M805550200 (2009).

229 Richard, J. P. *et al.* Cellular uptake of unconjugated TAT peptide involves clathrin-dependent endocytosis and heparan sulfate receptors. *J Biol Chem* **280**, 15300-15306, doi:10.1074/jbc.M401604200 (2005).

230 Lim, J. P. & Gleeson, P. A. Macropinocytosis: an endocytic pathway for internalising large gulps. *Immunol Cell Biol* **89**, 836-843, doi:10.1038/icb.2011.20 (2011).

231 Bloomfield, G. & Kay, R. R. Uses and abuses of macropinocytosis. *J Cell Sci* **129**, 2697-2705, doi:10.1242/jcs.176149 (2016).

232 Canton, J. Macropinocytosis: New Insights Into Its Underappreciated Role in Innate Immune Cell Surveillance. *Front Immunol* **9**, 2286, doi:10.3389/fimmu.2018.02286 (2018).

233 Nakase, I. *et al.* Cellular uptake of arginine-rich peptides: roles for macropinocytosis and actin rearrangement. *Mol Ther* **10**, 1011-1022, doi:10.1016/j.ymthe.2004.08.010 (2004).

234 Kaplan, I. M., Wadia, J. S. & Dowdy, S. F. Cationic TAT peptide transduction domain enters cells by macropinocytosis. *J Control Release* **102**, 247-253, doi:10.1016/j.jconrel.2004.10.018 (2005).

235 Gerbal-Chaloin, S. *et al.* First step of the cell-penetrating peptide mechanism involves Rac1 GTPase-dependent actin-network remodelling. *Biol Cell* **99**, 223-238, doi:10.1042/BC20060123 (2007).

236 Gump, J. M., June, R. K. & Dowdy, S. F. Revised role of glycosaminoglycans in TAT protein transduction domain-mediated cellular transduction. *J Biol Chem* **285**, 1500-1507, doi:10.1074/jbc.M109.021964 (2010).

237 Saar, K. *et al.* Cell-penetrating peptides: a comparative membrane toxicity study. *Anal Biochem* **345**, 55-65, doi:10.1016/j.ab.2005.07.033 (2005).

238 El-Andaloussi, S., Jarver, P., Johansson, H. J. & Langel, U. Cargo-dependent cytotoxicity and delivery efficacy of cell-penetrating peptides: a comparative study. *Biochem J* **407**, 285-292, doi:10.1042/BJ20070507 (2007).

239 Kilk, K., Mahlapuu, R., Soomets, U. & Langel, U. Analysis of in vitro toxicity of five cell-penetrating peptides by metabolic profiling. *Toxicology* **265**, 87-95, doi:10.1016/j.tox.2009.09.016 (2009).

240 Amantana, A. *et al.* Pharmacokinetics, biodistribution, stability and toxicity of a cell-penetrating peptide-morpholino oligomer conjugate. *Bioconjug Chem* **18**, 1325-1331, doi:10.1021/bc070060v (2007).

241 Aguilera, T. A., Olson, E. S., Timmers, M. M., Jiang, T. & Tsien, R. Y. Systemic in vivo distribution of activatable cell penetrating peptides is superior to that of cell penetrating peptides. *Integr Biol (Camb)* **1**, 371-381, doi:10.1039/b904878b (2009).

242 Khafagy el, S., Kamei, N., Nielsen, E. J., Nishio, R. & Takeda-Morishita, M. One-month subchronic toxicity study of cell-penetrating peptides for insulin nasal delivery in rats. *Eur J Pharm Biopharm* **85**, 736-743, doi:10.1016/j.ejpb.2013.09.014 (2013).

243 Lim, S., Koo, J. H. & Choi, J. M. Use of Cell-Penetrating Peptides in Dendritic Cell-Based Vaccination. *Immune Netw* **16**, 33-43, doi:10.4110/in.2016.16.1.33 (2016).

244 Martin, R. M., Tunnemann, G., Leonhardt, H. & Cardoso, M. C. Nucleolar marker for living cells. *Histochem Cell Biol* **127**, 243-251, doi:10.1007/s00418-006-0256-4 (2007).

245 Haase, H. *et al.* Minigenes encoding N-terminal domains of human cardiac myosin light chain-1 improve heart function of transgenic rats. *FASEB J* **20**, 865-873, doi:10.1096/fj.05-5414com (2006).

246 Cardo, L. *et al.* Accessible Synthetic Probes for Staining Actin inside Platelets and Megakaryocytes by Employing Lifeact Peptide. *Chembiochem* **16**, 1680-1688, doi:10.1002/cbic.201500120 (2015).

247 Santos-Cuevas, C. L. *et al.* 99mTc-N2S2-Tat (49-57)-bombesin internalized in nuclei of prostate and breast cancer cells: kinetics, dosimetry and effect on cellular proliferation. *Nucl Med Commun* **32**, 303-313, doi:10.1097/MNM.0b013e328341b27f (2011).

248 Jimenez-Mancilla, N. *et al.* Multifunctional targeted therapy system based on (99m) Tc/(177) Lu-labeled gold nanoparticles-Tat(49-57)-Lys(3) -bombesin internalized in nuclei of prostate cancer cells. *J Labelled Comp Radiopharm* **56**, 663-671, doi:10.1002/jlcr.3087 (2013).

249 Christian, N. A. *et al.* Tat-functionalized near-infrared emissive polymersomes for dendritic cell labeling. *Bioconjug Chem* **18**, 31-40, doi:10.1021/bc0601267 (2007).

250 Wender, P. A. *et al.* Real-time analysis of uptake and bioactivatable cleavage of luciferin-transporter conjugates in transgenic reporter mice. *Proc Natl Acad Sci U S A* **104**, 10340-10345, doi:10.1073/pnas.0703919104 (2007).

251 Jiang, T. *et al.* Tumor imaging by means of proteolytic activation of cell-penetrating peptides. *Proc Natl Acad Sci U S A* **101**, 17867-17872, doi:10.1073/pnas.0408191101 (2004).

252 Weinstain, R., Savariar, E. N., Felsen, C. N. & Tsien, R. Y. In vivo targeting of hydrogen peroxide by activatable cell-penetrating peptides. *J Am Chem Soc* **136**, 874-877, doi:10.1021/ja411547j (2014).

253 Walling, M. A., Novak, J. A. & Shepard, J. R. Quantum dots for live cell and in vivo imaging. *Int J Mol Sci* **10**, 441-491, doi:10.3390/ijms10020441 (2009).

254 Ruan, G., Agrawal, A., Marcus, A. I. & Nie, S. Imaging and tracking of tat peptide-conjugated quantum dots in living cells: new insights into nanoparticle uptake, intracellular transport, and vesicle shedding. *J Am Chem Soc* **129**, 14759-14766, doi:10.1021/ja074936k (2007).

255 Lei, Y. *et al.* Applications of mesenchymal stem cells labeled with Tat peptide conjugated quantum dots to cell tracking in mouse body. *Bioconjug Chem* **19**, 421-427, doi:10.1021/bc0700685 (2008).

256 Wiessner, C. *et al.* Neuron-specific transgene expression of Bcl-XL but not Bcl-2 genes reduced lesion size after permanent middle cerebral artery occlusion in mice. *Neurosci Lett* **268**, 119-122, doi:10.1016/s0304-3940(99)00392-4 (1999).

257 Cao, G. *et al.* In Vivo Delivery of a Bcl-xL Fusion Protein Containing the TAT Protein Transduction Domain Protects against Ischemic Brain Injury and Neuronal Apoptosis. *J Neurosci* **22**, 5423-5431, doi:20026550 (2002).

258 Asoh, S. *et al.* Protection against ischemic brain injury by protein therapeutics. *Proc Natl Acad Sci U S A* **99**, 17107-17112, doi:10.1073/pnas.262460299 (2002).

259 Martorana, F. *et al.* The BH4 domain of Bcl-X(L) rescues astrocyte degeneration in amyotrophic lateral sclerosis by modulating intracellular calcium signals. *Hum Mol Genet* **21**, 826-840, doi:10.1093/hmg/ddr513 (2012).

260 Borsello, T. *et al.* A peptide inhibitor of c-Jun N-terminal kinase protects against excitotoxicity and cerebral ischemia. *Nat Med* **9**, 1180-1186, doi:10.1038/nm911 (2003).

261 Sclip, A. *et al.* c-Jun N-terminal kinase has a key role in Alzheimer disease synaptic dysfunction in vivo. *Cell Death Dis* **5**, e1019, doi:10.1038/cddis.2013.559 (2014).

262 Suckfuell, M. *et al.* Efficacy and safety of AM-111 in the treatment of acute sensorineural hearing loss: a double-blind, randomized, placebo-controlled phase II study. *Otol Neurotol* **35**, 1317-1326, doi:10.1097/MAO.0000000000000466 (2014).

263 Touchard, E. *et al.* A peptide inhibitor of c-Jun N-terminal kinase for the treatment of endotoxin-induced uveitis. *Invest Ophthalmol Vis Sci* **51**, 4683-4693, doi:10.1167/iovs.09-4733 (2010).

264 Szabo, I., Orban, E., Schlosser, G., Hudecz, F. & Banoczi, Z. Cell-penetrating conjugates of pentaglutamylated methotrexate as potential anticancer drugs against resistant tumor cells. *Eur J Med Chem* **115**, 361-368, doi:10.1016/j.ejmech.2016.03.034 (2016).

265 Movafegh, B., Jalal, R., Mohammadi, Z. & Aldaghi, S. A. Poly-L-arginine: Enhancing Cytotoxicity and Cellular Uptake of Doxorubicin and Necrotic Cell Death. *Anticancer Agents Med Chem* **18**, 1448-1456, doi:10.2174/1871520618666180412114750 (2018).

266 Zhang, P., Cheetham, A. G., Lock, L. L. & Cui, H. Cellular uptake and cytotoxicity of drug-peptide conjugates regulated by conjugation site. *Bioconjug Chem* **24**, 604-613, doi:10.1021/bc300585h (2013).

267 Soudy, R., Chen, C. & Kaur, K. Novel peptide-doxorubucin conjugates for targeting breast cancer cells including the multidrug resistant cells. *J Med Chem* **56**, 7564-7573, doi:10.1021/jm400647r (2013).

268 Yu, M. *et al.* New Cell-Penetrating Peptide (KRP) with Multiple Physicochemical Properties Endows Doxorubicin with Tumor Targeting and Improves Its Therapeutic Index. *ACS Appl Mater Interfaces* **11**, 2448-2458, doi:10.1021/acsami.8b21027 (2019).

269 Ventura, A. *et al.* Restoration of p53 function leads to tumour regression in vivo. *Nature* **445**, 661-665, doi:10.1038/nature05541 (2007).

270 Snyder, E. L., Meade, B. R., Saenz, C. C. & Dowdy, S. F. Treatment of terminal peritoneal carcinomatosis by a transducible p53-activating peptide. *PLoS Biol* **2**, E36, doi:10.1371/journal.pbio.0020036 (2004).

271 Sarkar, F. H., Li, Y., Wang, Z. & Kong, D. NF-kappaB signaling pathway and its therapeutic implications in human diseases. *Int Rev Immunol* **27**, 293-319, doi:10.1080/08830180802276179 (2008).

272 May, M. J. *et al.* Selective inhibition of NF-kappaB activation by a peptide that blocks the interaction of NEMO with the IkappaB kinase complex. *Science* **289**, 1550-1554, doi:10.1126/science.289.5484.1550 (2000).

273 Peterson, J. M. *et al.* Peptide-based inhibition of NF-kappaB rescues diaphragm muscle contractile dysfunction in a murine model of Duchenne muscular dystrophy. *Mol Med* **17**, 508-515, doi:10.2119/molmed.2010.00263 (2011).

274 Wang, Y. F. *et al.* A cell-penetrating peptide suppresses inflammation by inhibiting NF-kappaB signaling. *Mol Ther* **19**, 1849-1857, doi:10.1038/mt.2011.82 (2011).

275 Splith, K. & Neundorf, I. Antimicrobial peptides with cell-penetrating peptide properties and vice versa. *Eur Biophys J* **40**, 387-397, doi:10.1007/s00249-011-0682-7 (2011).

276 Zhu, W. L., Hahm, K. S. & Shin, S. Y. Cell selectivity and mechanism of action of short antimicrobial peptides designed from the cell-penetrating peptide Pep-1. *J Pept Sci* **15**, 569-575, doi:10.1002/psc.1145 (2009).

277 Jung, H. J., Park, Y., Hahm, K. S. & Lee, D. G. Biological activity of Tat (47-58) peptide on human pathogenic fungi. *Biochem Biophys Res Commun* **345**, 222-228, doi:10.1016/j.bbrc.2006.04.059 (2006).

278 Zhu, W. L. & Shin, S. Y. Effects of dimerization of the cell-penetrating peptide Tat analog on antimicrobial activity and mechanism of bactericidal action. *J Pept Sci* **15**, 345-352, doi:10.1002/psc.1120 (2009).

279 Lee, H. *et al.* Conjugation of Cell-Penetrating Peptides to Antimicrobial Peptides Enhances Antibacterial Activity. *ACS Omega* **4**, 15694-15701, doi:10.1021/acsomega.9b02278 (2019).

280 Nagahara, H. *et al.* Transduction of full-length TAT fusion proteins into mammalian cells: TAT-p27Kip1 induces cell migration. *Nat Med* **4**, 1449-1452, doi:10.1038/4042 (1998).

281 Schwarze, S. R., Ho, A., Vocero-Akbani, A. & Dowdy, S. F. In vivo protein transduction: delivery of a biologically active protein into the mouse. *Science* **285**, 1569-1572, doi:10.1126/science.285.5433.1569 (1999).

282 Nagy, A. Cre recombinase: the universal reagent for genome tailoring. *Genesis* **26**, 99-109 (2000).

283 Tunnemann, G. *et al.* Cargo-dependent mode of uptake and bioavailability of TAT-containing proteins and peptides in living cells. *FASEB J* **20**, 1775-1784, doi:10.1096/fj.05-5523com (2006).

284 Patel, S. G. *et al.* Cell-penetrating peptide sequence and modification dependent uptake and subcellular distribution of green florescent protein in different cell lines. *Sci Rep* **9**, 6298, doi:10.1038/s41598-019-42456-8 (2019).

285 Anderson, D. C. *et al.* Tumor cell retention of antibody Fab fragments is enhanced by an attached HIV TAT protein-derived peptide. *Biochem Biophys Res Commun* **194**, 876-884, doi:10.1006/bbrc.1993.1903 (1993).

286 Pooga, M. *et al.* Cellular translocation of proteins by transportan. *FASEB J* **15**, 1451-1453, doi:10.1096/fj.00-0780fje (2001).

287 Inomata, K. *et al.* High-resolution multi-dimensional NMR spectroscopy of proteins in human cells. *Nature* **458**, 106-109, doi:10.1038/nature07839 (2009).

288 Takeuchi, T. *et al.* Direct and rapid cytosolic delivery using cell-penetrating peptides mediated by pyrenebutyrate. *ACS Chem Biol* **1**, 299-303, doi:10.1021/cb600127m (2006).

289 Suresh, B., Ramakrishna, S. & Kim, H. Cell-Penetrating Peptide-Mediated Delivery of Cas9 Protein and Guide RNA for Genome Editing. *Methods Mol Biol* **1507**, 81-94, doi:10.1007/978-1-4939-6518-2_7 (2017).

290 Nischan, N. *et al.* Covalent attachment of cyclic TAT peptides to GFP results in protein delivery into live cells with immediate bioavailability. *Angewandte Chemie* **54**, 1950-1953, doi:10.1002/anie.201410006 (2015).

291 Fuchs, S. M. & Raines, R. T. Arginine grafting to endow cell permeability. *ACS Chem Biol* **2**, 167-170, doi:10.1021/cb600429k (2007).

292 Cronican, J. J. *et al.* Potent delivery of functional proteins into Mammalian cells in vitro and in vivo using a supercharged protein. *ACS Chem Biol* **5**, 747-752, doi:10.1021/cb1001153 (2010).

293 Bruce, V. J., Lopez-Islas, M. & McNaughton, B. R. Resurfaced cell-penetrating nanobodies: A potentially general scaffold for intracellularly targeted protein discovery. *Protein Sci* **25**, 1129-1137, doi:10.1002/pro.2926 (2016).

294 Menichetti, R., Kanekal, K. H. & Bereau, T. Drug-Membrane Permeability across Chemical Space. *ACS Cent Sci* **5**, 290-298, doi:10.1021/acscentsci.8b00718 (2019).

295 Beaumont, K., Webster, R., Gardner, I. & Dack, K. Design of ester prodrugs to enhance oral absorption of poorly permeable compounds: challenges to the discovery scientist. *Curr Drug Metab* **4**, 461-485, doi:10.2174/1389200033489253 (2003).

296 Mix, K. A., Lomax, J. E. & Raines, R. T. Cytosolic Delivery of Proteins by Bioreversible Esterification. *J Am Chem Soc* **139**, 14396-14398, doi:10.1021/jacs.7b06597 (2017).

297 Ressler, V. T., Mix, K. A. & Raines, R. T. Esterification Delivers a Functional Enzyme into a Human Cell. *ACS Chem Biol* **14**, 599-602, doi:10.1021/acschembio.9b00033 (2019).

298 Palomo, J. M. Solid-phase peptide synthesis: an overview focused on the preparation of biologically relevant peptides. *RSC Advances* **4**, 32658-32672, doi:10.1039/C4RA02458C (2014).

299 Merrifield, R. B. Solid Phase Peptide Synthesis. I. The Synthesis of a Tetrapeptide. *Journal of the American Chemical Society* **85**, 2149-2154, doi:10.1021/ja00897a025 (1963).

300 Merrifield, B. Solid phase synthesis. *Science* **232**, 341-347, doi:10.1126/science.3961484 (1986).

301 Pedersen, S. L., Tofteng, A. P., Malik, L. & Jensen, K. J. Microwave heating in solid-phase peptide synthesis. *Chem Soc Rev* **41**, 1826-1844, doi:10.1039/c1cs15214a (2012).

302 Carpino, L. A. The 9-fluorenylmethyloxycarbonyl family of base-sensitive amino-protecting groups. *Accounts of Chemical Research* **20**, 401-407, doi:10.1021/ar00143a003 (1987).

303 Wong, C. H. & Zimmerman, S. C. Orthogonality in organic, polymer, and supramolecular chemistry: from Merrifield to click chemistry. *Chem Commun (Camb)* **49**, 1679-1695, doi:10.1039/c2cc37316e (2013).

304 Palomo, J. M., Lumbierres, M. & Waldmann, H. Efficient solid-phase lipopeptide synthesis employing the ellman sulfonamide linker. *Angewandte Chemie* **45**, 477-481, doi:10.1002/anie.200503298 (2006).

305 Galan, M. C., Dumy, P. & Renaudet, O. Multivalent glyco(cyclo)peptides. *Chemical Society Reviews* **42**, 4599-4612, doi:10.1039/C2CS35413F (2013).

306 Gaidzik, N., Westerlind, U. & Kunz, H. The development of synthetic antitumour vaccines from mucin glycopeptide antigens. *Chemical Society Reviews* **42**, 4421-4442, doi:10.1039/C3CS35470A (2013).

307 Broncel, M., Falenski, J. A., Wagner, S. C., Hackenberger, C. P. & Koksch, B. How post-translational modifications influence amyloid formation: a systematic study of phosphorylation and glycosylation in model peptides. *Chemistry* **16**, 7881-7888, doi:10.1002/chem.200902452 (2010).

308 Hojlys-Larsen, K. B. & Jensen, K. J. Solid-phase synthesis of phosphopeptides. *Methods Mol Biol* **1047**, 191-199, doi:10.1007/978-1-62703-544-6_13 (2013).

309 Bertran-Vicente, J. *et al.* Chemoselective synthesis and analysis of naturally occurring phosphorylated cysteine peptides. *Nat Commun* **7**, 12703, doi:10.1038/ncomms12703 (2016).

310 Avan, I., Hall, C. D. & Katritzky, A. R. Peptidomimetics via modifications of amino acids and peptide bonds. *Chem Soc Rev* **43**, 3575-3594, doi:10.1039/c3cs60384a (2014).

311 Wu, J. C. *et al.* Recent advances in peptide nucleic acid for cancer bionanotechnology. *Acta Pharmacol Sin* **38**, 798-805, doi:10.1038/aps.2017.33 (2017).

312 Sainlos, M. & Imperiali, B. Tools for investigating peptide-protein interactions: peptide incorporation of environment-sensitive fluorophores through SPPS-based 'building block' approach. *Nat Protoc* **2**, 3210-3218, doi:10.1038/nprot.2007.443 (2007).

313 Li, H., Aneja, R. & Chaiken, I. Click chemistry in peptide-based drug design. *Molecules* **18**, 9797-9817, doi:10.3390/molecules18089797 (2013).

314 Kohli, R. M., Walsh, C. T. & Burkart, M. D. Biomimetic synthesis and optimization of cyclic peptide antibiotics. *Nature* **418**, 658-661, doi:10.1038/nature00907 (2002).

315 Chow, H. Y., Zhang, Y., Matheson, E. & Li, X. Ligation Technologies for the Synthesis of Cyclic Peptides. *Chem Rev* **119**, 9971-10001, doi:10.1021/acs.chemrev.8b00657 (2019).

316 Behrendt, R., White, P. & Offer, J. Advances in Fmoc solid-phase peptide synthesis. *J Pept Sci* **22**, 4-27, doi:10.1002/psc.2836 (2016).

317 Dawson, P. E. & Kent, S. B. Synthesis of native proteins by chemical ligation. *Annu Rev Biochem* **69**, 923-960, doi:10.1146/annurev.biochem.69.1.923 (2000).

318 Monbaliu, J. C. & Katritzky, A. R. Recent trends in Cys- and Ser/Thr-based synthetic strategies for the elaboration of peptide constructs. *Chem Commun (Camb)* **48**, 11601-11622, doi:10.1039/c2cc34434c (2012).

319 Yan, L. Z. & Dawson, P. E. Synthesis of peptides and proteins without cysteine residues by native chemical ligation combined with desulfurization. *J Am Chem Soc* **123**, 526-533, doi:10.1021/ja003265m (2001).

320 Rohde, H. & Seitz, O. Ligation-desulfurization: a powerful combination in the synthesis of peptides and glycopeptides. *Biopolymers* **94**, 551-559, doi:10.1002/bip.21442 (2010).

321 Li, J. *et al.* One-pot native chemical ligation of peptide hydrazides enables total synthesis of modified histones. *Organic & Biomolecular Chemistry* **12**, 5435-5441, doi:10.1039/C4OB00715H (2014).

322 Raibaut, L. *et al.* Highly efficient solid phase synthesis of large polypeptides by iterative ligations of bis(2-sulfanylethyl)amido (SEA) peptide segments. *Chemical Science* **4**, 4061-4066, doi:10.1039/C3SC51824H (2013).

323 Nilsson, B. L., Kiessling, L. L. & Raines, R. T. Staudinger ligation: a peptide from a thioester and azide. *Org Lett* **2**, 1939-1941, doi:10.1021/ol0060174 (2000).

324 Tam, A. & Raines, R. T. Protein engineering with the traceless Staudinger ligation. *Methods Enzymol* **462**, 25-44, doi:10.1016/S0076-6879(09)62002-4 (2009).

325 Cai, H. *et al.* Towards a Fully Synthetic MUC1-Based Anticancer Vaccine: Efficient Conjugation of Glycopeptides with Mono-, Di-, and Tetravalent Lipopeptides Using Click Chemistry. **17**, 6396-6406, doi:10.1002/chem.201100217 (2011).

326 Hackenberger, C. P. & Schwarzer, D. Chemoselective ligation and modification strategies for peptides and proteins. *Angewandte Chemie* **47**, 10030-10074, doi:10.1002/anie.200801313 (2008).

327 Shadish, J. A. & DeForest, C. A. Site-Selective Protein Modification: From Functionalized Proteins to Functional Biomaterials. *Matter* **2**, 50-77, doi:https://doi.org/10.1016/j.matt.2019.11.011 (2020).

328 Spicer, C. D. & Davis, B. G. Selective chemical protein modification. *Nat Commun* **5**, 4740, doi:10.1038/ncomms5740 (2014).

329 Boutureira, O. & Bernardes, G. J. Advances in chemical protein modification. *Chem Rev* **115**, 2174-2195, doi:10.1021/cr500399p (2015).

330 Erlanson, D. A., Chytil, M. & Verdine, G. L. The leucine zipper domain controls the orientation of AP-1 in the NFAT.AP-1.DNA complex. *Chem Biol* **3**, 981-991, doi:10.1016/s1074-5521(96)90165-9 (1996).

331 Tolbert, T. J., Franke, D. & Wong, C. H. A new strategy for glycoprotein synthesis: ligation of synthetic glycopeptides with truncated proteins expressed in E. coli as TEV protease cleavable fusion protein. *Bioorg Med Chem* **13**, 909-915, doi:10.1016/j.bmc.2004.06.047 (2005).

332 Hackenberger, C. P., Chen, M. M. & Imperiali, B. Expression of N-terminal Cys-protein fragments using an intein refolding strategy. *Bioorg Med Chem* **14**, 5043-5048, doi:10.1016/j.bmc.2006.03.003 (2006).

333 Macmillan, D. & Arham, L. Cyanogen bromide cleavage generates fragments suitable for expressed protein and glycoprotein ligation. *J Am Chem Soc* **126**, 9530-9531, doi:10.1021/ja047855m (2004).

334 Gentle, I. E., De Souza, D. P. & Baca, M. Direct production of proteins with N-terminal cysteine for site-specific conjugation. *Bioconjug Chem* **15**, 658-663, doi:10.1021/bc049965o (2004).

335 Kane, P. M. *et al.* Protein splicing converts the yeast TFP1 gene product to the 69-kD subunit of the vacuolar H(+)-adenosine triphosphatase. *Science* **250**, 651-657, doi:10.1126/science.2146742 (1990).

336 Muir, T. W., Sondhi, D. & Cole, P. A. Expressed protein ligation: a general method for protein engineering. *Proc Natl Acad Sci U S A* **95**, 6705-6710 (1998).

337 Chong, S. *et al.* Single-column purification of free recombinant proteins using a self-cleavable affinity tag derived from a protein splicing element. *Gene* **192**, 271-281, doi:10.1016/s0378-1119(97)00105-4 (1997).

338 Wu, H., Hu, Z. & Liu, X. Q. Protein trans-splicing by a split intein encoded in a split DnaE gene of Synechocystis sp. PCC6803. *Proc Natl Acad Sci U S A* **95**, 9226-9231, doi:10.1073/pnas.95.16.9226 (1998).

339 Giriat, I. & Muir, T. W. Protein semi-synthesis in living cells. *J Am Chem Soc* **125**, 7180-7181, doi:10.1021/ja034736i (2003).

340 Sun, W., Yang, J. & Liu, X. Q. Synthetic two-piece and three-piece split inteins for protein trans-splicing. *J Biol Chem* **279**, 35281-35286, doi:10.1074/jbc.M405491200 (2004).

341 Burton, A. J., Haugbro, M., Parisi, E. & Muir, T. W. Live-cell protein engineering with an ultra-short split intein. *Proc Natl Acad Sci U S A* **117**, 12041-12049, doi:10.1073/pnas.2003613117 (2020).

342 Ludwig, C., Pfeiff, M., Linne, U. & Mootz, H. D. Ligation of a synthetic peptide to the N terminus of a recombinant protein using semisynthetic protein trans-splicing. *Angewandte Chemie* **45**, 5218-5221, doi:10.1002/anie.200600570 (2006).

343 Rashidian, M., Dozier, J. K. & Distefano, M. D. Enzymatic labeling of proteins: techniques and approaches. *Bioconjug Chem* **24**, 1277-1294, doi:10.1021/bc400102w (2013).

344 Zhang, Y., Park, K. Y., Suazo, K. F. & Distefano, M. D. Recent progress in enzymatic protein labelling techniques and their applications. *Chem Soc Rev* **47**, 9106-9136, doi:10.1039/c8cs00537k (2018).

345 Chang, T. K., Jackson, D. Y., Burnier, J. P. & Wells, J. A. Subtiligase: a tool for semisynthesis of proteins. *Proc Natl Acad Sci U S A* **91**, 12544-12548, doi:10.1073/pnas.91.26.12544 (1994).

346 Antos, J. M. *et al.* Site-Specific Protein Labeling via Sortase-Mediated Transpeptidation. *Curr Protoc Protein Sci* **89**, 15 13 11-15 13 19, doi:10.1002/cpps.38 (2017).

347 Antos, J. M., Truttmann, M. C. & Ploegh, H. L. Recent advances in sortase-catalyzed ligation methodology. *Curr Opin Struct Biol* **38**, 111-118, doi:10.1016/j.sbi.2016.05.021 (2016).

348 Suzuki, S. *et al.* Purification and characterization of novel transglutaminase from Bacillus subtilis spores. *Biosci Biotechnol Biochem* **64**, 2344-2351, doi:10.1271/bbb.64.2344 (2000).

349 Oteng-Pabi, S. K., Clouthier, C. M. & Keillor, J. W. Design of a glutamine substrate tag enabling protein labelling mediated by Bacillus subtilis transglutaminase. *PLoS One* **13**, e0197956, doi:10.1371/journal.pone.0197956 (2018).

350 Steffen, W. *et al.* Discovery of a microbial transglutaminase enabling highly site-specific labeling of proteins. *J Biol Chem* **292**, 15622-15635, doi:10.1074/jbc.M117.797811 (2017).

351 Schumacher, D. *et al.* Versatile and Efficient Site-Specific Protein Functionalization by Tubulin Tyrosine Ligase. *Angewandte Chemie* **54**, 13787-13791, doi:10.1002/anie.201505456 (2015).

352 Schumacher, D. *et al.* Broad substrate tolerance of tubulin tyrosine ligase enables one-step site-specific enzymatic protein labeling. *Chem Sci* **8**, 3471-3478, doi:10.1039/c7sc00574a (2017).

353 Cohen, J. D., Zou, P. & Ting, A. Y. Site-specific protein modification using lipoic acid ligase and bis-aryl hydrazone formation. *Chembiochem* **13**, 888-894, doi:10.1002/cbic.201100764 (2012).

354 Rush, J. S. & Bertozzi, C. R. New aldehyde tag sequences identified by screening formylglycine generating enzymes in vitro and in vivo. *J Am Chem Soc* **130**, 12240-12241, doi:10.1021/ja804530w (2008).

355 Koniev, O. & Wagner, A. Developments and recent advancements in the field of endogenous amino acid selective bond forming reactions for bioconjugation. *Chem Soc Rev* **44**, 5495-5551, doi:10.1039/c5cs00048c (2015).

356 Lang, K. & Chin, J. W. Bioorthogonal reactions for labeling proteins. *ACS Chem Biol* **9**, 16-20, doi:10.1021/cb4009292 (2014).

357 Kalkhof, S. & Sinz, A. Chances and pitfalls of chemical cross-linking with amine-reactive N-hydroxysuccinimide esters. *Anal Bioanal Chem* **392**, 305-312, doi:10.1007/s00216-008-2231-5 (2008).

358 Gray, G. R. The direct coupling of oligosaccharides to proteins and derivatized gels. *Arch Biochem Biophys* **163**, 426-428, doi:10.1016/0003-9861(74)90495-0 (1974).

359 Todrick, A. & Walker, E. A note on the combination of cysteine with allyl isothiocyanate. *Biochem J* **31**, 297-298, doi:10.1042/bj0310297 (1937).

360 Hacker, S. M. *et al.* Global profiling of lysine reactivity and ligandability in the human proteome. *Nat Chem* **9**, 1181-1190, doi:10.1038/nchem.2826 (2017).

361 Gunnoo, S. B. & Madder, A. Chemical Protein Modification through Cysteine. *Chembiochem* **17**, 529-553, doi:10.1002/cbic.201500667 (2016).

362 Thornton, J. M. Disulphide bridges in globular proteins. *J Mol Biol* **151**, 261-287, doi:10.1016/0022-2836(81)90515-5 (1981).

363 Stephanopoulos, N. & Francis, M. B. Choosing an effective protein bioconjugation strategy. *Nat Chem Biol* **7**, 876-884, doi:10.1038/nchembio.720 (2011).

364 Ravasco, J., Faustino, H., Trindade, A. & Gois, P. M. P. Bioconjugation with Maleimides: A Useful Tool for Chemical Biology. *Chemistry* **25**, 43-59, doi:10.1002/chem.201803174 (2019).

365 Huang, W. *et al.* Maleimide-thiol adducts stabilized through stretching. *Nat Chem* **11**, 310-319, doi:10.1038/s41557-018-0209-2 (2019).

366 Lyon, R. P. *et al.* Self-hydrolyzing maleimides improve the stability and pharmacological properties of antibody-drug conjugates. *Nat Biotechnol* **32**, 1059-1062, doi:10.1038/nbt.2968 (2014).

367 Kalia, D., Malekar, P. V. & Parthasarathy, M. Exocyclic Olefinic Maleimides: Synthesis and Application for Stable and Thiol-Selective Bioconjugation. *Angewandte Chemie* **55**, 1432-1435, doi:10.1002/anie.201508118 (2016).

368 Kasper, M. A. *et al.* Cysteine-Selective Phosphonamidate Electrophiles for Modular Protein Bioconjugations. *Angewandte Chemie* **58**, 11625-11630, doi:10.1002/anie.201814715 (2019).

369 Smith, M. E. B. *et al.* Protein Modification, Bioconjugation, and Disulfide Bridging Using Bromomaleimides. *Journal of the American Chemical Society* **132**, 1960-1965, doi:10.1021/ja908610s (2010).

370 Schafer, O. & Barz, M. Of Thiols and Disulfides: Methods for Chemoselective Formation of Asymmetric Disulfides in Synthetic Peptides and Polymers. *Chemistry* **24**, 12131-12142, doi:10.1002/chem.201800681 (2018).

371 Fontana, A., Scoffone, E. & Benassi, C. A. Sulfenyl halides as modifying reagents for polypeptides and proteins. II. Modification of cysteinyl residues. *Biochemistry* **7**, 980-986, doi:10.1021/bi00843a015 (1968).

372 King, T. P., Li, Y. & Kochoumian, L. Preparation of protein conjugates via intermolecular disulfide bond formation. *Biochemistry* **17**, 1499-1506, doi:10.1021/bi00601a022 (1978).

373 Yang, J., Chen, H., Vlahov, I. R., Cheng, J. X. & Low, P. S. Evaluation of disulfide reduction during receptor-mediated endocytosis by using FRET imaging. *Proc Natl Acad Sci U S A* **103**, 13872-13877, doi:10.1073/pnas.0601455103 (2006).

374 Ou, M. *et al.* Novel biodegradable poly(disulfide amine)s for gene delivery with high efficiency and low cytotoxicity. *Bioconjug Chem* **19**, 626-633, doi:10.1021/bc700397x (2008).

375 Taylor, M. T., Nelson, J. E., Suero, M. G. & Gaunt, M. J. A protein functionalization platform based on selective reactions at methionine residues. *Nature* **562**, 563-568, doi:10.1038/s41586-018-0608-y (2018).

376 Seim, K. L., Obermeyer, A. C. & Francis, M. B. Oxidative modification of native protein residues using cerium(IV) ammonium nitrate. *J Am Chem Soc* **133**, 16970-16976, doi:10.1021/ja206324q (2011).

377 Li, X., Ma, H., Dong, S., Duan, X. & Liang, S. Selective labeling of histidine by a designed fluorescein-based probe. *Talanta* **62**, 367-371, doi:10.1016/j.talanta.2003.08.004 (2004).

378 Kiick, K. L., Saxon, E., Tirrell, D. A. & Bertozzi, C. R. Incorporation of azides into recombinant proteins for chemoselective modification by the Staudinger ligation. *Proc Natl Acad Sci U S A* **99**, 19-24, doi:10.1073/pnas.012583299 (2002).

379 Wang, L., Brock, A., Herberich, B. & Schultz, P. G. Expanding the genetic code of Escherichia coli. *Science* **292**, 498-500, doi:10.1126/science.1060077 (2001).

380 Chin, J. W. *et al.* Addition of p-azido-L-phenylalanine to the genetic code of Escherichia coli. *J Am Chem Soc* **124**, 9026-9027, doi:10.1021/ja027007w (2002).

381 Plass, T., Milles, S., Koehler, C., Schultz, C. & Lemke, E. A. Genetically encoded copper-free click chemistry. *Angewandte Chemie* **50**, 3878-3881, doi:10.1002/anie.201008178 (2011).

382 Lang, K. *et al.* Genetic Encoding of bicyclononynes and trans-cyclooctenes for site-specific protein labeling in vitro and in live mammalian cells via rapid fluorogenic Diels-Alder reactions. *J Am Chem Soc* **134**, 10317-10320, doi:10.1021/ja302832g (2012).

383 Schafer, R. J. B., Aronoff, M. R. & Wennemers, H. Recent Advances in Bioorthogonal Reactions. *Chimia (Aarau)* **73**, 308-312, doi:10.2533/chimia.2019.308 (2019).

384 Saxon, E., Armstrong, J. I. & Bertozzi, C. R. A "traceless" Staudinger ligation for the chemoselective synthesis of amide bonds. *Org Lett* **2**, 2141-2143, doi:10.1021/ol006054v (2000).

385 Kleineweischede, R. & Hackenberger, C. P. Chemoselective peptide cyclization by traceless Staudinger ligation. *Angewandte Chemie* **47**, 5984-5988, doi:10.1002/anie.200801514 (2008).

386 Chan, T. R., Hilgraf, R., Sharpless, K. B. & Fokin, V. V. Polytriazoles as copper(I)-stabilizing ligands in catalysis. *Org Lett* **6**, 2853-2855, doi:10.1021/ol0493094 (2004).

387 Camakaris, J., Voskoboinik, I. & Mercer, J. F. Molecular mechanisms of copper homeostasis. *Biochem Biophys Res Commun* **261**, 225-232, doi:10.1006/bbrc.1999.1073 (1999).

388 Codelli, J. A., Baskin, J. M., Agard, N. J. & Bertozzi, C. R. Second-generation difluorinated cyclooctynes for copper-free click chemistry. *J Am Chem Soc* **130**, 11486-11493, doi:10.1021/ja803086r (2008).

389 Mahal, L. K., Yarema, K. J. & Bertozzi, C. R. Engineering chemical reactivity on cell surfaces through oligosaccharide biosynthesis. *Science* **276**, 1125-1128, doi:10.1126/science.276.5315.1125 (1997).

390 Rashidian, M. *et al.* A highly efficient catalyst for oxime ligation and hydrazone-oxime exchange suitable for bioconjugation. *Bioconjug Chem* **24**, 333-342, doi:10.1021/bc3004167 (2013).

391 Blackman, M. L., Royzen, M. & Fox, J. M. Tetrazine ligation: fast bioconjugation based on inverse-electron-demand Diels-Alder reactivity. *J Am Chem Soc* **130**, 13518-13519, doi:10.1021/ja8053805 (2008).

392 Darko, A. *et al.* Conformationally Strained trans-Cyclooctene with Improved Stability and Excellent Reactivity in Tetrazine Ligation. *Chem Sci* **5**, 3770-3776, doi:10.1039/C4SC01348D (2014).

393 Peng, T. & Hang, H. C. Site-Specific Bioorthogonal Labeling for Fluorescence Imaging of Intracellular Proteins in Living Cells. *J Am Chem Soc* **138**, 14423-14433, doi:10.1021/jacs.6b08733 (2016).

394 Selvaraj, R. *et al.* Tetrazine-trans-cyclooctene ligation for the rapid construction of integrin alphavbeta(3) targeted PET tracer based on a cyclic RGD peptide. *Bioorg Med Chem Lett* **21**, 5011-5014, doi:10.1016/j.bmcl.2011.04.116 (2011).

395 Lin, Y. A. *et al.* Rapid cross-metathesis for reversible protein modifications via chemical access to Se-allyl-selenocysteine in proteins. *J Am Chem Soc* **135**, 12156-12159, doi:10.1021/ja403191g (2013).

396 Wang, J. *et al.* A biosynthetic route to photoclick chemistry on proteins. *J Am Chem Soc* **132**, 14812-14818, doi:10.1021/ja104350y (2010).

397 Litman, G. W. *et al.* Phylogenetic diversification of immunoglobulin genes and the antibody repertoire. *Mol Biol Evol* **10**, 60-72, doi:10.1093/oxfordjournals.molbev.a040000 (1993).

398 Vidarsson, G., Dekkers, G. & Rispens, T. IgG subclasses and allotypes: from structure to effector functions. *Front Immunol* **5**, 520, doi:10.3389/fimmu.2014.00520 (2014).

399 Market, E. & Papavasiliou, F. N. V(D)J recombination and the evolution of the adaptive immune system. *PLoS Biol* **1**, E16, doi:10.1371/journal.pbio.0000016 (2003).

400 Diaz, M. & Casali, P. Somatic immunoglobulin hypermutation. *Curr Opin Immunol* **14**, 235-240, doi:10.1016/s0952-7915(02)00327-8 (2002).

401 Coombs, R. R., Mourant, A. E. & Race, R. R. A new test for the detection of weak and incomplete Rh agglutinins. *Br J Exp Pathol* **26**, 255-266 (1945).

402 Engvall, E. & Perlmann, P. Enzyme-linked immunosorbent assay (ELISA). Quantitative assay of immunoglobulin G. *Immunochemistry* **8**, 871-874 (1971).

403 Coons, A. H. & Kaplan, M. H. Localization of antigen in tissue cells; improvements in a method for the detection of antigen by means of fluorescent antibody. *J Exp Med* **91**, 1-13, doi:10.1084/jem.91.1.1 (1950).

404 Vira, S., Mekhedov, E., Humphrey, G. & Blank, P. S. Fluorescent-labeled antibodies: Balancing functionality and degree of labeling. *Anal Biochem* **402**, 146-150, doi:10.1016/j.ab.2010.03.036 (2010).

405 Szabo, A. *et al.* The Effect of Fluorophore Conjugation on Antibody Affinity and the Photophysical Properties of Dyes. *Biophys J* **114**, 688-700, doi:10.1016/j.bpj.2017.12.011 (2018).

406 Schroeder, H. W., Jr. & Cavacini, L. Structure and function of immunoglobulins. *J Allergy Clin Immunol* **125**, S41-52, doi:10.1016/j.jaci.2009.09.046 (2010).

407 Carter, P. J. & Lazar, G. A. Next generation antibody drugs: pursuit of the 'high-hanging fruit'. *Nat Rev Drug Discov* **17**, 197-223, doi:10.1038/nrd.2017.227 (2018).

408 Miersch, S. & Sidhu, S. S. Intracellular targeting with engineered proteins. *F1000Res* **5**, doi:10.12688/f1000research.8915.1 (2016).

409 Riabowol, K. T., Vosatka, R. J., Ziff, E. B., Lamb, N. J. & Feramisco, J. R. Microinjection of fos-specific antibodies blocks DNA synthesis in fibroblast cells. *Mol Cell Biol* **8**, 1670-1676, doi:10.1128/mcb.8.4.1670 (1988).

410 Gire, V. & Wynford-Thomas, D. Reinitiation of DNA synthesis and cell division in senescent human fibroblasts by microinjection of anti-p53 antibodies. *Mol Cell Biol* **18**, 1611-1621, doi:10.1128/mcb.18.3.1611 (1998).

411 Freund, G. *et al.* Targeting endogenous nuclear antigens by electrotransfer of monoclonal antibodies in living cells. *MAbs* **5**, 518-522, doi:10.4161/mabs.25084 (2013).

412 Carlson, J. R. A new means of inducibly inactivating a cellular protein. *Mol Cell Biol* **8**, 2638-2646, doi:10.1128/mcb.8.6.2638 (1988).

413 Southwell, A. L., Ko, J. & Patterson, P. H. Intrabody gene therapy ameliorates motor, cognitive, and neuropathological symptoms in multiple mouse models of Huntington's disease. *J Neurosci* **29**, 13589-13602, doi:10.1523/JNEUROSCI.4286-09.2009 (2009).

414 Kim, T. K. & Eberwine, J. H. Mammalian cell transfection: the present and the future. *Anal Bioanal Chem* **397**, 3173-3178, doi:10.1007/s00216-010-3821-6 (2010).

415 Zhao, Y., Lou, D., Burkett, J. & Kohler, H. Chemical engineering of cell penetrating antibodies. *J Immunol Methods* **254**, 137-145, doi:10.1016/s0022-1759(01)00410-0 (2001).

416 Mie, M. *et al.* Intracellular delivery of antibodies using TAT fusion protein A. *Biochem Biophys Res Commun* **310**, 730-734, doi:10.1016/j.bbrc.2003.09.071 (2003).

417 Zhao, Y., Brown, T. L., Kohler, H. & Muller, S. MTS-conjugated-antiactive caspase 3 antibodies inhibit actinomycin D-induced apoptosis. *Apoptosis* **8**, 631-637, doi:10.1023/A:1026139627930 (2003).

418 Chen, B. X. & Erlanger, B. F. Cell cycle inhibition by an anti-cyclin D1 antibodychemically modified for intracellular delivery. *Cancer Lett* **244**, 71-75, doi:10.1016/j.canlet.2005.12.011 (2006).

419 Wang, S. *et al.* Light-Controlled Delivery of Monoclonal Antibodies for Targeted Photoinactivation of Ki-67. *Mol Pharm* **12**, 3272-3281, doi:10.1021/acs.molpharmaceut.5b00260 (2015).

420 Dalkara, D., Zuber, G. & Behr, J. P. Intracytoplasmic delivery of anionic proteins. *Mol Ther* **9**, 964-969, doi:10.1016/j.ymthe.2004.03.007 (2004).

421 Courtete, J. *et al.* Suppression of cervical carcinoma cell growth by intracytoplasmic codelivery of anti-oncoprotein E6 antibody and small interfering RNA. *Mol Cancer Ther* **6**, 1728-1735, doi:10.1158/1535-7163.MCT-06-0808 (2007).

422 Chiu, H. Y. *et al.* Intracellular chromobody delivery by mesoporous silica nanoparticles for antigen targeting and visualization in real time. *Sci Rep* **6**, 25019, doi:10.1038/srep25019 (2016).

423 Helma, J., Cardoso, M. C., Muyldermans, S. & Leonhardt, H. Nanobodies and recombinant binders in cell biology. *J Cell Biol* **209**, 633-644, doi:10.1083/jcb.201409074 (2015).

424 Wurch, T. *et al.* Development of novel protein scaffolds as alternatives to whole antibodies for imaging and therapy: status on discovery research and clinical validation. *Curr Pharm Biotechnol* **9**, 502-509, doi:10.2174/138920108786786385 (2008).

425 Worn, A. & Pluckthun, A. Stability engineering of antibody single-chain Fv fragments. *J Mol Biol* **305**, 989-1010, doi:10.1006/jmbi.2000.4265 (2001).

426 Tanha, J. *et al.* Improving solubility and refolding efficiency of human V(H)s by a novel mutational approach. *Protein Eng Des Sel* **19**, 503-509, doi:10.1093/protein/gzl037 (2006).

427 Hamers-Casterman, C. *et al.* Naturally occurring antibodies devoid of light chains. *Nature* **363**, 446-448, doi:10.1038/363446a0 (1993).

428 De Genst, E. *et al.* Molecular basis for the preferential cleft recognition by dromedary heavy-chain antibodies. *Proc Natl Acad Sci U S A* **103**, 4586-4591, doi:10.1073/pnas.0505379103 (2006).

429 Muyldermans, S., Atarhouch, T., Saldanha, J., Barbosa, J. A. & Hamers, R. Sequence and structure of VH domain from naturally occurring camel heavy chain immunoglobulins lacking light chains. *Protein Eng* **7**, 1129-1135 (1994).

430 Maass, D. R., Sepulveda, J., Pernthaner, A. & Shoemaker, C. B. Alpaca (Lama pacos) as a convenient source of recombinant camelid heavy chain antibodies (VHHs). *J Immunol Methods* **324**, 13-25, doi:10.1016/j.jim.2007.04.008 (2007).

431 Steeland, S., Vandenbroucke, R. E. & Libert, C. Nanobodies as therapeutics: big opportunities for small antibodies. *Drug Discov Today* **21**, 1076-1113, doi:10.1016/j.drudis.2016.04.003 (2016).

432 Michaely, P., Tomchick, D. R., Machius, M. & Anderson, R. G. Crystal structure of a 12 ANK repeat stack from human ankyrinR. *EMBO J* **21**, 6387-6396, doi:10.1093/emboj/cdf651 (2002).

433 Binz, H. K. *et al.* High-affinity binders selected from designed ankyrin repeat protein libraries. *Nat Biotechnol* **22**, 575-582, doi:10.1038/nbt962 (2004).

434 Steiner, D., Forrer, P. & Pluckthun, A. Efficient selection of DARPins with sub-nanomolar affinities using SRP phage display. *J Mol Biol* **382**, 1211-1227, doi:10.1016/j.jmb.2008.07.085 (2008).

435 Koide, A., Bailey, C. W., Huang, X. & Koide, S. The fibronectin type III domain as a scaffold for novel binding proteins. *J Mol Biol* **284**, 1141-1151, doi:10.1006/jmbi.1998.2238 (1998).

436 Koide, A., Gilbreth, R. N., Esaki, K., Tereshko, V. & Koide, S. High-affinity single-domain binding proteins with a binary-code interface. *Proc Natl Acad Sci U S A* **104**, 6632-6637, doi:10.1073/pnas.0700149104 (2007).

437 Nord, K. *et al.* Binding proteins selected from combinatorial libraries of an alpha-helical bacterial receptor domain. *Nat Biotechnol* **15**, 772-777, doi:10.1038/nbt0897-772 (1997).

438 Schumacher, D., Helma, J., Schneider, A. F. L., Leonhardt, H. & Hackenberger, C. P. R. Nanobodies: Chemical Functionalization Strategies and Intracellular Applications. *Angewandte Chemie* **57**, 2314-2333, doi:10.1002/anie.201708459 (2018).

439 Massa, S. *et al.* Site-specific labeling of cysteine-tagged camelid single-domain antibody-fragments for use in molecular imaging. *Bioconjug Chem* **25**, 979-988, doi:10.1021/bc500111t (2014).

440 Witte, M. D. *et al.* Preparation of unnatural N-to-N and C-to-C protein fusions. *Proc Natl Acad Sci U S A* **109**, 11993-11998, doi:10.1073/pnas.1205427109 (2012).

441 Gray, M. A., Tao, R. N., DePorter, S. M., Spiegel, D. A. & McNaughton, B. R. A Nanobody Activation Immunotherapeutic that Selectively Destroys HER2-Positive Breast Cancer Cells. *Chembiochem* **17**, 155-158, doi:10.1002/cbic.201500591 (2016).

442 Marschall, A. L. *et al.* Delivery of antibodies to the cytosol: debunking the myths. *MAbs* **6**, 943-956, doi:10.4161/mabs.29268 (2014).

443 Klein, A. *et al.* Live-cell labeling of endogenous proteins with nanometer precision by transduced nanobodies. *Chem Sci* **9**, 7835-7842, doi:10.1039/c8sc02910e (2018).

444 Roder, R. *et al.* Intracellular Delivery of Nanobodies for Imaging of Target Proteins in Live Cells. *Pharm Res* **34**, 161-174, doi:10.1007/s11095-016-2052-8 (2017).

445 Kirchhofer, A. *et al.* Modulation of protein properties in living cells using nanobodies. *Nat Struct Mol Biol* **17**, 133-138, doi:10.1038/nsmb.1727 (2010).

446 Herce, H. D. *et al.* Cell-permeable nanobodies for targeted immunolabelling and antigen manipulation in living cells. *Nat Chem* **9**, 762-771, doi:10.1038/nchem.2811 (2017).

447 Dang, C. V. & Lee, W. M. Identification of the human c-myc protein nuclear translocation signal. *Mol Cell Biol* **8**, 4048-4054, doi:10.1128/mcb.8.10.4048 (1988).

448 Riedl, J. *et al.* Lifeact: a versatile marker to visualize F-actin. *Nat Methods* **5**, 605-607, doi:10.1038/nmeth.1220 (2008).

449 McBride, H. M., Neuspiel, M. & Wasiak, S. Mitochondria: more than just a powerhouse. *Curr Biol* **16**, R551-560, doi:10.1016/j.cub.2006.06.054 (2006).

450 Chan, D. C. Mitochondria: dynamic organelles in disease, aging, and development. *Cell* **125**, 1241-1252, doi:10.1016/j.cell.2006.06.010 (2006).

451 Anderson, S. *et al.* Sequence and organization of the human mitochondrial genome. *Nature* **290**, 457-465, doi:10.1038/290457a0 (1981).

452 Dudek, J., Rehling, P. & van der Laan, M. Mitochondrial protein import: common principles and physiological networks. *Biochim Biophys Acta* **1833**, 274-285, doi:10.1016/j.bbamcr.2012.05.028 (2013).

453 Verner, K. Co-translational protein import into mitochondria: an alternative view. *Trends Biochem Sci* **18**, 366-371, doi:10.1016/0968-0004(93)90090-a (1993).

454 Mayer, A., Neupert, W. & Lill, R. Mitochondrial protein import: reversible binding of the presequence at the trans side of the outer membrane drives partial translocation and unfolding. *Cell* **80**, 127-137, doi:10.1016/0092-8674(95)90457-3 (1995).

455 Gorman, G. S. *et al.* Mitochondrial diseases. *Nat Rev Dis Primers* **2**, 16080, doi:10.1038/nrdp.2016.80 (2016).

456 Smith, R. A., Hartley, R. C., Cocheme, H. M. & Murphy, M. P. Mitochondrial pharmacology. *Trends Pharmacol Sci* **33**, 341-352, doi:10.1016/j.tips.2012.03.010 (2012).

457 Schneider, A. F. L., Wallabregue, A. L. D., Franz, L. & Hackenberger, C. P. R. Targeted Subcellular Protein Delivery Using Cleavable Cyclic Cell-Penetrating Peptides. *Bioconjug Chem* **30**, 400-404, doi:10.1021/acs.bioconjchem.8b00855 (2019).

458 Goedhart, J. *et al.* Structure-guided evolution of cyan fluorescent proteins towards a quantum yield of 93%. *Nat Commun* **3**, 751, doi:10.1038/ncomms1738 (2012).

459 von Heijne, G. Membrane-protein topology. *Nat Rev Mol Cell Biol* **7**, 909-918, doi:10.1038/nrm2063 (2006).

460 Thuduppathy, G. R., Craig, J. W., Kholodenko, V., Schon, A. & Hill, R. B. Evidence that membrane insertion of the cytosolic domain of Bcl-xL is governed by an electrostatic mechanism. *J Mol Biol* **359**, 1045-1058, doi:10.1016/j.jmb.2006.03.052 (2006).

461 Goni, F. M. Non-permanent proteins in membranes: when proteins come as visitors (Review). *Mol Membr Biol* **19**, 237-245, doi:10.1080/0968768021000035078 (2002).

462 Ferri, N., Paoletti, R. & Corsini, A. Lipid-modified proteins as biomarkers for cardiovascular disease: a review. *Biomarkers* **10**, 219-237, doi:10.1080/13547500500216660 (2005).

463 Chen, B., Sun, Y., Niu, J., Jarugumilli, G. K. & Wu, X. Protein Lipidation in Cell Signaling and Diseases: Function, Regulation, and Therapeutic Opportunities. *Cell Chem Biol* **25**, 817-831, doi:10.1016/j.chembiol.2018.05.003 (2018).

464 Ko, P. J. & Dixon, S. J. Protein palmitoylation and cancer. *EMBO Rep* **19**, doi:10.15252/embr.201846666 (2018).

465 Agudo-Ibanez, L., Herrero, A., Barbacid, M. & Crespo, P. H-ras distribution and signaling in plasma membrane microdomains are regulated by acylation and deacylation events. *Mol Cell Biol* **35**, 1898-1914, doi:10.1128/MCB.01398-14 (2015).

466 Gross, L. A., Baird, G. S., Hoffman, R. C., Baldridge, K. K. & Tsien, R. Y. The structure of the chromophore within DsRed, a red fluorescent protein from coral. *Proc Natl Acad Sci U S A* **97**, 11990-11995, doi:10.1073/pnas.97.22.11990 (2000).

Aus Datenschutzgründen ist der Lebenslauf in der Online-Version nicht enthalten.